ESA Climate Change Initiative “Plus” (CCI+)

Product Validation and Intercomparison Report (PVIR) for data set CRDP8

for the Essential Climate Variable (ECV)

Greenhouse Gases (GHG):

XCO_2 and/or XCH_4 from

OCO-2, Sentinel-5-Precursor and GOSAT-2

Written by: GHG-CCI+ Phase 2 project team

Lead author: Michael Buchwitz, Institute of Environmental Physics (IUP), University of Bremen, Germany

Co-authors:

Bart Dils (BIRA-IASB, Belgium, Brussels)

Maximilian Reuter, Oliver Schneising-Weigel, Michael Hilker (IUP, Univ. Bremen, Germany)

Andrew Barr, Tobias Borsdorff, (SRON, Leiden, The Netherlands)

Change log:

Version Nr.	Date	Status	Reason for change
Version 1.1	13-Mar-2020	Approved	New document for CRDP5
Version 2.0	10-Feb-2021	Submitted	Update for CRDP6
Version 2.1	19-Mar-2021	Approved	Content for Sect. 4.2.2 added on request of ESA.
Version 3.0	16-Feb-2022	Approved	Update for CRDP7
Version 4.0	29-Aug-2023	Submitted	Update for CRDP8

Table of Contents

1 Executive Summary

This document is the Product Validation and Intercomparison Report (PVIR) version 4.0 (v4.0), which is a deliverable of the ESA project GHG-CCI+ (https://climate.esa.int/en/projects/ghgs/) Phase 2.

Phase 2 of the GHG-CCI+ project started in September 2022 and is carrying out research and development (R&D) as needed to generate new and/or improve existing Greenhouse Gas (GHG) Essential Climate Variable (ECV) satellite-derived CO_2 and CH_4 data products.

These products are column-averaged dry-air mole fractions of carbon dioxide (CO_2), denoted XCO_2, and methane (CH_4), denoted XCH_4, from these satellites / satellite sensors using European scientific retrieval algorithms:

- XCO_2 from OCO-2 using the University of Bremen FOCAL algorithm (product **CO2_OC2_FOCA**),
- XCH_4 from Sentinel-5 Precursor (S5P) using University of Bremen's WFM-DOAS (or WFMD) algorithm (product **CH4_S5P_WFMD**),
- XCO_2 and XCH_4 from GOSAT-2 using SRON's RemoTeC algorithm (products **CO2_GO2_SRFP, CH4_GO2_SRFP, CH4_GO2_SRPR**)

This project aims to generate GHG ECV data products in-line with GCOS (Global Climate Observing System) requirements. GCOS defines the ECV GHG as follows (see Sect. 2 for comments related to the recent update of the GCOS requirements): "Retrievals of greenhouse gases, such as CO_2 and CH_4, of sufficient quality to estimate regional sources and sinks". Within the GHG-CCI+ project satellite-derived XCO_2 (in ppm) and XCH_4 (in ppb) data products are retrieved from satellite radiance observations in the Short-Wave-Infra-Red (SWIR) spectral region. These instruments are used because their measurements are sensitive also to the lowest atmospheric layer and therefore provide information on the regional surface sources and sinks of CO_2 and CH_4. All products are generated with independent retrieval algorithms developed to convert GOSAT-2, OCO-2 and TROPOMI/S5P radiance spectra into Level 2 (L2) XCO_2 and/or XCH_4 data products.

In this document the validation and intercomparison results are presented. The validation is based on comparisons with TCCON (Total Carbon Column Observation Network) ground-based XCO_2 and XCH_4 retrievals. The validation has been carried out by the GHG-CCI+ independent Validation Team (VALT) and by the data provider (DP) of a given product.

For each data product and each assessment method the following validation summary "figures of merit" have been determined and are reported in this document: (i) Single measurement precision, (ii) mean bias (global offset), (iii) relative systematic error (or relative accuracy), (iv) stability (linear bias drift or trend). Furthermore, also the reported XCO_2 and XCH_4 uncertainties have been validated by computing a quantity called "Uncertainty ratio", which is the ratio of the (mean value of the) reported uncertainty and the standard deviation of satellite minus TCCON differences. The results are summarized in **Table 1-1** for the XCO_2 products and **Table 1-2** for the XCH_4 product.

Table 1-1: *Summary of the validation of XCO_2 products CO2_OC2_FOCA and CO2_GO2_SRFP of data set Climate Research Data Package No. 8 (CRDP#8, to be released in September 2023) via comparison with TCCON ground-based XCO_2 retrievals. VALT refers to the assessment results of the GHG-CCI+ independent validation team and DP refers to the assessment results of the data provider. (*) Excluding a possible global offset, which is reported separately in this document. The range reported for VALT results in square brackets […] correspond with the upper and lower 95% confidence bound on the parameter. "n.a." means "not applicable" and "n.e." means "not evaluated (e.g., because time series too short).*

Summary validation results GHG-CCI+ CRDP#8 XCO_2 products

by comparisons with TCCON

Product CO2_OC2_FOCA (v10.1, global, 9.2014 – 2.2022)

Parameter	Achieved	Required	Comments
Random error (single obs., 1σ) [ppm]	VALT: 1.52 [1.37,1.55] DP: 1.77	T:<8; B:<3; G:<1	T=threshold; B=breakthrough; G=goal
Systematic error [ppm]	VALT: 0.35 [0.12, 0.50] / 0.54 [0.43, 0.67] DP: 0.55 / 0.61	< 0.5	"Relative accuracy" (*) Spatial / spatio-temp.
Stability: Linear bias trend [ppm/year]	VALT: -0.02 [-0.10, 0.03] DP: -0.02 ± 0.19	< 0.5	1σ uncertainty

Product CO2_GO2_SRFP (v02.0.2, global, 2.2019 – 12.2021)

Parameter	Achieved	Required	Comments
Random error (single obs., 1σ) [ppm]	VALT: 2.07 [1.94, 2.18] DP: 2.21	T:<8; B:<3; G:<1	T=threshold; B=breakthrough; G=goal
Systematic error [ppm]	VALT: 0.47 [0.09, 0.74] / 0.81 [0.53, 1.05] DP: 0.5 / 1.0	< 0.5	"Relative accuracy" (*) Spatial / spatio-temp.
Stability: Linear bias trend [ppm/year]	VALT: 0.12 [-0.05, 0.44] DP: 0.46	< 0.5	1σ uncertainty Only short time period

Table 1-2: *Summary of the validation of XCH_4 products CH4_S5P_WFMD of data set Climate Research Data Package No. 8 (CRDP#8, to be released in September 2023) via comparison with TCCON ground-based XCH_4 retrievals. VALT refers to the assessment results of the GHG-CCI+ independent validation team and DP refers to the assessment results of the data provider. (*) Excluding a possible global offset, which is reported separately in this document. The range reported for VALT results in square brackets […] correspond with the upper and lower 95% confidence bound on the parameter. "n.a." means "not applicable" and "n.e." means "not evaluated (e.g., because time series is too short).*

Summary validation results GHG-CCI+ CRDP#8 XCH_4 products by comparisons with TCCON			
Product CH4_S5P_WFMD (v1.8, global, 11.2017– 12.2022)			
Parameter	**Achieved**	**Required**	**Comments**
Random error (single obs., 1σ) [ppb]	VALT: 13.7 [12.0, 14.8] DP: 12.4	T:<34; B:<17; G:<9	T=threshold; B=breakthrough; G=goal
Systematic error [ppb]	VALT: 3.9 [0.4, 6.2] / 5.9 [4.8, 7.4] DP: 5.2 / 5.4	< 10	"Relative accuracy" (*) Spatial / spatio-temp.
Stability: Linear bias trend [ppb/year]	VALT: 0.4 [0.1, 0.8] DP: -0.003	< 3	1σ uncertainty

Product CH4_GO2_SRFP (v02.0.2, global, 2.2019– 12.2021)			
Parameter	**Achieved**	**Required**	**Comments**
Random error (single obs., 1σ) [ppb]	VALT: 14.2 [12.6, 15.1] DP: 15.2	T:<34; B:<17; G:<9	T=threshold; B=breakthrough; G=goal
Systematic error [ppb]	VALT: 1.8 [0.1, 2.7] / 5.1 [3.4, 6.8] DP: 4.3 / 3.8	< 10	"Relative accuracy" (*) Spatial / spatio-temp.
Stability: Linear bias trend [ppb/year]	VALT: 3.8 [1.9, 4.8] DP: 2.5	< 3	1σ uncertainty

Table is continued on the following page …

Table 1-2: *Continued from previous page.*

Product CH4_GO2_SRPR (v02.0.2, global, 2.2019– 12.2021)			
Parameter	**Achieved**	**Required**	**Comments**
Random error (single obs., 1σ) [ppb]	VALT: 15.1 [14.1, 16.2] DP: 16.6	T:<34; B:<17; G:<9	T=threshold; B=breakthrough; G=goal
Systematic error [ppb]	VALT: 3.7 [1.8, 5.4] / 6.2 [4.6, 8.1] DP: 5.9 / n.a.	< 10	"Relative accuracy" (*) Spatial / spatio-temp.
Stability: Linear bias trend [ppb/year]	VALT: n.a. DP: n.a.	< 3	1σ uncertainty

2 Introduction

This document is the Product Validation and Intercomparison Report (PVIR) version 4.0 (v4.0), which is a deliverable of the ESA project GHG-CCI+ (https://climate.esa.int/en/projects/ghgs/) Phase 2.

GHG-CCI+ Phase 2 started in September 2022 and is carrying out the R&D needed to generate new or improve existing Greenhouse Gas (GHG) Essential Climate Variable (ECV) satellite-derived CO_2 and CH_4 data products.

These products are column-averaged dry-air mole fractions of carbon dioxide (CO_2), denoted XCO_2, and methane (CH_4), denoted XCH_4, from these satellites / satellite sensors using European scientific retrieval algorithms:

- XCO_2 from OCO-2,
- XCO_2 and XCH_4 from GOSAT-2 and
- XCH_4 from S5P

This project aims to generate GHG ECV data products in-line with GCOS (Global Climate Observing System) requirements **/GCOS-154/ /GCOS-195/ /GCOS-200/**. GCOS defines the ECV GHG as follows: "Retrievals of greenhouse gases, such as CO_2 and CH_4, of sufficient quality to estimate regional sources and sinks".

Note that GCOS has recently (in 2022) published updated requirements **/GCOS-245/**. These requirements are on one hand more appropriate for our data products as "CO_2 column average dry air mixing ratio", i.e., XCO_2, and "CH_4 column average dry air mixing ratio", i.e., XCH_4, are now listed as ECV products (in contrast to earlier GCOS documents referring to products not generated by us (for good reasons) such as tropospheric columns, etc.) but on the other hand the requirements are less appropriate as they partially refer to future missions or cannot be met for the existing satellites we are using. For example, the XCO_2 threshold requirements for temporal resolution (72 hours; neither OCO-2 nor GOSAT-2 meet this requirement) and uncertainty (0.8 ppm, 1-sigma) refer to CO2M (launch 2026). The threshold stability requirement is 0.3 ppm per decade (0.03 ppm/year) which is according to our experience significantly smaller that the uncertainty of methods used to establish stability (taking into account "noise" due to sampling aspects, stability of the reference data, etc.). Similar for XCH_4: The required minimum (threshold) uncertainty is 10 ppb (1-sigma), which (for many locations on Earth) cannot be met by S5P. For the breakthrough requirement of 5 ppb, it is argued that this is based on "Expert judgement based on expected improvement of TROPOMI/S5P". Typical TROPOMI/S5P XCH_4 uncertainty is on the order of 15 ppb and this is mainly due to instrument noise and no improvement can change this (except by limiting retrievals to highly reflecting scenes). Furthermore, the arguably most important requirement for users who use our data products for inverse modelling of sources and sinks is related to systematic errors (high accuracy or low biases) but this is not addressed in **/GCOS-245/** as the uncertainty requirement is essentially a random error (dispersion, scatter) related requirement.

ECV GHG requirements for satellite-derived XCO_2 and XCH_4 products avoiding these limitations have been formulated by the GHG-CCI+ project Climate Research Group (CRG) and are document in the GHG-CCI+ User Requirements Document (URD) **/URDv3.0/**. In the past we assessed the achieved quality of our products in detail considering these URD requirements and we follow this approach also during GHG-CCI+ Phase 2.

Once the products are of sufficient quality for a climate service and cover a long enough time period, it is expected that the data will become part of the Copernicus Climate Change Service (C3S, https://climate.copernicus.eu/) as done for earlier products initially developed by GHG-CCI, see Copernicus Climate Data Store (CDS, https://cds.climate.copernicus.eu/):

- CO_2 products: https://cds.climate.copernicus.eu/cdsapp#!/dataset/satellite-carbon-dioxide?tab=overview
- CH_4 products: https://cds.climate.copernicus.eu/cdsapp#!/dataset/satellite-methane?tab=overview

Within GHG-CCI+ satellite-derived XCO_2 (in ppm) and XCH_4 (in ppb) data products are retrieved from satellite radiance observations in the Short-Wave-Infra-Red (SWIR) spectral region. These instruments are used because their measurements are sensitive also to the lowest atmospheric layer and therefore provide information on the regional surface sources and sinks of CO_2 and CH_4.

This document provides validation and intercomparison results for the XCO_2 and XCH_4 datasets as listed in **Table 2-1** for XCO_2 and **Table 2-2** for XCH_4.

All products are generated with independent retrieval algorithms developed to convert GOSAT-2, OCO-2 and/or TROPOMI/S5P radiance spectra into Level 2 (L2) XCO_2 and/or XCH_4 data products.

For more information on these products see also **Table 2-3**.

Table 2-1: *Overview GHG-CCI+ algorithms for XCO_2 retrieval.*

XCO_2 Product Identifier	Algorithm (version)	Institute	Technique	Reference
CO2_OC2_FOCA	FOCAL (v10.1)	IUP, Univ. Bremen, Germany	Optimal Estimation; approximation for an optically thin scattering layer	Reuter et al., 2017a, b
CO2_GO2_SRFP	SRFP or RemoTeC (v2.0.2)	SRON, Netherlands	Phillips-Tikhonov regularization	Butz et al., 2009, 2010

Table 2-2: *Overview GHG-CCI+ algorithms for XCH_4 retrieval.*

XCH_4 Product Identifier	Algorithm (version)	Institute	Technique	Reference
CH4_S5P_WFMD	WFM-DOAS (v1.8)	IUP, Univ. Bremen, Germany	Weighted least squares	Schneising et al., 2023
CH4_GO2_SRPR	SRPR or RemoTeC (v2.0.2)	SRON, Netherlands	Proxy (PR) retrieval method	Frankenberg et al., 2005
CH4_GO2_SRFP	SRFP or RemoTeC (v2.0.2)	SRON, Netherlands	Phillips-Tikhonov regularization; Full Physics (FP) method	Butz et al., 2009, 2010

Table 2-3: *Overview of (other) GHG-CCI+ product related documents. ATBD = Algorithm Theoretical Basis Document, PUG = Product User Guide, E3UB = End-to-End ECV Uncertainty Budget document.*

Product ID	Document	Link
CO2_OC2_FOCA	ATBD	Available from: https://www.iup.uni-bremen.de/carbon_ghg/cg_data.html#GHG-CCI and https://climate.esa.int/de/projekte/ghgs/key-documents/
-"-	PUG	- " -
-"-	E3UB	- " -
CH4_S5P_WFMD	ATBD	- " -
-"-	PUG	- " -
-"-	E3UB	- " -
CO2_GO2_SRFP	ATBD	- " -
-"-	PUG	- " -
-"-	E3UB	- " -
CH4_GO2_SRFP	ATBD	- " -
-"-	PUG	- " -
-"-	E3UB	- " -
CH4_GO2_SRPR	ATBD	- " -
-"-	PUG	- " -
-"-	E3UB	- " -

3 General description of the processing system

A schematic overview of the GHG-CCI+ processing system is given in **Figure 3-1**.

The processing system consists of the different algorithms (see **Tables 2-1 and 2-2**), running at the different responsible institutes. The different institutes have their own access to the required input data (satellite data, ECMWF meteorological data, model data for priors, spectroscopic databases, etc.), and their own computational facilities in the form of multi-CPU Unix/Linux systems. The Level-2 (L2) output data (XCO_2 and XCH_4) generated by the algorithms at the different institutes are available via the CCI Open Data Portal (*https://climate.esa.int/en/odp/#/dashboard*) and additional information is given at the GHG-CCI+ website (https://climate.esa.int/en/projects/ghgs/). The different parts of the GHG-CCI+ processing systems running at the different institutes are described in more detail in the System Specification Document (SSD) document **/Aben et al., 2019/**.

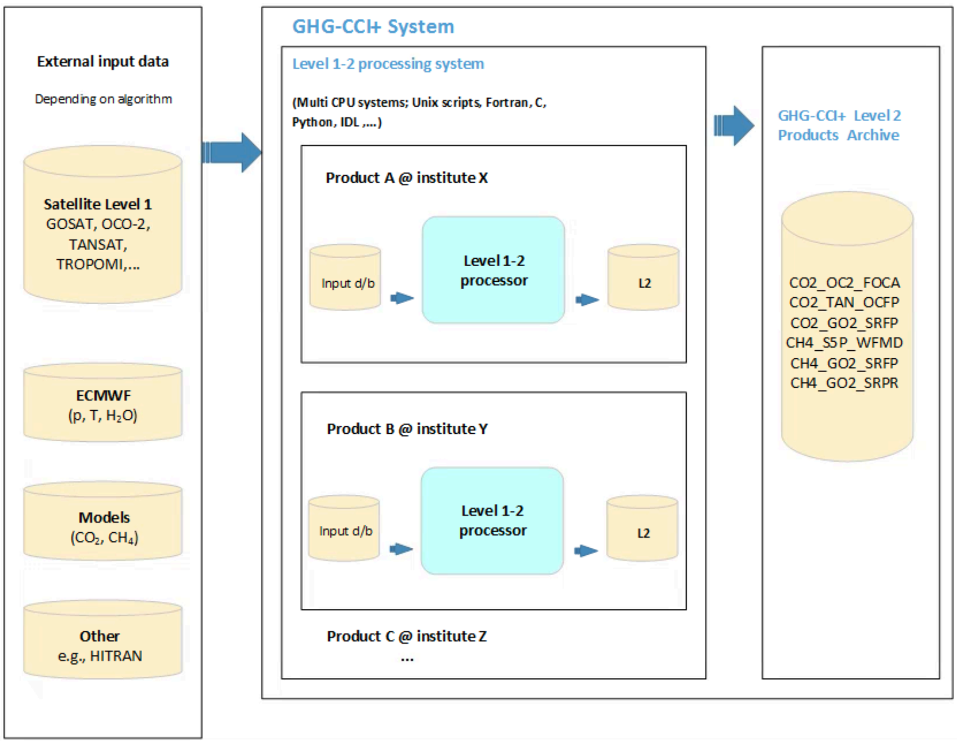

Figure 3-1: *Overview of the GHG-CCI+ processing system. Note that the GHG-CCI+ Level 2 product data archive is the CCI Open Data Portal (https://climate.esa.int/en/odp/#/dashboard). Note that product CO2_TAN_OCFP (XCO_2 from TanSat) has been generated (only) in Phase 1 of the GHG-CCI+ project.*

4 Independent validation by validation team

This chapter deals with the validation of the GHG-CCI+ retrieval products using ground-based FTIR remote sensing measurements from the Total Carbon Column Observing Network (TCCON) **/Wunch et al.2011/** and, in the case of XCH_4, the Network for the Detection of Atmospheric Composition Change (NDACC) **/De Mazière et al. 2018/**. Take note that NDACC's data protocol is less harmonized as compared to TCCON's. For instance, it allows the use of 2 retrieval algorithms (SFIT4 and PROFFIT9). However, analysis between the two algorithms showed no bias between them **/Hase et al. 2004/**). It also features more stations in what we may call 'challenging environments', that being high altitude sites (Zugspitze, Jungfraujoch, Izaña, Mauna Loa, Reunion (Maido) and Altzomoni), near major urban sites (Toronto, Altzomoni (Mexico City)) and high latitude sites (Eureka, Ny Alesund, Thule, Arrival Heights). It also relies on the surface pressure to derive the dry air mole fraction (see equation 1 in **/Deutscher et al., 2010/**) as it cannot rely on a retrieved CH_4/O_2 ratio to reduce errors in the retrieval process.

TCCON also benefits from an extensive calibration campaign, which results in a calibration factor to reduce its systematic bias **/Wunch et al., 2011/**. TCCON's network accuracy can be determined by the uncertainty on this calibration factor, and amounts to 0.1% for XCO_2, and 0.2% for XCH_4. **/Wunch et al. 2010/.** The random uncertainty of TCCON is about 0.5% for XCH_4 and 0.25% for XCO_2. **/Wunch et al. 2015/.**

For NDACC, the systematic and random uncertainties of CH_4 total columns are estimated to be 3.0% and 1.5%, respectively. The first is mainly coming from the uncertainty of the spectroscopy.

Comparisons between TCCON and NDACC XCH_4 measurements **/Ostler et al., 2014**/ do demonstrated that there is no overall bias between both TCCON and NDACC XCH_4 retrieval methods. Therefore, we feel confident to include NDACC in our analysis, as it may provide some insight into regions that are not sampled by TCCON (Latin America being a prime example). An added benefit of the NDACC data is that it does not use a profile scaling retrieval method, but uses optimal estimation instead, retrieving profiles with ~2.5 degrees of freedom. This should, in principle, reduce the smoothing error, when we apply the satellite averaging kernels as it does not rely on the assumption that the real profile conforms to a pre-determined shape. Nor is the data used in post-retrieval bias-correction methods, that are employed by various satellite algorithms, to reduce the effect of residual systematic error components. While this approach is certainly valid, it also results in retrieval data that is optimized in some sense to the TCCON retrieval sites.

That said, the summary numbers in the tables, are still based on the TCCON analysis only. Mainly due to the much higher prevalence of high altitude/ high latitude sites and higher interstation biases in the NDACC network.

In our previous analysis we made use of all public GGG2014 data. Since then TCCON has transitioned to GGG2020 (a list of the main 2014-2020 feature differences, including a new way to calculate the *a priori* profiles **/Laughner et al., 2023/**, can be found here: https://tccon-wiki.caltech.edu/Main/DataDescriptionGGG2020). Unfortunately at the time of this analysis some stations still need to reanalyze their complete datasets. Therefore, no comparisons could be made with Bialystok, Zugspitze, Anmeyondo, Ascension, Darwin and Wollongong data. Note that data from the latter 2 stations have very recently become available, alas not in time for this report. New stations are Harwell (UK) and Xianghe (China, near Beijing). This also implies that the analysis of the Southern hemisphere particularly is currently restricted to 2 stations only (Reunion and Lauder) of which the latter only features a long-running uninterrupted time series. While maybe not 100% complete we opted to use all public TCCON GGG2020 data as available on the TCCON Data Archive (https://tccondata.org/) as well as all publicly available data on the NDACC archive (https://www-air.larc.nasa.gov/missions/ndacc/data.html) on the 1st of July 2023. We also included data from Garmisch, Sodankylä and Porto Velho, which are currently not officially part of NDACC but perform observations and data analysis fully compatible with NDACC guidelines.

Table 4.1: TCCON station coordinates and references.

STATION	Lat	Lon	Alt (km)	Ref
EUREKA	80.05 N	86.42 W	0.61	**/Strong et al., 2022/**
NY ALESUND	78.92 N	11.92 E	0.02	**/Buschmann et al., 2022/**
SODANKYLA	67.37N	26.62E	0.19	**/Kivi et al., 2022/**
EASTTROUTLAKE	54.35 N	104.99 W	0.50	**/Wunch et al., 2022/**
BREMEN	53.10 N	8.85 E	0.03	**/Notholt et al., 2022/**
HARWELL	51.57 N	1.32 W	0.14	**/Wiedmann et al., 2023/**
KARLSRUHE	49.10 N	8.44 E	0.12	**/Hase et al., 2023/**
PARIS	48.85 N	2.36 E	0.06	**/Té et al., 2022/**
ORLEANS	47.97 N	2.11 E	0.13	**/Warneke et al., 2022/**
GARMISCH	47.48 N	11.06 E	0.74	**/Sussmann et al., 2023/**
PARKFALLS	45.95 N	90.27 W	0.44	**/Wennberg et al., 2022/**
RIKUBETSU	43.46 N	143.77 E	0.38	**/Morino et al., 2022a/**
XIANGHE	39.80 N	116.69 E	0.04	**/Zhou et al., 2022/**
LAMONT	36.60 N	97.49 W	0.32	**/Wennberg et al., 2022b/**
TSUKUBA	36.05 N	140.12 E	0.03	**/Morino et al., 2022b/**
NICOSIA	35.14 N	33.38 E	0.18	**/Petri et al., 2022/**
EDWARDS	34.96 N	117.88 W	0.70	**/Iraci et al., 2022/**
JPL	34.20 N	118.18 W	0.39	**/Wennberg et al. 2022b/**
PASADENA	34.14 N	118.13 W	0.23	**/Wennberg et al. 2022c/**
SAGA	33.24 N	130.29 E	0.01	**/Shiomi et al. 2022/**
HEFEI	31.91 N	117.17 E	0.03	**/Liu et al. 2022/**
IZAÑA	28.30 N	16.50 W	2.37	**/Garcia et al., 2022/**
BURGOS	18.53 N	120.65 E	0.04	**/Morino et al., 2022c/**
REUNION	20.90 S	55.49 E	0.09	**/De Mazière et al., 2022/**
LAUDER	45.04 S	169.68 E	0.37	**/Sherlock et al., 2022/**

Table 4-2: NDACC station coordinates and institutes/references.

STATION	Lat	Lon	Alt (km)	Institutes
EUREKA	80.05 N	86.42 W	0.61	**U. of Toronto, /Batchelor et al., 2009/,/Strong 2021/**
NY ALESUND	78.92 N	11.93 E	0.01	**U. of Bremen, /Notholt et al., 2021a/**
THULE	78.90 N	68.77 W	0.02	**NCAR /Hannigan et al., 2021/**
KIRUNA	67.84 N	20.40 E	0.2	**KIT-ASF, IRF Kiruna /Blumenstock et al., 2020/**
SODANKYLA	67.37 N	26.65 E	0.18	**FMI, BIRA-IASB**
HARESTUA	60.20 N	10.80 E	0.60	**Chalmers, /Mellqvist et al., 2021/**
St. PETERSBURG	59.88 N	29.83 E	0.02	**SPbU, /Marakova et al., 2017/**
BREMEN	53.11 N	8.85 E	0.03	**U. of Bremen, /Notholt et al., 2021b/**
GARMISCH	47.48 N	11.06 E	0.74	**KIT-IFU**
ZUGSPITZE	47.42 N	10.98 E	2.96	**KIT-IFU, /Sussmann et al., 2018/**
JUNGFRAUJOCH	46.55 N	7.98 E	3.58	**U. of Liège, /Mahieu, 2017/**
TORONTO	43.60 N	79.36 W	0.17	**U. of Toronto, /Wiacek et al., 2007/**
RIKUBETSU	43,46 N	143.77 E	0.38	**Nagoya U, NIES**
BOULDER	40.04 N	105.24 W	1.61	**NCAR, /Ortega et al. 2019/**
IZAÑA	28.30 N	16.50 E	2.37	**AEMET, KIT-ASF**
MAUNA LOA	19.54 N	155.57 W	3.40	**NCAR**
ALTZOMONI	19.12 N	98.66 W	3.98	**UNAM**
PARAMARIBO	5.81 S	55.21 W	0.03	**U. of Bremen**
PORTO VELHO	8.77 S	296.13 W	0.09	**BIRA-IASB**
REUNION (MAÏDO)	21.08 S	55.38 E	2.16	**BIRA-IASB**
WOLLONGONG	34.41 S	150.88 E	0.03	**U. of Wollongong**
LAUDER	45.04 S	169.68 E	0.37	**NIWA**
ARRIVAL HEIGHTS	77.82 S	166.65	0.20	**NIWA**

As before, the key concept behind this validation is to apply an as uniform as possible validation strategy for all the involved algorithms. We uphold the same methodology as in the previous PVIR (see **/PVIR GHG-CCI+ v3.0, 2022**/ for details) analysis.

Choosing collocation criteria is a balance between minimizing the potential collocation error and still retaining a large enough sample so as to be able to derive adequate statistics. Also of note is that some of the current available algorithms have processed data for a limited time span only, which hampers certain aspects of the analysis.

Concerning the Figures of Merit (FoM), we did not employ any pre-analysis averaging and looked at individual satellite-TCCON pairs. This was done mainly to have statistical parameters that relate to the quality of the original data. Users of the data however should keep in mind that some algorithms opt to have a high-density dataset with a larger random error component versus a much stricter quality-flagged low density dataset with a smaller random error component. After averaging (in space or time) the first might outperform the latter.

4.1 Validation method

Each individual satellite measurement is paired, if the criteria are met, with an individual FTS measurement (from TCCON or NDACC). This particular, FTS measurements needs to be taken within 2 hours and within 500 km of the satellite measurement. Only for CH4_S5P_WFMD is the collocation criteria tightened to within 100 km and within 1 hour (TCCON) or 2 hours (NDACC) due to its high data density. If more than one FTS measurement fits the above criteria, the FTS measurement that has been measured closest (in time) to the satellite coordinates will be the one paired with said satellite measurement. This creates a collocated dataset with unique individual satellite-FTS pairs.

Prior to the FoM analysis we try to limit the impact of differences in *a priori* and vertical sensitivity between FTS and the satellite product (**/Rodgers, 2000/**). To limit the impact of the former we adjust the satellite dry air mole fraction using the FTS *a priori* as in

$$\hat{c}_{S,adj} = \hat{c}_S + \sum_l pw_l\,(1 - A_l)(x^l_{F,a} - x^l_{S,a})$$

where, $\hat{c}_S$ represents the originally retrieved satellite column-averaged dry air mole fraction, l is the index of the vertical layer, A_l the corresponding column averaging kernel of the satellite algorithm, $\boldsymbol{x}_{S,a}$ and $\boldsymbol{x}_{F,a}$ are the satellite and FTS *a priori* dry air mole fraction profiles respectively. pw_l is the pressure weight associated with level or layer l.

Likewise, to address the latter we apply the satellite averaging kernel onto the FTS data.

Unlike NDACC which directly yields retrieved profiles ($x_{F,r}$), TCCON provides total column dry air mole fractions only. So here we apply this smoothing onto the scaled TCCON *a priori,* where the scaling factor takes into account the actual retrieval (which is based on a scaling an *a priori* profile) as well as the post retrieval correction to bring TCCON in line with in situ measurements. Thus, the scaled TCCON profile ($x_{F,r}$) corresponds with

$$x_{F,r} = x_{F,a} \times \hat{c}_{F,r}/\hat{c}_{F,a}$$

where $x_{F,a}$ is the TCCON *a priori* profile. $\hat{c}_{F,r}\ and\ \hat{c}_{F,a}$ are the TCCON retrieved and *a priori* column-averaged dry air mole fractions.

The adjusted FTS dry air mole fraction then corresponds with

$$\hat{c}_{F,adj} = \sum_l pw_l\,(x^l_{F,a} + (x^l_{F,r} - x^l_{F,a})A_l)$$

where, pw_l again represents the pressure weight associated with the level or vertical layer with index l and A_l the corresponding column averaging kernel of the satellite algorithm. $\boldsymbol{x}_{F,a}$ and $\boldsymbol{x}_{F,r}$ are the FTS *a priori* and scaled dry air mole fraction profiles respectively.

Prior to these adjustments, the FTS *a priori* needs to be interpolated onto the satellite product vertical grid. This is done using a regridding method that preserves mass (**/Langerock et al., 2015/**) and in case the satellite pixel surface altitude is below that of the FTS site, the regridded FTS profile is extrapolated towards the surface assuming a constant dry air molefraction.

This approach should minimize the differences between satellite and ground-based retrievals, regardless of the algorithm and target species involved.

The bias is defined as the median difference between the individual satellite and FTS pairs

$$\tilde{X}_{bias} = median(\hat{c}_{S,adj} - \hat{c}_{T,adj})$$

This is done for each station after which the overall Bias FoM is defined as the median of all calculated station biases. One could also group all individual measurements, regardless of station, into one sample onto which we calculate the bias, but this would increase the impact of stations where the data density is high. Since having a high data density, does not necessarily correspond with the highest quality data (or best collocation environment), we deem our median of station biases approach more accurate.

The scatter at each station corresponds with the median absolute deviation (mad) scaled by 1.4826 which is a statistically more robust proxy for the standard deviation (std) of said difference as in:

$$scatter = 1.4826 \times median(|X_{bias} - \tilde{X}_{bias}|)$$

where

$$X_{bias} = \hat{c}_{S,adj} - \hat{c}_{F,adj}$$

Again for the overall assessment of the scatter we take the median of all individual station scatter values.

Both parameters, bias and scatter, are presented with their 95% confidence interval in the validation summary tables (see **Tables 4-4, 4-6, 4-8, 4-11, 4-14, 4-17**). These confidence bands have been determined using a bootstrap methodology (**/Lunneborg, 2020/**), where the 95% confidence limits around the median $\tilde{X}$ corresponds with

[$\tilde{X}$ - *(97.5%tile -* $\tilde{X}$*),* $\tilde{X}$ + *(*$\tilde{X}$*- 0.25%tile)*]

Using medians and scaled median absolute deviations instead of means and standard deviations makes for a more robust assessment as it is far less impacted by outliers. These outliers could be haphazard single outliers (in the satellite data as well as for the FTS measurements, due to cloud interference etc.) when calculation the station bias and scatter values, but also caused by far from ideal collocation circumstances, limited data, etc. at various FTS sites when calculating the overall FoMs.

Other FoM are the Relative Accuracy (RA) and Seasonal Relative Accuracy (SRA), which give an indication of the spatial and spatio-temporal accuracy of the algorithm. We define RA as the scaled median absolute deviation on the overall median biases (derived from individual data) obtained at each station. The "Seasonal Relative Accuracy" (SRA), differs from the relative accuracy in that it uses the seasonal bias medians at each station, instead of the overall biases obtained at each station, it is thus the scaled median absolute deviation over all station seasonal median bias results. The seasonal bias results are constructed, for each FTS station, from all data pairs which fall within the months of January till March (JFM), April till June (AMJ), July till September (JAS) or October till December (OND), regardless of the year the measurements are taken. Some stations feature only limited data during certain seasons, which sometimes results in erratic (seasonal) bias results. To avoid the inclusion of these results into the RA and SRA calculation, we do not include those results which are derived from less than 4 individual SAT-FTS pairs. This may seem as a low threshold, but combined with the fact that we draw upon median values, we deem this sufficient.

To verify the stability of the algorithm over time we fit a linear trend and seasonal cycle through the bias timeseries:

$$X = i + s.t + A.\sin(2\pi.(t + ph))$$

Here, *X* represents the satellite minus FTS difference, *i* the intercept, *s* the slope which corresponds with the linear drift, *A* the amplitude of the seasonal cycle and *ph* the phase shift. While the slope yields information on any potential drift, the amplitude in the above fit results gives us information on the potential mismatch between Satellite and FTS seasonal cycles. Ideally there should be no difference between these cycles which would yield a slope and amplitude=0 in the bias timeseries. This is done for all stations provided that the overlapping station satellite timeseries covers a timespan of at least 2 years. The overall long-term stability then corresponds with the median slope over all these stations as we expect the linear drift to be consistent for the entire dataset.

Figures 4-6, 4-10, 4-14, 4-22, 4-23, 4-30, 4-31, 4-38 and 4-39 show the monthly medians of all data within certain latitude bands. To determine the seasonal cycle, as with the determination of the long-term stability, a fit as outlined above is performed on the (now monthly median instead of individual) data. For the seasonal cycle representation, we then subtract the linear part from the medians and calculate the mean of all medians for each given month.

Another Figure of Merit is the so-called Uncertainty Ratio, which is defined as the ratio between the algorithm's reported uncertainty and the above mentioned scatter. If the reported uncertainty is correctly assessed, the uncertainty ratio should approach unity. However, this baseline number ignores any aspect of temporal, spatial or FTS variability embedded in the scatter.

We therefore also calculate an improved Uncertainty Ratio, which is the ratio between the reported uncertainty and the uncertainty on the Satellite (σ_{SAT}) as determined from the scatter using the method outlined below. Both are reported in the summary tables of each algorithm (see **Tables 4-4, 4-6, 4-8, 4-11, 4-14, 4-17**), where the improved uncertainty ratio is marked by an *.

Taking into account the variability of the FTS reference data and the collocation error, when assuming independence, the scatter can be written down as:

$$\text{scatter}=\sqrt{(\sigma_{SAT}^2 + \sigma_{FTS}^2 + \sigma_{Collocation}^2)}$$

where σ_{SAT} is the standard deviation due to variability of the satellite product, σ_{FTS} due to variability within the FTS measurements and $\sigma_{Collocation}$ due to variability in time and space. σ_{SAT} as derived from our comparison between the satellite and FTS measurements is thus:

$$\sigma_{SAT} = \sqrt{(scatter^2 - \sigma_{FTS}^2 - \sigma_{Collocation}^2)}$$

The standard deviation on the ground-based FTS measurements can be readily calculated from the average variability of the FTIR measurements within the collocation timeframe (4 hours).

The Collocation uncertainty is harder to define and consists of a spatial and temporal component. The latter can be ignored since it is already embedded in our calculation of the FTS uncertainty (which is based on the actual variability of the FTS measurements in time and thus also contains the temporal natural variability).

Unfortunately, we have no solid information on the spatial collocation uncertainty. One method to at least visualize potential collocation biases is to take the satellite data and calculate the bias of all measurements within a satellite overpass with respect to the satellite data point that precisely targets the FTIR site location. After which the obtained biases can be averaged within certain predefined grid cells. This yields plots as in **Figure 4-1**, wherein WFMD XCH4 was used to visualize spatial biases within WFMD XCH4 around the Edwards (Dryden) and Pasadena (Caltech) sites. While located relatively close to one another, they nevertheless operate from very different environments. The Pasadena site is located in the Los Angeles basin, while Edwards is located in the Mojave Desert. As a result, we expect most of the measurements that are taken outside of the Los Angeles basin to have a negative bias towards the data taken at Pasadena, with the exception of data taken over the California Central Valley which features strong emissions from agriculture and petroleum extraction. Inversely, the Edwards site is surrounded by many areas that have a positive bias. While this certainly gives us insight into collocation aspects, it depends on relatively wide-swath high density satellite products and is thus currently restricted to S5P WFMD XCH4 only. Furthermore, the obtained gridded biases should be averaged to such an extent that no temporal/random noise error component is in play. This can potentially be achieved by lowering the spatial resolution, at least for those stations where the data density is high enough. However, at some point this will certainly remove real spatial collocation features. While we certainly want to explore this further in more detail (either to have a better idea of the collocation bias or as a method to better select collocation areas), we currently maintain the method as described in the previous PVIR analysis.

Therefore, our current best, universally applicable, but flawed, estimate of this factor can be derived from fitting a linear equation through the sat-TCCON residuals as a function of distance between the FTS site and the satellite pixel center points (we do this for all satellite FTS pairs drawn from all stations, see **Figure 4-2**). From the obtained slope a, we can then estimate the uncertainty associated with the collocation by simply taking the standard deviation of points along the slope (a×dist(i)), where dist(i) is the distance between the FTS station and satellite centre point for a given sat-FTS pair with index i. Note that we here use the normal standard deviation as, by default, there are no outliers in the points that constitute the slope.

As already mentioned, this is a mere estimate and corresponds more with a lower bound threshold, as station to station bias results can differ profoundly. Most noticeable is to look at bias value differences between sites where the collocation areas overlap to a large degree, such as Pasadena and Edwards (see **Tables 4-3, 4-5, 4-7, 4-9, 4-12, 4-15**).

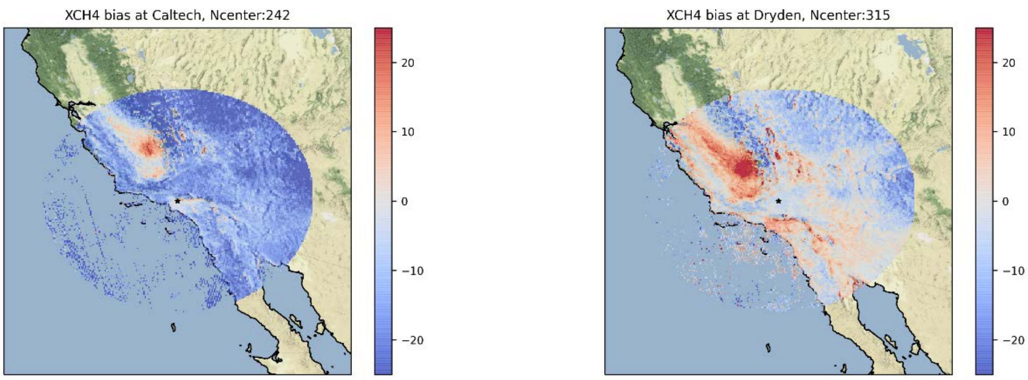

Figure 4-1: Average bias seen by WFMD XCH4 within the same overpass, with respect to WFMD XCH4 data taken over the TCCON site location at Pasadena (left) and Edwards (right).

As can be seen in **Figure 4-2**, which shows all the 'bias as a function of distance' plots, the effect is fairly limited. For XCO_2, values range between 0.01 and 0.06 ppm/100 km, for XCH_4 we see values between -0.37 and 0.52 ppb/100km for TCCON and between -3.23 and -1.31ppb/100km for NDACC.

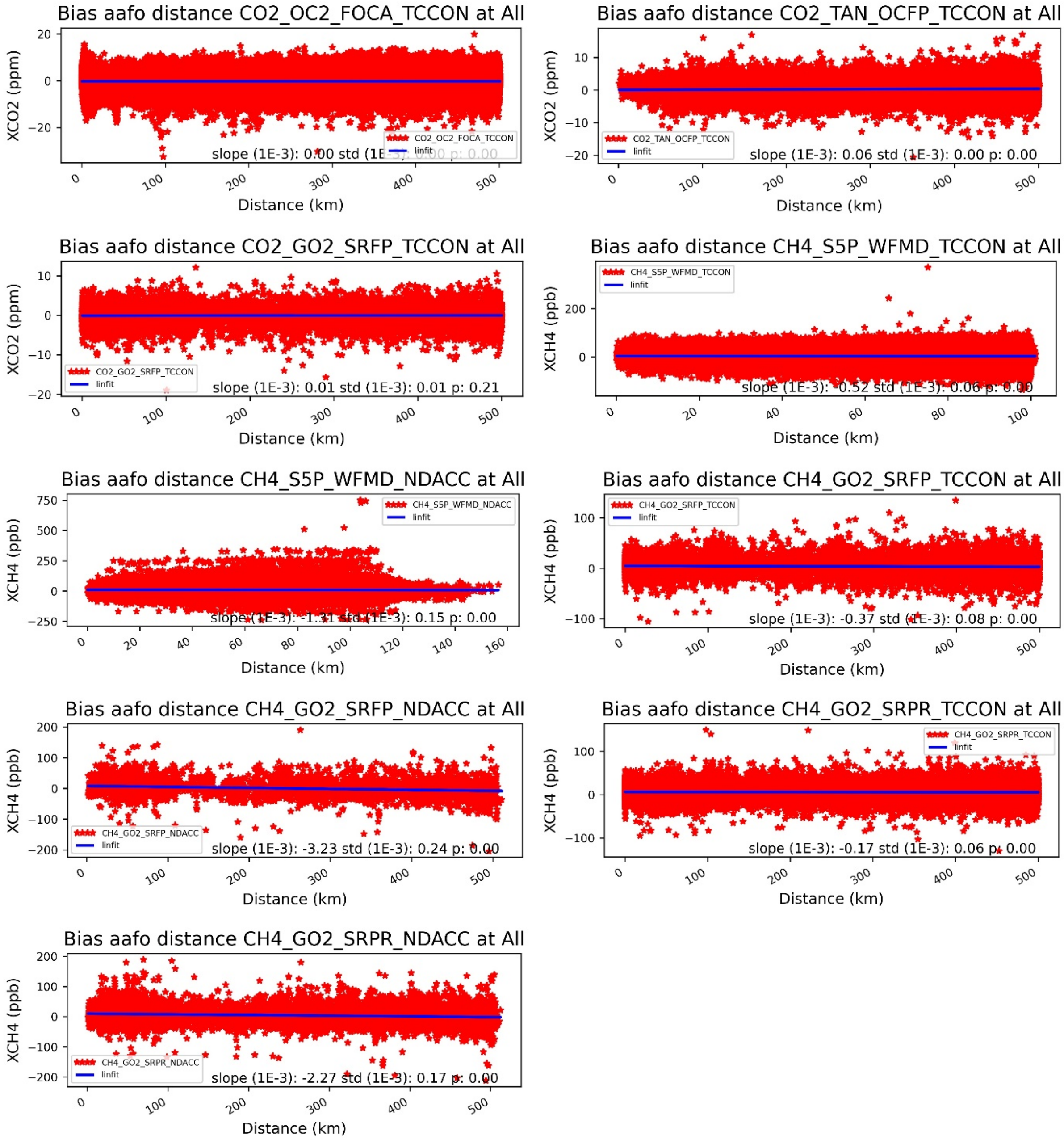

Figure 4-2: Satellite-TCCON or NDACC bias as a function of (aafo) distance between the satellite and TCCON/NDACC sampling point, for all algorithms in this study. Slope in ppm/100 km for XCO_2 and ppb/100 km for XCH_4.

4.2 Validation results

This section lists all validation results for the algorithms presently available in this study. First we show, for each algorithm, a general overview of the collocated data.

This comprises of a Taylor plot and a mosaic overview of the obtained timeseries.

The Taylor plot shows the correlation between the various FTS sites and the retrieval algorithm (straight lines), the standard deviation of the FTS data at each site, relative to the standard deviation of the satellite (normalized to 1) (light grey arches) and the root mean square error of the sat-fts difference (dark grey arches).

After this we discuss the different statistical parameters as obtained on a per station level.

Then the temporal variability is discussed, showing all the station timeseries as well as a more broad 'latitudinal band' based discussion on the long-term trend (if any) and seasonality.

After this we discuss the overall FoM, obtained from the analysis of individual data, and their statistical reliability.

Thus, in each section, we show:

1) A Taylor and Mosaic overview plot.
2) A table listing all Bias, Scatter, correlation (R), number of collocated data pairs (N) for all stations, and, if the timeseries allows, the slopes and amplitudes of the trend fits.
3) Example timeseries of individual data.
4) Monthly averaged timeseries and seasonal plots for broader latitude bands.
5) A Summary table of the Figures of Merit drawn from the values, drawn from individual measurements, at all stations.

4.2.1 Validation results for product CO2_OC2_FOCA

Below we show the validation results of the XCO_2 concentrations as derived by the CO2_OC2_FOCA v10.1 algorithm using OCO-2 spectra. Data was available from September 2014 until the end of February 2022. The FOCAL algorithm provides *a priori* and column averaging kernel data on a 5-layer profile. Compared to the last PVIR iteration little has changed in terms of its comparisons with TCCON. There are slight changes in the FoM but never abruptly and always within the previously established confidence bounds.

4.2.1.1 Detailed results

The Taylor diagram below in **Figure 4-3** yields a concise overview of the capabilities of the CO2_OC2_FOCA algorithm. Most TCCON sites cluster between the 0.9 and 0.95 correlation line. Also, the normalized standard deviation of most sites is close to 1, indicating that the variability of both datasets (due to natural variability and random error) is comparable. The normalized standard deviation of the bias (std(sat-fts)/std(sat)) sits (for most sites) at and even below (an improvement with respect to the previous analysis) 0.4, which is very encouraging as it indicates that a large fraction of the variability (we can only assume it is the natural variability part) within the TCCON time series is also captured by the satellite.

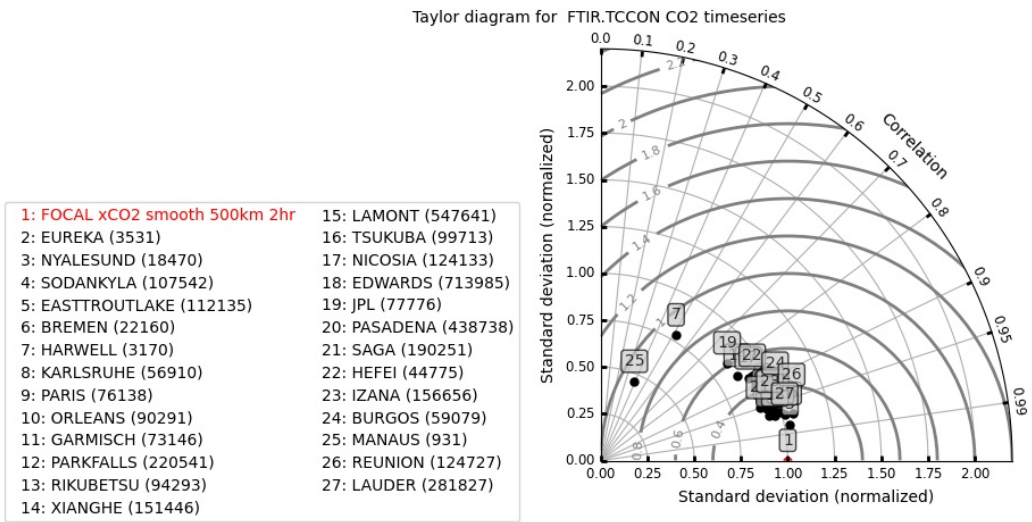

Figure 4-3: Tayor plot of XCO_2 TCCON values relative to CO2_OC2_FOCA . Straight lines correspond with the correlation, light grey lines yield the variability of the TCCON data relative to the satellite variability and the dark grey lines correspond with the variability of the Satellite -TCCON bias relative to the satellite variability.

Notable outliers are Manaus and Harwell with lower correlations (~0.4 and ~0.5) but both datasets only cover a limited fraction of the sampled time period (see **Figure 4-4**)

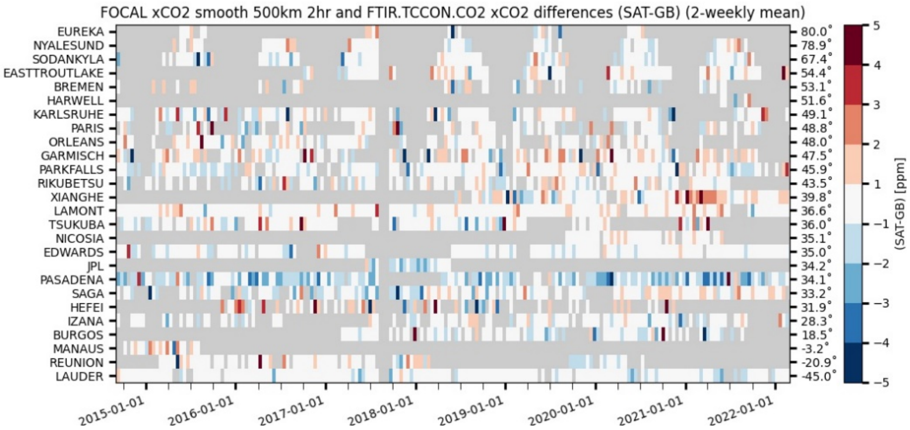

Figure 4-4: Mosaic plot of bi-weekly mean CO2_OC2_FOCA-TCCON XCO_2 biases as a function of time and TCCON station.

It is hard to discern a pattern in the above mosaic plot (**Figure 4-4**), which shows the mean bi-weekly bias between the satellite and TCCON measurement pairs. One can see the seasonal unavailability of data during winter (not visible for the Southern hemisphere as Lauder (New Zealand) still sits at a modest 45°S). Pasadena has consistent negative biases (see also **Table 4-3**) but far less outspoken compared to the previous analysis (v10 vs. TCCON GGG2014). This is not surprising as it is located within the Los Angeles basin and typically measures larger concentrations than what is present outside the basin. The nearby Edwards site which to a large degree has an overlapping collocation area (see **Figure 4-1**) features much different bias values (-0.50 ppm compared to -1.59 ppm at Pasadena). The algorithm produces on average ~97000 data pairs per station. Which roughly corresponds with around 21000 data pairs per station per year. Of the stations, only 6 out of 26 have a correlation coefficient under 0.90 and 3 of those still have a correlation of more than 0.75. The correlation of all data (regardless of station) equals 0.95. The bias ranges between -1.59 ppm (Pasadena) and 1.28 ppm (Manaus) and the scatter between 2.24 ppm (Xianghe) and 1.05 ppm (Lauder). Long term trends on the bias (the so-called drift) range between -0.22 ppm/year (Reunion) and 0.57 ppm/year (Xianghe). Note that we only calculated long-term trends for stations whose collocated dataset spans at least 2 years. The amplitude on the other hand ranges between 0.14ppm at Saga and 2.81 ppm at Eureka. However, at high latitude sites, such as Eureka, the FTIR time series feature large seasonal gaps which affects the quality of the seasonal amplitude fit.

Table 4-3: Number of collocated data pairs (N), Correlation (R), Bias, Scatter, long term trend difference (ltt) and uncertainty thereon (ltt_err), seasonal amplitude difference (A) and uncertainty thereon (A_err) as well as the latitude of the TCCON station. The last row lists the median values over all stations. Product: CO2_OC2_FOCA.

STATION	N	R	Bias	Scat	ltt	ltt_err	A	A_err	Lat
EUREKA	3531	0.93	0.53	1.69	-0.12	0.18	2.81	1.8	80
NYALESUND	18470	0.98	-0.06	1.09	-0.1	0.08	1.21	0.78	78.9
SODANKYLA	107542	0.95	-0.27	1.52	0.06	0.05	0.49	0.32	67.4
EASTTROUTLAKE	112135	0.94	0.29	1.59	0.09	0.07	1.01	0.22	54.4
BREMEN	22160	0.97	-0.03	1.55	-0.11	0.12	0.66	0.34	53.1
HARWELL	3170	0.52	0.05	1.92	-	-	-	-	51.6
KARLSRUHE	56910	0.94	-0.07	1.68	0.02	0.06	0.57	0.17	49.1
PARIS	76138	0.95	-0.05	1.51	-0.01	0.05	0.38	0.22	48.8
ORLEANS	90291	0.94	0.28	1.39	-0.04	0.04	0.36	0.14	48
GARMISCH	73146	0.95	0.45	1.67	0.17	0.09	0.26	0.21	47.5
PARKFALLS	220541	0.97	-0.28	1.5	0.16	0.04	0.47	0.12	45.9
RIKUBETSU	94293	0.97	-0.08	1.45	0.06	0.06	0.48	0.16	43.5
XIANGHE	151446	0.85	0.43	2.24	0.57	0.16	0.64	0.19	39.8
LAMONT	547641	0.96	0.22	1.52	0	0.03	0.41	0.09	36.6
TSUKUBA	99713	0.95	-0.27	1.51	0.14	0.07	0.16	0.17	36
NICOSIA	124133	0.87	0.1	1.48	-	-	-	-	35.1
EDWARDS	713985	0.97	-0.5	1.49	-0.04	0.02	0.27	0.08	35
JPL	77776	0.79	-1.43	1.9	-	-	-	-	34.2
PASADENA	438738	0.94	-1.59	1.75	-0.06	0.04	0.3	0.11	34.1
SAGA	190251	0.95	-0.25	1.55	0.24	0.05	0.14	0.12	33.2
HEFEI	44775	0.87	0.95	1.98	-0.06	0.2	0.68	0.38	31.9
IZANA	156656	0.94	-0.46	1.28	-0.02	0.05	0.28	0.12	28.3
BURGOS	59079	0.91	-0.24	1.09	-0.19	0.08	0.71	0.16	18.5
MANAUS	931	0.39	1.28	1.79	-	-	-	-	-3.2
REUNION	124727	0.95	0.12	1.14	-0.22	0.09	0.34	0.18	-20.9
LAUDER	281827	0.97	-0.02	1.05	-0.08	0.03	0.36	0.07	-45
MEDIAN	**97003**	**0.95**	**-0.04**	**1.52**	**-0.02**	**0.06**	**0.44**	**0.17**	**38.2**

The timeseries below in **Figure 4-5** show individual satellite and ground-based fts measurements. The capture of the seasonal cycle and long term trend is similar to that of TCCON. Some (mostly low concentration) outliers are still present in the data (for instance in the Hefei, Saga or Park Falls plots) but overall most measurements yield good comparison results.

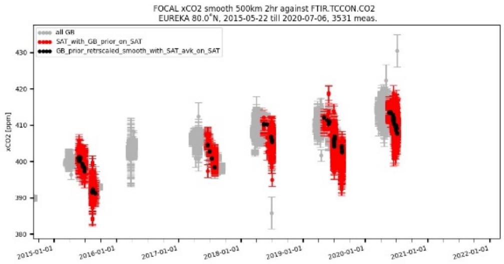
FOCAL xCO2 smooth 500km 2hr against FTIR.TCCON.CO2
EUREKA 80.0˚N, 2015-05-22 till 2020-07-06, 3531 meas.
all GB
SAT_with_GB_prior_on_SAT
GB_prior_retrscaled_smooth_with_SAT_avk_on_SAT
xCO2 [ppm]

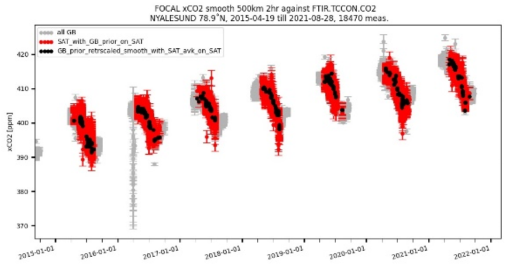
FOCAL xCO2 smooth 500km 2hr against FTIR.TCCON.CO2
NYALESUND 78.9˚N, 2015-04-19 till 2021-08-28, 18470 meas.
all GB
SAT_with_GB_prior_on_SAT
GB_prior_retrscaled_smooth_with_SAT_avk_on_SAT
xCO2 [ppm]

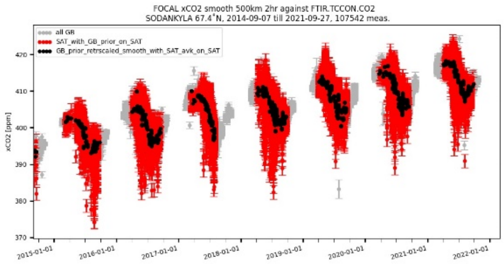
FOCAL xCO2 smooth 500km 2hr against FTIR.TCCON.CO2
SODANKYLA 67.4˚N, 2014-09-07 till 2021-09-27, 107542 meas.
all GB
SAT_with_GB_prior_on_SAT
GB_prior_retrscaled_smooth_with_SAT_avk_on_SAT
xCO2 [ppm]

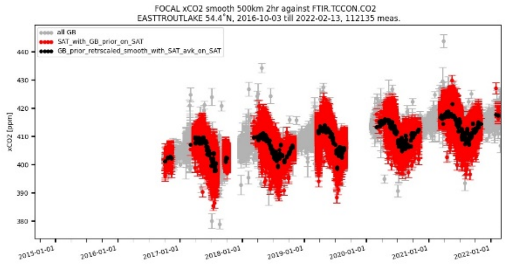
FOCAL xCO2 smooth 500km 2hr against FTIR.TCCON.CO2
EASTTROUTLAKE 54.4˚N, 2016-10-03 till 2022-02-13, 112135 meas.
all GB
SAT_with_GB_prior_on_SAT
GB_prior_retrscaled_smooth_with_SAT_avk_on_SAT
xCO2 [ppm]

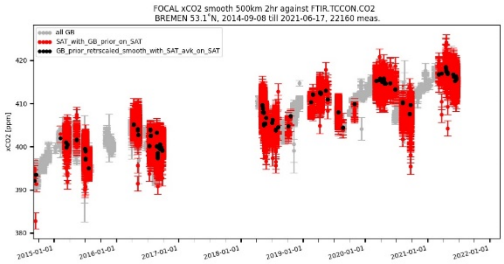
FOCAL xCO2 smooth 500km 2hr against FTIR.TCCON.CO2
BREMEN 53.1˚N, 2014-09-08 till 2021-06-17, 22160 meas.
all GB
SAT_with_GB_prior_on_SAT
GB_prior_retrscaled_smooth_with_SAT_avk_on_SAT
xCO2 [ppm]

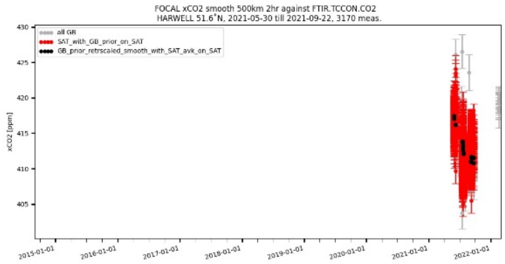
FOCAL xCO2 smooth 500km 2hr against FTIR.TCCON.CO2
HARWELL 51.6˚N, 2021-05-30 till 2021-09-22, 3170 meas.
all GB
SAT_with_GB_prior_on_SAT
GB_prior_retrscaled_smooth_with_SAT_avk_on_SAT
xCO2 [ppm]

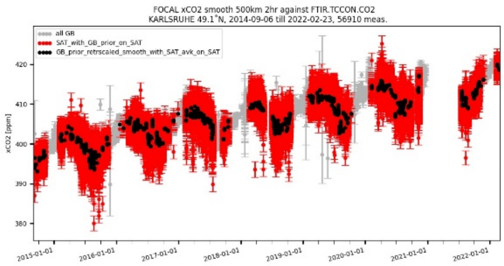
FOCAL xCO2 smooth 500km 2hr against FTIR.TCCON.CO2
KARLSRUHE 49.1˚N, 2014-09-06 till 2022-02-23, 56910 meas.
all GB
SAT_with_GB_prior_on_SAT
GB_prior_retrscaled_smooth_with_SAT_avk_on_SAT
xCO2 [ppm]

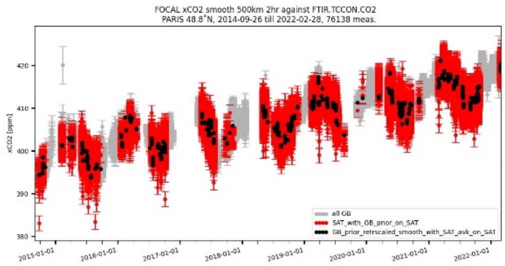
FOCAL xCO2 smooth 500km 2hr against FTIR.TCCON.CO2
PARIS 48.8˚N, 2014-09-26 till 2022-02-28, 76138 meas.
all GB
SAT_with_GB_prior_on_SAT
GB_prior_retrscaled_smooth_with_SAT_avk_on_SAT
xCO2 [ppm]

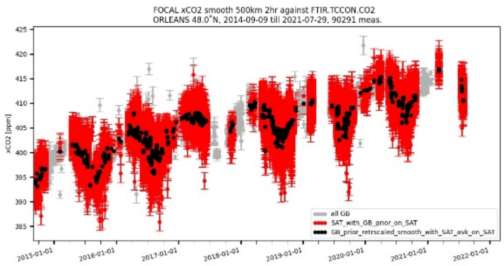
FOCAL xCO2 smooth 500km 2hr against FTIR.TCCON.CO2
ORLEANS 48.0˚N, 2014-09-09 till 2021-07-29, 90291 meas.
all GB
SAT_with_GB_prior_on_SAT
GB_prior_retrscaled_smooth_with_SAT_avk_on_SAT
xCO2 [ppm]

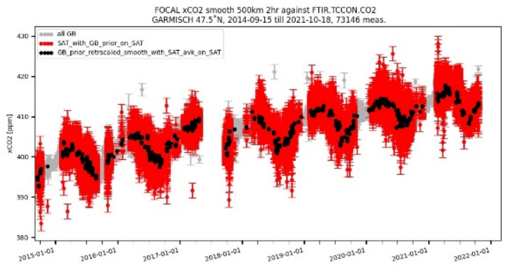
FOCAL xCO2 smooth 500km 2hr against FTIR.TCCON.CO2
GARMISCH 47.5˚N, 2014-09-15 till 2021-10-18, 73146 meas.
all GB
SAT_with_GB_prior_on_SAT
GB_prior_retrscaled_smooth_with_SAT_avk_on_SAT
xCO2 [ppm]

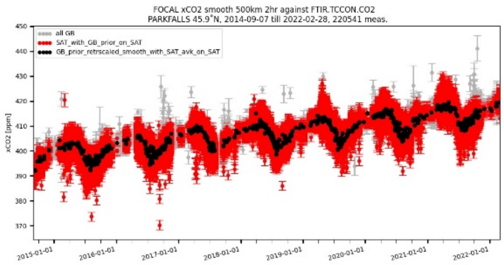

FOCAL xCO2 smooth 500km 2hr against FTIR.TCCON.CO2
PARKFALLS 45.9°N, 2014-09-07 till 2022-02-28, 220541 meas.
all GB
SAT_with_GB_prior_on_SAT
GB_prior_retrscaled_smooth_with_SAT_avk_on_SAT

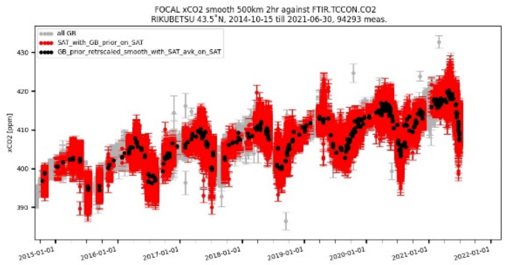

FOCAL xCO2 smooth 500km 2hr against FTIR.TCCON.CO2
RIKUBETSU 43.5°N, 2014-10-15 till 2021-06-30, 94293 meas.
all GB
SAT_with_GB_prior_on_SAT
GB_prior_retrscaled_smooth_with_SAT_avk_on_SAT

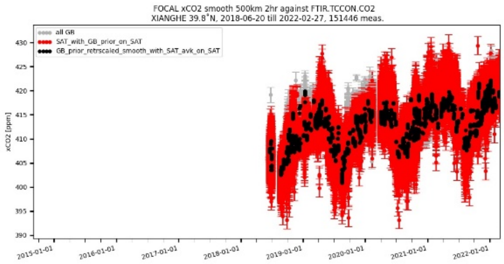

FOCAL xCO2 smooth 500km 2hr against FTIR.TCCON.CO2
XIANGHE 39.8°N, 2018-06-20 till 2022-02-27, 151446 meas.
all GB
SAT_with_GB_prior_on_SAT
GB_prior_retrscaled_smooth_with_SAT_avk_on_SAT

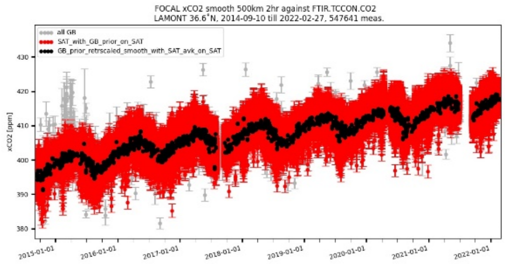

FOCAL xCO2 smooth 500km 2hr against FTIR.TCCON.CO2
LAMONT 36.6°N, 2014-09-10 till 2022-02-27, 547641 meas.
all GB
SAT_with_GB_prior_on_SAT
GB_prior_retrscaled_smooth_with_SAT_avk_on_SAT

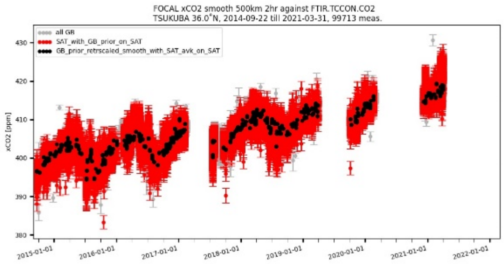

FOCAL xCO2 smooth 500km 2hr against FTIR.TCCON.CO2
TSUKUBA 36.0°N, 2014-09-22 till 2021-03-31, 99713 meas.
all GB
SAT_with_GB_prior_on_SAT
GB_prior_retrscaled_smooth_with_SAT_avk_on_SAT

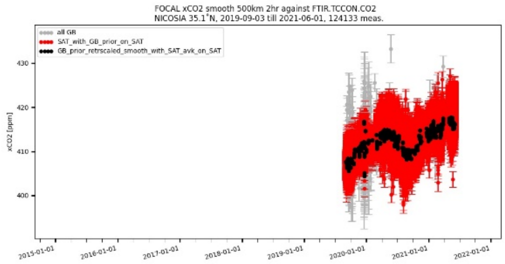

FOCAL xCO2 smooth 500km 2hr against FTIR.TCCON.CO2
NICOSIA 35.1°N, 2019-09-03 till 2021-06-01, 124133 meas.
all GB
SAT_with_GB_prior_on_SAT
GB_prior_retrscaled_smooth_with_SAT_avk_on_SAT

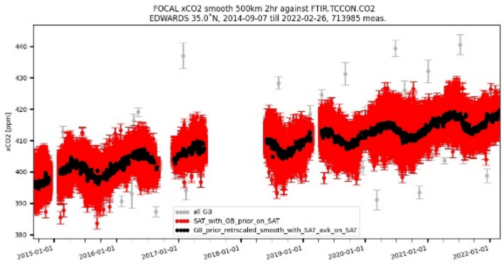

FOCAL xCO2 smooth 500km 2hr against FTIR.TCCON.CO2
EDWARDS 35.0°N, 2014-09-07 till 2022-02-26, 713985 meas.
all GB
SAT_with_GB_prior_on_SAT
GB_prior_retrscaled_smooth_with_SAT_avk_on_SAT

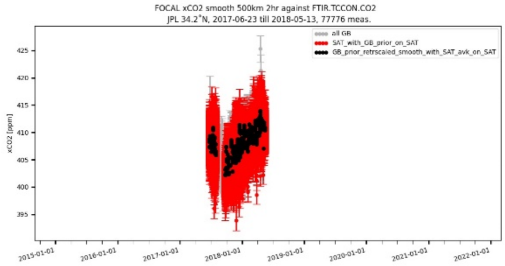

FOCAL xCO2 smooth 500km 2hr against FTIR.TCCON.CO2
JPL 34.2°N, 2017-06-23 till 2018-05-13, 77776 meas.
all GB
SAT_with_GB_prior_on_SAT
GB_prior_retrscaled_smooth_with_SAT_avk_on_SAT

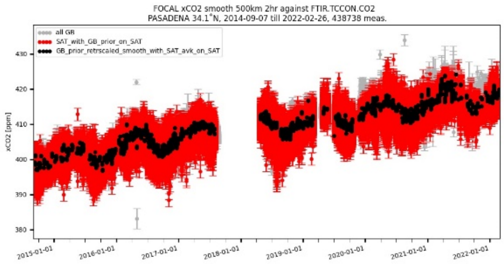

FOCAL xCO2 smooth 500km 2hr against FTIR.TCCON.CO2
PASADENA 34.1°N, 2014-09-07 till 2022-02-26, 438738 meas.
all GB
SAT_with_GB_prior_on_SAT
GB_prior_retrscaled_smooth_with_SAT_avk_on_SAT

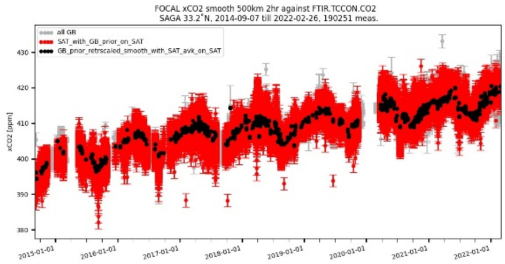

FOCAL xCO2 smooth 500km 2hr against FTIR.TCCON.CO2
SAGA 33.2°N, 2014-09-07 till 2022-02-26, 190251 meas.
all GB
SAT_with_GB_prior_on_SAT
GB_prior_retrscaled_smooth_with_SAT_avk_on_SAT

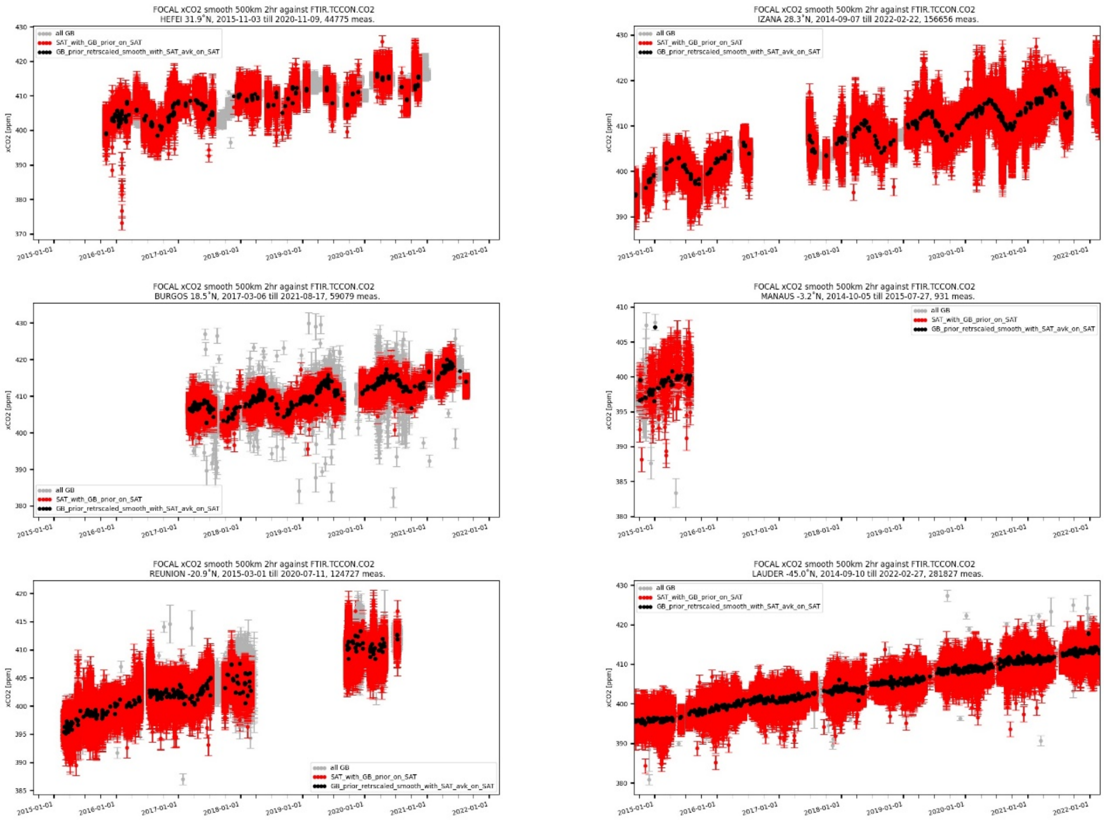

Figure 4-5: XCO_2 timeseries at all TCCON sites (red= CO2_OC2_FOCA data, black is collocated TCCON data and grey are the uncollocated TCCON data).

Figure 4-6 shows monthly median timeseries for TCCON and FOCAL XCO_2 for all data that fall within certain latitude bands, namely all sites north of 40°N latitude (top), all sites between 40°N and the equator (mid) and all sites in the Southern hemisphere (bottom). Again, note that the Southern Hemisphere is only covered by Reunion and Lauder. As can be seen, for all bands, the TCCON and FOCAL data feature long term trends that differ by 0.1 ppm/year only which is well within its uncertainty bounds. On the right hand side of each figure is the detrended monthly median values as a function of month. Again this clearly shows that FOCAL accurately captures the seasonal cycle. The median amplitude derived from seasonal fits through the individual bias data at each station amounts to 0.44 [0.27, 0.54] ppm.

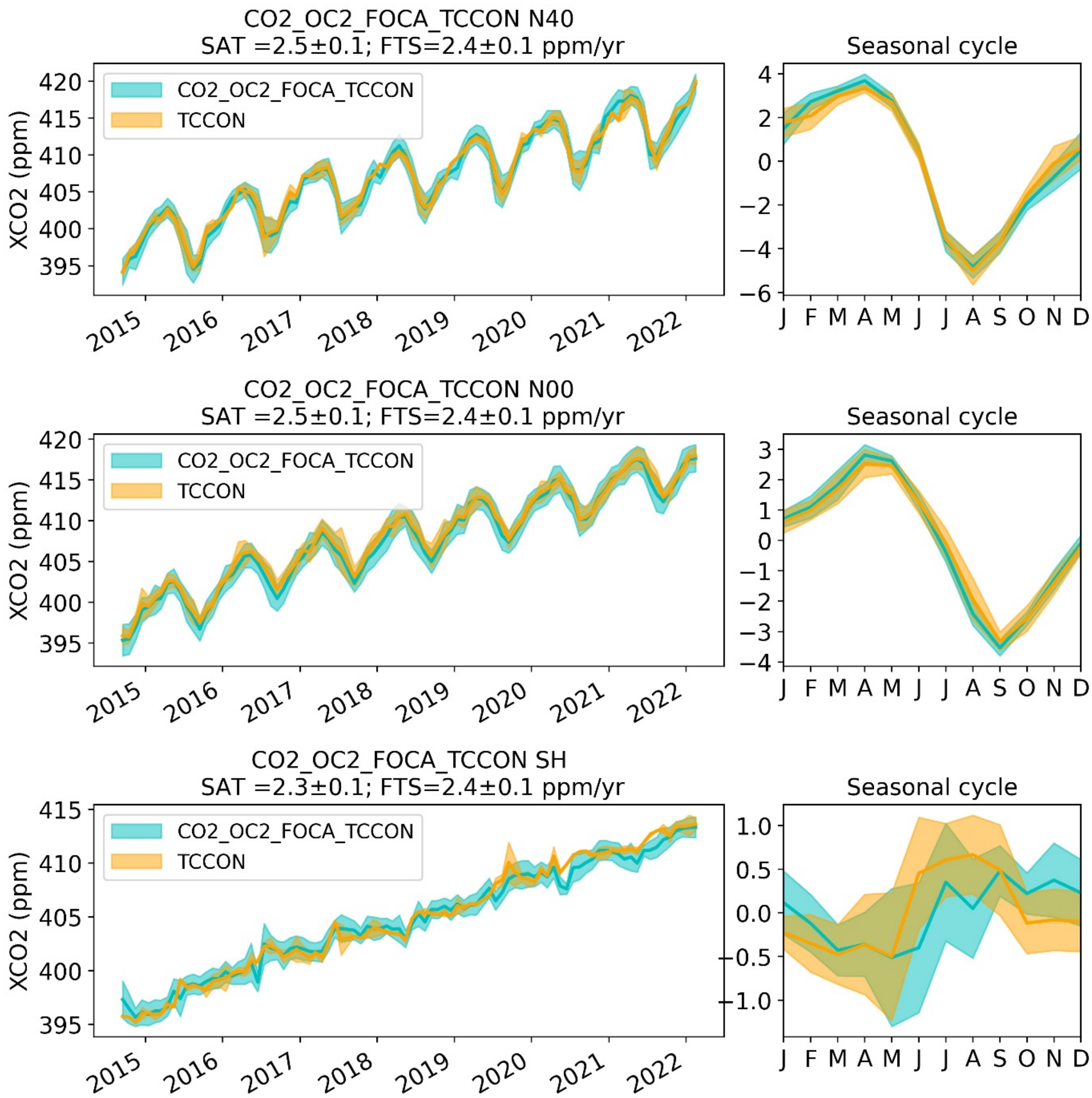

Figure 4-6: Monthly median collocated Sat and TCCON XCO_2 concentrations as a function of time and the detrended monthly medians as a function of season. The shaded areas correspond with the scaled median absolute deviation.

4.2.1.2 Summary

Listed in the table below (**Table 4-4**) are the Figure of Merit parameters as derived from the individual data pairs at the different TCCON stations. Values in square brackets [ ] correspond with the upper and lower 95% confidence bound on the parameter. The uncertainty ratio features 2 numbers as outlined in the validation method.

Also important to note is that the results not only pertain to the actual data quality but also contain a collocation error component. For instance, the difference in the observed bias at the relatively close by Pasadena and Edwards stations is 1.09 ppm. The same holds true for Paris and Orleans (0.33 ppm difference). However, compared to the previous analysis using TCCON GGG2014, these interstation differences have decreased (1.46 and 1.00 ppm respectively)

Overall, the CO2_OC2_FOCA product delivers data that matches very well with that of TCCON. This is apparent in the Taylor diagram time series plots as well as the Figures of Merit.

In our previous assessment **/PVIR GHG-CCI+ v3.0, 2022**/ the determined Relative Accuracy (0.62) was slightly higher than the <0.5 ppm accuracy requirements, but with confidence bands that still overlapped. The Seasonal Relative Accuracy (SRA at 0.83) did not have overlapping confidence bands with the target. Currently the estimated Relative Accuracy sits at 0.35 [0.12, 0.50] ppm, while the Seasonal Relative Accuracy equals 0.54 [0.43, 0.67] ppm. This is a market improvement, but we need to take into account that the number of TCCON sites has been reduced from 30 to 26. Take note that the accuracy requirements of < 0.5 ppm, assumes the abolishment of any collocation influence, nor any station-to-station differences within the TCCON network (its network accuracy is estimated to be within 0.4 ppm), all of which do contribute to the obtained RA and SRA values.

The reported uncertainty is, when compared to the scatter, very accurate (1.10 or 1.17) and even slightly too high. The scatter itself (1.52 ppm) has reached the so-called breakthrough levels (< 3 ppm). From the timeseries plots and Taylor diagram we in fact see that the variability closely matches this of TCCON. The overall bias is essentially zero (-0.04 [-0.24, 0.15]). And finally the dataset shows no significant long term drift.

Table 4-4: presents an overview of the estimated data quality of CO2_OC2_FOCA, as obtained by the VALT team, from comparisons with TCCON ground-based reference observations. Values in square brackets [ ] correspond with the upper and lower 95% confidence bound on the parameter. The uncertainty ratio features 2 numbers as outlined in the validation method.

Product Quality Summary Table for Product: CO2_OC2_FOCA **Level: 2, Version: v10.1, Time period covered: 9.2014 – 2.2022** **Assessment: Validation Team (VALT)**			
Parameter [unit]	**Achieved performance**	**Requirement**	**Comments**
Single measurement precision (1-sigma) in [ppm]	1.52 [1.37, 1.55]	< 8 (T) < 3 (B) < 1 (G)	Computed as the median over all station scaled median absolute differences to TCCON
Uncertainty ratio [-]: Ratio reported uncertainty to standard deviation of satellite-TCCON difference	1.10, 1.17*	-	No requirement but value close to unity expected for a high quality data product with reliable reported uncertainty.
Median bias (global offset) [ppm]	-0.04 [-0.24, 0.15]	-	No requirement but value close to zero expected for a high quality data product.
Accuracy: Relative systematic error [ppm]	Spatial: 0.35 [0.12, 0.50] Spatio-temporal: 0.54 [0.43, 0.67]	< 0.5	Spatial: Computed as standard deviation of the biases at the various TCCON sites. Spatio-temporal: As "Spatial" but also considering seasonal biases.
Stability: Drift [ppm/year]	-0.02 [-0.10, 0.03]	< 0.5	Linear drift

4.2.2 Validation results for product CO2_TAN_OCFP

Here we present the VALT validation results for the CO2_TAN_OCFP product. The analysis pertains to the global v1.2 dataset, which is exactly the same algorithm as used in the previous study. Data is available from March 2017 up to and including May 2018 (again no change). The only change with respect to the previous analysis is the TCCON dataset used (GGG2020 vs. GGG2014). The OCFP algorithm provides *a priori* and column averaging kernel information on a 20 level profile. Given the very limited time period that is covered by this product, these validation results will be rather preliminary in nature, nor can we make useful statements about long term trends.

4.2.2.1 Detailed results

The Taylor diagram below in **Figure 4-7** shows a short overview of the capabilities of the CO2_TAN_OCFP product. Most TCCON sites are clustered between the 0.6 and 0.9 0.75 correlation value, but with negative correlation values for Bremen, likely due its extremely limited collocated dataset (Bremen has not yet processed all its data to GGG2020). Other stations with low correlation values (<0.2) are Izaña, Burgos and Reunion(all featuring very limited temporal overlap). The normalized standard deviation ranges between 0.5 and 1.25 with most sites clustering around the 0.75 mark, indicating that the variability of the TCCON data is (in most cases) smaller. The normalized standard deviation of the bias sits (for most sites) between 1 and 0.6. All this indicates that while OCFP data features a stronger variability (random error and/or seasonal variability) than the TCCON data, the biases still harbors less variability then either of them, an indication of OCFP capturing the natural variability.

There is no real discernible pattern in the mosaic plot (**Figure 4-8**), which shows the mean bi-weekly bias between the satellite and TCCON measurement pairs. August seems to exhibit some more outspoken biases (negative and positive), but since the period covered by the plot is very limited, it is hard to tell if this is indeed a systematic feature or merely coincidence.

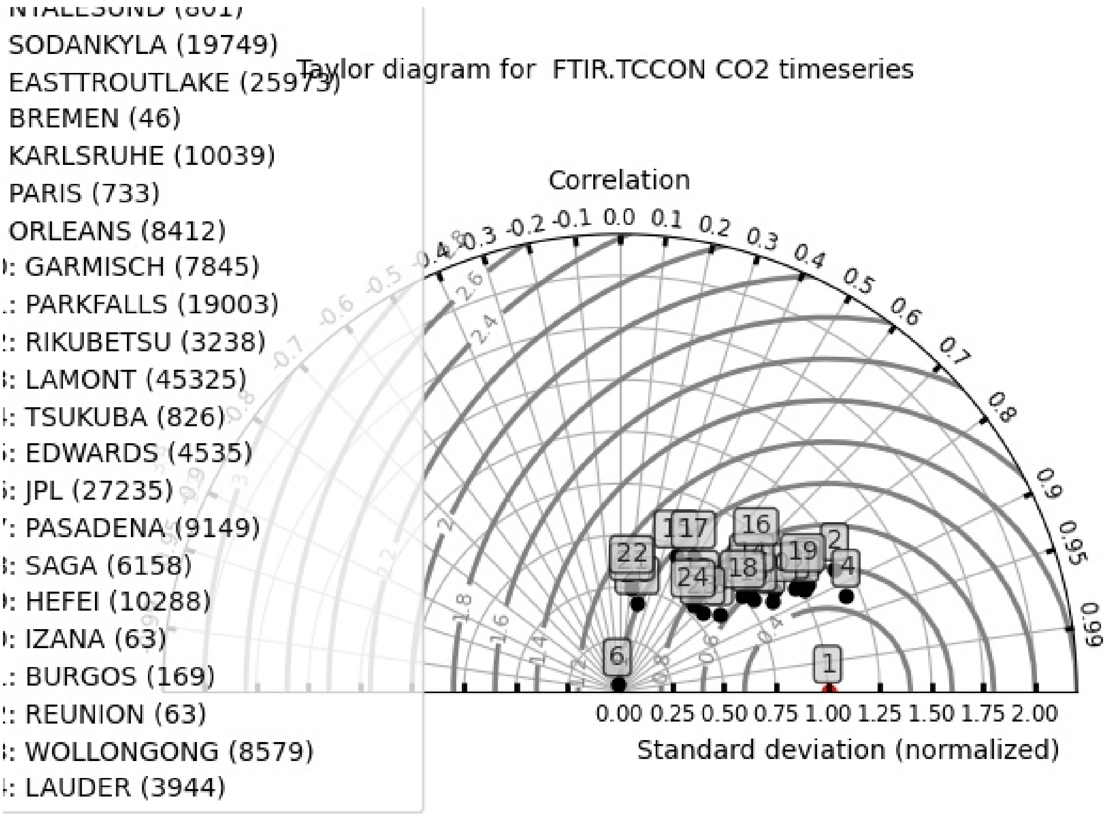

Figure 4-7: Taylor plot of daily averaged XCO_2 TCCON values relative to product CO2_TAN_OCFP. Straight lines correspond with the correlation, light grey lines yield the variability of the TCCON data relative to the satellite variability and the dark grey lines correspond with the variability of the Satellite - TCCON bias relative to the satellite variability.

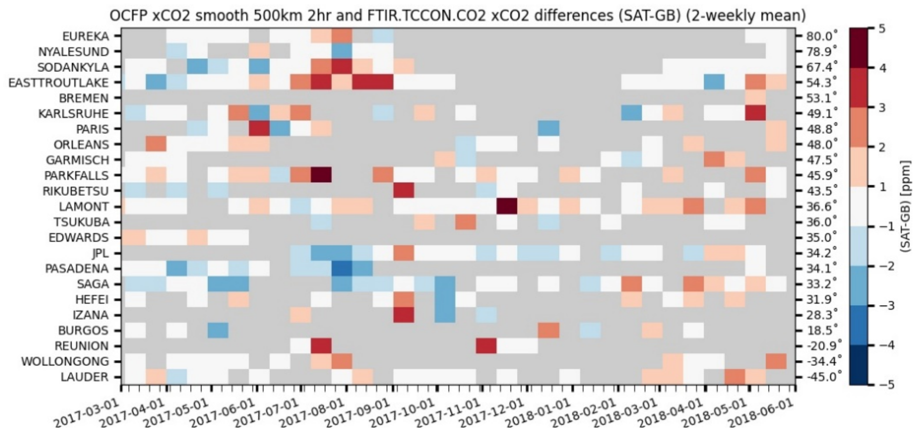

Figure 4-8: Mosaic plot of bi-weekly mean CO2_TAN_OCFP-TCCON XCO_2 biases as a function of time and TCCON station.

Table 4-5 lists all bias and scatter results derived from individual data pairs at all TCCON stations. The algorithm produces on average ~6150 data pairs per station which corresponds with ~4900 pairs per station per year. The observed median bias ranges between -0.95 (Rikubetsu) and 1.95 ppm (Bremen), while the scatter ranges between 3.15 ppm (Izaña) and 0.63 ppm (Wollongong). Note that large bias results are observed at stations that are quite close to one another. One in the Los Angeles basin (Pasadena) and the other just outside on the other side of the San Gabriel Mountain range (Edwards), which separates the basin from the Mojave Desert. Correlation values range between -0.33 (Bremen) and 0.92 (Sodankyla), with the median over all stations equal to 0.79. The correlation using all data regardless of station equals 0.83. Given the limited timespan covered by the product, we did not calculate any long term trend. But as can be seen in **Figures 4-9 and 4-10** no clear-cut drift is observable.

Table 4-5: Number of collocated data pairs (N), Correlation (R), Bias, Scatter, long term trend difference (ltt) and uncertainty thereon (ltt_err), seasonal amplitude difference (A) and uncertainty thereon (A_err) as well as the latitude of the TCCON station. The last row lists the median values over all stations. Product: CO2_TAN_OCFP.

STATION	N	R	Bias	Scat	ltt	ltt_err	A	A_err	lat
EUREKA	928	0.87	1.01	1.56	-	-	-	-	80
NYALESUND	801	0.86	-0.57	1.12	-	-	-	-	78.9
SODANKYLA	19749	0.92	0.35	1.27	-	-	-	-	67.4
EASTTROUTLAKE	25973	0.87	0.56	1.71	-	-	-	-	54.3
BREMEN	46	-0.33	1.95	0.91	-	-	-	-	53.1
KARLSRUHE	10039	0.88	0.27	1.42	-	-	-	-	49.1
PARIS	733	0.86	1.21	1.05	-	-	-	-	48.8
ORLEANS	8412	0.79	0.49	1.05	-	-	-	-	48
GARMISCH	7845	0.84	0.22	1.72	-	-	-	-	47.5
PARKFALLS	19003	0.79	0	1.66	-	-	-	-	45.9
RIKUBETSU	3238	0.63	-0.95	1.7	-	-	-	-	43.5
LAMONT	45325	0.83	0.56	1.42	-	-	-	-	36.6
TSUKUBA	826	0.76	-0.44	1.69	-	-	-	-	36
EDWARDS	4535	0.38	0.79	1.18	-	-	-	-	35
JPL	27235	0.7	-0.52	1.86	-	-	-	-	34.2
PASADENA	9149	0.48	-0.59	1.69	-	-	-	-	34.1
SAGA	6158	0.79	-0.2	1.69	-	-	-	-	33.2
HEFEI	10288	0.85	1.16	1.61	-	-	-	-	31.9
IZANA	63	0.19	-0.24	3.15	-	-	-	-	28.3
BURGOS	169	0.12	0.72	1.29	-	-	-	-	18.5
REUNION	63	0.11	0.83	0.84	-	-	-	-	-20.9
WOLLONGONG	8579	0.73	0.63	1.59	-	-	-	-	-34.4
LAUDER	3944	0.65	0.77	1.28	-	-	-	-	-45
MEDIAN	**6158**	**0.79**	**0.49**	**1.56**	**-**	**-**	**-**	**-**	**36.6**

The timeseries below in **Figure 4-9** show individual satellite and ground-based fts measurements. As can be seen, and was already apparent from the Taylor diagram, OCFP XCO_2 features a somewhat higher scatter than TCCON, but overall the seasonality is well captured. An occasional outlier is still noticeable (both in the TCCON and OCFP dataset).

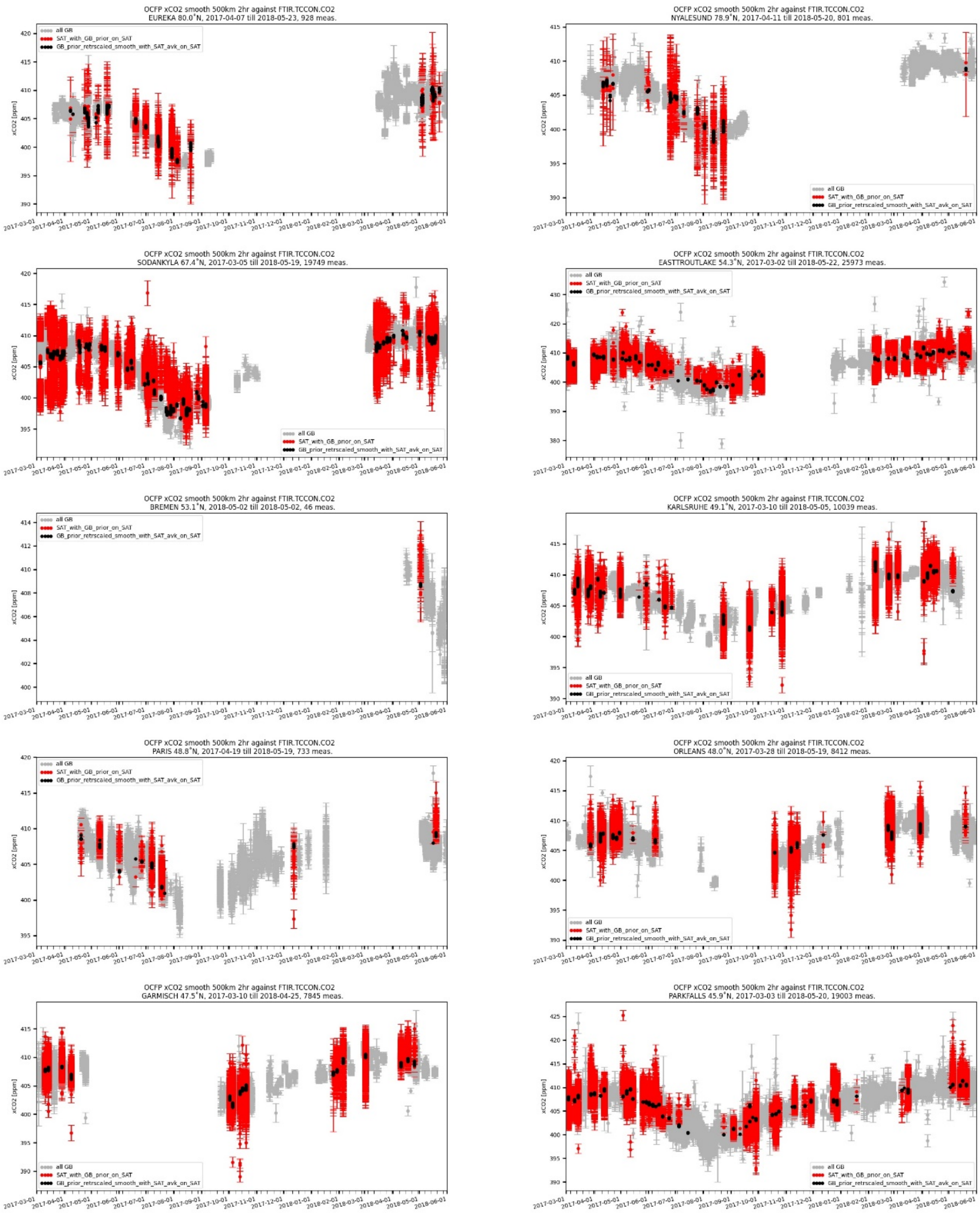

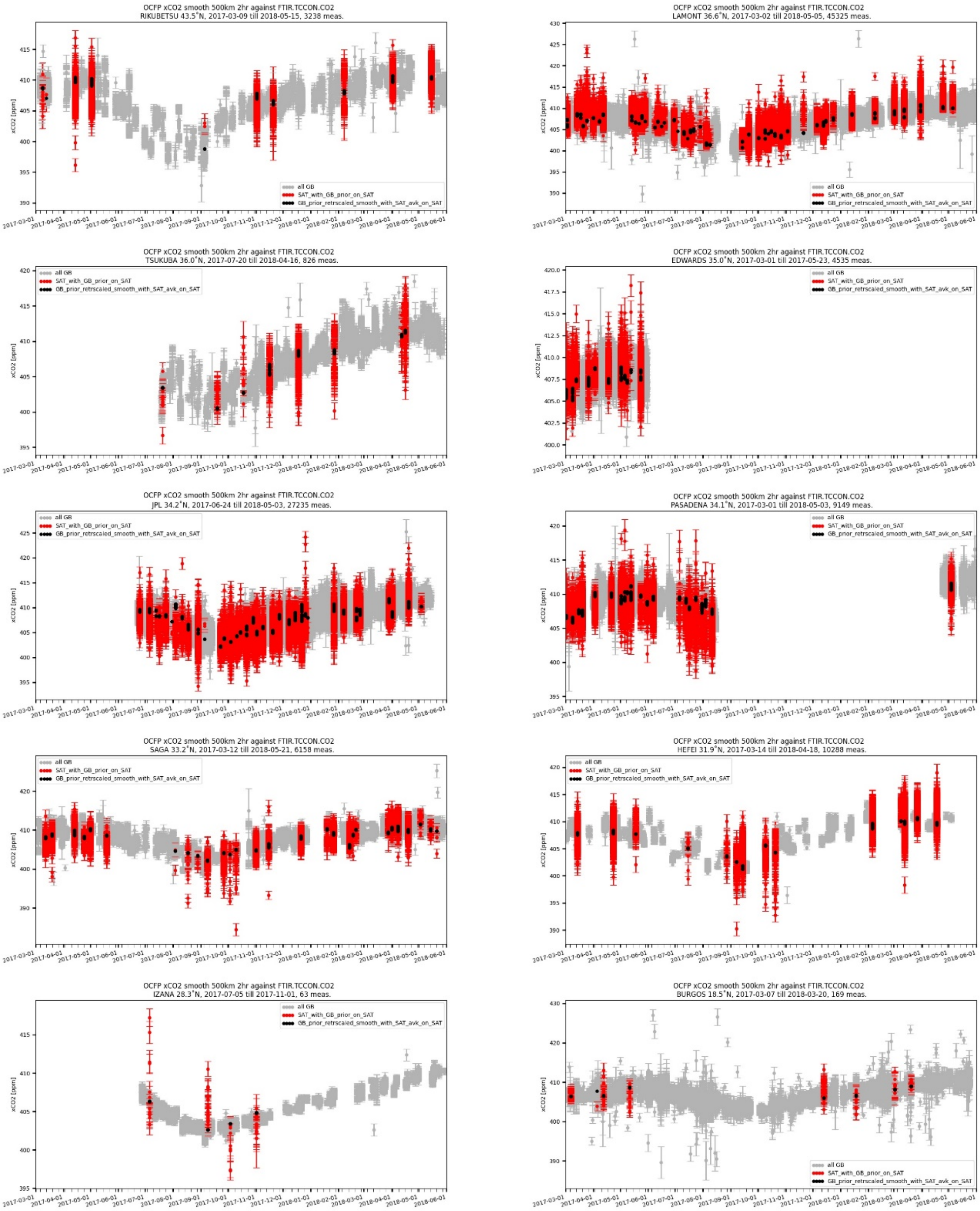
OCFP xCO2 smooth 500km 2hr against FTIR.TCCON.CO2
RIKUBETSU 43.5°N, 2017-03-09 till 2018-05-15, 3238 meas.
OCFP xCO2 smooth 500km 2hr against FTIR.TCCON.CO2
LAMONT 36.6°N, 2017-03-02 till 2018-05-05, 45325 meas.
OCFP xCO2 smooth 500km 2hr against FTIR.TCCON.CO2
TSUKUBA 36.0°N, 2017-07-20 till 2018-04-16, 826 meas.
OCFP xCO2 smooth 500km 2hr against FTIR.TCCON.CO2
EDWARDS 35.0°N, 2017-03-01 till 2017-05-23, 4535 meas.
OCFP xCO2 smooth 500km 2hr against FTIR.TCCON.CO2
JPL 34.2°N, 2017-06-24 till 2018-05-03, 27235 meas.
OCFP xCO2 smooth 500km 2hr against FTIR.TCCON.CO2
PASADENA 34.1°N, 2017-03-01 till 2018-05-03, 9149 meas.
OCFP xCO2 smooth 500km 2hr against FTIR.TCCON.CO2
SAGA 33.2°N, 2017-03-12 till 2018-05-21, 6158 meas.
OCFP xCO2 smooth 500km 2hr against FTIR.TCCON.CO2
HEFEI 31.9°N, 2017-03-14 till 2018-04-18, 10288 meas.
OCFP xCO2 smooth 500km 2hr against FTIR.TCCON.CO2
IZANA 28.3°N, 2017-07-05 till 2017-11-01, 63 meas.
OCFP xCO2 smooth 500km 2hr against FTIR.TCCON.CO2
BURGOS 18.5°N, 2017-03-07 till 2018-03-20, 169 meas.
all GB
SAT_with_GB_prior_on_SAT
GB_prior_retrscaled_smooth_with_SAT_avk_on_SAT
xCO2 [ppm]

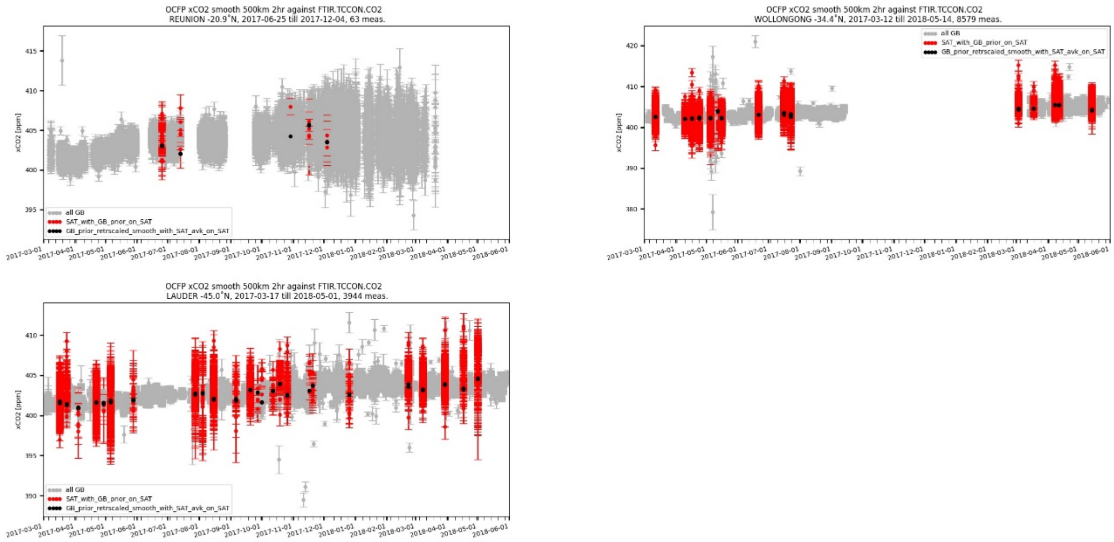

Figure 4-9: XCO_2 timeseries at all TCCON sites (red= CO2_TAN_OCFP data, black is collocated TCCON data and grey are the uncollocated TCCON data).

Figure 4-10 shows monthly median timeseries for TCCON and OCFP XCO_2 for all data that falls within certain latitude bands, namely all sites North of 40°N latitude (top), all sites between 40°N and the equator (mid) and all sites in the Southern hemisphere (bottom). It also features the values for a trend+seasonal fit through both datasets. The obtained long term trends have overlapping standard deviations apart from the Southern hemisphere analysis. Also both FTIR and OCFP XCO_2 seem to follow the same seasonal cycle in the Northern Hemisphere but again not for the Southern hemisphere. However, the observed trend values are, given the short timeframe covered, and limited Southern Hemisphere data, not robust. Combined with the limited seasonal variability in the Southern hemisphere it is not surprising that we see differences in the fitting parameters.

All in all, we can state that OCFP clearly captures the overall seasonality.

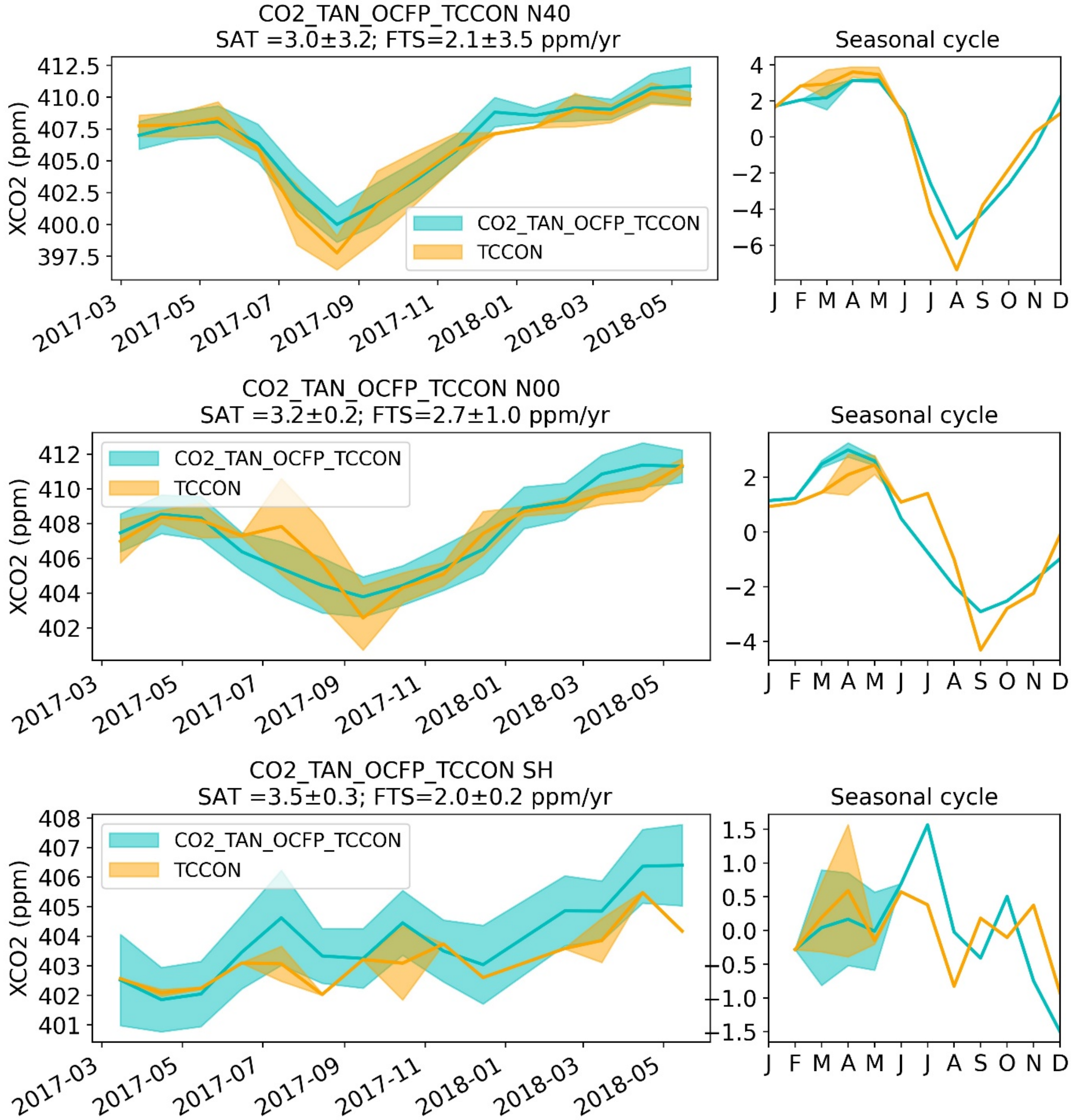

Figure 4-10: Monthly median collocated Sat and TCCON XCO_2 concentrations as a function of time. The shaded areas correspond with the scaled median absolute deviation.

4.2.2.2 Summary

Despite the limited amount of collocated data and the relatively small time period covered, we can already state that we see no obvious defects embedded within the CO2_TAN_OCFP product.

The OCFP reported uncertainty is underestimated by roughly 15% (Uncertainty ratio = 0.85) and the overall bias equals 0.49 ppm and the scatter equals 1.56 ppm. The spatial relative accuracy (RA), using GGG2014 TCCON, had even (just) reached the stated goal requirement (0.5 ppm) and the spatio-temporal relative accuracy (SRA) was 0.96 ppm. With GGG2020, the RA and SRA have worsened slightly to 0.72 and 1.01 respectively but with substantially overlapping confidence bands with respect to the previous analysis. The confidence bands for RA still overlap with the stated goal requirement of (>0.5 ppm) but not those of the SRA. As already mentioned in the analysis of FOCAL XCO2, these numbers ignore TCCON network and collocation errors. Due to the limited temporal coverage, no Stability parameter has been calculated, but we did not see any apparent problems in this area. All in all the differences with respect to the previous analysis are, as expected, minute.

Table 4-6 presents an overview of the estimated data quality of CO2_TAN_OCFP, as obtained by the VALT team, from comparisons with TCCON ground-based reference observations. Values in square brackets [ ] correspond with the upper and lower 95% confidence bound on the parameter. The uncertainty ratio features 2 numbers as outlined in the validation method.

Product Quality Summary Table for Product: CO2_TAN_OCFP Level: 2, Version: v01.2.0, Time period covered: 03.2017 – 05.2018 Assessment: Validation Team (VALT)			
Parameter [unit]	**Achieved performance**	**Requirement**	**Comments**
Single measurement precision (1-sigma) in [ppm]	1.56 [1.42, 1.85]	< 8 (T) < 3 (B) < 1 (G)	Computed as the median over all station scaled median absolute differences to TCCON
Uncertainty ratio [-]: Ratio reported uncertainty to standard deviation of satellite-TCCON difference	0.76, 0.85*	-	No requirement but value close to unity expected for a high quality data product with reliable reported uncertainty.
Mean bias (global offset) [ppm]	0.49 [0.21,0.97]	-	No requirement but value close to zero expected for a high quality data product.
Accuracy: Relative systematic error [ppm]	Spatial: 0.72 [0.35, 1.13] Spatio-temporal: 1.01 [0.76, 1.28]	< 0.5	Spatial: Computed as standard deviation of the biases at the various TCCON sites. Spatio-temporal: As "Spatial" but also considering seasonal biases.
Stability: Drift [ppm/year]	-	< 0.5	Linear drift

4.2.3 Validation results for product CO2_GO2_SRFP

Below we show the validation results of the XCO_2 concentrations as derived by the CO2_GO2_SRFP v2.0.2 algorithm using GOSAT-2 spectra. Data was available from February 2019 up to and including December 2021. The SRFP algorithm provides *a priori* and column averaging kernel information on a 12 layers profile. The covered time period has thus been significantly expanded (end date shifted from August 2020 to December 2021), and has thus reached the full 2 years to make an initial analysis on any long term-trend issues.

4.2.3.1 Detailed results

The Taylor diagram below in **Figure 4-11** shows a short overview of the capabilities of the CO2_GO2_SRFP product. Most TCCON sites cluster around the intercept of the 0.7 correlation line and a normalized standard deviation of ~0.85, with Reunion, Eureka, Harwell and Hefei, notable exceptions. However, all of these outlier stations have limited collocated data. The normalized standard deviation of most sites range between 0.5 and 1.2, with most being smaller than 1, indicating that on average the variability of the TCCON data is smaller. The normalized standard deviation of the bias sits (for most sites) around 0.6. All this indicates that while SRFP data features a slightly stronger variability (random error and/or seasonal variability) than the TCCON data, the biases still harbors less variability then either of them, an indication of SRFP capturing the natural variability.

There is no strong discernible pattern in the mosaic plot (**Figure 4-12**), which shows the mean bi-weekly bias between the satellite and TCCON measurement pairs. The period between 10-2019 and 7-2020 appears to have lower biases across almost all latitude stations compared to the rest of the timeframe but this feature is not clear for all stations. Furthermore, the period covered by the above plot is limited and there are many gaps in the timeseries, either do due unavailability of TCCON data during winter at high latitudes, interruptions in the measurement cycle or instruments moving to other locations. Sometimes it is merely the result of the sparseness of either data, yielding extremely limiting overlap.

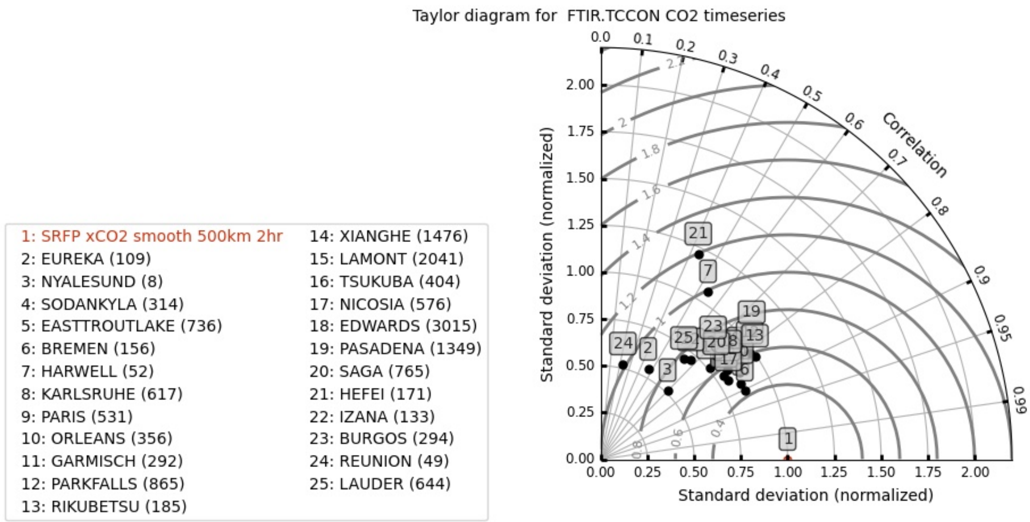

Figure 4-11: Tayor plot of daily averaged XCO_2 TCCON values relative to product CO2_GO2_SRFP. Straight lines correspond with the correlation, light grey lines yield the variability of the TCCON data relative to the satellite variability and the dark grey lines correspond with the variability of the Satellite - TCCON bias relative to the satellite variability.

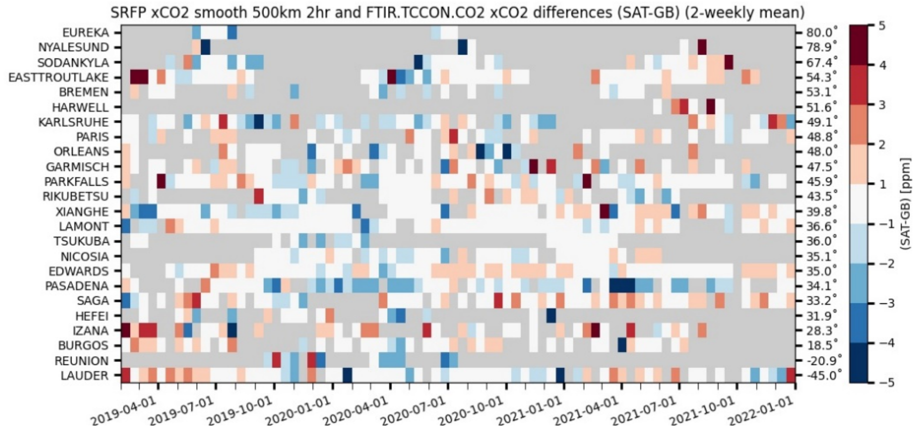

Figure 4-12: Mosaic plot of bi-weekly mean CO2_GO2_SRFP-TCCON XCO_2 biases as a function of time and TCCON station.

Table 4-7 lists all bias and scatter results derived from individual data pairs at all TCCON stations. The algorithm produces on average ~380 data pairs per station which corresponds with ~120 pairs per station per year. The observed median bias ranges between -1.86 ppm (Reunion) and 1.77 ppm (Harwell), while the scatter ranges between 1.48 ppm (Reunion) and 2.51 (EastTroutLake). Correlation values range between 0.23 (Reunion) and 0.90 (Bremen), with most correlation values sitting around 0.8. Of course the limited dataset hampers the correlation values at certain stations. The correlation using all data regardless of station equals 0.81. The median long term trend equals 0.12 ppm/year with values ranging between -0.84 (Orleans) and 4.99 (Ny Alesund). However given the extremely limited amount of data (8 pairs) the latter number is not reliable. The second largest positive trend value is 1.09 (Sodankyla). In **Figures 4-13 and 4-14** no clear-cut drift is observable.

Table 4-7: Number of collocated data pairs (N), Correlation (R), Bias, Scatter, long term trend difference (ltt) and uncertainty thereon (ltt_err), seasonal amplitude difference (A) and uncertainty thereon (A_err) as well as the latitude of the TCCON station. The last row lists the median values over all stations. Product: CO2_GO2_SRFP.

STATION	N	R	Bias	Scat	ltt	ltt_err	A	A_err	Lat
EUREKA	109	0.47	-1.21	2.34	-	-	-	-	80
NYALESUND	8	0.7	0.1	2.4	4.99	0.73	40.79	11.19	78.9
SODANKYLA	314	0.88	-0.77	2.32	1.09	0.36	0.12	0.92	67.4
EASTTROUTLAKE	736	0.82	0.05	2.51	-0.2	0.24	0.96	0.37	54.3
BREMEN	156	0.9	-0.14	2.07	-0.3	0.31	1.27	0.67	53.1
HARWELL	52	0.54	1.77	1.59	-	-	-	-	51.6
KARLSRUHE	617	0.76	-0.39	2.21	0.24	0.36	0.33	0.29	49.1
PARIS	531	0.8	0.35	2.07	0.01	0.19	0.77	0.3	48.8
ORLEANS	356	0.85	0.1	1.93	-0.84	0.7	1.01	0.46	48
GARMISCH	292	0.77	0.65	2.21	0.12	0.42	0.54	0.4	47.5
PARKFALLS	865	0.81	0.09	2.18	-0.21	0.2	0.36	0.24	45.9
RIKUBETSU	185	0.83	0.27	1.53	0.24	0.33	0.75	0.37	43.5
XIANGHE	1476	0.83	0	2.5	0.99	0.21	0.27	0.21	39.8
LAMONT	2041	0.81	-0.03	1.68	0.33	0.16	0.47	0.13	36.6
TSUKUBA	404	0.77	-1.03	1.99	0.31	0.3	0.76	0.45	36
NICOSIA	576	0.85	0.1	1.77	-	-	-	-	35.1
EDWARDS	3015	0.79	0.48	1.95	0.26	0.14	0.5	0.13	35
PASADENA	1349	0.77	-1.31	2.2	-0.49	0.33	0.48	0.19	34.1
SAGA	765	0.77	0.54	2.11	0.29	0.2	0.18	0.23	33.2
HEFEI	171	0.43	0.22	2.09	-	-	-	-	31.9
IZANA	133	0.67	0.43	2.04	0.11	0.55	0.93	0.48	28.3
BURGOS	294	0.71	0.4	1.96	-0.36	0.23	0.58	0.28	18.5
REUNION	49	0.23	-1.86	1.48	-	-	-	-	-20.9
LAUDER	644	0.64	0.65	2.01	-0.02	0.24	0.66	0.26	-45
MEDIAN	**380**	**0.77**	**0.1**	**2.07**	**0.12**	**0.3**	**0.58**	**0.3**	**41.65**

The timeseries below in **Figure 4-13** show individual satellite and ground-based fts measurements. As can be seen, and was already apparent from the Taylor diagram, SRFP XCO_2 features at most stations a somewhat higher scatter than TCCON, but overall the seasonality is well captured.

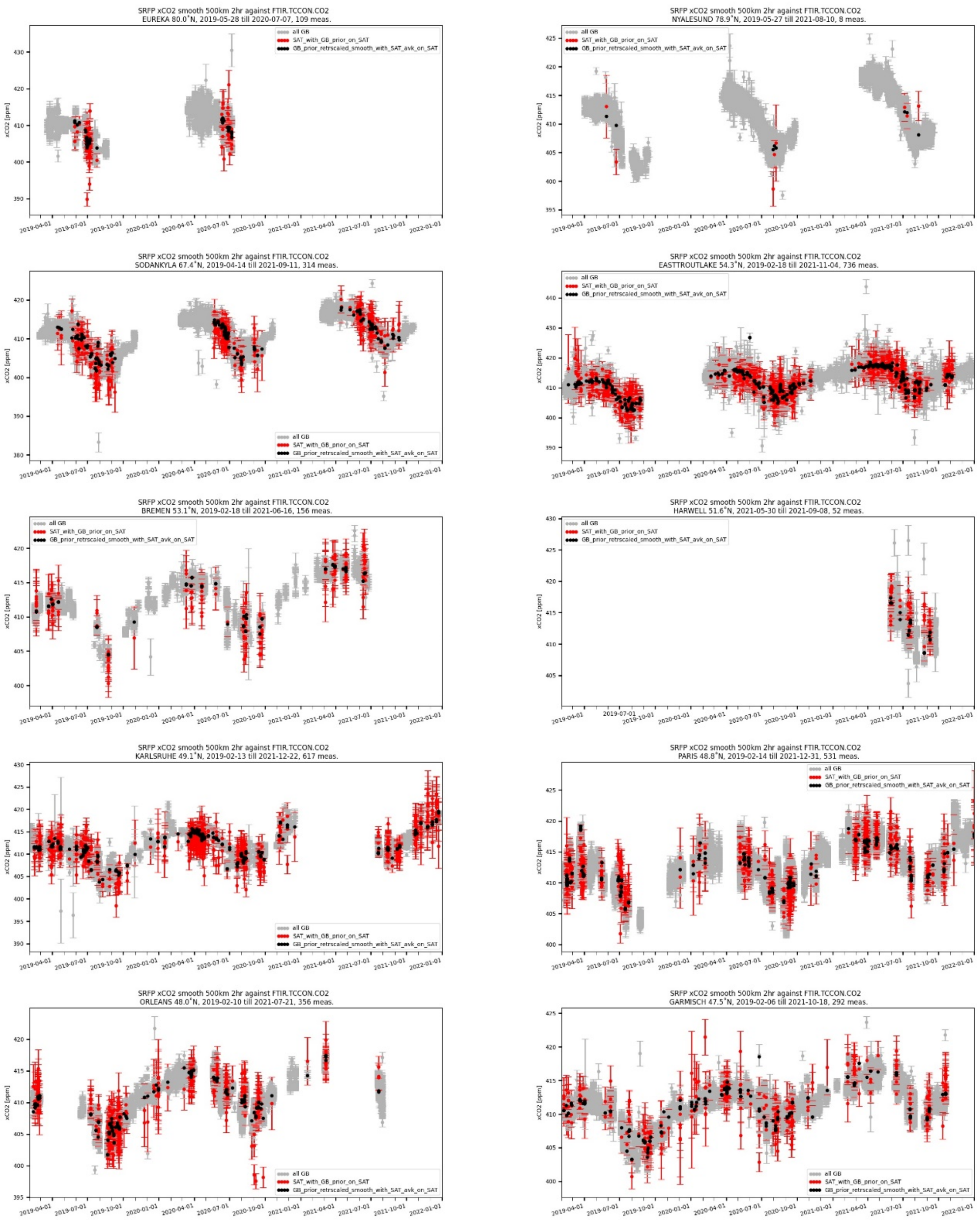

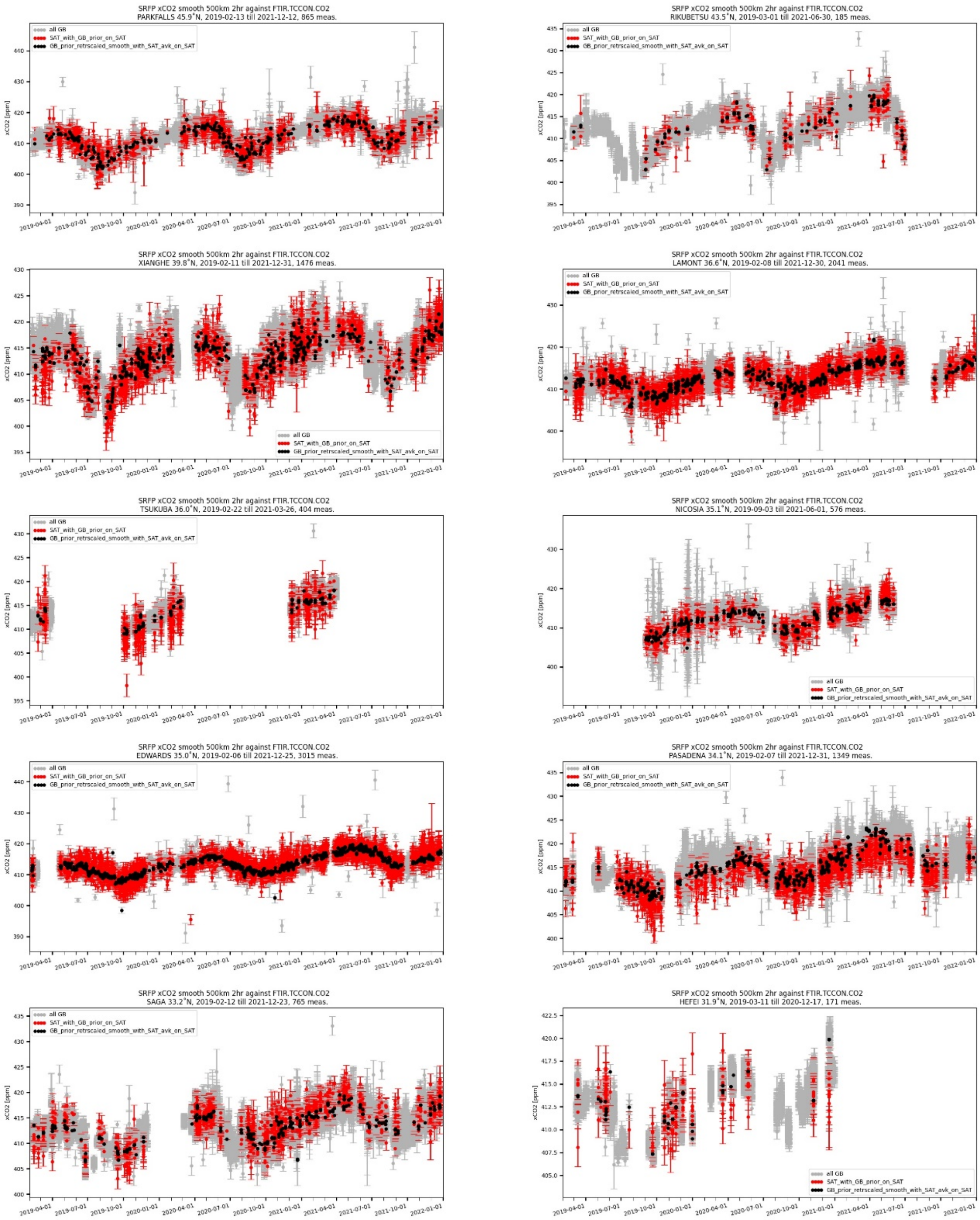

SRFP xCO2 smooth 500km 2hr against FTIR.TCCON.CO2
PARKFALLS 45.9°N, 2019-02-13 till 2021-12-12, 865 meas.
SRFP xCO2 smooth 500km 2hr against FTIR.TCCON.CO2
RIKUBETSU 43.5°N, 2019-03-01 till 2021-06-30, 185 meas.
SRFP xCO2 smooth 500km 2hr against FTIR.TCCON.CO2
XIANGHE 39.8°N, 2019-02-11 till 2021-12-31, 1476 meas.
SRFP xCO2 smooth 500km 2hr against FTIR.TCCON.CO2
LAMONT 36.6°N, 2019-02-08 till 2021-12-30, 2041 meas.
SRFP xCO2 smooth 500km 2hr against FTIR.TCCON.CO2
TSUKUBA 36.0°N, 2019-02-22 till 2021-03-26, 404 meas.
SRFP xCO2 smooth 500km 2hr against FTIR.TCCON.CO2
NICOSIA 35.1°N, 2019-09-03 till 2021-06-01, 576 meas.
SRFP xCO2 smooth 500km 2hr against FTIR.TCCON.CO2
EDWARDS 35.0°N, 2019-02-06 till 2021-12-25, 3015 meas.
SRFP xCO2 smooth 500km 2hr against FTIR.TCCON.CO2
PASADENA 34.1°N, 2019-02-07 till 2021-12-31, 1349 meas.
SRFP xCO2 smooth 500km 2hr against FTIR.TCCON.CO2
SAGA 33.2°N, 2019-02-12 till 2021-12-23, 765 meas.
SRFP xCO2 smooth 500km 2hr against FTIR.TCCON.CO2
HEFEI 31.9°N, 2019-03-11 till 2020-12-17, 171 meas.
all GB
SAT_with_GB_prior_on_SAT
GB_prior_retrscaled_smooth_with_SAT_avk_on_SAT
xCO2 [ppm]

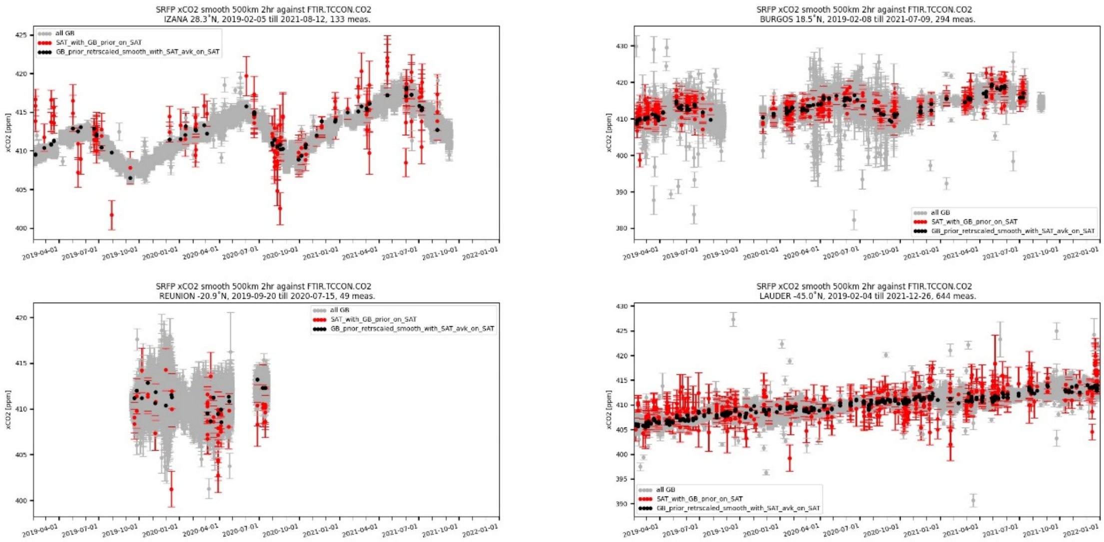

Figure 4-13: XCO_2 timeseries at all TCCON sites (red= CO2_GO2_SRFP data, black is collocated TCCON data and grey are the uncollocated TCCON data).

Figure 4-14 shows monthly median timeseries for TCCON and SRFP XCO_2 for all data that falls within certain latitude bands, namely all sites North of 40°N latitude (top), all sites between 40°N and the equator (mid) and all sites in the Southern hemisphere (bottom). It also features the values for a trend+seasonal fit through both datasets. For all bands , the differences in the obtained long term trends (0.4 ppm/year for sites North of 40° latitude and 0.2 for the remainder) can be covered by their respective standard deviations.

All in all, we can state that SRFP clearly captures the overall seasonality.

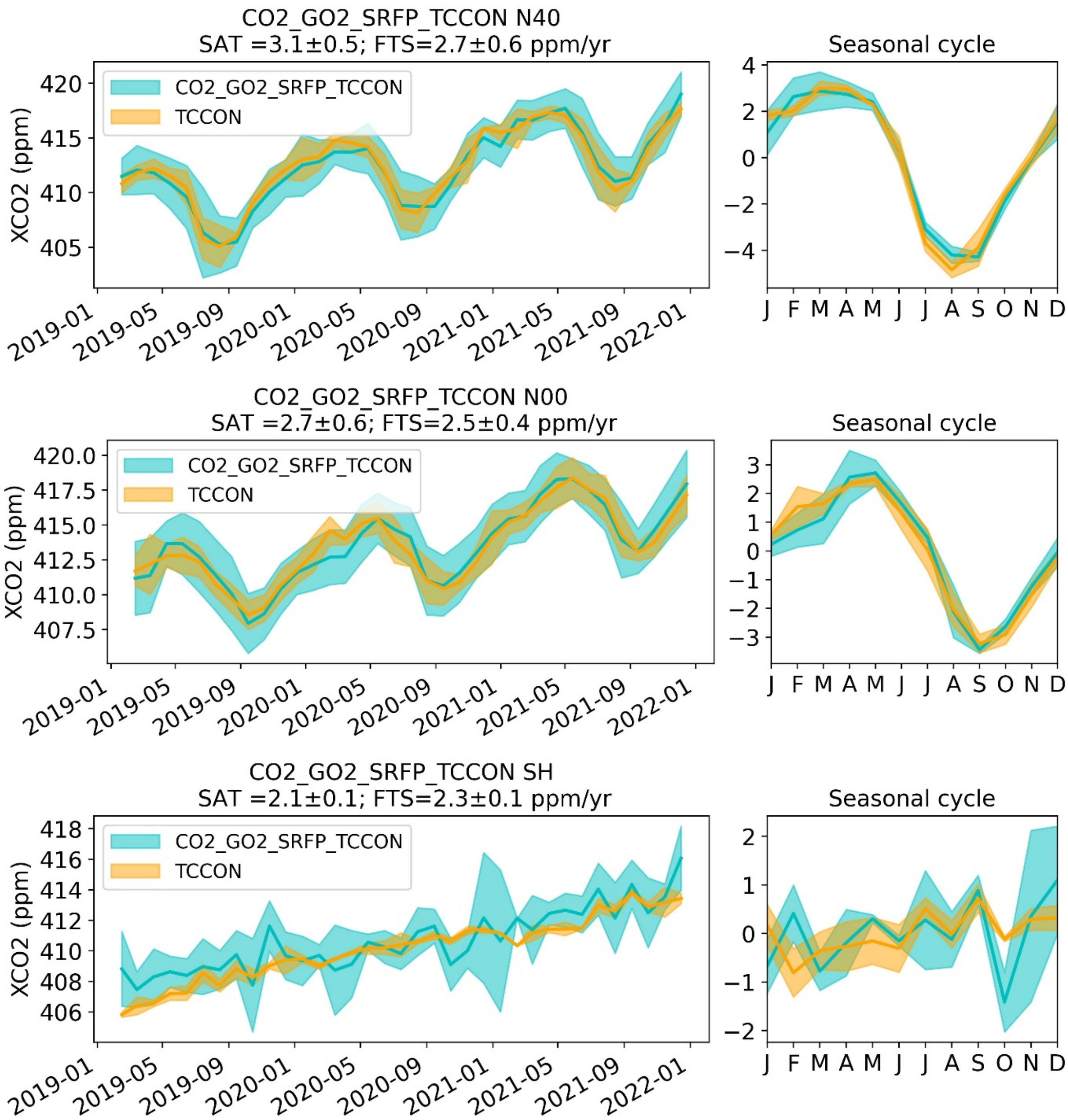

Figure 4-14: Monthly median collocated Sat and TCCON XCO_2 concentrations as a function of time. The shaded areas correspond with the scaled median absolute deviation.

4.2.3.2 Summary

Despite the limited amount of collocated data and the limited time period covered, we can already state that we see no obvious defects embedded within the CO2_GO2_SRFP product. The SRFP reported uncertainty corresponds closely with our analysis (Uncertainty ratio = 0.85). The spatial (RA), 0.47 ppm has met the stated goal requirement of (>0.5 ppm), but the spatio-temporal relative accuracy (SRA) has not, nor do its confidence interval overlap [0.53, 1.05]. The long term stability (0.12 ppm/year) meets the linear drift requirements (<0.5 ppm/year), its confidence interval range encompassing 0.

Table 4-8 presents an overview of the estimated data quality of CO2_GO2_SRFP, as obtained by the VALT team, from comparisons with TCCON ground-based reference observations. Values in square brackets [ ] correspond with the upper and lower 95% confidence bound on the parameter. The uncertainty ratio features 2 numbers as outlined in the validation method.

Product Quality Summary Table for Product: CO2_GO2_SRFP Level: 2, Version: v02.0.2, Time period covered: 2.2019 – 12.2021 Assessment: Validation Team (VALT)			
Parameter [unit]	**Achieved performance**	**Requirement**	**Comments**
Single measurement precision (1-sigma) in [ppm]	2.07 [1.94,2.18]	< 8 (T) < 3 (B) < 1 (G)	Computed as the median over all station scaled median absolute differences to TCCON
Uncertainty ratio [-]: Ratio reported uncertainty to standard deviation of satellite-TCCON difference	0.83, 0.85*	-	No requirement but value close to unity expected for a high quality data product with reliable reported uncertainty.
Mean bias (global offset) [ppm]	0,10 [-0.15, 0.23]	-	No requirement but value close to zero expected for a high quality data product.
Accuracy: Relative systematic error [ppm]	Spatial: 0.47 [0.09, 0.74] Spatio-temporal: 0.81 [0.53, 1.05]	< 0.5	Spatial: Computed as standard deviation of the biases at the various TCCON sites. Spatio-temporal: As "Spatial" but also considering seasonal biases.
Stability: Drift [ppm/year]	0.12 [-0.05, 0.44]	< 0.5	Linear drift

4.2.4 Validation results for product CH4_S5P_WFMD

Below we show the validation results of the XCH_4 concentrations as derived by the CH4_S5P_WFMD v1.8 algorithm using S5P spectra. Data was available from November 2017 up to and including April 2022. The WFMD algorithm provides *a priori* and column averaging kernel data on a 20 layers vertical profile. We have made comparisons with data from both the TCCON and NDACC networks. Note that instead of 'within 500 km and 2 hour' collocation criteria, we here have used 'within 100km and 1 hours' for TCCON and 'within 100km and 2 hours' for NDACC. In the plots and tables below, the TCCON figure/table is always shown first. The obtained Figures of Merit in the summary table (**table 4-11**) pertain to the TCCON analysis only, partly to ensure continuity with previous assessments, but also due to the higher systematic uncertainty and high prevalence of high-latitude and mountain sites in the NDACC network, which might distort our analysis.

4.2.4.1 Detailed results

The Taylor plot for product CH4_S5P_WFMD is shown in **Figure 4-15**. Most FTIR sites are clustered between the 0.5 and 0.8 correlation line, with the standard deviation of the differences sitting between 0.75 and 1 times the standard deviation of the satellite data itself. The variability on the TCCON data is consistently smaller than that of WFMD apart from the Reunion station. In fact the Reunion site is the only station that stands out, other stations are fairly well grouped together. This indicates a good consistency of both Satellite product and station network. Note that the Reunion site is an island site with the lowest collocation pair density.

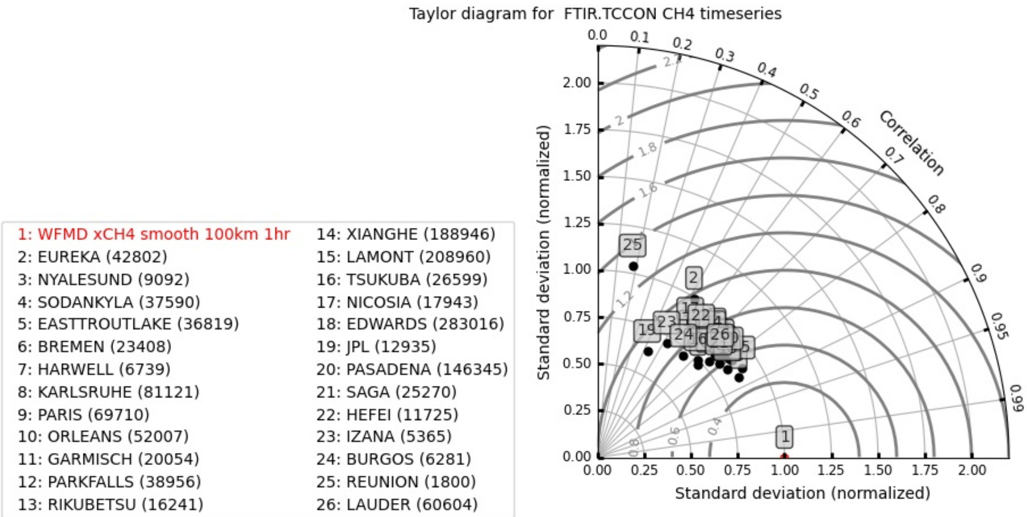

Figure 4-15: Tayor plot of daily averaged XCH4 TCCON values relative to CH4_S5P_WFMD. Straight lines correspond with the correlation, light grey lines yield the variability of the TCCON data relative to the satellite variability and the dark grey lines correspond with the variability of the Satellite -TCCON bias relative to the satellite variability.

The NDACC Taylorplot shows way more dispersion, indicating either less consistency within the network, less ideal collocation circumstances or a satellite product that is less attuned to the NDACC network. Also the correlation, standard deviation of the difference and standard deviation of the satellite data relative to NDACC yields poorer results. Correlations, on average with a lot of leeway, sits around 0.6, while the standard deviation on the Satellite data has a wide range relative to the NDACC data with some stations showing lower and other higher scatter than NDACC. The scatter on the SAT-NDACC difference, relative to the scatter of the NDACC data itself sits around 1.0 but with many outliers. Notable outliers are Eureka, Toronto and La Reunion Maïdo, with much lower correlation values. Toronto and Bremen also feature very high scatter values with respect to the satellite data.

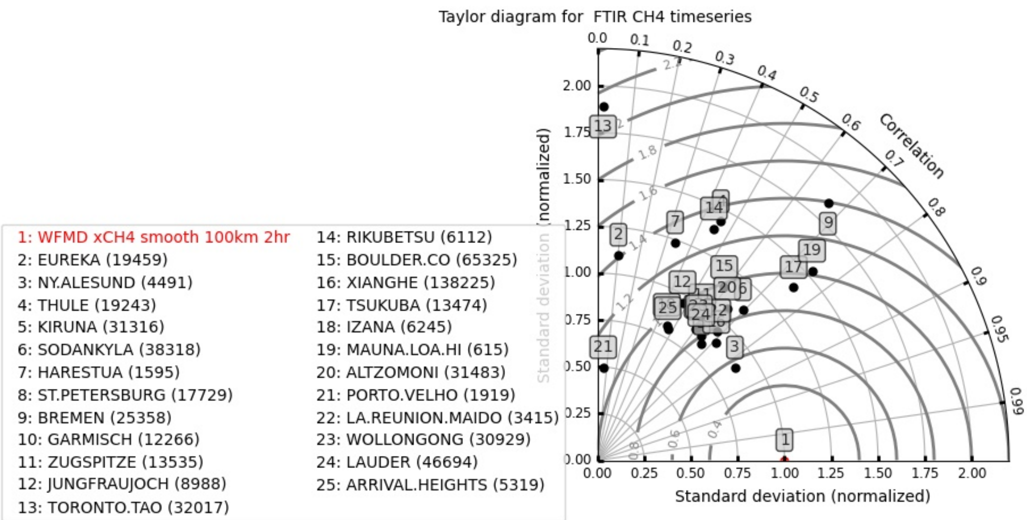

Figure 4-16: Tayor plot of daily averaged XCH4 NDACC values relative to CH4_S5P_WFMD. Straight lines correspond with the correlation, light grey lines yield the variability of the NDACC data relative to the satellite variability and the dark grey lines correspond with the variability of the Satellite -NDACC bias relative to the satellite variability..

The mosaic overview of bi-weekly sat-TCCON biases (**Figure 4-17**) does not reveal any systematic trend over time, nor any as a function of latitude. There are some very pronounced biases (negative in Parkfalls and positive in Izaña, the latter, being a high altitude stations).

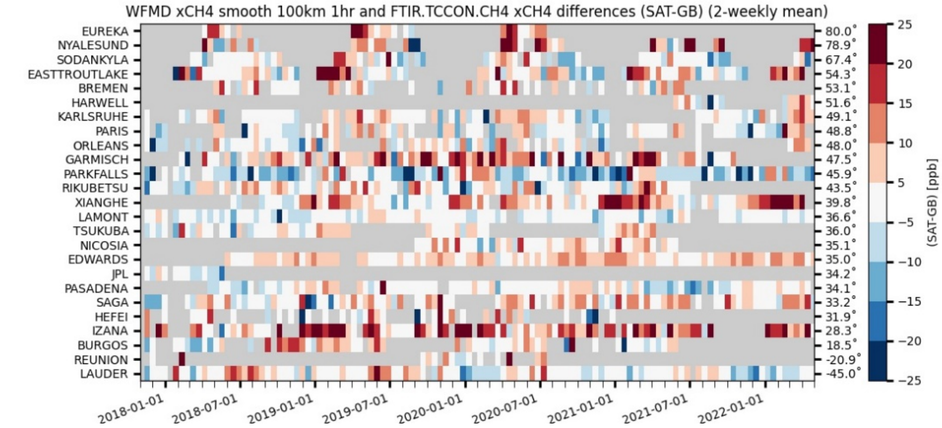

Figure 4-17: Mosaic plot of bi-weekly mean CH4_S5P_WFMD - TCCON XCH_4 biases as a function of time and TCCON station.

For NDACC we see more pronounced differences with strong positive biases at Thule, Altzomoni and Arrival Heights and negative ones at Jungfraujoch, Wollongong and Lauder. For Toronto we even see a shifting bias, with lower values at the start and higher values at the end of the observed timeframe. This corresponds with a significant increase in the Toronto FTIR scatter (see **Figure 4-21**). Paramaribo (only 2 collocation data pairs!), Porto Velho and Reunion (Maïdo) cover only a tiny fraction of the retrieved timeseries.

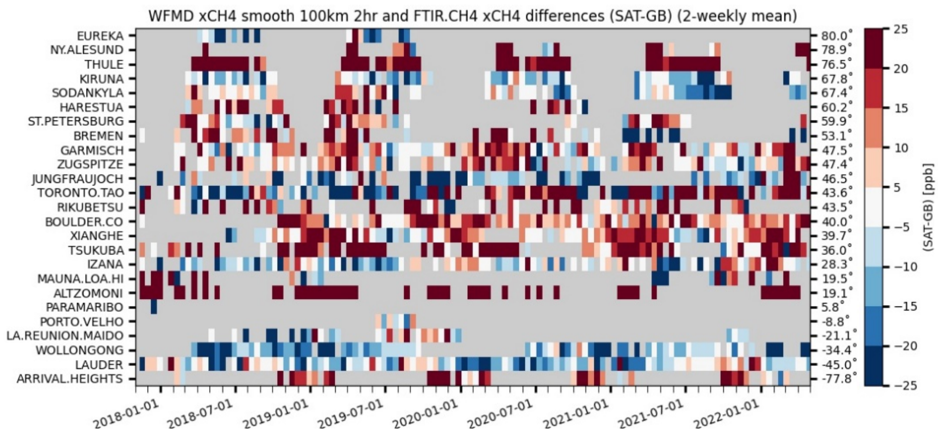

Figure 4-18: Mosaic plot of bi-weekly mean CH4_S5P_WFMD - NDACC XCH_4 biases as a function of time and NDACC station.

Tables 4-9 and 4-10 lists all bias and scatter results derived from individual data pairs at all TCCON and NDACC stations respectively. For TCCON, the algorithm produces on average ~26500 data pairs per station which corresponds with ~6000 pairs per station per year. Also keep in mind that the collocation criteria are substantially stricter. The observed median bias ranges between -6.66 ppb (Parkfalls) and 17.21 ppb (Eureka), while the scatter ranges between 11.11 ppb (Lamont) and 21.15 ppb (Easttroutlake). Correlation values range between 0.18 (Reunion) and 0.87 (Ny Alesund), with most correlation values sitting between 0.6 and 0.76. The correlation of all data, regardless of station, equals 0.89. The long term trend on the bias ranges between -5.26 ppb/year at Reunion and 4.3 ppb/year at Eureka. Finally, the seasonal amplitude present in the sat-TCCON bias ranges between 0.76 ppb (Lamont) and 17.17 ppb (Eureka). Of course the latter, being a high latitude station, misses data during autumn and wintertime and cannot capture the full seasonal cycle.

For NDACC (**Table 4-11**), the overall and median correlations are lower (0.77 and 0.60 respectively). Biases range from a staggering -118.0 ppb (Paramaribo) to 57.3 ppb (Altzomoni). However for the first we only have 2 datapoints, and the latter is a particularly challenging site as it sits in the mountains near Mexico City. It is certainly the case that the simple profile extension we employ does not yield satisfying results. If we generate the same plot (**Figure 4-19**) for Altzomoni as for Dryden and Caltech (see **Figure 4-1**), we immediately see that the data density is far less, but also that all datapoints within the vicinity of Altzomoni feature XCH4 concentrations, significantly larger than at the mountain site itself. Scatter numbers range from 1.9 (Paramaribo again) and 53.6 ppb (Toronto). This site seems to suffer from a degradation in the data quality from the start of 2021 onwards (see **Figure 4-21**). Long term trends range between -13.3 ppb/year (Bremen) and 18.2 ppb/year (Toronto). The latter is a clear outlier with the next highest positive trends are at 4.88 (Jungfraujoch).

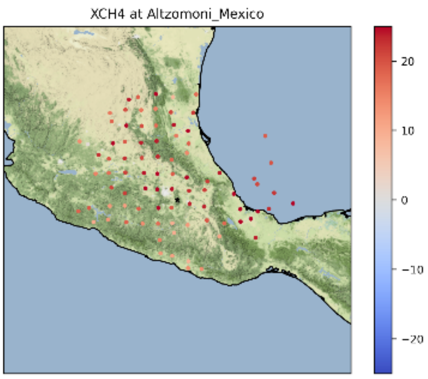

Figure 4-19: Bias between WFMD XCH_4 around and at the Altzomoni site within the same overpass.

Table 4-9: Number of collocated data pairs (N), Correlation (R), Bias, Scatter, long term trend difference (ltt) and uncertainty thereon (ltt_err), seasonal amplitude difference (A) and uncertainty thereon (A_err) as well as the latitude of the TCCON station. The last row lists the median values over all stations. Product: CH4_S5P_WFMD.

STATION	N	R	Bias	Scat	ltt	ltt_err	A	A_err	lat
EUREKA	42802	0.52	17.21	18.78	4.3	4	17.17	4.15	80
NYALESUND	9092	0.87	13.01	18.65	0.86	1.82	9.46	5.15	78.9
SODANKYLA	37590	0.75	2.31	16.09	-0.59	0.94	3.14	1.36	67.4
EASTTROUTLAKE	36819	0.72	10.19	21.15	0.22	0.93	4.4	1.06	54.3
BREMEN	23408	0.72	6.03	11.75	0.3	0.79	5.79	1.44	53.1
HARWELL	6739	0.73	4.88	12.51	-	-	-	-	51.6
KARLSRUHE	81121	0.79	5.75	12.49	0.36	0.58	5.51	0.73	49.1
PARIS	69710	0.81	3.36	12.36	0.97	0.57	3.7	0.89	48.8
ORLEANS	52007	0.76	4.07	11.77	1.72	0.8	2.47	1.01	48
GARMISCH	20054	0.63	11.12	14.59	-0.25	1.31	4.71	1.2	47.5
PARKFALLS	38956	0.76	-6.66	14.08	0.75	0.77	6.84	0.93	45.9
RIKUBETSU	16241	0.76	1.84	15.35	0.7	1.04	3.81	1.1	43.5
XIANGHE	188946	0.71	8.43	17.85	2.31	0.6	10.8	0.81	39.8
LAMONT	208960	0.85	-1.93	11.11	-0.26	0.42	0.76	0.53	36.6
TSUKUBA	26599	0.72	4.02	12.28	1.81	0.9	3.25	1.09	36
NICOSIA	17943	0.59	4.96	12.52	-	-	-	-	35.1
EDWARDS	283016	0.83	6.07	11.27	0.63	0.33	3.35	0.4	35
JPL	12935	0.43	-2.31	14.66	-	-	-	-	34.2
PASADENA	146345	0.8	-0.1	13.68	-0.17	0.5	3.48	0.49	34.1
SAGA	25270	0.79	7.88	15.48	0.79	0.64	3.94	0.96	33.2
HEFEI	11725	0.65	6.1	13.55	-0.67	1.92	5.5	2.07	31.9
IZANA	5365	0.52	6.7	18.83	0.44	1.04	3.58	1.38	28.3
BURGOS	6281	0.65	5.34	12.81	0.4	1.31	4.26	1.33	18.5
REUNION	1800	0.18	3.82	14.42	-5.26	3.82	11.87	4.55	-20.9
LAUDER	60604	0.77	-1.07	13.39	-2	0.37	6.77	0.62	-45
MEDIAN	**26599**	**0.73**	**4.96**	**13.68**	**0.42**	**0.85**	**4.33**	**1.075**	**39.8**

Table 4-10: Number of collocated data pairs (N), Correlation (R), Bias, Scatter, long term trend difference (ltt) and uncertainty thereon (ltt_err), seasonal amplitude difference (A) and uncertainty

thereon (A_err) as well as the latitude of the NDACC station. The last row lists the median values over all stations. Product: CH4_S5P_WFMD.

STATION	N	R	Bias	Scat	ltt	ltt_err	A	A_err	lat
EUREKA	19459	0.1	-1.9	24.68	-	-	-	-	79.8
NY.ALESUND	4491	0.83	40.7	19.43	0.57	2.63	20.49	4.76	78.9
THULE	19243	0.46	43.01	22.99	0.04	2.11	17.6	5.43	76.3
KIRUNA	31316	0.67	-5.96	18.03	-0.55	1.41	3.24	1.39	67.7
SODANKYLA	38318	0.69	2.36	20.34	-5.34	0.97	6.14	1.94	67.2
HARESTUA	1595	0.34	20.58	20.89	-3.87	3.61	9.65	5.4	60.1
ST.PETERSBURG	17729	0.6	11.25	18.17	1.39	1.09	8.97	1.82	59.7
BREMEN	25358	0.67	15.17	25.69	-13.27	9.44	2.55	3.79	52.9
GARMISCH	12266	0.6	8.28	18.52	0.3	1.19	10.75	1.43	47.4
ZUGSPITZE	13535	0.59	10.37	17.7	-0.32	0.88	11.83	1.49	47.3
JUNGFRAUJOCH	8988	0.47	-11.59	21.7	4.88	2.74	13.6	2.07	46.4
TORONTO.TAO	32017	0.02	6.07	53.62	18.2	3.56	6.12	4.55	43.5
RIKUBETSU	6112	0.45	18.2	30.72	-0.89	5.47	37.02	4.63	43.3
BOULDER.CO	65325	0.59	10.02	15.89	-0.76	1.16	0.67	1.41	39.9
XIANGHE	138225	0.71	12.41	18.48	-0.78	0.9	15.23	0.98	39.7
TSUKUBA	13474	0.75	19.47	20.1	-6.05	1.58	9.93	2.96	36
IZANA	6245	0.46	-13.34	22.13	2.99	1.43	6.09	1.54	28.2
MAUNA.LOA.HI	615	0.75	23.95	22.72	-3.85	4.24	10.49	10.54	19.5
ALTZOMONI	31483	0.65	57.34	19.67	-2.29	1.55	11.98	3.54	19.1
PARAMARIBO	2	-1	-117.98	1.93	-	-	-	-	5.8
PORTO.VELHO	1919	0.06	-2.01	17.63	-	-	-	-	-8.7
LA.REUNION.MAIDO	3415	0.68	-4.75	13.17	5.96	5.57	9.22	6.24	-21
WOLLONGONG	30929	0.61	-10.94	17.41	1.33	1.19	9.84	1.65	-34.4
LAUDER	47005	0.64	-7.52	16.84	-0.18	0.82	5.43	1.16	-45
ARRIVAL.HEIGHTS	5319	0.47	23.42	20.92	-2.85	1.76	18.82	5.16	-77.7
MEDIAN	**13535**	**0.60**	**10.02**	**19.67**	**-0.44**	**1.565**	**9.88**	**2.52**	**43.3**

Figure 4-20 shows all collocated WFMD and TCCON data time series. From these figures, it is clear that the variability of WFMD XCH_4 is substantially stronger. Also a fair amount of, particularly negative, outliers is present at many stations.

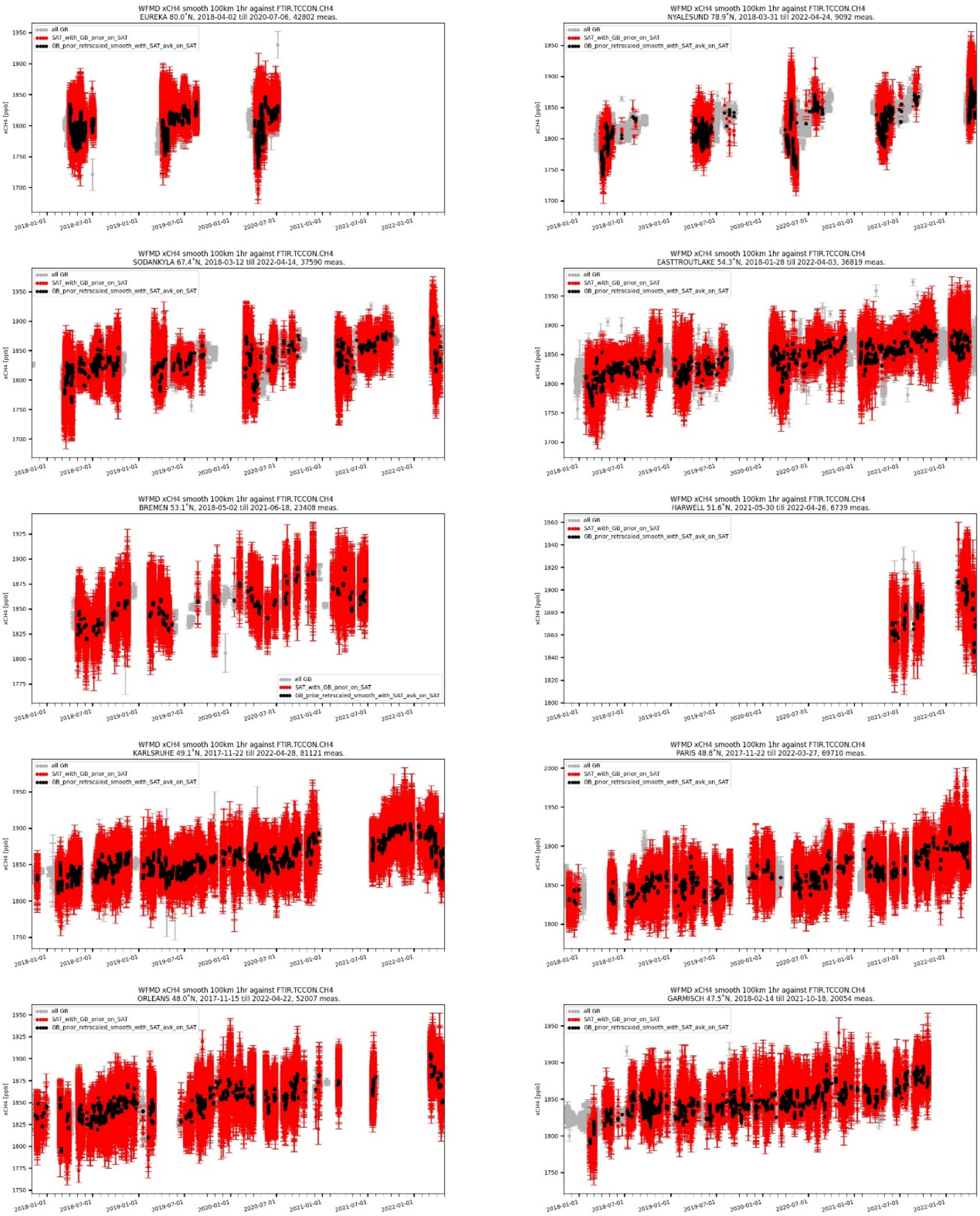

WFMD xCH4 smooth 100km 1hr against FTIR.TCCON.CH4
EUREKA 80.0°N, 2018-04-02 till 2020-07-06, 42802 meas.
WFMD xCH4 smooth 100km 1hr against FTIR.TCCON.CH4
NYALESUND 78.9°N, 2018-03-31 till 2022-04-24, 9092 meas.
WFMD xCH4 smooth 100km 1hr against FTIR.TCCON.CH4
SODANKYLA 67.4°N, 2018-03-12 till 2022-04-14, 37590 meas.
WFMD xCH4 smooth 100km 1hr against FTIR.TCCON.CH4
EASTTROUTLAKE 54.3°N, 2018-01-28 till 2022-04-03, 36819 meas.
WFMD xCH4 smooth 100km 1hr against FTIR.TCCON.CH4
BREMEN 53.1°N, 2018-05-02 till 2021-06-18, 23408 meas.
WFMD xCH4 smooth 100km 1hr against FTIR.TCCON.CH4
HARWELL 51.6°N, 2021-05-30 till 2022-04-26, 6739 meas.
WFMD xCH4 smooth 100km 1hr against FTIR.TCCON.CH4
KARLSRUHE 49.1°N, 2017-11-22 till 2022-04-28, 81121 meas.
WFMD xCH4 smooth 100km 1hr against FTIR.TCCON.CH4
PARIS 48.8°N, 2017-11-22 till 2022-03-27, 69710 meas.
WFMD xCH4 smooth 100km 1hr against FTIR.TCCON.CH4
ORLEANS 48.0°N, 2017-11-15 till 2022-04-22, 52007 meas.
WFMD xCH4 smooth 100km 1hr against FTIR.TCCON.CH4
GARMISCH 47.5°N, 2018-02-14 till 2021-10-18, 20054 meas.
all GB
SAT_with_GB_prior_on_SAT
GB_prior_retrscaled_smooth_with_SAT_avk_on_SAT
xCH4 [ppb]

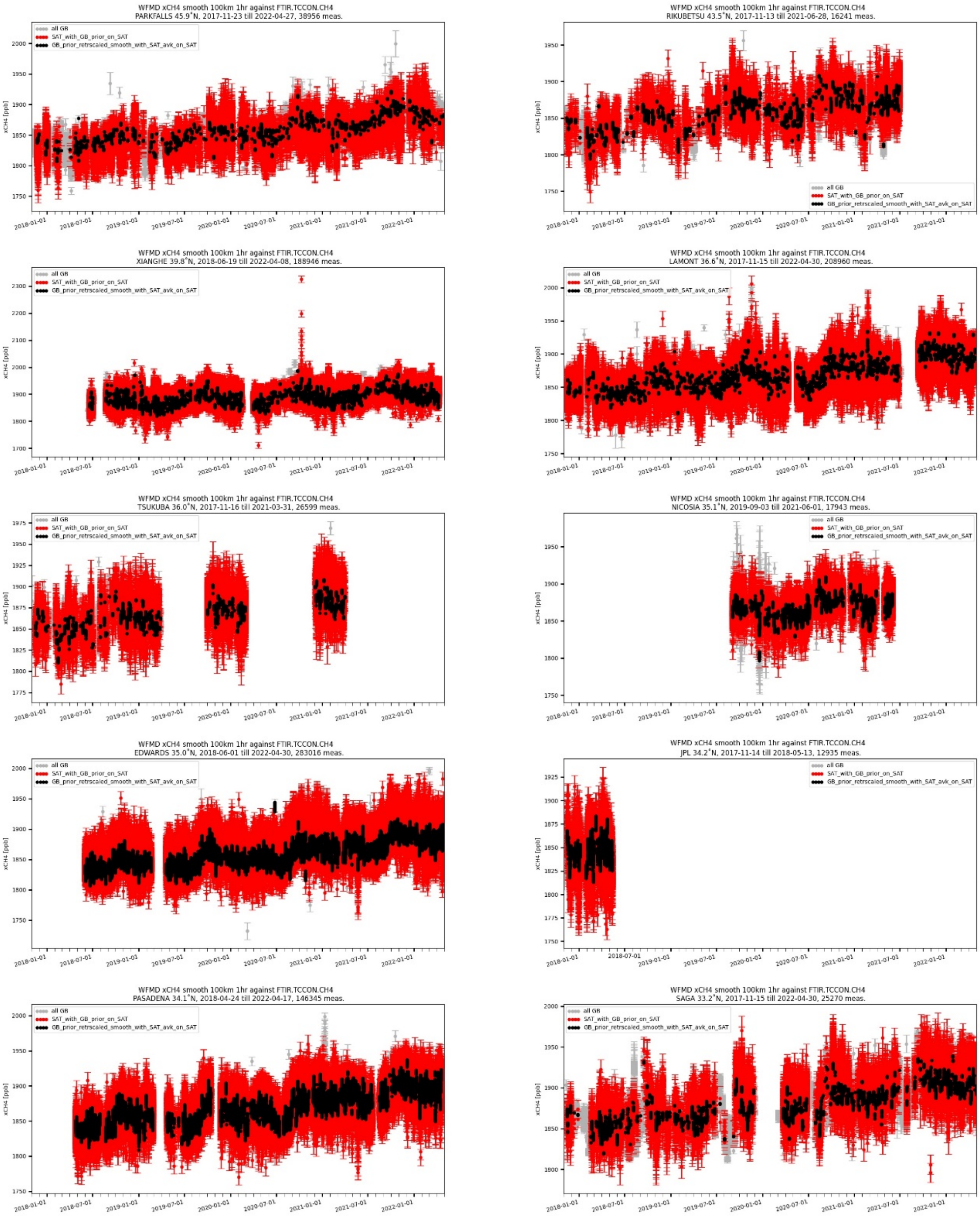
WFMD xCH4 smooth 100km 1hr against FTIR.TCCON.CH4
PARKFALLS 45.9°N, 2017-11-23 till 2022-04-27, 38956 meas.
WFMD xCH4 smooth 100km 1hr against FTIR.TCCON.CH4
RIKUBETSU 43.5°N, 2017-11-13 till 2021-06-28, 16241 meas.
WFMD xCH4 smooth 100km 1hr against FTIR.TCCON.CH4
XIANGHE 39.8°N, 2018-06-19 till 2022-04-08, 188946 meas.
WFMD xCH4 smooth 100km 1hr against FTIR.TCCON.CH4
LAMONT 36.6°N, 2017-11-15 till 2022-04-30, 208960 meas.
WFMD xCH4 smooth 100km 1hr against FTIR.TCCON.CH4
TSUKUBA 36.0°N, 2017-11-16 till 2021-03-31, 26599 meas.
WFMD xCH4 smooth 100km 1hr against FTIR.TCCON.CH4
NICOSIA 35.1°N, 2019-09-03 till 2021-06-01, 17943 meas.
WFMD xCH4 smooth 100km 1hr against FTIR.TCCON.CH4
EDWARDS 35.0°N, 2018-06-01 till 2022-04-30, 283016 meas.
WFMD xCH4 smooth 100km 1hr against FTIR.TCCON.CH4
JPL 34.2°N, 2017-11-14 till 2018-05-13, 12935 meas.
WFMD xCH4 smooth 100km 1hr against FTIR.TCCON.CH4
PASADENA 34.1°N, 2018-04-24 till 2022-04-17, 146345 meas.
WFMD xCH4 smooth 100km 1hr against FTIR.TCCON.CH4
SAGA 33.2°N, 2017-11-15 till 2022-04-30, 25270 meas.
all GB
SAT_with_GB_prior_on_SAT
GB_prior_retrscaled_smooth_with_SAT_avk_on_SAT
xCH4 [ppb]

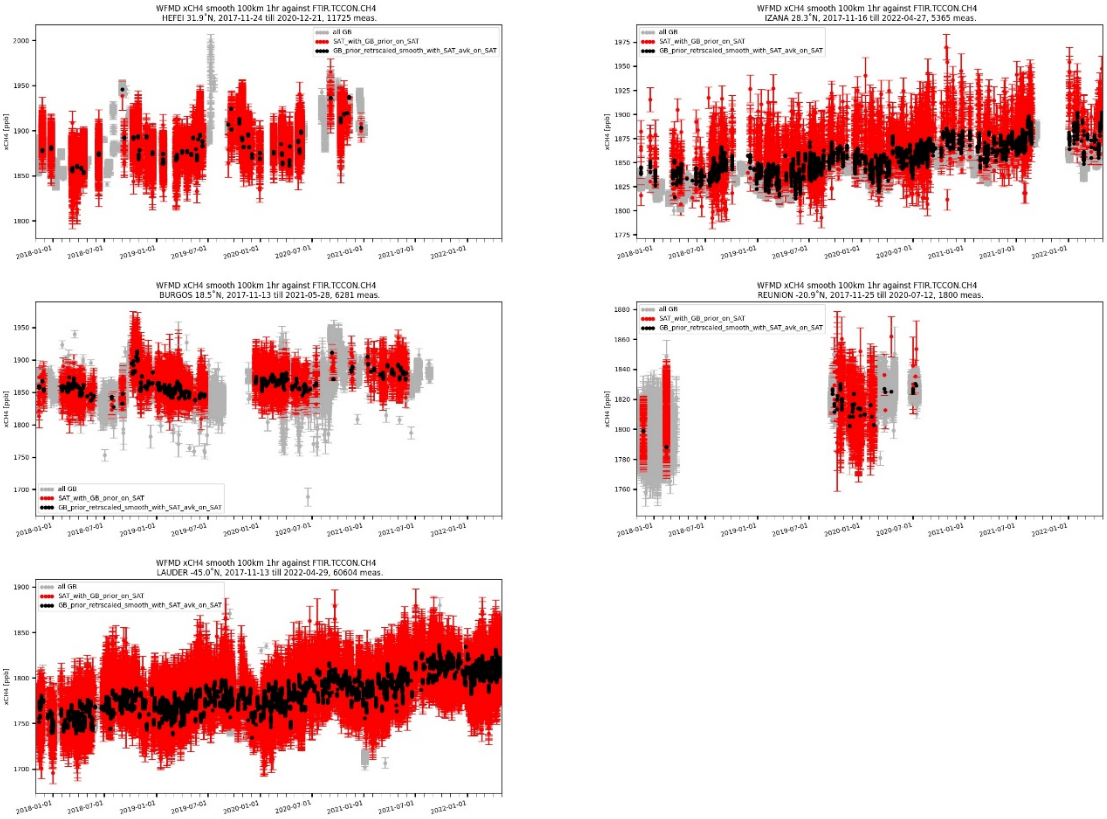

Figure 4-20: Timeseries of XCH_4 TCCON (collocated=black, all=grey) and CH4_S5P_WFMD (red) data at selected TCCON sites.

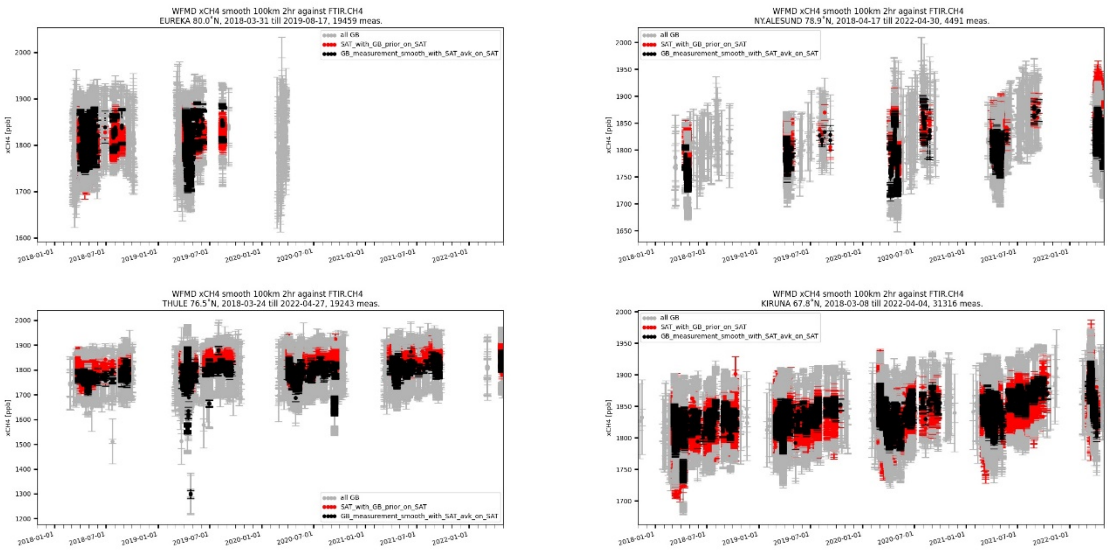

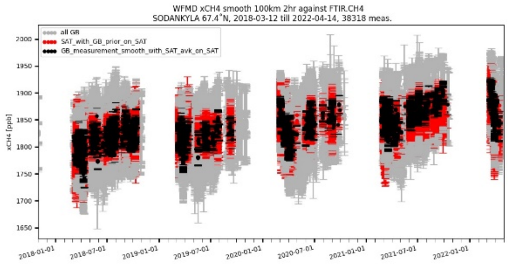
WFMD xCH4 smooth 100km 2hr against FTIR.CH4
SODANKYLA 67.4°N, 2018-03-12 till 2022-04-14, 38318 meas.

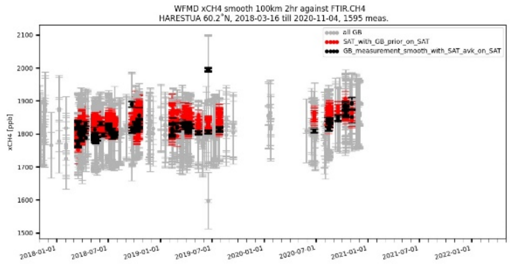
WFMD xCH4 smooth 100km 2hr against FTIR.CH4
HARESTUA 60.2°N, 2018-03-16 till 2020-11-04, 1595 meas.

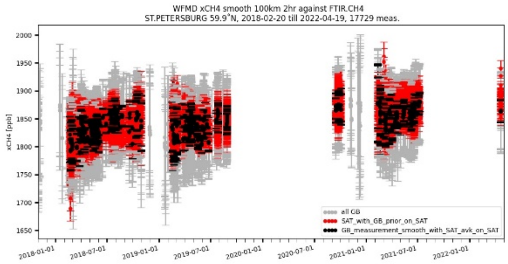
WFMD xCH4 smooth 100km 2hr against FTIR.CH4
ST.PETERSBURG 59.9°N, 2018-02-20 till 2022-04-19, 17729 meas.

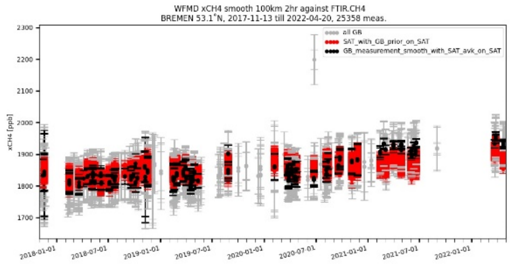
WFMD xCH4 smooth 100km 2hr against FTIR.CH4
BREMEN 53.1°N, 2017-11-13 till 2022-04-20, 25358 meas.

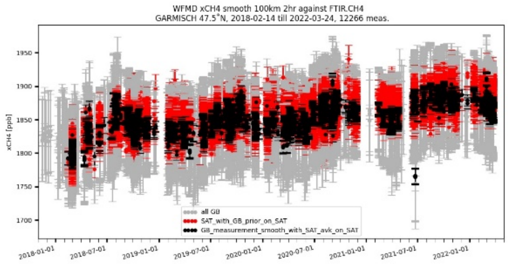
WFMD xCH4 smooth 100km 2hr against FTIR.CH4
GARMISCH 47.5°N, 2018-02-14 till 2022-03-24, 12266 meas.

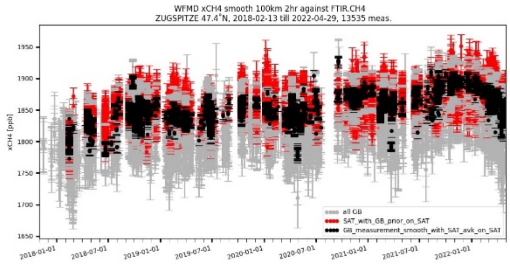
WFMD xCH4 smooth 100km 2hr against FTIR.CH4
ZUGSPITZE 47.4°N, 2018-02-13 till 2022-04-29, 13535 meas.

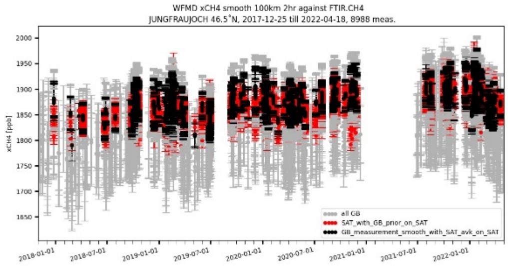
WFMD xCH4 smooth 100km 2hr against FTIR.CH4
JUNGFRAUJOCH 46.5°N, 2017-12-25 till 2022-04-18, 8988 meas.

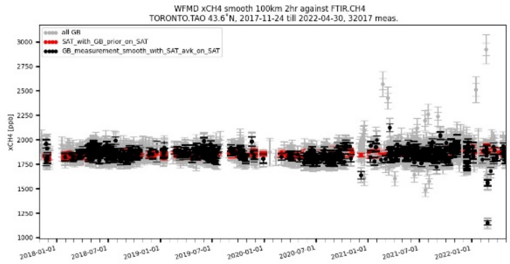
WFMD xCH4 smooth 100km 2hr against FTIR.CH4
TORONTO.TAO 43.6°N, 2017-11-24 till 2022-04-30, 32017 meas.

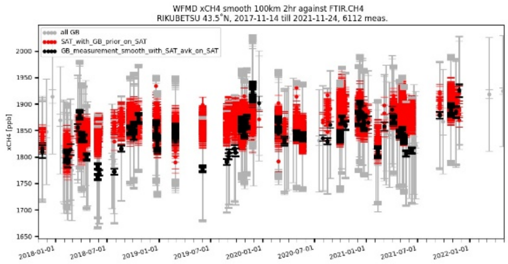
WFMD xCH4 smooth 100km 2hr against FTIR.CH4
RIKUBETSU 43.5°N, 2017-11-14 till 2021-11-24, 6112 meas.

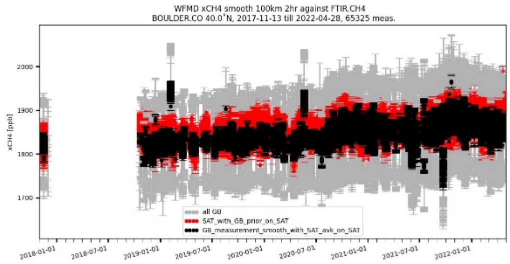
WFMD xCH4 smooth 100km 2hr against FTIR.CH4
BOULDER.CO 40.0°N, 2017-11-13 till 2022-04-28, 65325 meas.

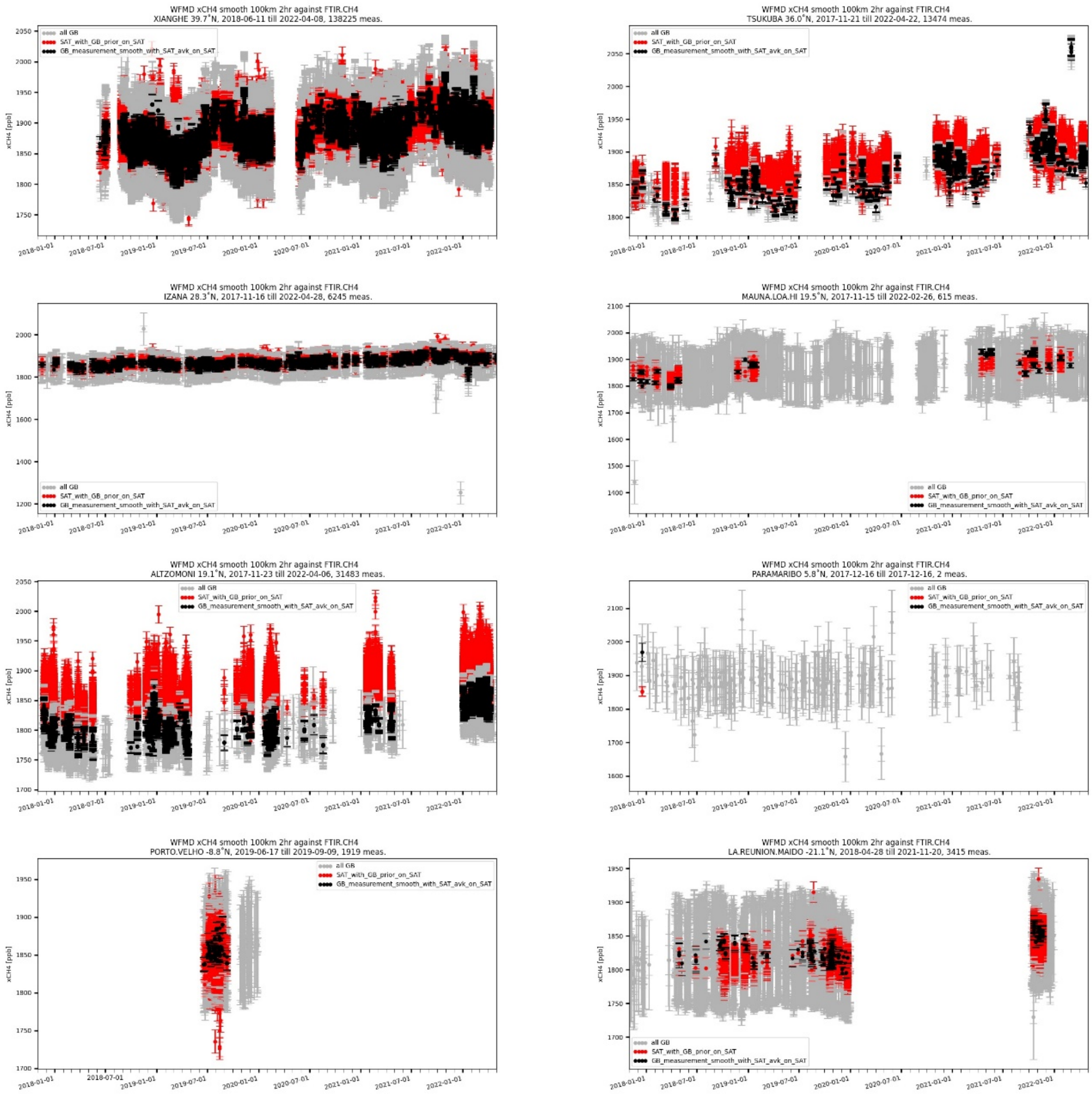

WFMD xCH4 smooth 100km 2hr against FTIR.CH4
XIANGHE 39.7˚N, 2018-06-11 till 2022-04-08, 138225 meas.
WFMD xCH4 smooth 100km 2hr against FTIR.CH4
TSUKUBA 36.0˚N, 2017-11-21 till 2022-04-22, 13474 meas.
WFMD xCH4 smooth 100km 2hr against FTIR.CH4
IZANA 28.3˚N, 2017-11-16 till 2022-04-28, 6245 meas.
WFMD xCH4 smooth 100km 2hr against FTIR.CH4
MAUNA.LOA.HI 19.5˚N, 2017-11-15 till 2022-02-26, 615 meas.
WFMD xCH4 smooth 100km 2hr against FTIR.CH4
ALTZOMONI 19.1˚N, 2017-11-23 till 2022-04-06, 31483 meas.
WFMD xCH4 smooth 100km 2hr against FTIR.CH4
PARAMARIBO 5.8˚N, 2017-12-16 till 2017-12-16, 2 meas.
WFMD xCH4 smooth 100km 2hr against FTIR.CH4
PORTO.VELHO -8.8˚N, 2019-06-17 till 2019-09-09, 1919 meas.
WFMD xCH4 smooth 100km 2hr against FTIR.CH4
LA.REUNION.MAIDO -21.1˚N, 2018-04-28 till 2021-11-20, 3415 meas.
all GB
SAT_with_GB_prior_on_SAT
GB_measurement_smooth_with_SAT_avk_on_SAT
xCH4 [ppb]

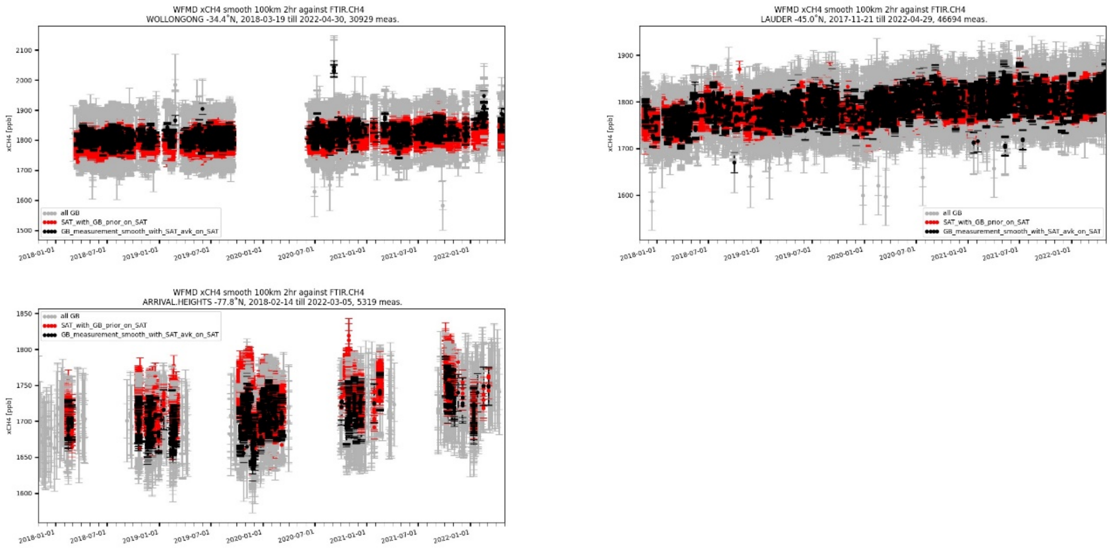

Figure 4-21: Timeseries of XCH_4 NDACC (collocated=black, all=grey) and CH4_S5P_WFMD (red) data at selected NDACC sites.

Figure 4-22 shows monthly median timeseries for TCCON and WFMD XCH_4 for all data that fall within certain latitude bands, namely all sites North of 40°N latitude (top), all sites between 40°N and the equator (mid) and all sites in the Southern hemisphere (bottom). The figures clearly show that WFMD is capable of capturing the larger scale temporal evolution of XCH_4 as well as seasonal variability.

Figure 4-23 shows the same for NDACC with high altitude stations and the Toronto site removed from the data pool. Here we see good agreement for all latitude bands, with the largest difference in slope being 0.6 (well within uncertainty bounds) at high latitudes. Also no strong deviations in the seasonality are observed.

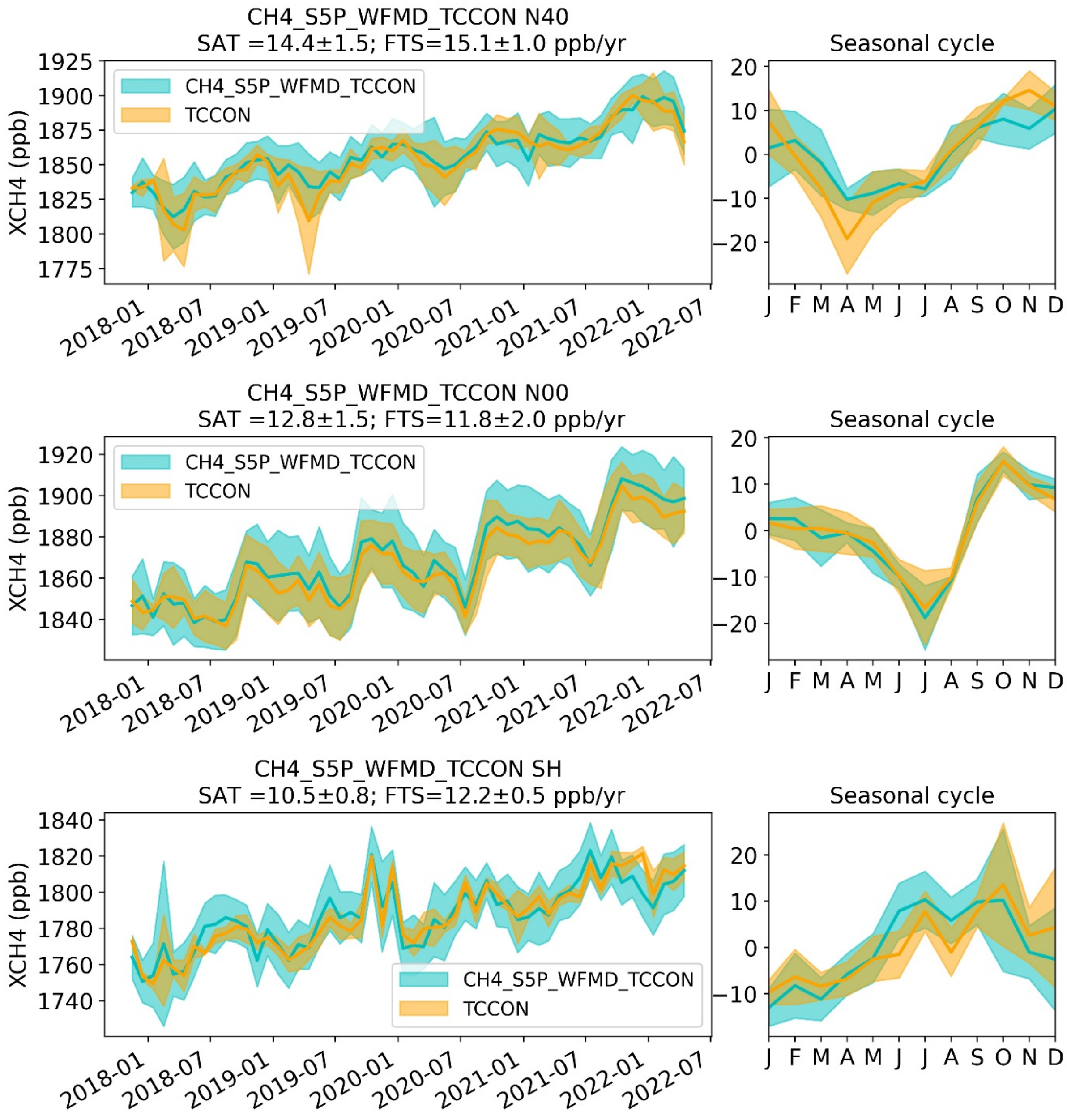

Figure 4-22: Monthly median collocated Sat and TCCON XCH_4 concentrations as a function of time and the detrended monthly medians as a function of season. The shaded areas correspond with the scaled median absolute deviation.

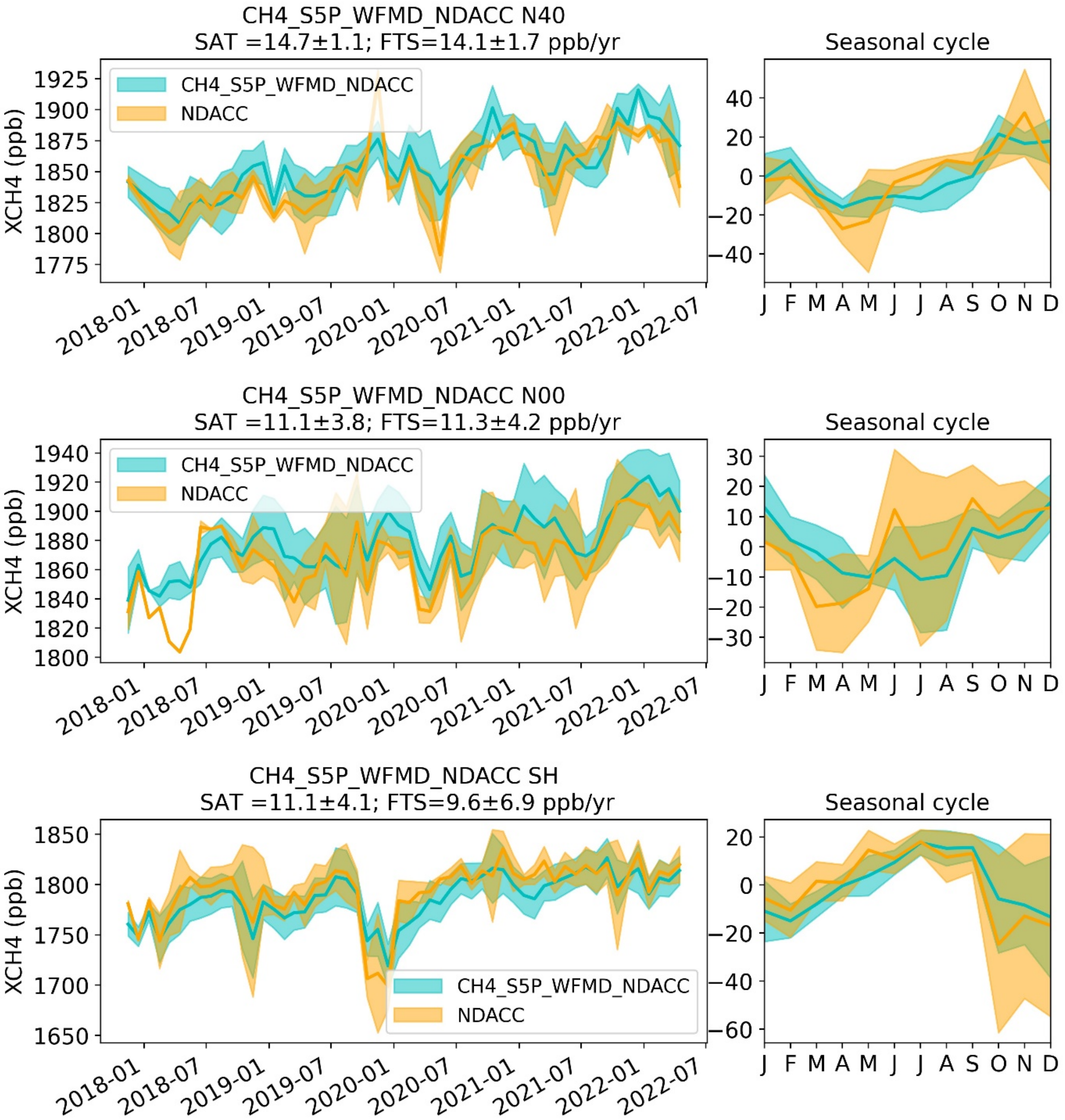

Figure 4-23: Monthly median collocated Sat and NDACC XCH_4 concentrations as a function of time and the detrended monthly medians as a function of season. The shaded areas correspond with the scaled median absolute deviation.

4.2.4.2 Summary

As with our previous assessment the current CH4_S5P_WFMD data contains little noticeable outliers. The seasonal cycles and long-term trends seem well captured. The obtained Stability equals 0.4 ppb/year with confidence bands that do not overlap 0. There could therefore be a significant but very small trend in the retrieval (still far below the linear drift requirement of <3 ppb/year). The single measurement precision equals 13.7 (previously 13.8 ppb), thus reaching the breakthrough < 17 ppb target value. The reported uncertainty sits at 0.88 times what we find in our analysis. The overall bias sits at 5.0 ppb (used to be 0).

The Relative and Seasonal relative accuracies equal 3.95 and 5.9 ppb respectively, thus reaching the <10 ppb target.

For NDACC, when excluding the high-altitude sites and Toronto, we obtain a single measurement precision 19.4 [17.9,20.8] ppb, an overall bias of 11.2 [3.0,24.4] ppb and relative accuracy values: RA 13.8 [0.4, 21.8] and SRA 16.9 [12.5,22.7]. The confidence bands for NDACC are significantly wider indicating larger inter-station differences. This naturally also manifests itself in the relative accuracy numbers, where RA strongly overlaps with the <10 ppb target, while the SRA does not. It is however safe to say that inter-station biases (even after removing high altitude sites) between the NDACC stations contribute to this number.

Table 4-11 presents an overview of the estimated data quality of CH4_S5P_WFMD, as obtained by the VALT team, from comparisons with TCCON ground-based reference observations. Values in square brackets [ ] correspond with the upper and lower 95% confidence bound on the parameter. The uncertainty ratio features 2 numbers as outlined in the validation method.

Product Quality Summary Table for Product: CH4_S5P_WFMD Level: 2, Version: v1.8, Time period covered: 11.2017 – 12.2022 Assessment: Validation Team (VALT)			
Parameter [unit]	**Achieved performance**	**Requirement**	**Comments**
Single measurement precision (1-sigma) in [ppb]	13.7 [12.0,14.8]	< 34 (T) < 17 (B) < 9 (G)	Computed as the median over all station scaled median absolute differences to TCCON
Uncertainty ratio [-]: Ratio reported uncertainty to standard deviation of satellite-TCCON difference	0.87, 0.88*	-	No requirement but value close to unity expected for a high quality data product with reliable reported uncertainty.
Mean bias (global offset) [ppb]	5.0 [3.8, 0.6]	-	No requirement but value close to zero expected for a high quality data product.
Accuracy: Relative systematic error [ppb]	Spatial: 3.9 [0.4,6.2] Spatio-temporal: 5.9 [4.8,7.4]	< 10	Spatial: Computed as standard deviation of the biases at the various TCCON sites. Spatio-temporal: As “Spatial” but also considering seasonal biases.
Stability: Drift [ppb/year]	0.4 [0.1,0.8]	< 3	Linear drift

4.2.5 Validation results for product CH4_GO2_SRFP

Below we show the validation results of the XCH_4 concentrations as derived by the CH4_GO2_SRFP v2.0.2 algorithm using GOSAT-2 spectra, FP standing for the Full Physics version of the algorithm developed at SRON. Data was available from February 2019 up to and including December 2021. The SRFP algorithm provides *a priori* and column averaging kernel information on a 12 layer profile.

4.2.5.1 Detailed results

The Taylor diagram above in **Figure 4-24** yields a concise overview of the capabilities of the CH4_GO2_SRFP algorithm with respect to the TCCON network. Most TCCON sites are nicely clustered apart from Eureka (negative correlation) which exhibits a limited seasonal cycle (only FTIR measurements in spring-summer) and data pair availability. Also Harwell and Reunion have lower correlation and relative standard deviations (again limited data and temporal coverage). All other sites cluster between the 0.5 and 0.8 correlation line. TCCON yields standard deviations that are 0.5 to 0.9 times that of the algorithm and the relative standard deviation of the bias sits around 0.8.

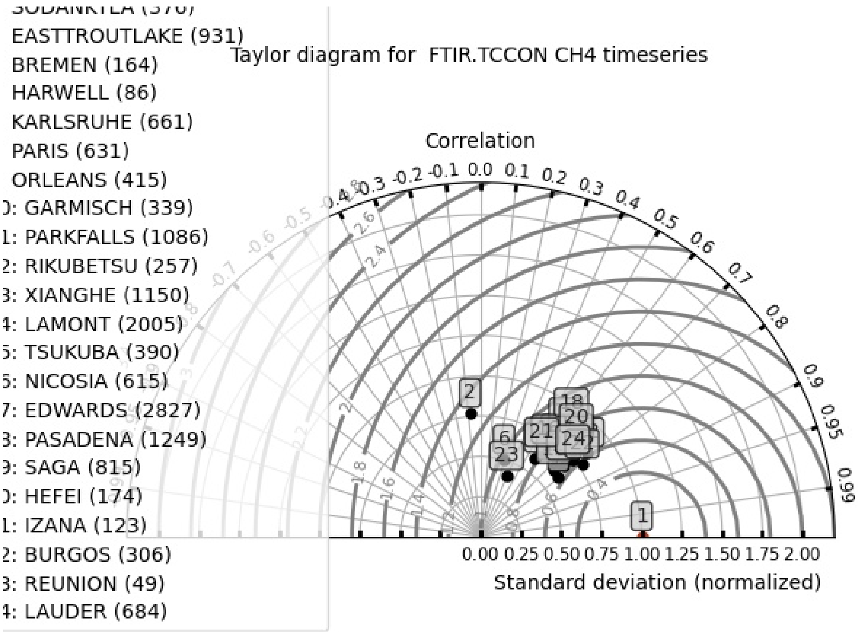

Figure 4-24: Tayor plot of XCH_4 TCCON values relative to CH4_GO2_SRFP. Straight lines correspond with the correlation, light grey lines yield the variability of the TCCON data relative to the satellite variability and the dark grey lines correspond with the variability of the Satellite -TCCON bias relative to the satellite variability.

For NDACC (**Figure 4-25**) we again see much more dispersion with strong outliers at Toronto, Mauna Loa and Rikubetsu. Correlations are generally weaker compared to TCCON, whereas its variability relative to the FTIR measurements is lower (indicating higher variability in NDACC).

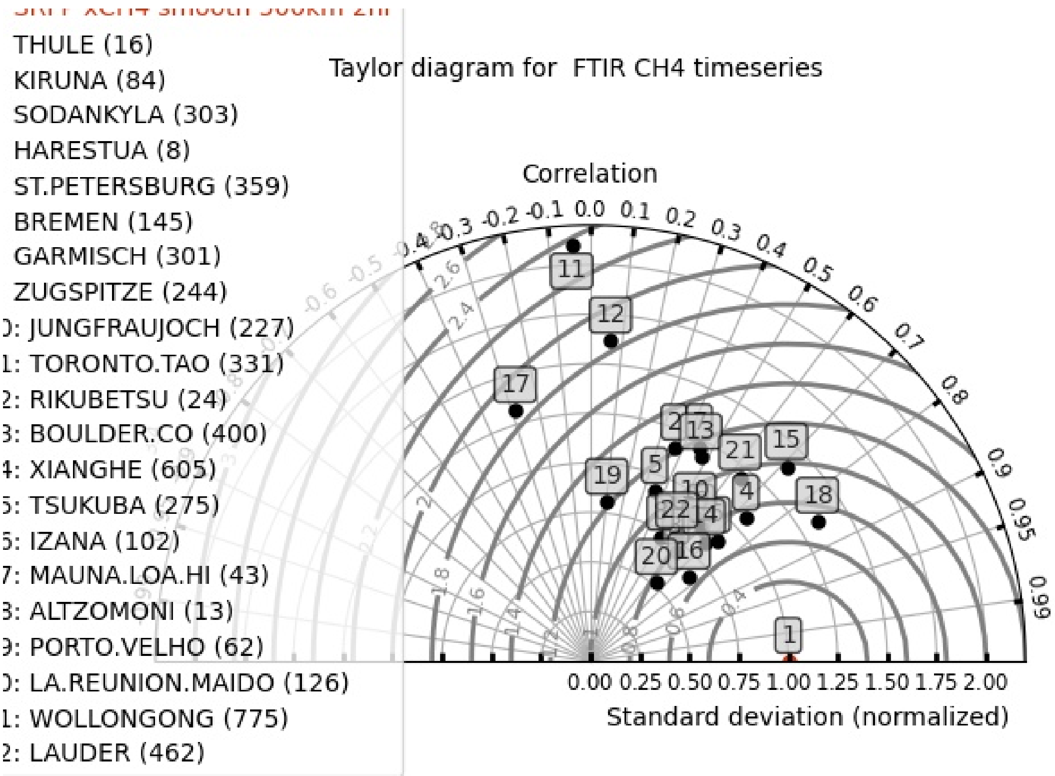

Figure 4-25: Tayor plot of XCH_4 NDACC values relative to CH4_GO2_SRFP. Straight lines correspond with the correlation, light grey lines yield the variability of the TCCON data relative to the satellite variability and the dark grey lines correspond with the variability of the Satellite -TCCON bias relative to the satellite variability.

Again, it is hard to discern a pattern in the mosaic plots which shows the mean bi-weekly bias between the satellite and FTS measurement pairs (**Figure 4-26 and 4-27**), particularly for NDACC which shows substantial data gaps across all latitudes. One of the few stations for which we have a near complete coverage, namely Toronto, again (as with WFMD XCH_4) shows a shift in the bias over time, most likely due to a degradation in the Toronto data quality (see **Figure 4-29**). For TCCON. no station clearly stands out. Less obvious as with its XCO2 counterpart, one could again notice slightly more prevalent negative biases in the 10-2019 to 7-2020 time window, but again not across all stations. Inversely one could also state that biases seem to increase around January 2021. At this point it is too early to say that these are clear indications of any issues with the algorithm. However, they do point to areas of interest for further investigation.

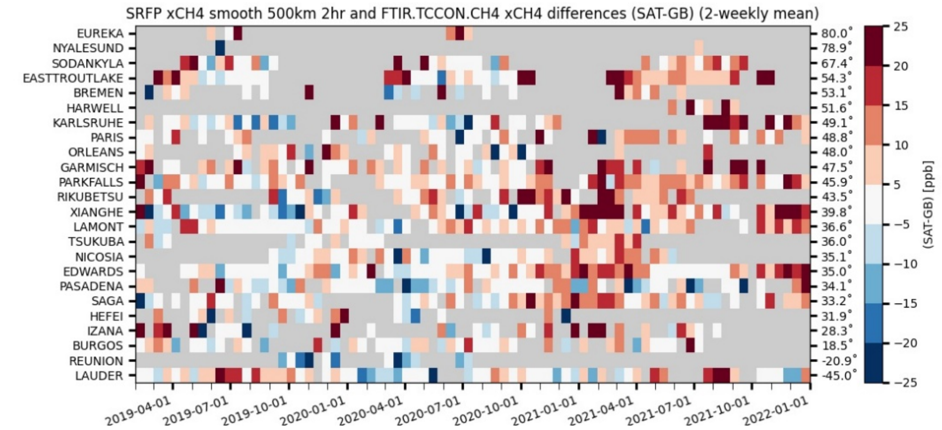

Figure 4-26. Mosaic plot of bi-weekly mean CH4_GO2_SRFP – TCCON XCH_4 biases as a function of time and TCCON station.

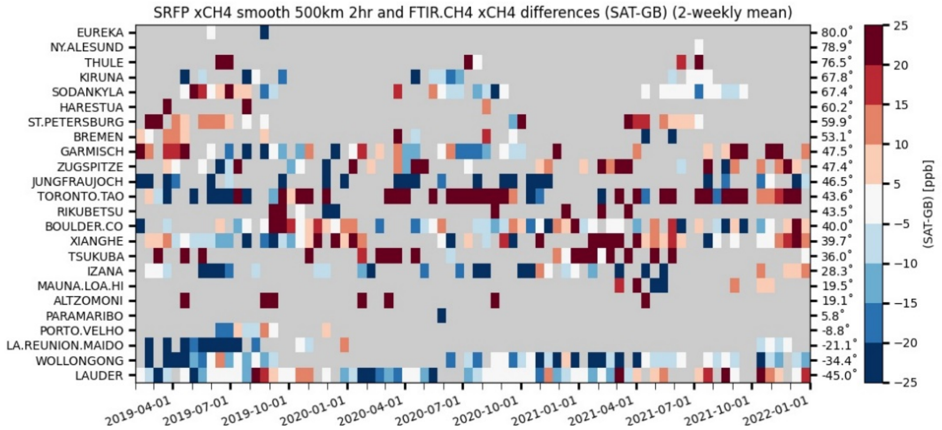

Figure 4-27. Mosaic plot of bi-weekly mean CH4_GO2_SRFP – NDACC XCH_4 biases as a function of time and NDACC station.

Table 4-12 lists all bias and scatter results derived from individual data pairs at all TCCON stations. The algorithm produces on average 400 data pairs per station (slightly more than its XCO2 counterpart), which corresponds with ~125 pairs per station per year. Several stations however have far less collocated measurements (Ny Alesund has only 3 data pairs, Reunion and Eureka less than 50) hampering an accurate assessment of the data quality at these sites. The observed median bias ranges between -19.2 (Ny Alesund) and 11.4 (Harwell), while the scatter ranges between 11.0 ppb (Reunion) and 17.8 ppb (Ny Alesund. The long term bias ranges between -2.0 ppb/year (Orleans) and 9.7 ppb/year (Xianghe). Apart from 2 sites (Orleans and Pasadena, all trends are positive. The overall correlation using all collocated data regardless of station equals 0.84.

Table 4-12: Number of collocated data pairs (N), Correlation (R), Bias, Scatter, long term trend difference (ltt) and uncertainty thereon (ltt_err), seasonal amplitude difference (A) and uncertainty thereon (A_err) as well as the latitude of the TCCON station. The last row lists the median values over all stations. Product: CH4_GO2_SRFP.

STATION	N	R	Bias	Scat	ltt	ltt_err	A	A_err	lat
EUREKA	48	-0.09	5.29	17.78	-	-	-	-	80
NYALESUND	3	0.99	-19.22	15.94	-	-	-	-	78.9
SODANKYLA	376	0.72	5.19	13.37	3.68	1.99	13.74	5.40	67.4
EASTTROUTLAKE	931	0.69	5.39	15.27	4.04	1.34	11.54	2.22	54.3
BREMEN	164	0.63	4.56	16.31	4.70	2.58	4.01	5.60	53.1
HARWELL	86	0.29	11.36	11.69	-	-	-	-	51.6
KARLSRUHE	661	0.79	3.48	15.64	8.72	3.72	0.93	2.20	49.1
PARIS	631	0.73	5.52	14.27	6.07	1.55	3.65	2.08	48.8
ORLEANS	415	0.57	4.62	14.08	-2.03	2.57	2.94	2.98	48
GARMISCH	339	0.72	8.26	17.27	6.79	2.87	4.99	2.46	47.5
PARKFALLS	1086	0.73	5.58	15.37	2.65	1.15	3.37	1.51	45.9
RIKUBETSU	257	0.79	9.03	12.67	7.65	3.53	3.55	2.71	43.5
XIANGHE	1150	0.63	2.99	21.6	9.66	1.41	12.34	1.95	39.8
LAMONT	2005	0.74	4.34	14.17	3.93	1.07	0.57	1.20	36.6
TSUKUBA	390	0.74	1.58	12.88	5.34	1.91	4.57	2.32	36
NICOSIA	615	0.61	4.12	13.01	-	-	-	-	35.1
EDWARDS	2827	0.76	4.98	15.72	3.53	1.17	5.24	1.04	35
PASADENA	1249	0.62	-2.98	16.78	-0.33	1.45	5.57	1.68	34.1
SAGA	815	0.77	3.68	13.48	2.81	1.84	5.65	1.74	33.2
HEFEI	174	0.7	2.89	13.27	-	-	-	-	31.9
IZANA	123	0.59	2.1	17.62	2.99	2.89	14.11	3.20	28.3
BURGOS	306	0.81	3.11	11.47	2.39	1.44	2.36	1.72	18.5
REUNION	49	0.39	-9.9	11.04	-	-	-	-	-20.9
LAUDER	684	0.77	1.99	12.96	2.13	1.82	10.30	1.63	-45
MEDIAN	**402.5**	**0.72**	**4.23**	**14.22**	**3.81**	**1.83**	**4.78**	**2.14**	**41.7**

Table 4-13: Number of collocated data pairs (N), Correlation (R), Bias, Scatter, long term trend difference (ltt) and uncertainty thereon (ltt_err), seasonal amplitude difference (A) and uncertainty thereon (A_err) as well as the latitude of the NDACC station. The last row lists the median values over all stations. Product: CH4_GO2_SRFP.

STATION	N	R	Bias	Scat	ltt	ltt_err	A	A_err	lat
EUREKA	2	-1	-16.1	24.37	-	-	-	-	80
NY.ALESUND	1	nan	-1.22	0	-	-	-	-	78.8
THULE	16	0.37	28.2	17.54	1.21	3.53	243.48	99.27	76.5
KIRUNA	84	0.62	-8.14	12.71	6.45	3.39	3.07	13.2	67.8
SODANKYLA	303	0.74	-1.88	14.47	-4.06	2.27	9.11	6.18	67.3
HARESTUA	8	0.35	31.14	14.15	-	-	-	-	60.1
ST.PETERSBURG	359	0.72	8.67	12.2	2.37	2.12	11.91	3.01	59.7
BREMEN	145	0.45	7.8	19.07	-5.8	23.63	11.64	15.73	53
GARMISCH	301	0.49	-1.18	23.37	9.46	7.63	13.59	3.38	47.4
ZUGSPITZE	244	0.64	4.66	21.91	11.91	2.59	8.82	4.89	47.4
JUNGFRAUJOCH	227	0.59	-29.27	25.19	9.59	6.34	8.33	5.58	46.5
TORONTO.TAO	331	-0.04	28.27	45.13	23.61	12.96	5.56	8.23	43.5
RIKUBETSU	24	0.06	47.76	23.89	-	-	-	-	43.4
BOULDER.CO	400	0.48	1.14	16.73	0.29	4.16	5.91	3.28	40
XIANGHE	605	0.69	1.53	19.67	6.28	1.44	14.56	2.15	39.7
TSUKUBA	275	0.71	28.7	21.07	-6.51	3.98	10.46	7.77	36
IZANA	102	0.76	-14.24	15.36	-0.37	3.51	13.51	3.12	28.3
MAUNA.LOA.HI	43	-0.29	-10.15	33.06	-	-	-	-	19.5
ALTZOMONI	13	0.85	55.36	8.13	-0.37	4.34	7.26	8.95	19.1
PARAMARIBO	1	nan	-211.62	0	-	-	-	-	5.8
PORTO.VELHO	62	0.1	-2.68	16.21	-	-	-	-	-8.7
LA.REUNION.MAIDO	126	0.64	-12.93	16.61	1.24	6.4	12.11	4.46	-21.1
WOLLONGONG	775	0.63	-9.22	16.57	5.17	2.73	16.25	2.98	-34.4
LAUDER	462	0.57	-1.13	16.28	6.76	3.42	10.57	2.51	-45
MEDIAN	**135.5**	**0.58**	**-1.155**	**16.67**	**2.37**	**3.53**	**10.57**	**4.89**	**43.45**

Table 4-13 lists the same variables but now for the NDACC stations. Here again we sometimes have very little overlap between the ground-based and satellite measurements. Ny Alesund, Harestua, Paramaribo (1 data pair!) feature less than 10 data pairs, Thule, Rikubetsu, Mauna Loa and Altzomoni less than 50. Ignoring these low data volume stations, the correlation coefficient ranges between 0.10 (Porto Velho) and 0.76 (Izaña). The bias ranges between -29.3 ppb (Jungfraujoch) and 28.3 ppb (Toronto) while the scatter ranges between 12.2 ppb (St. Petersburg) and 25.2 ppb (Jubgfraujoch). Note that the scatter at Toronto is 45.1 ppb, but (as can be seen in **Figure 4-29** this is mainly due to the large amount of scatter present in the ground-based FTIR data at this location.

The timeseries below in **Figure 4-28** show individual satellite and ground-based TCCON measurements, while **Figure 4-29** does the same for NDACC. For TCCON we see that SRFP generally manages to capture the seasonal cycle. While the scatter is somewhat higher for SRFP XCH_4, compared to TCCON, it is relatively free of outliers..

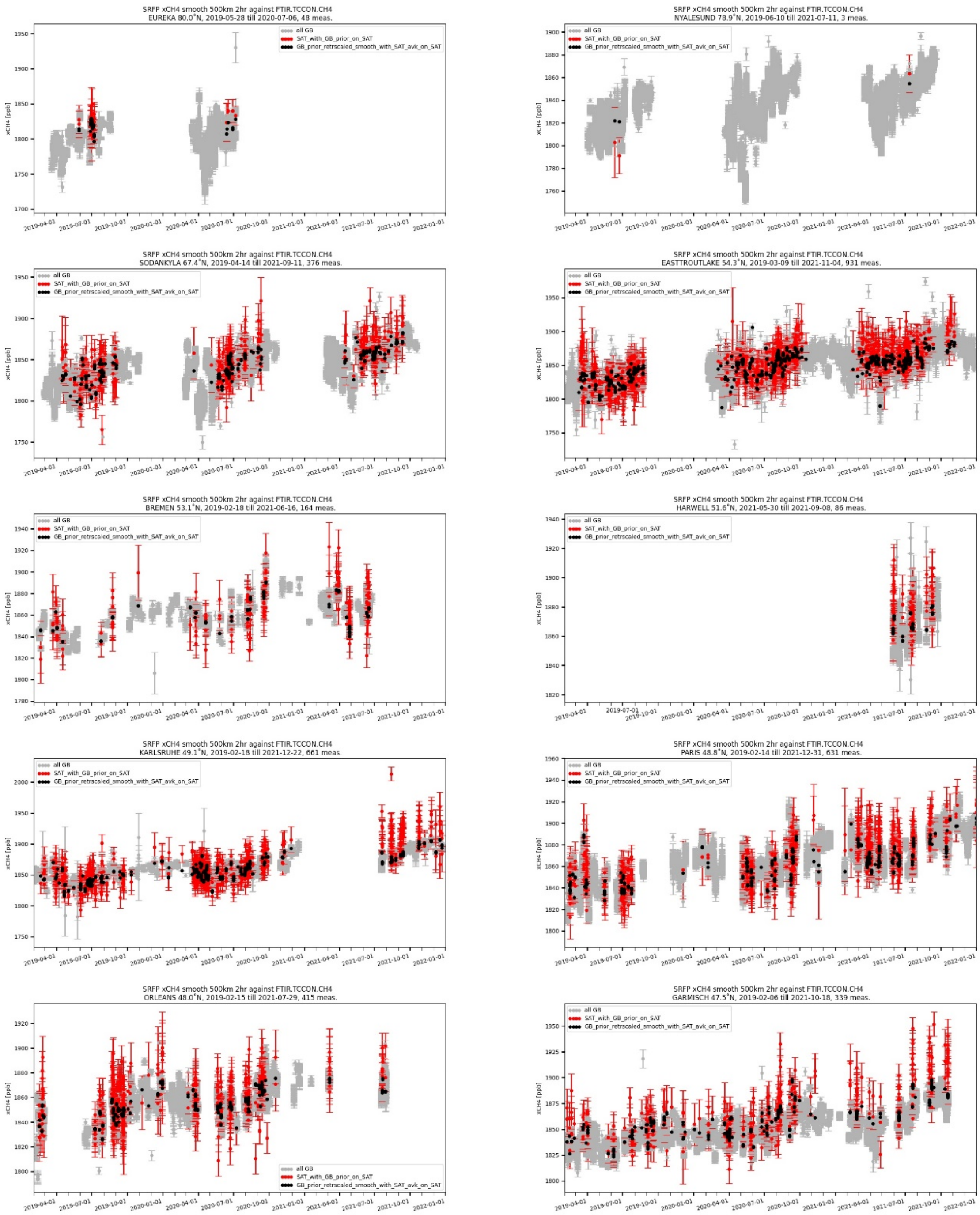

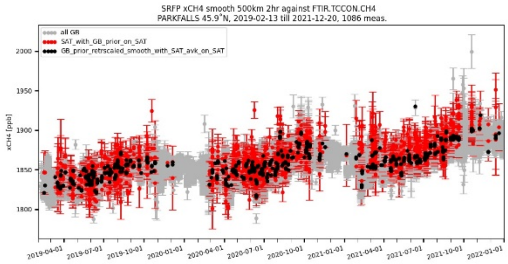
SRFP xCH4 smooth 500km 2hr against FTIR.TCCON.CH4
PARKFALLS 45.9°N, 2019-02-13 till 2021-12-20, 1086 meas.
all GB
SAT_with_GB_prior_on_SAT
GB_prior_retrscaled_smooth_with_SAT_avk_on_SAT

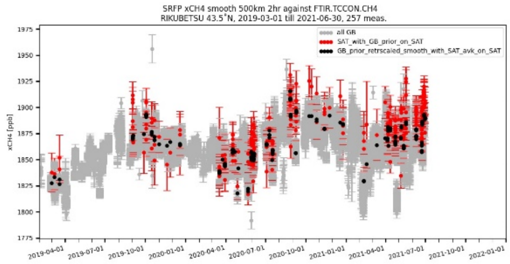
SRFP xCH4 smooth 500km 2hr against FTIR.TCCON.CH4
RIKUBETSU 43.5°N, 2019-03-01 till 2021-06-30, 257 meas.
all GB
SAT_with_GB_prior_on_SAT
GB_prior_retrscaled_smooth_with_SAT_avk_on_SAT

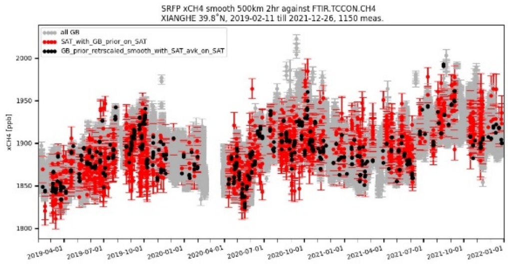
SRFP xCH4 smooth 500km 2hr against FTIR.TCCON.CH4
XIANGHE 39.8°N, 2019-02-11 till 2021-12-26, 1150 meas.
all GB
SAT_with_GB_prior_on_SAT
GB_prior_retrscaled_smooth_with_SAT_avk_on_SAT

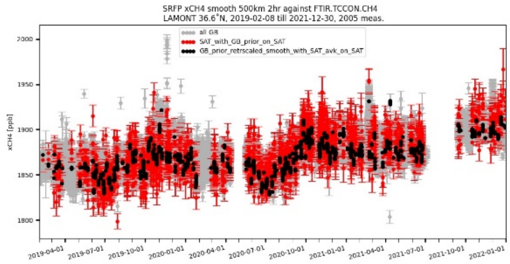
SRFP xCH4 smooth 500km 2hr against FTIR.TCCON.CH4
LAMONT 36.6°N, 2019-02-08 till 2021-12-30, 2005 meas.
all GB
SAT_with_GB_prior_on_SAT
GB_prior_retrscaled_smooth_with_SAT_avk_on_SAT

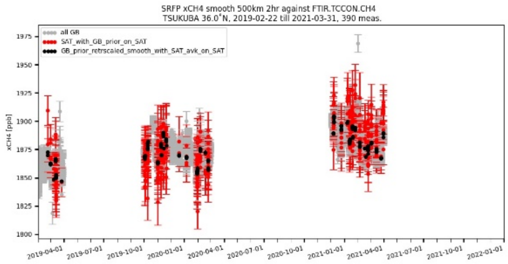
SRFP xCH4 smooth 500km 2hr against FTIR.TCCON.CH4
TSUKUBA 36.0°N, 2019-02-22 till 2021-03-31, 390 meas.
all GB
SAT_with_GB_prior_on_SAT
GB_prior_retrscaled_smooth_with_SAT_avk_on_SAT

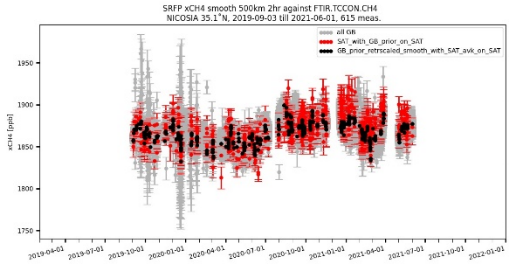
SRFP xCH4 smooth 500km 2hr against FTIR.TCCON.CH4
NICOSIA 35.1°N, 2019-09-03 till 2021-06-01, 615 meas.
all GB
SAT_with_GB_prior_on_SAT
GB_prior_retrscaled_smooth_with_SAT_avk_on_SAT

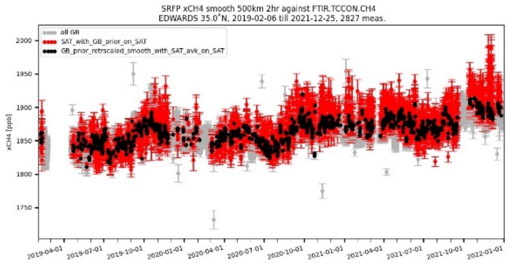
SRFP xCH4 smooth 500km 2hr against FTIR.TCCON.CH4
EDWARDS 35.0°N, 2019-02-06 till 2021-12-25, 2827 meas.
all GB
SAT_with_GB_prior_on_SAT
GB_prior_retrscaled_smooth_with_SAT_avk_on_SAT

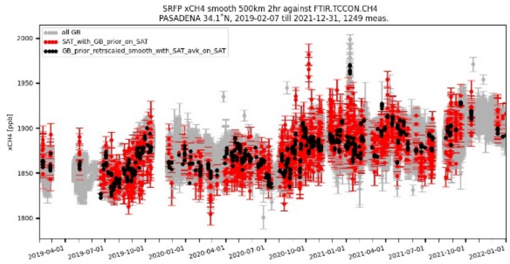
SRFP xCH4 smooth 500km 2hr against FTIR.TCCON.CH4
PASADENA 34.1°N, 2019-02-07 till 2021-12-31, 1249 meas.
all GB
SAT_with_GB_prior_on_SAT
GB_prior_retrscaled_smooth_with_SAT_avk_on_SAT

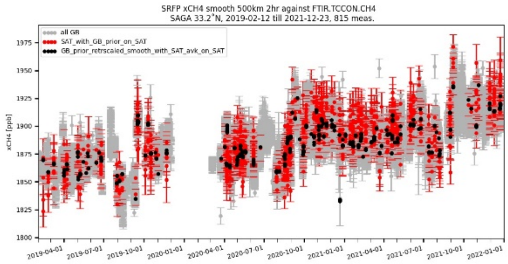
SRFP xCH4 smooth 500km 2hr against FTIR.TCCON.CH4
SAGA 33.2°N, 2019-02-12 till 2021-12-23, 815 meas.
all GB
SAT_with_GB_prior_on_SAT
GB_prior_retrscaled_smooth_with_SAT_avk_on_SAT

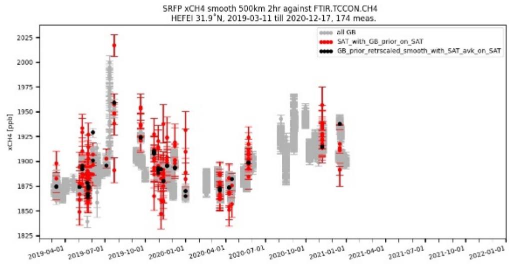
SRFP xCH4 smooth 500km 2hr against FTIR.TCCON.CH4
HEFEI 31.9°N, 2019-03-11 till 2020-12-17, 174 meas.
all GB
SAT_with_GB_prior_on_SAT
GB_prior_retrscaled_smooth_with_SAT_avk_on_SAT

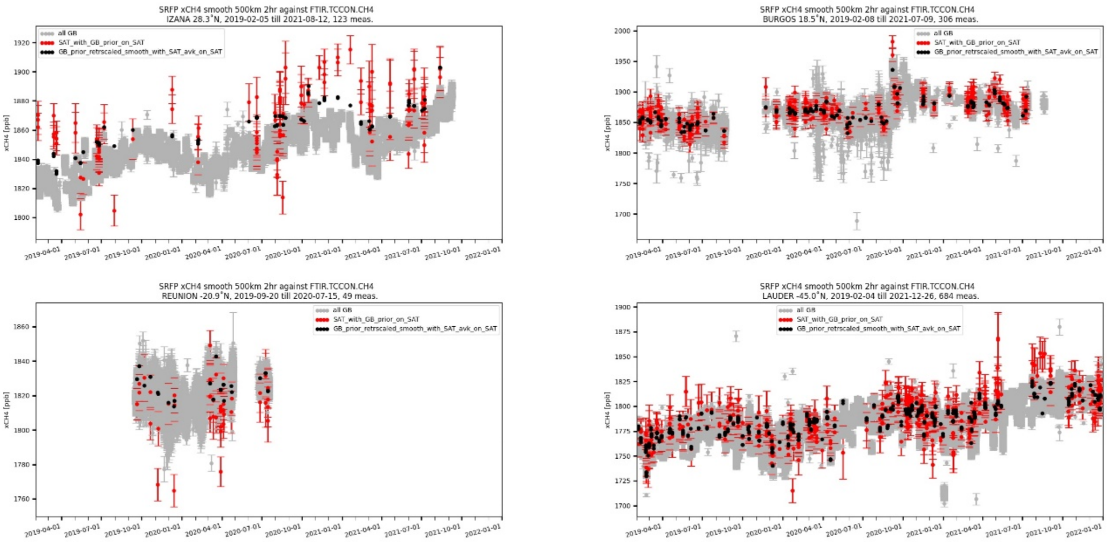

Figure 4-28: XCH_4 timeseries at all TCCON sites (red= CH4_GO2_SRFP data, black is collocated TCCON data and grey are the uncollocated TCCON data).

For NDACC it is clear that SRFP exhibits the same or at some stations even smaller temporal variability than NDACC. Also crealy visible is the sparsness of the dataset, with either little coverage at all, or significant datagaps in the timeseries. For stations where we do have consistent longer sampling, such as Garmisch, Boulder and Lauder, we see that NDACC and SRFP are in good agreement. For Toronto we clearly see the high variability in the NDACC data, worsening in the later stages of the time series, it is therefore not clear whether the strong trend that is observed at this station is real or a sampling issue.

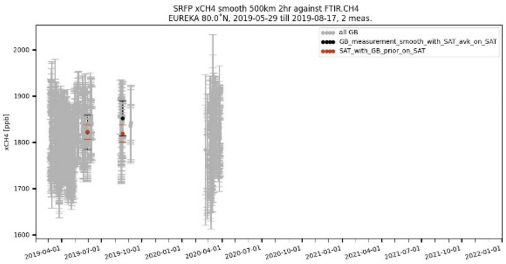
SRFP xCH4 smooth 500km 2hr against FTIR.CH4
EUREKA 80.0°N, 2019-05-29 till 2019-08-17, 2 meas.

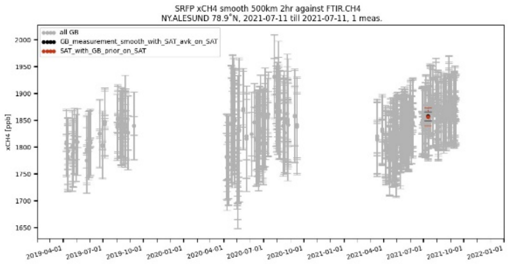
SRFP xCH4 smooth 500km 2hr against FTIR.CH4
NYALESUND 78.9°N, 2021-07-11 till 2021-07-11, 1 meas.

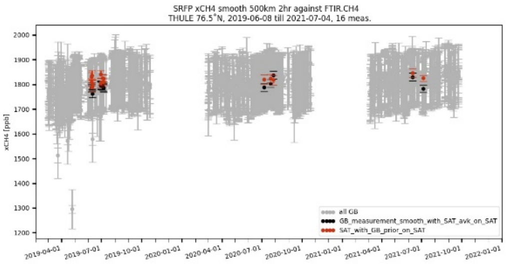
SRFP xCH4 smooth 500km 2hr against FTIR.CH4
THULE 76.5°N, 2019-06-08 till 2021-07-04, 16 meas.

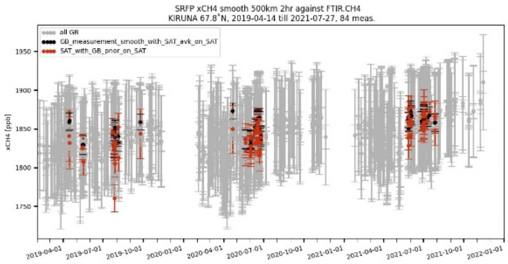
SRFP xCH4 smooth 500km 2hr against FTIR.CH4
KIRUNA 67.8°N, 2019-04-14 till 2021-07-27, 84 meas.

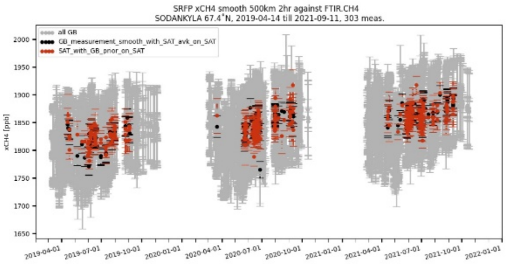
SRFP xCH4 smooth 500km 2hr against FTIR.CH4
SODANKYLA 67.4°N, 2019-04-14 till 2021-09-11, 303 meas.

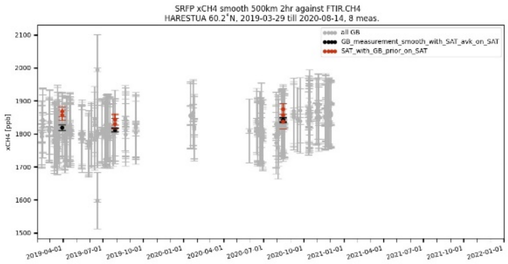
SRFP xCH4 smooth 500km 2hr against FTIR.CH4
HARESTUA 60.2°N, 2019-03-29 till 2020-08-14, 8 meas.

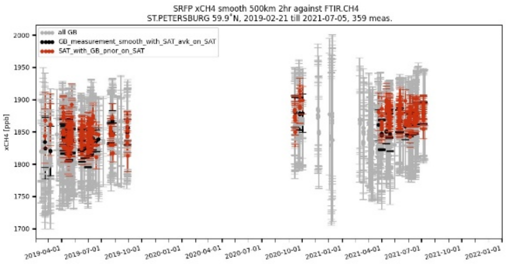
SRFP xCH4 smooth 500km 2hr against FTIR.CH4
ST.PETERSBURG 59.9°N, 2019-02-21 till 2021-07-05, 359 meas.

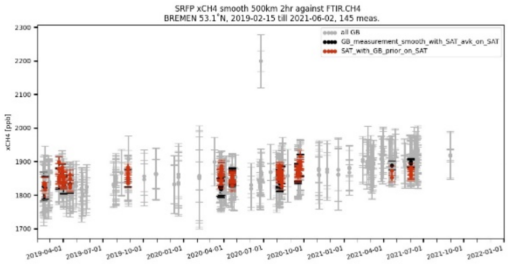
SRFP xCH4 smooth 500km 2hr against FTIR.CH4
BREMEN 53.1°N, 2019-02-15 till 2021-06-02, 145 meas.

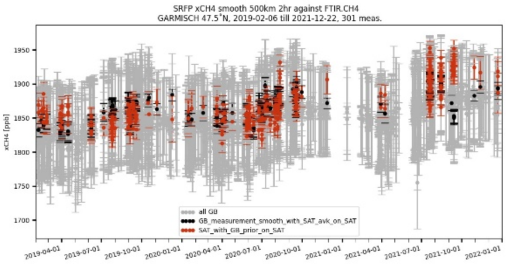
SRFP xCH4 smooth 500km 2hr against FTIR.CH4
GARMISCH 47.5°N, 2019-02-06 till 2021-12-22, 301 meas.

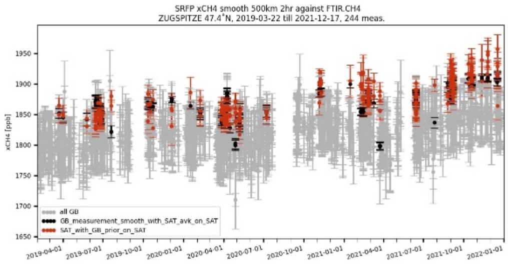
SRFP xCH4 smooth 500km 2hr against FTIR.CH4
ZUGSPITZE 47.4°N, 2019-03-22 till 2021-12-17, 244 meas.

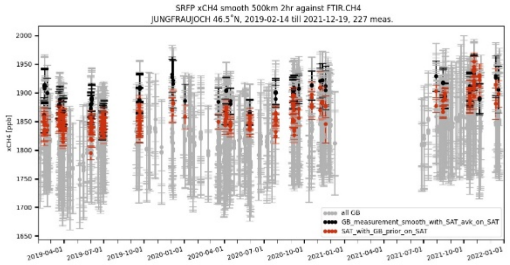
SRFP xCH4 smooth 500km 2hr against FTIR.CH4
JUNGFRAUJOCH 46.5°N, 2019-02-14 till 2021-12-19, 227 meas.
all GB
GB_measurement_smooth_with_SAT_avk_on_SAT
SAT_with_GB_prior_on_SAT

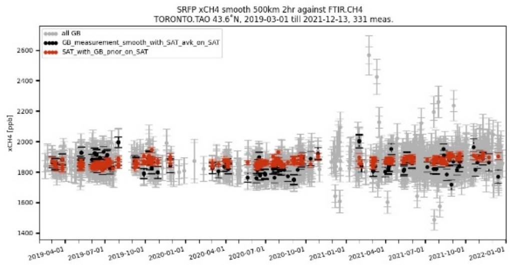
SRFP xCH4 smooth 500km 2hr against FTIR.CH4
TORONTO.TAO 43.6°N, 2019-03-01 till 2021-12-13, 331 meas.
all GB
GB_measurement_smooth_with_SAT_avk_on_SAT
SAT_with_GB_prior_on_SAT

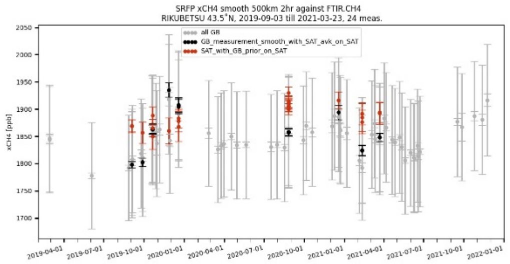
SRFP xCH4 smooth 500km 2hr against FTIR.CH4
RIKUBETSU 43.5°N, 2019-09-03 till 2021-03-23, 24 meas.
all GB
GB_measurement_smooth_with_SAT_avk_on_SAT
SAT_with_GB_prior_on_SAT

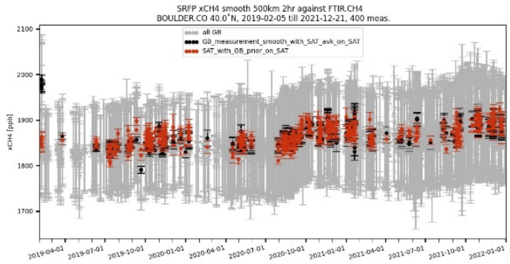
SRFP xCH4 smooth 500km 2hr against FTIR.CH4
BOULDER.CO 40.0°N, 2019-02-05 till 2021-12-21, 400 meas.
all GB
GB_measurement_smooth_with_SAT_avk_on_SAT
SAT_with_GB_prior_on_SAT

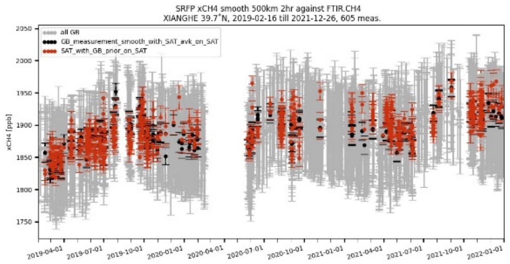
SRFP xCH4 smooth 500km 2hr against FTIR.CH4
XIANGHE 39.7°N, 2019-02-16 till 2021-12-26, 605 meas.
all GB
GB_measurement_smooth_with_SAT_avk_on_SAT
SAT_with_GB_prior_on_SAT

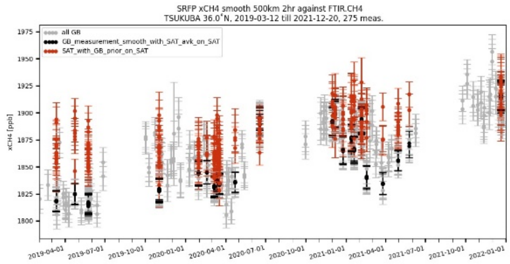
SRFP xCH4 smooth 500km 2hr against FTIR.CH4
TSUKUBA 36.0°N, 2019-03-12 till 2021-12-20, 275 meas.
all GB
GB_measurement_smooth_with_SAT_avk_on_SAT
SAT_with_GB_prior_on_SAT

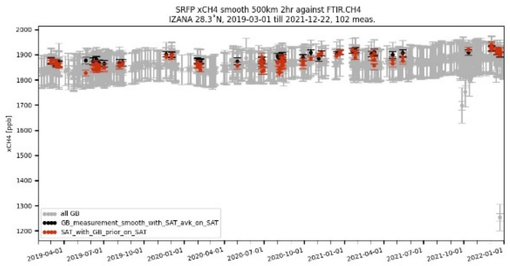
SRFP xCH4 smooth 500km 2hr against FTIR.CH4
IZANA 28.3°N, 2019-03-01 till 2021-12-22, 102 meas.
all GB
GB_measurement_smooth_with_SAT_avk_on_SAT
SAT_with_GB_prior_on_SAT

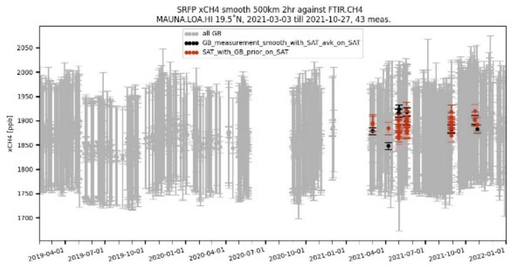
SRFP xCH4 smooth 500km 2hr against FTIR.CH4
MAUNA.LOA.HI 19.5°N, 2021-03-03 till 2021-10-27, 43 meas.
all GB
GB_measurement_smooth_with_SAT_avk_on_SAT
SAT_with_GB_prior_on_SAT

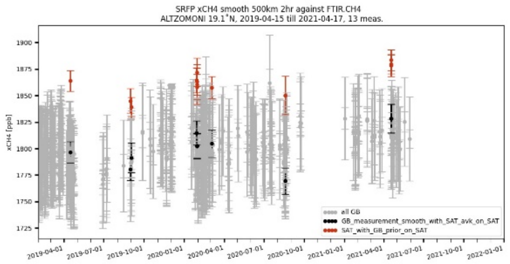
SRFP xCH4 smooth 500km 2hr against FTIR.CH4
ALTZOMONI 19.1°N, 2019-04-15 till 2021-04-17, 13 meas.
all GB
GB_measurement_smooth_with_SAT_avk_on_SAT
SAT_with_GB_prior_on_SAT

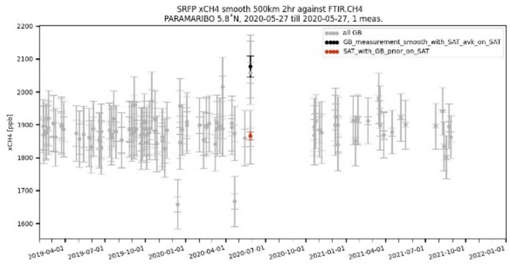
SRFP xCH4 smooth 500km 2hr against FTIR.CH4
PARAMARIBO 5.8°N, 2020-05-27 till 2020-05-27, 1 meas.
all GB
GB_measurement_smooth_with_SAT_avk_on_SAT
SAT_with_GB_prior_on_SAT

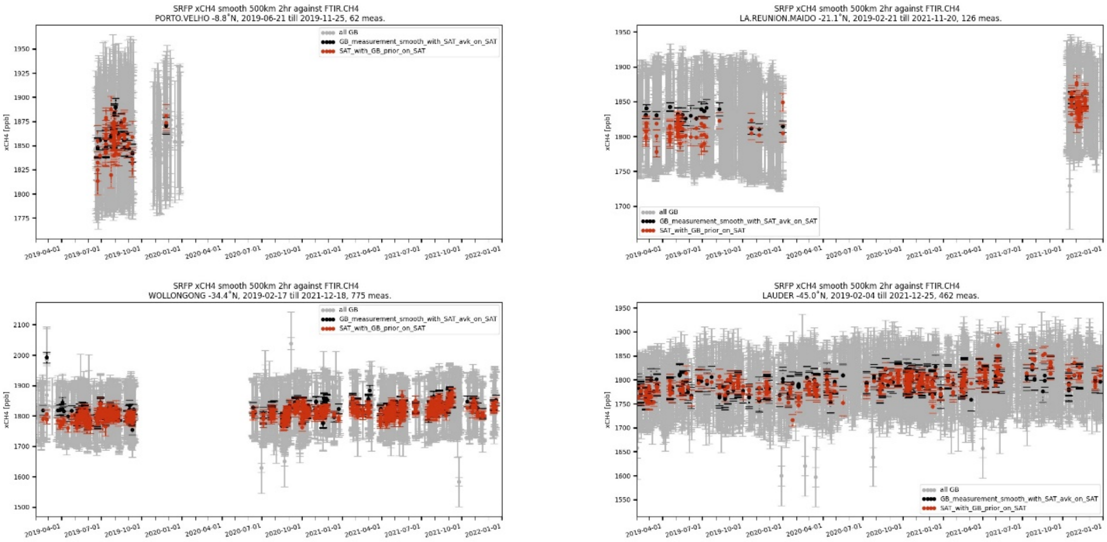

Figure 4-29: Timeseries of XCH_4 NDACC (collocated=black, all=grey) and CH4_GO2_SRFP (red) data at all NDACC sites.

Figure 4-30 shows monthly median timeseries for TCCON and SRFP XCH_4 for all data that fall within certain latitude bands, namely all sites North of 40°N latitude (top), all sites between 40°N and the equator (mid) and all sites in the Southern hemisphere (bottom). The plots also show the trend results of a trend+seasonality fit. Here we see ~5 ppb/year trend differences in the Northern hemisphere plots, with no overlap in errors. Rather than a gradual trend mismath the plot seems to indicate a bias shift around September 2020. Since this plot comprises of all timeseries taken at all stations within certain latitude bands and signifact gaps in timeseries do occur on a station by station level this could simply be a feature caused by changes in the overall constellation. However as the >40°N and 0° to 40°N latitude bands show a very consistent picture further investigation is certainly warrented. For the Southern Hemisphere the trend difference is less pronounced and fall within the combined uncertainty. The seasonality however is well captured.

Figure 4-31 shows the same but for NDACC (ignoring high altitude sites and Toronto again). Here again we see strong discrepancies in the long term trend, even up to 10 ppb/year for >40°N, which would confirm the onbservations made by TCCON. However the dataset used is extremely sparse which shows in the erratic behaviour of the NDACC data itself.

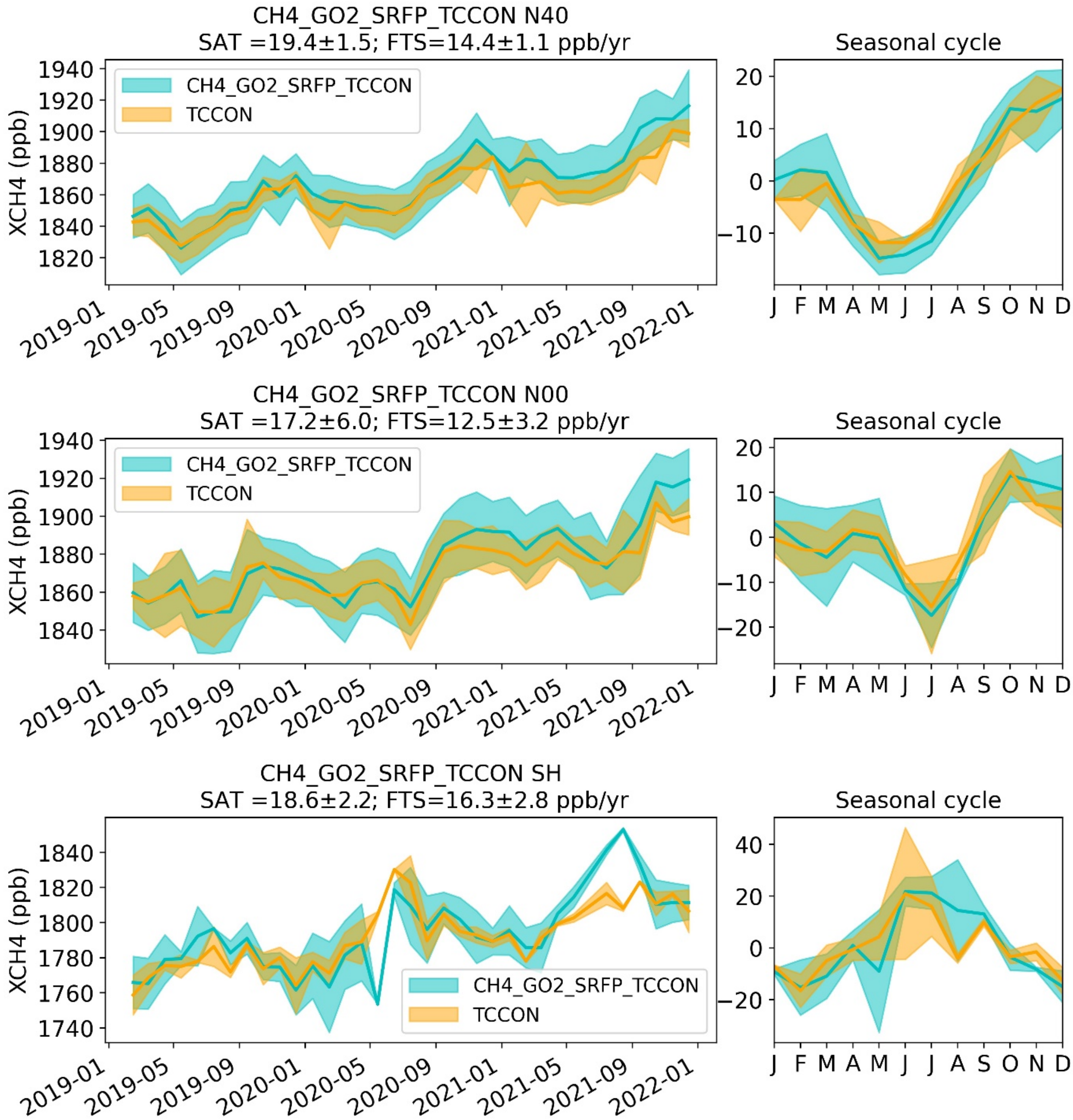

Figure 4-30: Monthly median collocated Sat and TCCON XCH_4 concentrations as a function of time. The shaded areas correspond with the scaled median absolute deviation.

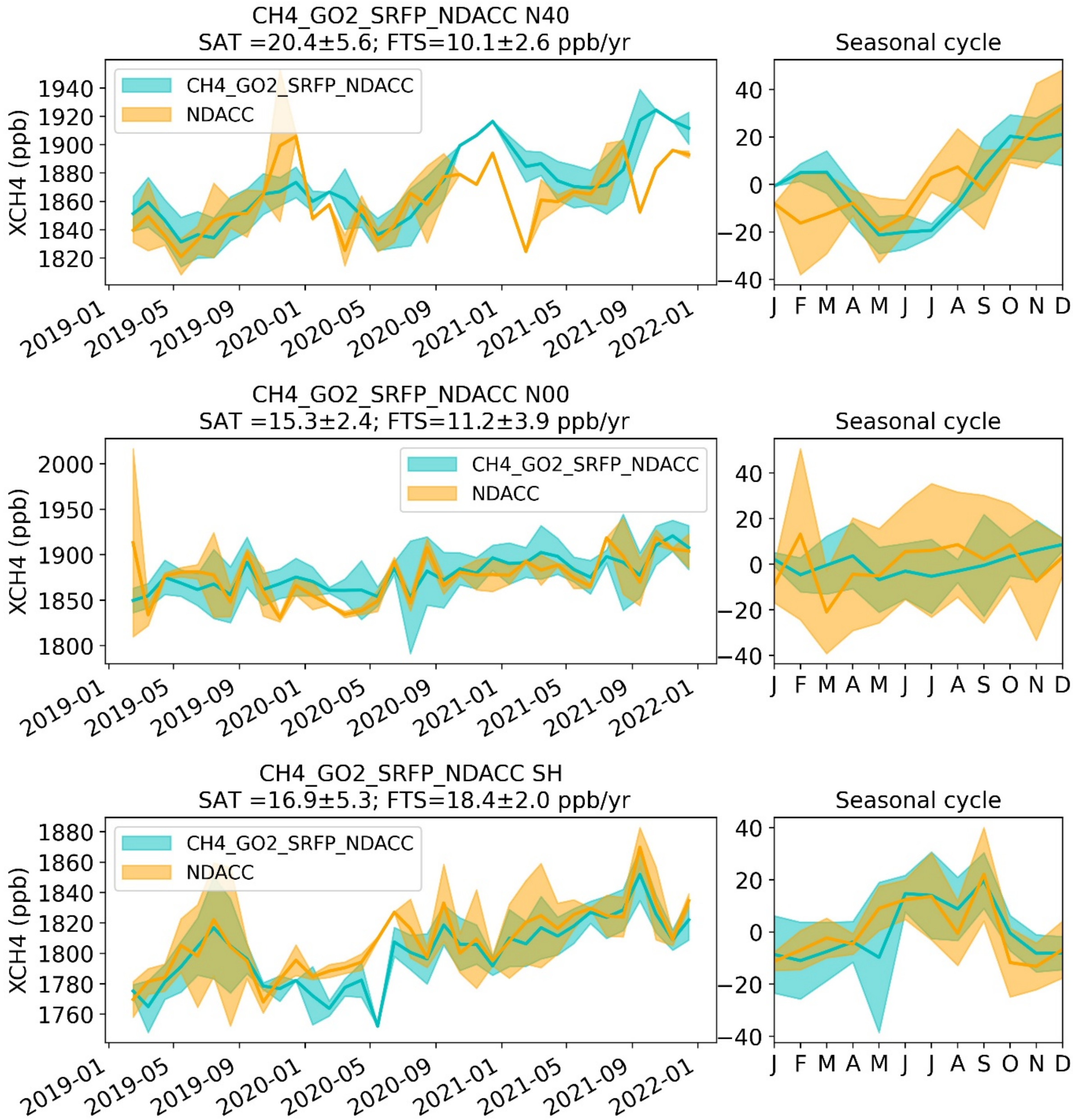

Figure 4-31: Monthly median collocated Sat and NDACC XCH_4 concentrations as a function of time. The shaded areas correspond with the scaled median absolute deviation.

4.2.5.2 Summary

Listed in the table below (**Table 4-14**) are the Figure of Merit parameters as derived from the individual collocated data pairs at each station.

SRFP XCH_4's single measurement precision equals 14.2 ppb, reaching the Breakthrough target of <17 ppb. The error assessment is slightly underestimated with an uncertainty ratio of 0.80. The median bias equals 4.3 ppb and is significant with confidence bands between 3.5 and 5.6 ppb. Both the spatial and spatio-temporal relative accuracies reach the <10 ppb target. A drift of 3.8 ppb/year is observed with confidence bands between 1.9 and 4.8 ppb/year. This is larger than the <3 ppb/year requirement. That said the confidence interval does overlap with the target and the available time period (just short of 3 years) is still fairly limited for a long term trend assessment.

For NDACC (ignoring high altitude sites and Toronto), we obtain a single measurement precision of 16.6 [13.6, 18.8] ppb, a positive but not significant median bias of 1.3 [-16.0, 4.6] pp. The median relative accuracy numbers do not meet the target but exhibit very large uncertainty bands (RA 10.2 [0, 18.2] ppb, SRA 12.7 [7.0, 18.1] ppb). Given these uncertainties, all obtained data overlap with our TCCON analysis.

Table 4-14 presents an overview of the estimated data quality of CH4_GO2_SRFP, as obtained by the VALT team, from comparisons with TCCON ground-based reference observations. Values in square brackets [ ] correspond with the upper and lower 95% confidence bound on the parameter. The uncertainty ratio features 2 numbers as outlined in the validation method.

Product Quality Summary Table for Product: CH4_GO2_SRFP Level: 2, Version: v02.0.2, Time period covered: 2.2019 – 12.2021 Assessment: Validation Team (VALT)			
Parameter [unit]	**Achieved performance**	**Requirement**	**Comments**
Single measurement precision (1-sigma) in [ppm]	14.2 [12.6,15.1]	< 34 (T) < 17 (B) < 9 (G)	Computed as the median over all station scaled median absolute differences to TCCON
Uncertainty ratio [-]: Ratio reported uncertainty to standard deviation of satellite-TCCON difference	0.78, 0.80*	-	No requirement but value close to unity expected for a high quality data product with reliable reported uncertainty.
Median bias (global offset) [ppm]	4.3 [3.5,5.6]	-	No requirement but value close to zero expected for a high quality data product.
Accuracy: Relative systematic error [ppm]	Spatial: 1.8 [0.1,2.7] Spatio-temporal: 5.1 [3.4,6.8]	< 10	Spatial: Computed as standard deviation of the biases at the various TCCON sites. Spatio-temporal: As “Spatial” but also considering seasonal biases.
Stability: Drift [ppm/year]	3.8 [1.9, 4.8]	< 3	Linear drift

4.2.6 Validation results for product CH4_GO2_SRPR

Below we show the validation results of the XCH_4 concentrations as derived by the CH4_GO2_SRPR v2.0.2 algorithm using GOSAT-2 spectra. 'PR' stands for the proxy version of the algorithm developed at SRON, whereby the retrieved CH_4 concentration is scaled by the modelled CO_2/retrieved CO_2 ratio. Data was available from February 2019 up to and including December 2021. The SRPR algorithm provides *a priori* and column averaging kernel data on a 3-layer vertical profile.

4.2.6.1 Detailed results

The Taylor diagram below in **Figure 4-32** yields a concise overview of the capabilities of the CH4_GO2_SRPR algorithm. Almost all TCCON sites cluster between the 0.5 and 0.8 correlation line. The TCCON scatter is smaller than that of SRPR while the variability of the bias roughly ranges between 0.8 and 1, relative to the SRPR variability. These results are very similar to the ones obtained from its Full Physics counterpart (see **Figure 4-24**).

Figure 4-33 yields the same information but for the NDACC comparisons. Again, we see more dispersion as compared to TCCON. Toronto, Rikubetsu, Tsukuba, Ny Alesund and Eureka stand out with much higher scatter in the NDACC data as compared to SRPR. The other stations are clustered between the 0.3 and 0.7 correlation line, with scatter values of the bias, being 0.8 to 1.2 times that of SRPR. Compared to SRFP (see **Figure 4-25**), these values seem to be internally more consistent between stations.

When looking at the mosaic plot for TCCON (**Figure 4-34**), we see almost consistent positive biases across all latitudes and times apart from the stations South of 45°N between July 2019 and roughly April 2020. With the limited available data it is hard to tell if this apparent bias shift is the result of a long term trend, seasonal mismatch (Oktober 2020 (and even 2021) does hint at again lower biases but not as outspoken) or something entirely different (and possibly transient in nature). Here the SRPR product does substantially differ from SRFP, where we see a lot less data coverage and more gaps in the timeseries.

Figure 4-44 shows the same but for NDACC. Here we see more data gaps which hampers our ability to draw conclusions. Station to station biases are also (again) far more outspoken. There are again traces of some sort of pattern in the biases (for instance recurring negative biases in Lauder around April 2019,2020,2021. The same for Garmish and Xianghe but at slightly shifted times). Toronto yet again features an outspoken trend.

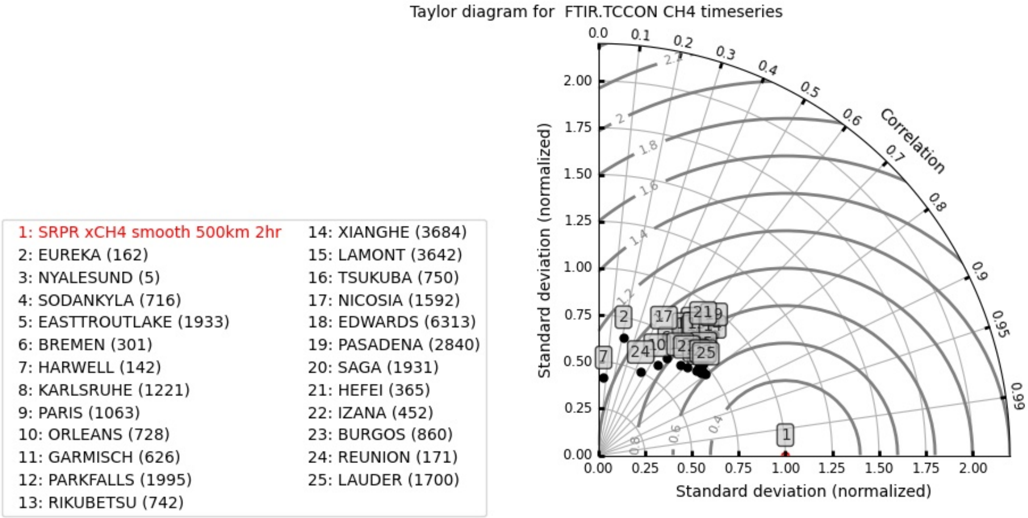

Figure 4-32: Tayor plot of XCH_4 TCCON values relative to CH4_GO2_SRPR. Straight lines correspond with the correlation, light grey lines yield the variability of the TCCON data relative to the satellite variability and the dark grey lines correspond with the variability of the Satellite -TCCON bias relative to the satellite variability.

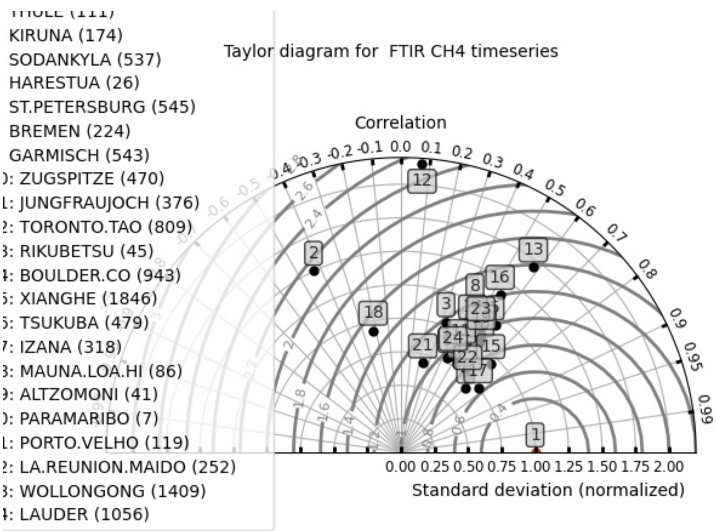

Figure 4-33: Tayor plot of XCH_4 NDACC values relative to CH4_GO2_SRPR. Straight lines correspond with the correlation, light grey lines yield the variability of the NDACC data relative to the satellite variability and the dark grey lines correspond with the variability of the Satellite –NDACC bias relative to the satellite variability.

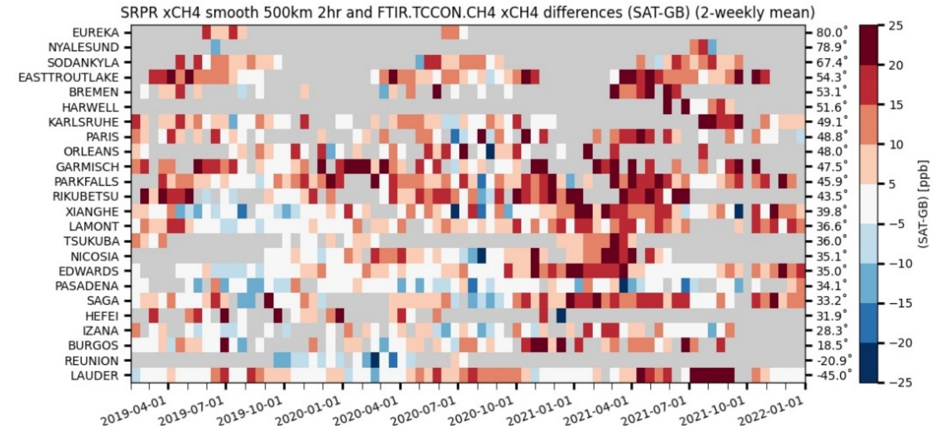

Figure 4-34. Mosaic plot of bi-weekly mean CH4_GO2_SRPR - TCCON XCH_4 biases as a function of time and TCCON station.

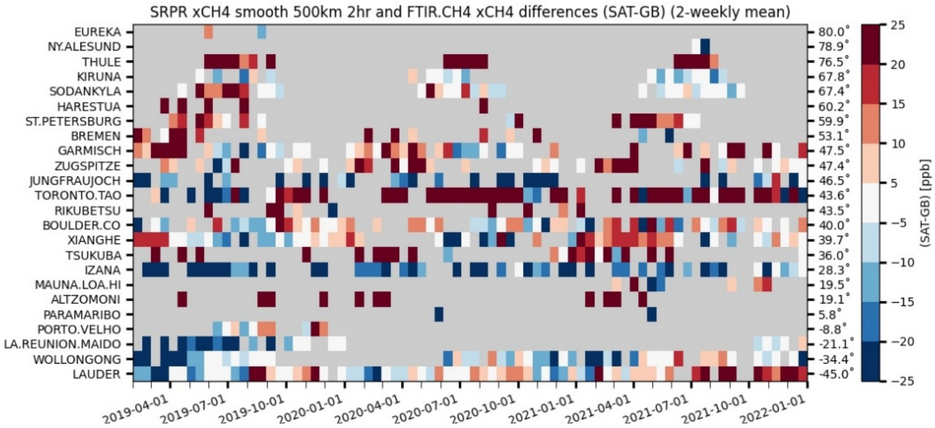

Figure 4-35. Mosaic plot of bi-weekly mean CH4_GO2_SRPR - NDACC XCH_4 biases as a function of time and NDACC station.

Table 4-15 lists all bias and scatter results derived from individual data pairs at all TCCON stations. The Proxy version of the algorithm produces roughly 2 times (note that in the previous PVIR iteration this was 10 times) as many collocated data pairs than its Full Physics counterpart, with on average ~800 data pairs per station, which corresponds with ~260 pairs per station per year. The only station that feature less than 100 collocated data pairs is Ny Alesund (5). While the data density is higher, the single measurement precision is also somewhat higher (15.1 ppb for SRPR vs. 14.2 ppb for SRFP) with values ranging (excluding Ny Alesund) between 12.0 ppb (Lauder) and 19.6 ppb (Xianghe). This in turn impacts the median correlation values (0.721 for SRFP vs. 0.66 for SRPR). SRFP only features a 8.1 ppb positive median bias compared to TCCON. The correlation using all data regardless of station yields 0.85 which is only slightly above SRFP's 0.84.

Table 4-15: Number of collocated data pairs (N), Correlation (R), Bias, Scatter, long term trend difference (ltt) and uncertainty thereon (ltt_err), seasonal amplitude difference (A) and uncertainty thereon (A_err) as well as the latitude of the TCCON station. The last row lists the median values over all stations. Product: CH4_GO2_SRPR.

STATION	N	R	Bias	Scat	ltt	ltt_err	A	A_err	lat
STATION	N	R	Bias	Std	ltt	ltt_err	A	A_err	lat
EUREKA	162	0.21	11.61	16.09	-	-	-	-	80
NYALESUND	5	0.73	10.6	8.69	-	-	-	-	78.9
SODANKYLA	716	0.64	10.04	17.34	0.38	1.57	2.45	2.35	67.4
EASTTROUTLAKE	1933	0.62	11.4	16.81	2.88	1.1	8.55	1.5	54.3
BREMEN	301	0.57	10.63	17.08	5.89	2.08	6.77	4	53.1
HARWELL	142	0.07	11.15	14.93	-	-	-	-	51.6
KARLSRUHE	1221	0.75	8.54	16.3	3.57	1.45	1.41	1.44	49.1
PARIS	1063	0.65	7.74	15.68	3.44	1.32	5.92	1.62	48.8
ORLEANS	728	0.55	6.21	13.47	2.07	2.26	2.12	1.92	48
GARMISCH	626	0.62	11.52	17.69	6.9	2.19	9.19	2.16	47.5
PARKFALLS	1995	0.67	9.54	15.86	1.46	1.23	9.62	1.24	45.9
RIKUBETSU	742	0.66	15.81	14.87	7.31	1.99	8.85	1.95	43.5
XIANGHE	3684	0.73	5.49	19.62	6.32	1.48	9.52	1.45	39.8
LAMONT	3642	0.75	7.01	14.61	4.73	0.79	2.39	0.87	36.6
TSUKUBA	750	0.67	6.72	13.72	2.12	0.59	2.95	1.84	36
NICOSIA	1592	0.49	6.53	13.73	-	-	-	-	35.1
EDWARDS	6313	0.78	4.43	14.54	3.81	0.88	6.12	0.81	35
PASADENA	2840	0.69	-3.18	15.2	1.65	1.26	4.8	1.27	34.1
SAGA	1931	0.76	8.89	15.51	3.28	1.66	8.89	1.29	33.2
HEFEI	365	0.65	8.83	16.07	-	-	-	-	31.9
IZANA	452	0.71	0.71	13.11	3.36	1.21	7.6	1.3	28.3
BURGOS	860	0.78	6.48	13.98	5.86	1.89	2.73	1.71	18.5
REUNION	171	0.46	-7.01	13.74	-	-	-	-	-20.9
LAUDER	1700	0.8	4.83	11.98	3.26	1.01	9.43	0.98	-45
MEDIAN	**805**	**0.665**	**8.14**	**15.07**	**3.4**	**1.385**	**6.445**	**1.475**	**41.65**

Table 4-16 shows the same but for NDACC. Consistent with previous NDACC analysis for other algorithms, we see lower data densities (Median at 285), with Eureka, Ny Alesund and Paramaribo featuring less than 10 data pairs. Excluding those stations. Correlation numbers range between -0.22 (Mauna LoaEureka) and 0.77 (Izaña) and scatter ranges between 10.5 ppb (Harestua) and 31.4 ppb (Rikubetsu. The median bias equals 3.3 ppb, but with much

larger interstation variability compared to SRFP (from -26.4 ppb at Jungfraujoch to 55.6 ppb at Altzomoni). Long term trend values range between -9.2 ppb/year at Sodankyla and 16.4 ppb/year at Toronto. The latter, as mentioned before, apparently having issues with degrading data quality.

Table 4-16: Number of collocated data pairs (N), Correlation (R), Bias, Scatter, long term trend difference (ltt) and uncertainty thereon (ltt_err), seasonal amplitude difference (A) and uncertainty thereon (A_err) as well as the latitude of the NDACC station. The last row lists the median values over all stations. Product: CH4_GO2_SRPR.

STATION	N	R	Bias	Scat	ltt	ltt_err	A	A_err	lat
EUREKA	9	-0.43	2.03	33.95	-	-	-	-	80
NY.ALESUND	2	-1	-18.65	27.85	-	-	-	-	78.8
THULE	111	0.33	33.12	15.72	7.38	4.48	22.45	11.75	76.5
KIRUNA	174	0.71	-5.38	14.85	-0.09	1.76	5.66	4.14	67.8
SODANKYLA	537	0.6	4.81	20.83	-9.21	2.01	11.18	7.17	67.3
HARESTUA	26	0.53	31.14	10.5	-	-	-	-	60.1
ST.PETERSBURG	545	0.61	16.7	17.48	3.12	2.12	15.12	4.26	59.8
BREMEN	224	0.44	14.37	19.36	-1	24.33	17.21	7.59	53
GARMISCH	543	0.44	4	24.19	10.13	5.2	12.46	3.08	47.4
ZUGSPITZE	470	0.58	3.86	20.75	5.28	4.29	11.09	4.15	47.4
JUNGFRAUJOCH	376	0.5	-26.43	24.19	13.37	6.72	13.89	5.07	46.5
TORONTO.TAO	809	0.07	36.71	42.64	16.43	6.78	8.49	7.35	43.5
RIKUBETSU	45	0.58	33.99	31.36	-	-	-	-	43.4
BOULDER.CO	943	0.49	3.32	19.13	4.03	2.47	2.88	3.06	40
XIANGHE	1846	0.71	3.35	21.01	2.19	1.8	13.13	1.88	39.7
TSUKUBA	479	0.53	33.51	23.39	-9.64	1.86	11.77	10.67	36
IZANA	318	0.77	-23.54	13.67	2.08	1.51	4.46	1.72	28.3
MAUNA.LOA.HI	86	-0.22	-11.73	29.61	-	-	-	-	19.5
ALTZOMONI	41	0.57	55.6	12.23	-4.03	1.73	15.11	6.96	19.1
PARAMARIBO	7	-0.69	-58.29	70.26	-	-	-	-	5.8
PORTO.VELHO	119	0.24	0	17.71	-	-	-	-	-8.7
LA.REUNION.MAIDO	252	0.65	-13.83	14.74	0.98	3.44	9.96	2.62	-21.1
WOLLONGONG	1409	0.53	-2.98	20.06	8.17	2.55	21.15	2.94	-34.4
LAUDER	1056	0.48	1.61	18.73	9.64	2.15	7.27	1.85	-45
MEDIAN	285	0.515	3.335	20.405	3.12	2.47	11.77	4.15	43.45

The timeseries in **Figure 4-36** show individual satellite and ground-based TCCON measurements. While the scatter is even somewhat higher for SRPR XCH_4 with respect to both TCCON and SRFP, it is again relatively free of outliers and manages to capture (in most cases) TCCON's temporal variability.

Figure 4-37 shows the NDACC correlative data timeseries and here again it is obvious that NDACC in itself shows more variability (which affects single measurement precision and correlation numbers). See for instance Toronto and Boulder.

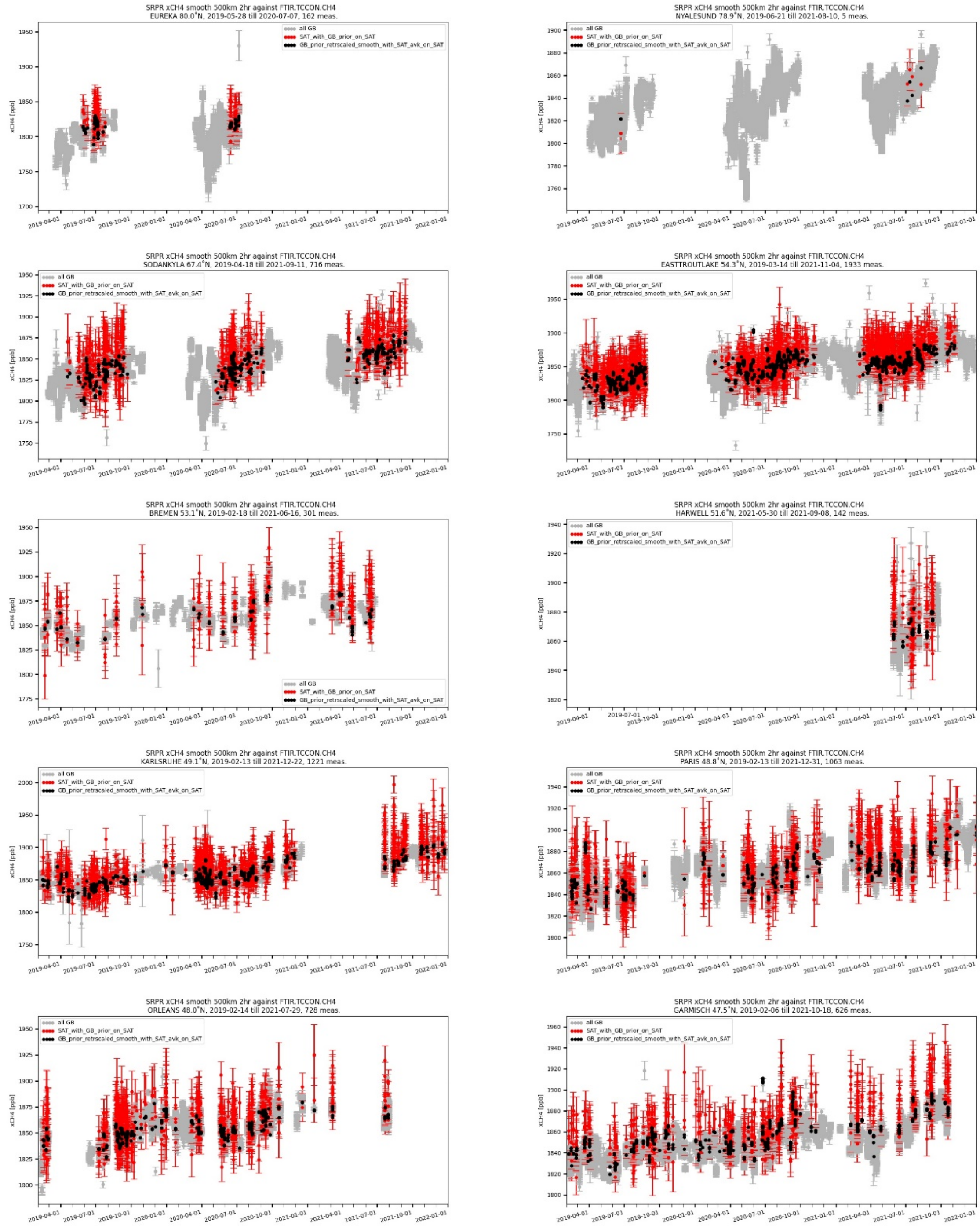

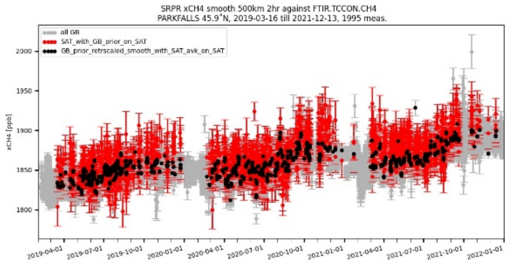
SRPR xCH4 smooth 500km 2hr against FTIR.TCCON.CH4
PARKFALLS 45.9°N, 2019-03-16 till 2021-12-13, 1995 meas.

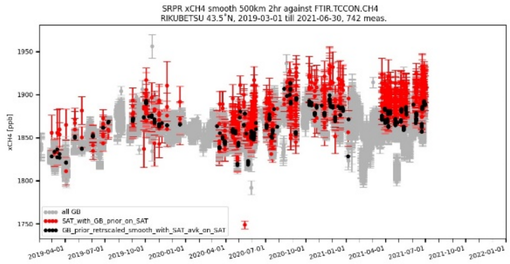
SRPR xCH4 smooth 500km 2hr against FTIR.TCCON.CH4
RIKUBETSU 43.5°N, 2019-03-01 till 2021-06-30, 742 meas.

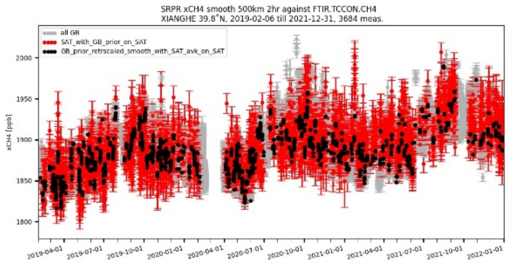
SRPR xCH4 smooth 500km 2hr against FTIR.TCCON.CH4
XIANGHE 39.8°N, 2019-02-06 till 2021-12-31, 3684 meas.

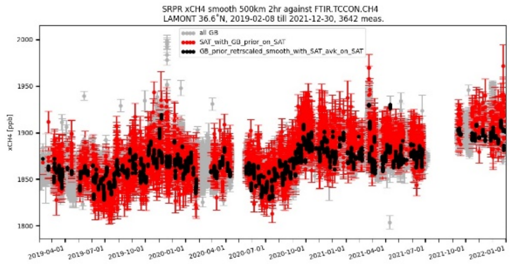
SRPR xCH4 smooth 500km 2hr against FTIR.TCCON.CH4
LAMONT 36.6°N, 2019-02-08 till 2021-12-30, 3642 meas.

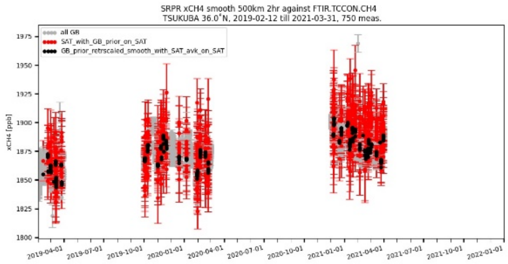
SRPR xCH4 smooth 500km 2hr against FTIR.TCCON.CH4
TSUKUBA 36.0°N, 2019-02-12 till 2021-03-31, 750 meas.

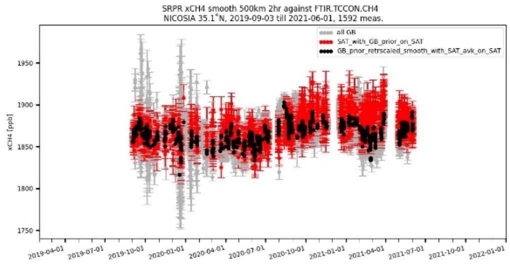
SRPR xCH4 smooth 500km 2hr against FTIR.TCCON.CH4
NICOSIA 35.1°N, 2019-09-03 till 2021-06-01, 1592 meas.

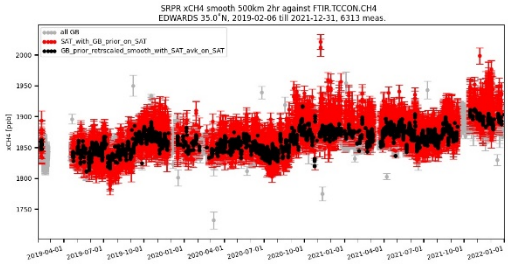
SRPR xCH4 smooth 500km 2hr against FTIR.TCCON.CH4
EDWARDS 35.0°N, 2019-02-06 till 2021-12-31, 6313 meas.

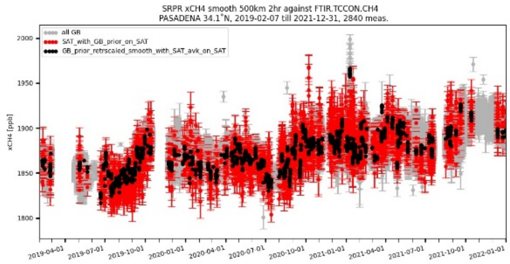
SRPR xCH4 smooth 500km 2hr against FTIR.TCCON.CH4
PASADENA 34.1°N, 2019-02-07 till 2021-12-31, 2840 meas.

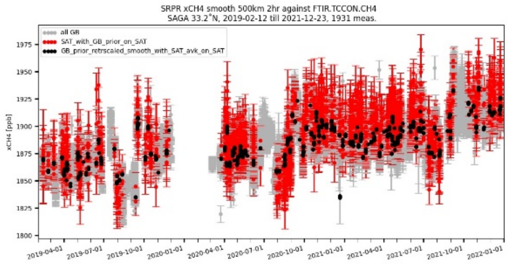
SRPR xCH4 smooth 500km 2hr against FTIR.TCCON.CH4
SAGA 33.2°N, 2019-02-12 till 2021-12-23, 1931 meas.

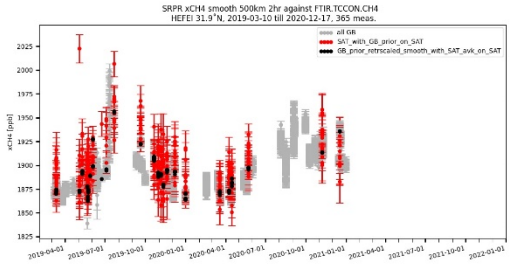
SRPR xCH4 smooth 500km 2hr against FTIR.TCCON.CH4
HEFEI 31.9°N, 2019-03-10 till 2020-12-17, 365 meas.

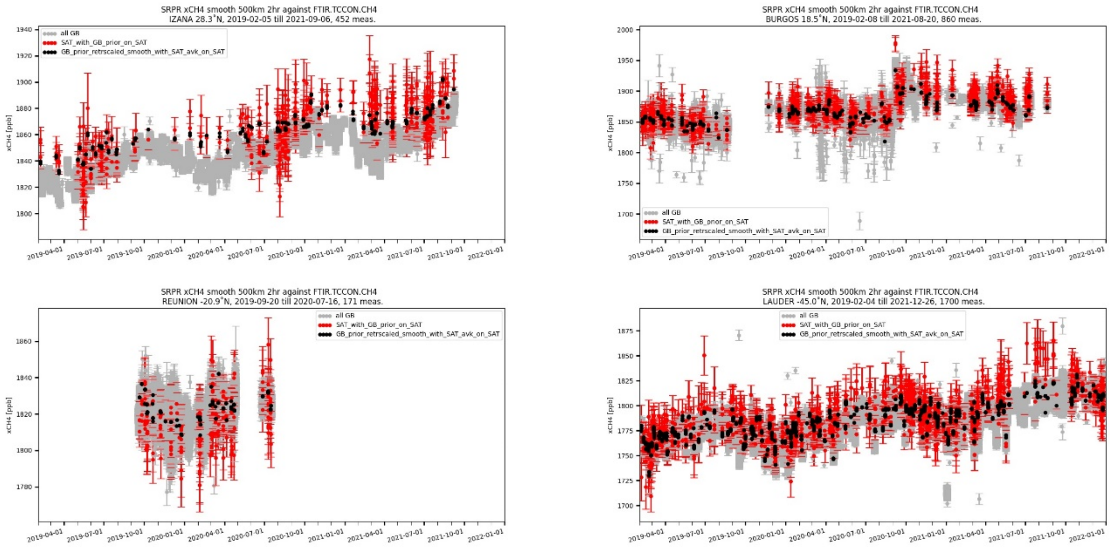

Figure 4-36: Timeseries of XCH_4 TCCON (collocated=black, all=grey) and CH4_GO2_SRPR (red) data at selected TCCON sites.

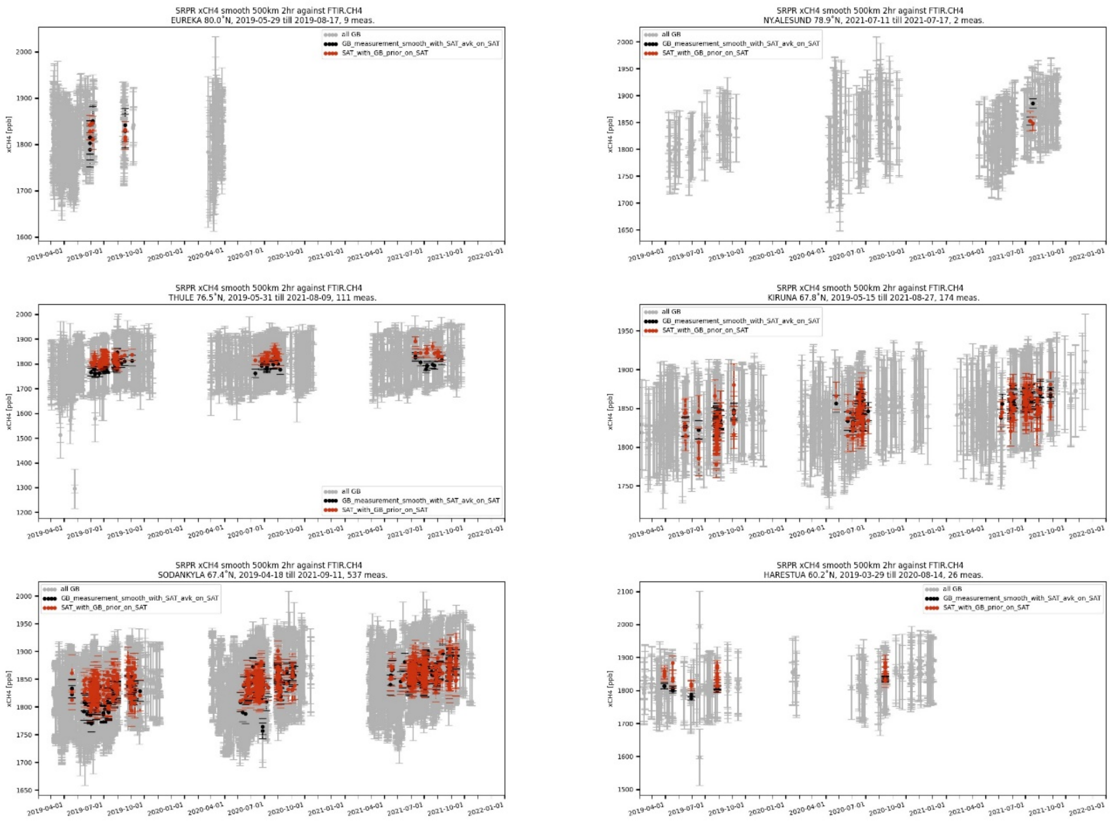

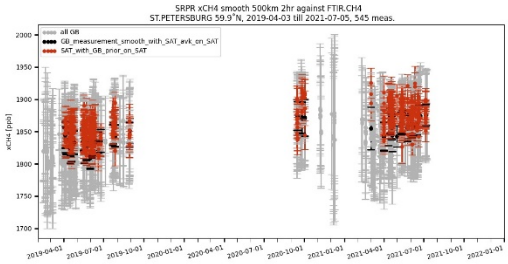
SRPR xCH4 smooth 500km 2hr against FTIR.CH4
ST.PETERSBURG 59.9°N, 2019-04-03 till 2021-07-05, 545 meas.

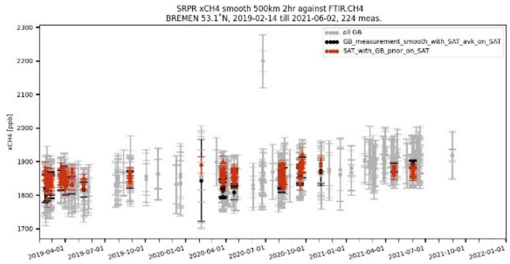
SRPR xCH4 smooth 500km 2hr against FTIR.CH4
BREMEN 53.1°N, 2019-02-14 till 2021-06-02, 224 meas.

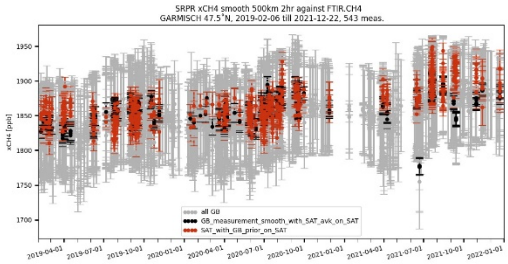
SRPR xCH4 smooth 500km 2hr against FTIR.CH4
GARMISCH 47.5°N, 2019-02-06 till 2021-12-22, 543 meas.

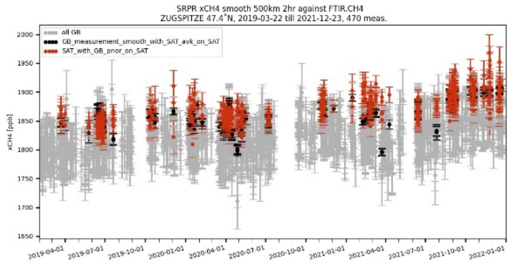
SRPR xCH4 smooth 500km 2hr against FTIR.CH4
ZUGSPITZE 47.4°N, 2019-03-22 till 2021-12-23, 470 meas.

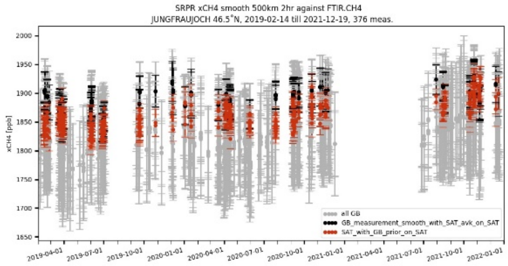
SRPR xCH4 smooth 500km 2hr against FTIR.CH4
JUNGFRAUJOCH 46.5°N, 2019-02-14 till 2021-12-19, 376 meas.

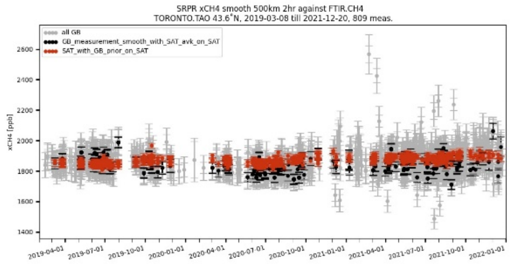
SRPR xCH4 smooth 500km 2hr against FTIR.CH4
TORONTO.TAO 43.6°N, 2019-03-08 till 2021-12-20, 809 meas.

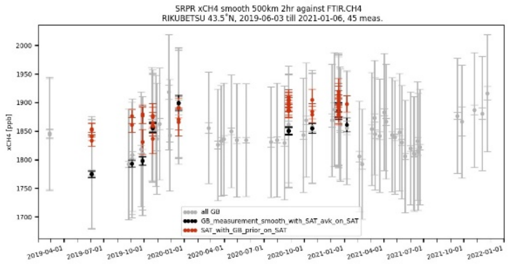
SRPR xCH4 smooth 500km 2hr against FTIR.CH4
RIKUBETSU 43.5°N, 2019-06-03 till 2021-01-06, 45 meas.

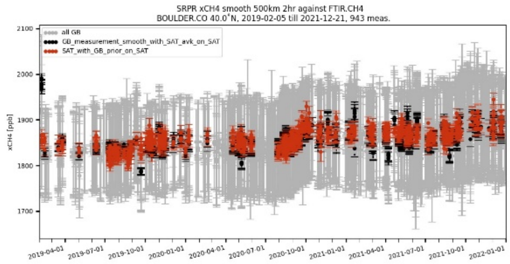
SRPR xCH4 smooth 500km 2hr against FTIR.CH4
BOULDER.CO 40.0°N, 2019-02-05 till 2021-12-21, 943 meas.

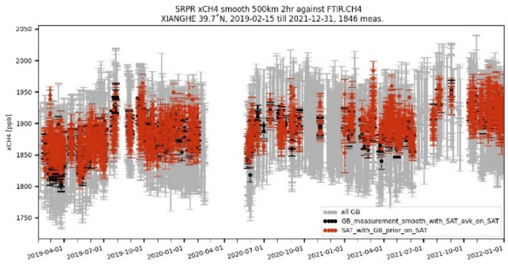
SRPR xCH4 smooth 500km 2hr against FTIR.CH4
XIANGHE 39.7°N, 2019-02-15 till 2021-12-31, 1846 meas.

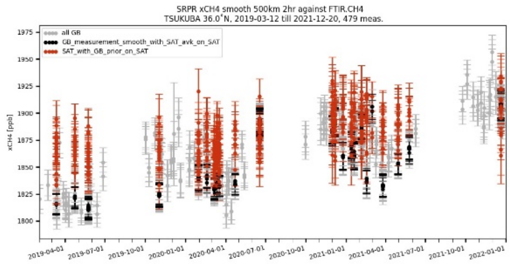
SRPR xCH4 smooth 500km 2hr against FTIR.CH4
TSUKUBA 36.0°N, 2019-03-12 till 2021-12-20, 479 meas.

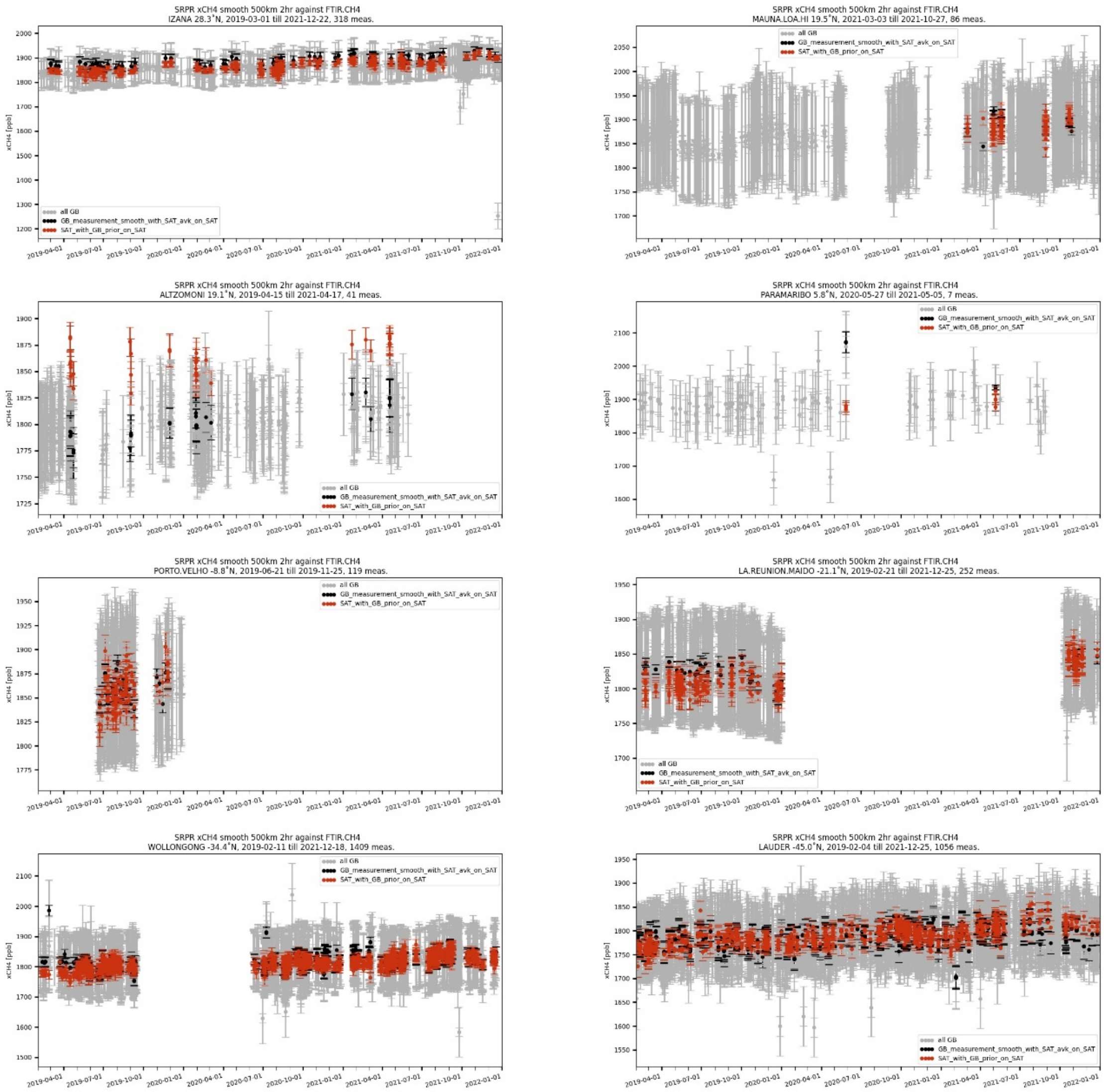

Figure 4-37: Timeseries of XCH$_4$ NDACC (collocated=black, all=grey) and CH4_GO2_SRPR (red) data at all NDACC sites.

Figure 4-38 shows monthly median timeseries for TCCON and SRPR XCH$_4$ for all data that fall within certain latitude bands, namely all sites North of 40°N latitude (top), all sites between 40°N and the equator (mid) and all sites in the Southern hemisphere (bottom). Here we see a picture that is very consistent with that of SRFP. For the Northern Hemisphere bands we again see a stronger annual trend than observed by TCCON. Wheither this is gradual or the result of a offset change remains to be investigated. As with the SRFP analysis we also need to contend with the fairly limited time covered and with changing station constellations that contribute to this plot in time which might skew our analysis. For the >40°N band we see a difference of 2.5 ppb/year, for the 0-40°N band we have a 4.3 ppb/ year difference, which is slighly less outspoken than those observed in SRFP. The seasonality seems to be well captured although in the top plot (>40°N) we might discern a phase shift, while in the middle plot a higher amplitude in the seasonality can be observed. This was not apparent in the SRFP plots (**Figure 4-30**).

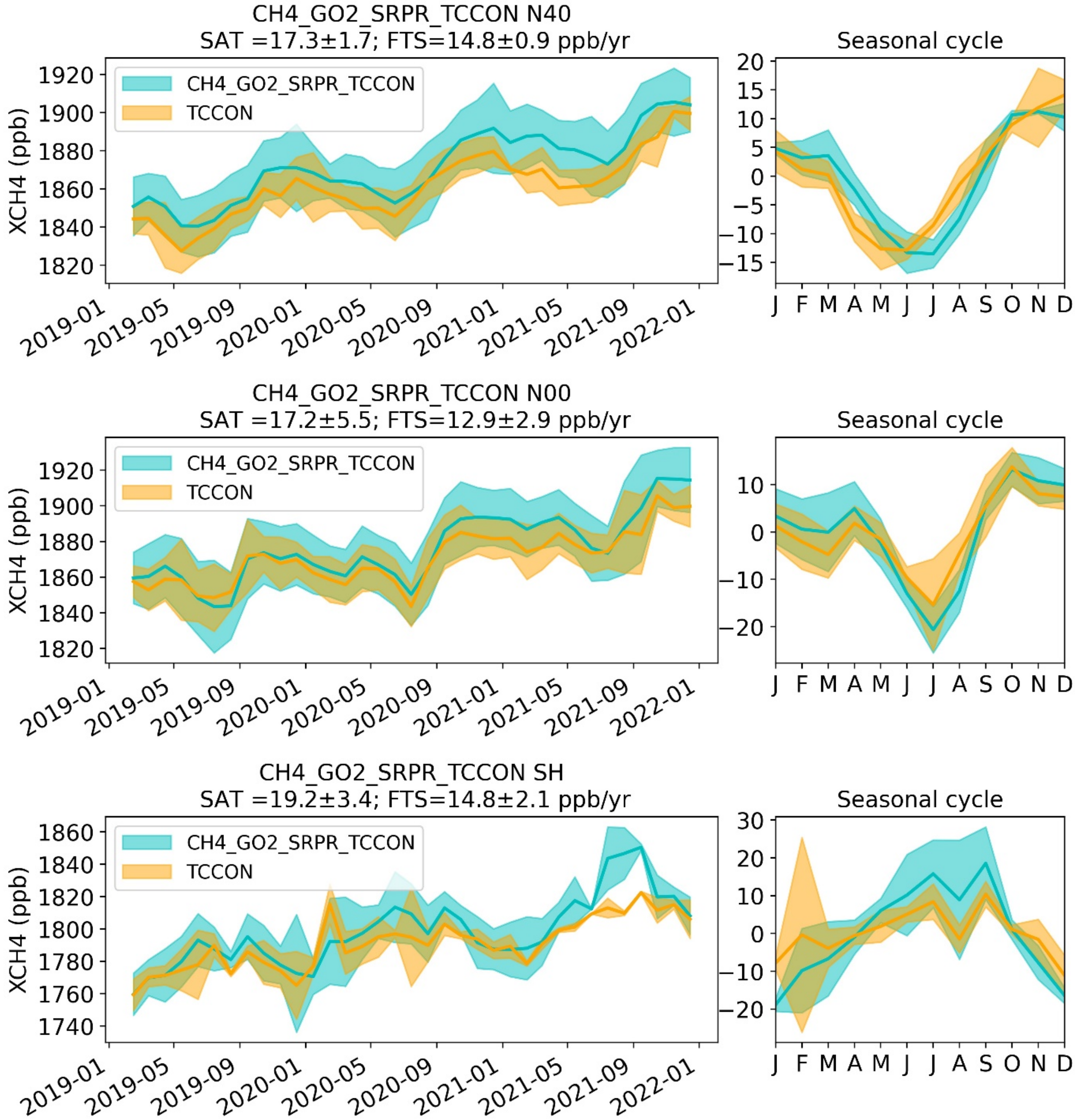

Figure 4-38: Monthly median collocated Sat and TCCON XCH_4 concentrations as a function of time. The shaded areas correspond with the scaled median absolute deviation.

Figure 4-39 shows the same but for NDACC (ignoring high altitude sites and Toronto). Due to the higher variability it is difficult to draw conclusions. SRPR's long term trend is consistently larger than that observed by NDACC, sometimes significantly so, sometimes not (for the 0° to 40° N band). Nor can we make meaningful conclusions for the seasonality. The findings do not contradict the observations made with TCCON but due to the uncertainty they do not confirm them either.

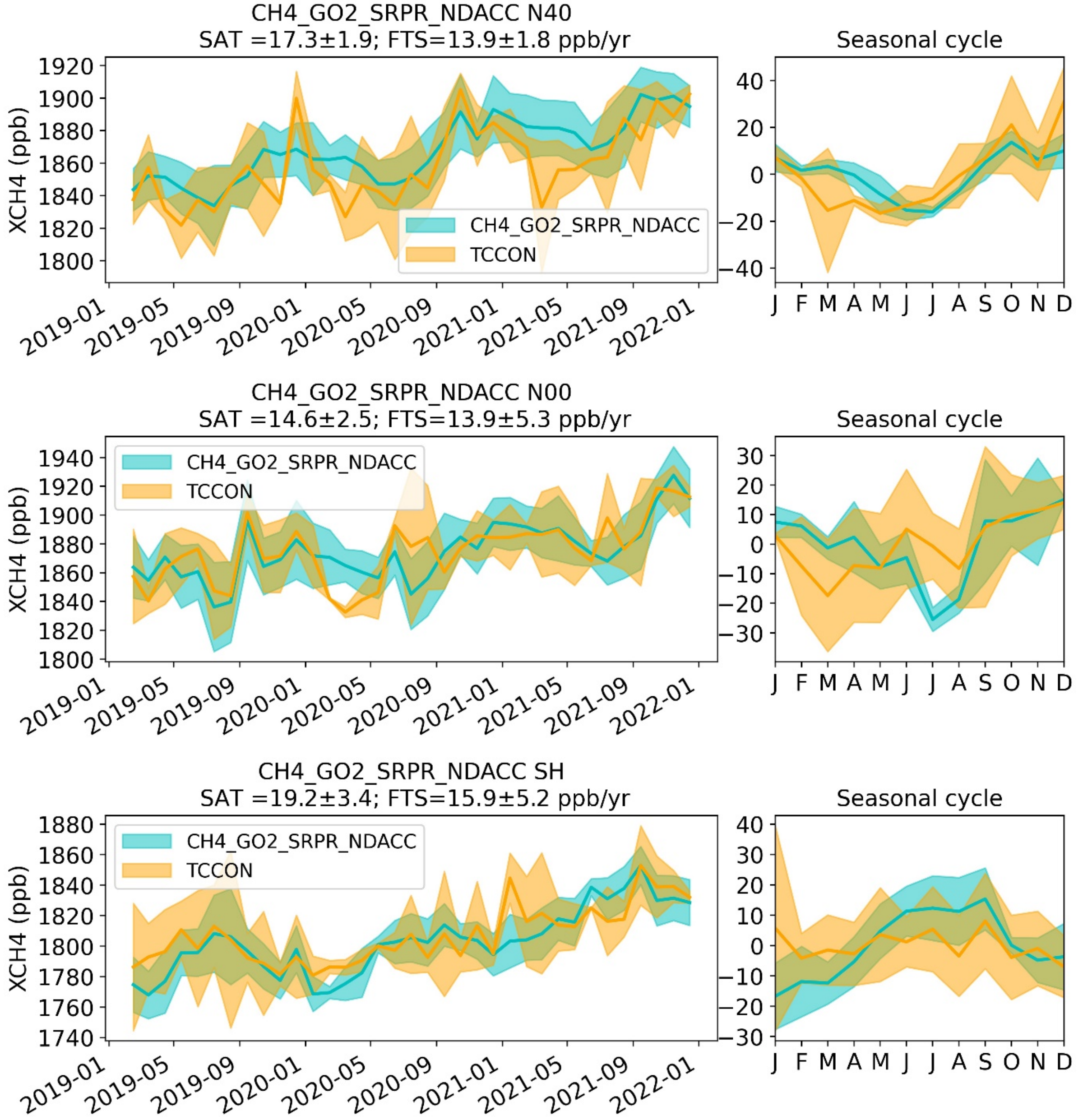

Figure 4-39: Monthly median collocated Sat and NDACC XCH_4 concentrations as a function of time. The shaded areas correspond with the scaled median absolute deviation.

4.2.6.2 Summary

Listed in the table below (**Table 4-17**) are the Figure of Merit parameters as derived from the individual collocated data pairs at each station.

SRPR XCH_4’s single measurement precision equals 15.1 ppb, reaching the Breakthrough target of <17 ppb. The error assessment is somewhat underestimated with an uncertainty ratio of 0.82. The median bias is significant at 8.1 ppb with confidence bands between 6.2 and 9.8 ppb. Both the spatial and spatio-temporal relative accuracies reach the <10 ppb target (3.7 and 6.2 ppb for the RA and SRA respectively (an improvement compared to the previous analysis at 5.0 and 9.4), which is slightly worse than SRFP’s RA and SRA (1.8 and 5.1 respectively).

In the previous analysis we saw far more (10 time) SRPR data compared to SRFP but with significantly more scatter. In this iteration of the algorithms the differences between them seem to have reduced.

Compared to NDACC we see a single measurement precision of 19.7 [16.0, 21.7] ppb, a likewise positive median bias of 3.7 [-10.6, 6.3] ppb, and relative accuracy values that do not meet the requirements (RA 11.6[0, 21.2] ppb, SRA 17.4 [12.8, 24.9] ppb), although the confidence interval of the RA is so large it overlaps with the target of <10 ppb. The latter no doubt in part to the higher inter-station variability within the NDACC network itself.

Table 4-17 presents an overview of the estimated data quality of CH4_GO2_SRPR, as obtained by the VALT team, from comparisons with TCCON ground-based reference observations. Values in square brackets [ ] correspond with the upper and lower 95% confidence bound on the parameter. The uncertainty ratio features 2 numbers as outlined in the validation method.

Product Quality Summary Table for Product: CH4_GO2_SRPR Level: 2, Version: v02.0.2, Time period covered: 2.2019 – 12.2021 Assessment: Validation Team (VALT)			
Parameter [unit]	**Achieved performance**	**Requirement**	**Comments**
Single measurement precision (1-sigma) in [ppm]	15.1 [14.1,16.2]	< 34 (T) < 17 (B) < 9 (G)	Computed as the median over all station scaled median absolute differences to TCCON
Uncertainty ratio [-]: Ratio reported uncertainty to standard deviation of satellite-TCCON difference	0.80,0.82*	-	No requirement but value close to unity expected for a high quality data product with reliable reported uncertainty.
Median bias (global offset) [ppm]	8,1 [6.2,9.8]	-	No requirement but value close to zero expected for a high quality data product.
Accuracy: Relative systematic error [ppm]	Spatial: 3.7 [1.8, 5.4] Spatio-temporal: 6.2 [4.6, 8.1]	< 10	Spatial: Computed as standard deviation of the biases at the various TCCON sites. Spatio-temporal: As "Spatial" but also considering seasonal biases.
Stability: Drift [ppm/year]	3.4 [1.5, 4.3]	< 3	Linear drift

5 Validation and intercomparisons results from data provider

5.1 Validation and intercomparison results for product CO2_OC2_FOCA

The validation results shown in this section are valid for version v10.1 of the OCO-2 XCO_2 retrieval algorithm CO2_OC2_FOCA. The applied methods are similar to those described in BESD's comprehensive error characterization Report **/CECRv3, 2017/** and product validation and inter-comparison reports (e.g., **/PVIRv5, 2017/)** of ESA's GHG CCI project and partly also in the publication of **/Reuter et al., 2020/**. For all comparisons, averaging kernels have been applied and the influence of the smoothing error reduced as described in Section 5.2 of ESA's GHG CCI+ product user guide version 4.1 (PUGv4.1) for the FOCAL XCO_2 OCO-2 data product CO2_OC2_FOCA **/PUGv4.1, 2023/**. The validation results shown in this section are part of ESA's GHG CCI+ end-to-end ECV uncertainty budget version 4.1 (E3UBv4.1) for the FOCAL XCO_2 OCO-2 data product CO2_OC2_FOCA **/E3UBv4.1, 2023/**.

5.1.1 Co-location

FOCAL's XCO_2 has been validated with TCCON **/Wunch et al., 2011/** GGG2020 measurements. The co-location criteria are defined by a maximum time difference of two hours, a maximum spatial distance of 500km, and a maximum surface elevation difference of 250m. Additionally, only TCCON sites with at least 1000 co-locations (4 in the case of daily, weekly, or monthly averages) covering a time period of at least two years are taken into account.

Figure 5.1 shows all 2329133 co-located FOCAL and TCCON XCO_2 retrieval results used for the validation study. One can see that the temporal sampling differs from site to site and that FOCAL captures the year-to-year increase and the seasonal features well.

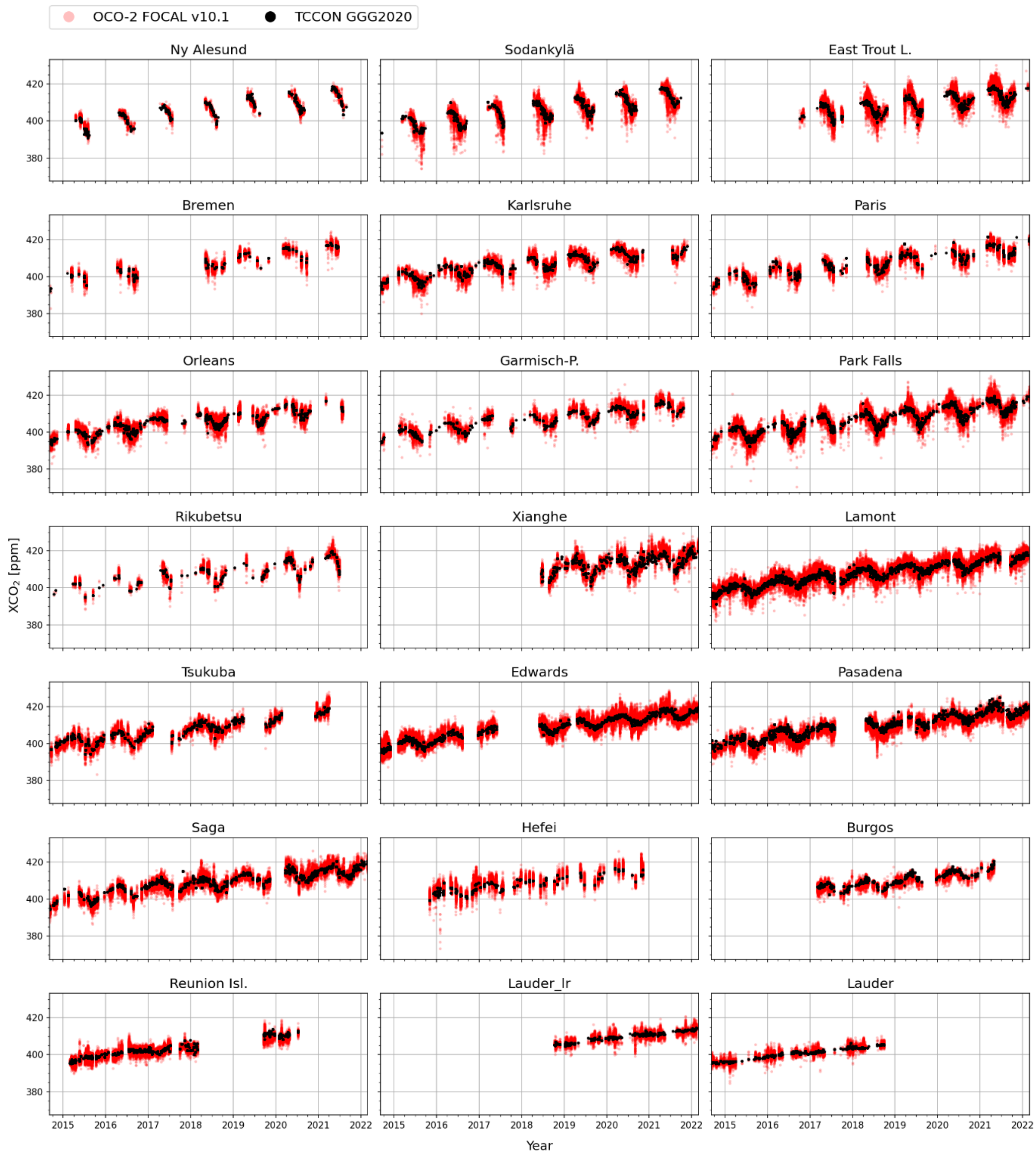

Figure 5.1: *Co-located FOCAL and TCCON XCO_2 retrieval results used for the validation study. The TCCON sites are ordered from top/left to bottom/right by average latitude of the co-located satellite soundings.*

5.1.2 Daily, weekly, and monthly averages

For some applications, it is expected that FOCAL XCO_2 data will be aggregated to "super soundings" averaging, e.g., all soundings of an orbit in a surrounding of a target. Also, FOCAL XCO_2 data might be used to compute L3 (level 3) products, e.g., in the manner of gridded monthly averages. With such application in the mind, we computed daily, weekly, and monthly averages of the FOCAL and TCCON co-locations at each TCCON site. In order to improve the robustness, daily, weekly, and monthly averages are only calculated when averaging at least 10, 30, or 50 individual soundings, respectively. As an example, Figure 5.2 shows the daily, weekly, and monthly FOCAL XCO_2 averages for the Lamont and Reunion Island TCCON sites. Due to OCO-2's data density, it is often the case that one overpass generates many co-colocations. This considerably reduces the scatter of the daily averages compared to the individual soundings.

Note that FOCAL reports only on the stochastic uncertainty of the individual soundings. In the case of daily, weekly, and monthly averages we computed the corresponding uncertainties by applying the rules of error propagation under the assumption of uncorrelated errors.

5.1.3 General overview

The overall agreement of the FOCAL data (and its averages) with TCCON data at all sites is illustrated in Figure 5.3. The histograms of the difference (FOCAL – TCCON) show in all cases a near Gaussian distribution with a center between -0.17ppm and -0.06ppm. The standard deviation of the difference reduces from 1.91ppm for individual soundings to 1.14ppm for monthly averages. The FOCAL vs. TCCON heat maps show a pronounced clustering along the one-to-one line for all cases. This is supported by a good agreement of the orthogonal distance regression with the one-to-one line and high Pearson correlation coefficients between 0.95 for individual soundings and 0.98 for monthly averages.

These results provide a first rough overview of FOCAL's agreement with TCCON. However, except for an average bias, they do not allow to separate systematic and stochastic error components.

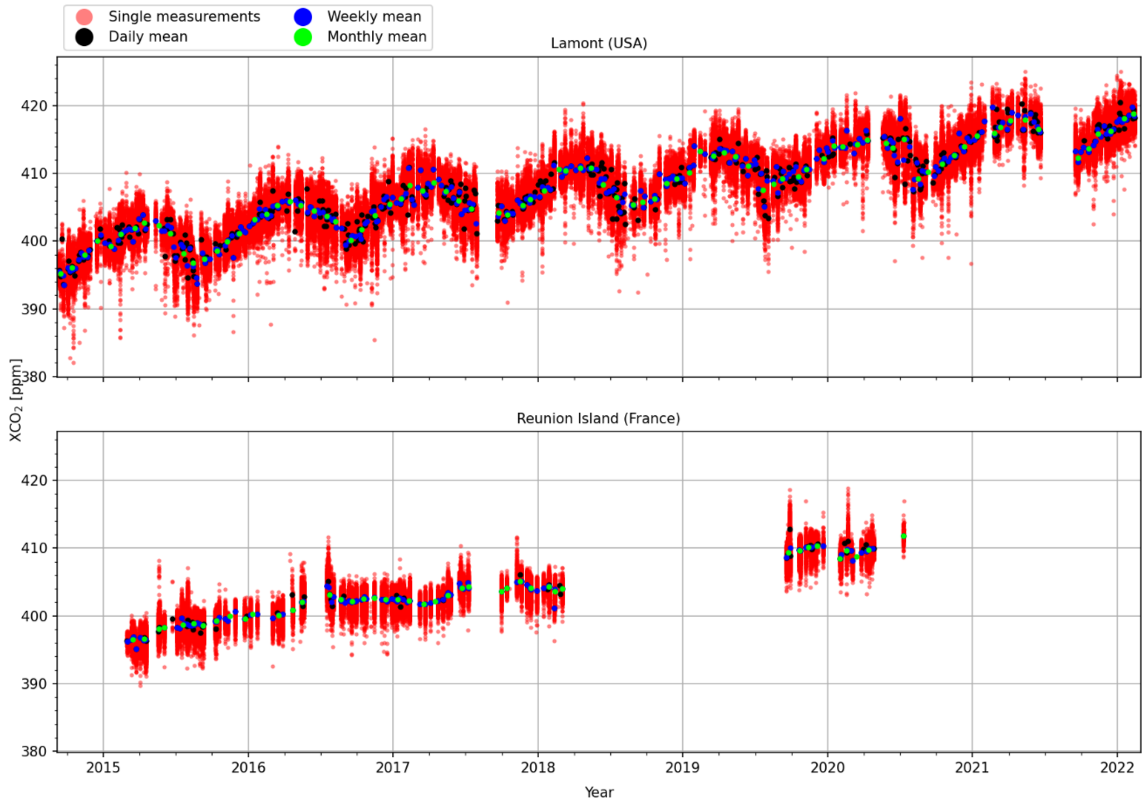

Figure 5.2: *Co-located FOCAL XCO_2 retrieval results and their daily, weekly, and monthly averages at the TCCON sites Lamont (top) and Reunion Island (bottom) used for the validation study.*

5.1.4 Stochastic and systematic error components

The method described in the following allows us to separate the stochastic errors from potential regional or seasonal biases as well as from a linear drift.

5.1.4.1 Per site performance statistics

For the co-locations of each site, we compute the FOCAL minus TCCON differences ΔX and fit the following bias model:

5-1
$$\Delta X = a_0 + a_1 t + a_2 \sin(2\pi t + a_3) + \varepsilon$$

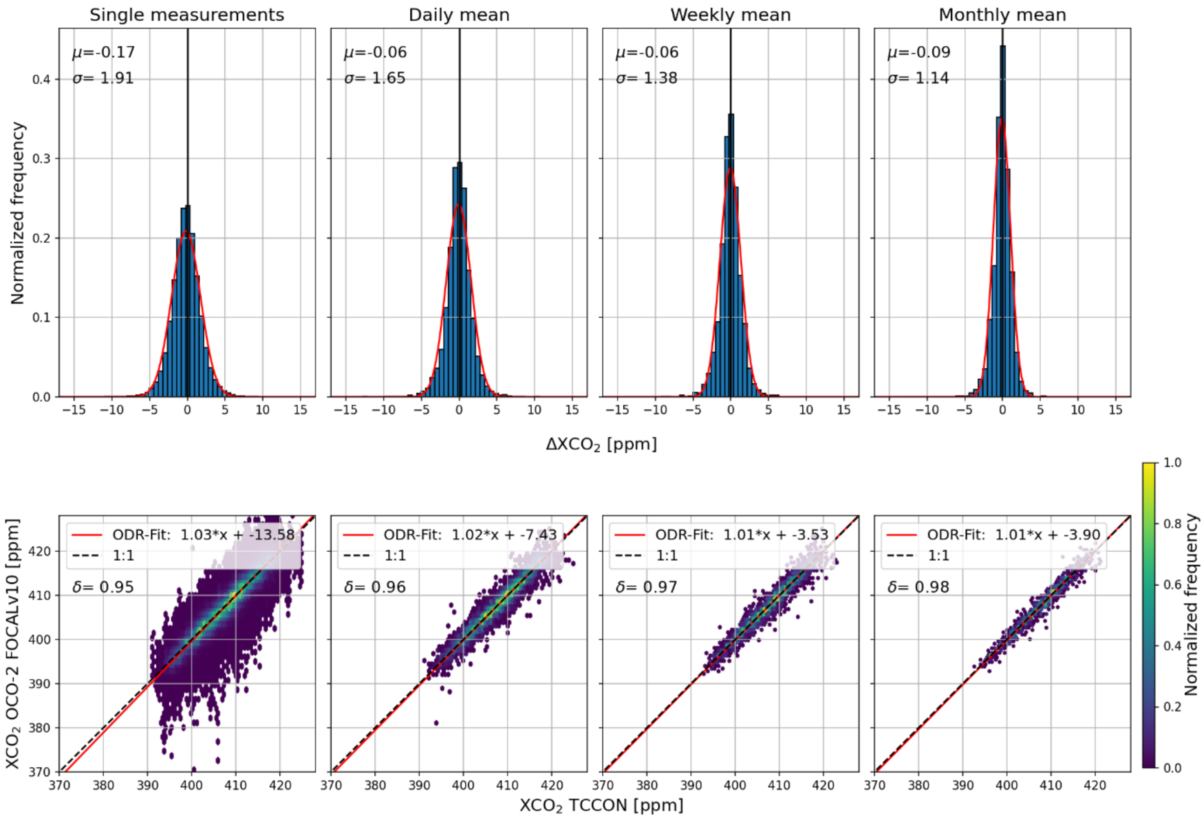

Figure 5.3: *Overall overview on the agreement of the FOCAL data (and its averages) with TCCON data at all sites. Top: Normalized histograms of the difference FOCAL – TCCON. Bottom: Heat maps TCCON vs. FOCAL including one-to-one line, orthogonal distance regression (ODR), and Pearson correlation coefficient* $\boldsymbol{\delta}$*.*

Here, t is the time of the measurements in fractional years, a_{0-3} the free fit parameters from which we compute the systematic error components, and ε the fit residuum. Figure 5.4 shows at the example of the TCCON sites Lamont and Reunion Island the fitted bias functions for the individual soundings, daily, weekly, and monthly averages.

We compute the station or regional bias Δ_{reg} from the average (ave) of the fit values:

5-2 $$\Delta_{reg} = \text{ave}[a_0 + a_1 t + a_2 \sin(2\pi t + a_3)]$$

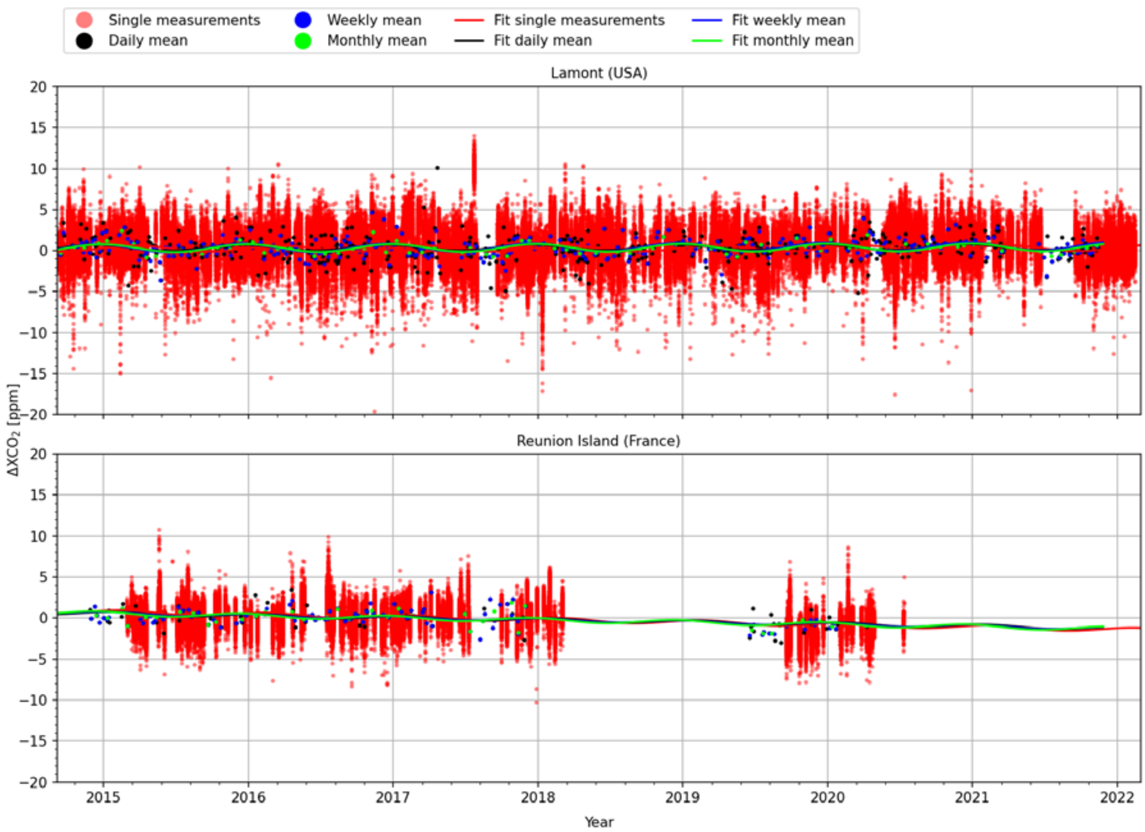

Figure 5.4: *ΔXCO_2 (FOCAL – TCCON) for the co-locations of the single measurements, daily, weekly, and monthly averages at the TCCON sites Lamont (top) and Reunion Island (bottom). Additionally, the corresponding fits of the bias model (Eq. 5-1) are shown.*

The seasonal bias Δ_{sea} is computed from the standard deviation (std) of the seasonal component of the fit:

5-3 $$\Delta_{sea} = \mathrm{std}[a_2 \sin(2\pi t + a_3)]$$

It shall be noted that the vector t consists only of the time of the measurements. This means, Δ_{sea} is only computed from those parts of the seasonal cycle actually covered by observations.

The linear drift corresponds to the fit parameter $\Delta_{dri} = a_1$, and the single sounding precision, i.e., the stochastic retrieval uncertainty σ, is computed from the standard deviation of the residuum.

5-4 $$\sigma = \mathrm{std}[\varepsilon]$$

We define the spatiotemporal bias Δ_{spt} as combination of regional and seasonal bias.

5-5 $$\Delta_{spt} = \sqrt{\Delta_{reg}{}^2 + \Delta_{sea}{}^2}$$

The FOCAL retrieval algorithm reports on the XCO_2 stochastic uncertainty σ'_{rep} for each sounding. From these values, we compute the average reported uncertainty σ_{rep} per station by:

5-6 $$\sigma_{rep} = \sqrt{\mathrm{ave}\left(\sigma'_{rep}{}^2\right)}$$

5.1.4.2 Summarizing performance statistics

Based on the per site statistics, the following summarizing performance statistics are calculated.

The average site bias $\overline{\Delta_{reg}}$ and the site-to-site variability is computed from the mean and the standard deviation of the individual site biases:

5-7 $$\overline{\Delta_{reg}} = \mathrm{ave}(\Delta_{reg}) \pm \mathrm{std}(\Delta_{reg})$$

The average seasonal bias $\overline{\Delta_{sea}}$ is computed by:

5-8 $$\overline{\Delta_{sea}} = \mathrm{avg}(\Delta_{sea})$$

The overall spatiotemporal bias $\overline{\Delta_{spt}}$ is computed by:

5-9 $$\overline{\Delta_{spt}} = \sqrt{\overline{\Delta_{reg}}^2 + \overline{\Delta_{sea}}^2}$$

The average drift and the drift uncertainty is computed by:

5-10 $$\overline{\Delta_{dri}} = \mathrm{ave}(\Delta_{dri}) \pm \mathrm{std}(\Delta_{dri})$$

As the linear drift can be assumed to be globally constant, the station-to-station standard deviation of the linear drift can be considered a measure of its uncertainty. The overall single sounding precision and reported uncertainty are computed by:

5-11 $$\overline{\sigma} = \sqrt{\mathrm{ave}(\sigma^2)}$$

5-12 $$\overline{\sigma_{rep}} = \sqrt{\mathrm{ave}\left({\sigma_{rep}}^2\right)}$$

5.1.5 Results

The results of all site performance statistics as well as the summarizing performance statistics for individual soundings, daily, weekly, and monthly averages are illustrated in Figure 5.5. Based on this figure, it can first be noted that averaging does not have a substantial impact on the validation results for the systematic error components. This is especially the case for the summarizing performance statistics which are similar for individual soundings, daily, weekly, and monthly averages. Therefore, it is sufficient that we primarily concentrate on the results for individual soundings from now on and Table 5.1 lists only values of the statistics for individual soundings.

However, the results for the stochastic error component show some important differences. The overall result for the stochastic error of the individual soundings amounts to 1.77ppm which agrees well with the corresponding reported uncertainty of 1.77ppm. This is not the case for the results of the averages. The actual stochastic error reduces for daily (1.45ppm), weekly (1.17ppm), and monthly (0.86ppm) averages, but the reduction is far less pronounced as for the reported uncertainty which has been computed under the assumption of uncorrelated errors. Therefore, it has to be expected that the separation of systematic and stochastic errors by Eq. 5-1 is incomplete at least for the individual soundings. In other words, it can be expected that parts of the residuum ε of Eq. 5-1 for the individual soundings are actually of systematic origin.

For this reason, we grouped the residuum into bins consisting of $n = 1, 2, 3, \cdots$ elements and analyzed its standard deviation as function of the bin size. As the reported retrieval precision is usually relatively constant at one TCCON site, it should be expected that the standard deviation of the binned residuum scales approximately with $1/\sqrt{n}$. We performed this experiment for the TCCON site Lamont because of the large number of co-locations. As shown in Figure 5.6 (top/left), the actual precision (standard deviation of the binned residuum) of the individual soundings does not follow the curve expected for uncorrelated errors. In contrast, the actual precision of daily (Figure 5.6, top/right), weekly (Figure 5.6, bottom/left), and monthly averages (Figure 5.6, bottom/right) agrees well with the expectation for uncorrelated errors. These results may differ in detail from TCCON site to TCCON site but indicates that the errors of the individual soundings may have additional systematic components not covered by the seasonal component of Eq. 5-1.

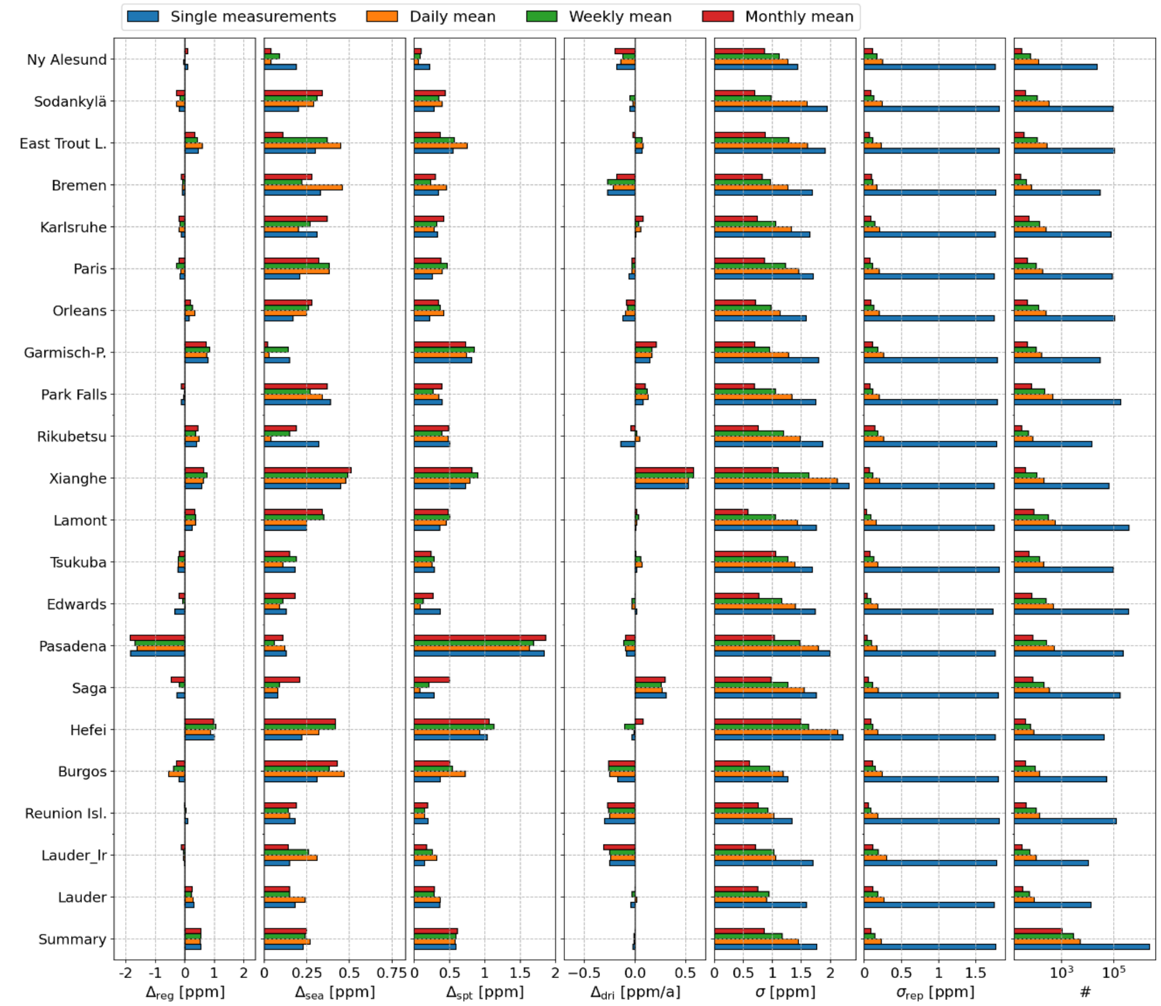

Figure 5.5: *Validation results for FOCAL single measurements, daily, weekly, and monthly averages. From left to right, the figure shows the per site performance statistics (Section 5.1.4.1) regional (Δ_{reg}), seasonal (Δ_{sea}), and spatiotemporal bias (Δ_{spt}), the linear drift (Δ_{dri}), the actual (σ) and reported precision (σ_{rep}), and the number of soundings (#). TCCON sites are order from top to bottom by average latitude of the co-located satellite soundings. The last row includes the summarizing performance statistics as defined in Section 5.1.4.2.*

Table 5.1: *Validation results for FOCAL single measurements. From left to right, the table lists the per site performance statistics (Section 5.1.4.1) regional (Δ_{reg}), seasonal (Δ_{sea}), and spatiotemporal bias (Δ_{spt}), the linear drift (Δ_{dri}), the actual (σ) and reported precision (σ_{rep}), and the number of soundings (#). TCCON sites are order from top to bottom by average latitude of the co-located satellite soundings. The last row includes the summarizing performance statistics as defined in Section 5.1.4.2.*

Station	Δ_{reg} [ppm]	Δ_{sea} [ppm]	Δ_{spt} [ppm]	Δ_{dri} [ppm/a]	σ [ppm]	σ_{rep} [ppm]	#
Ny Alesund	0.10	0.19	0.22	-0.18	1.44	1.76	22983
Sodankylä	-0.19	0.20	0.28	-0.05	1.94	1.81	98542
East Trout Lake	0.46	0.30	0.55	0.07	1.91	1.81	106147
Bremen	-0.08	0.33	0.34	-0.27	1.69	1.77	29961
Karlsruhe	-0.11	0.31	0.33	0.01	1.65	1.76	77705
Paris	-0.16	0.21	0.26	-0.06	1.71	1.75	89541
Orleans	0.14	0.17	0.22	-0.12	1.58	1.75	112416
Garmisch-P.	0.80	0.15	0.81	0.15	1.80	1.79	30128
Park Falls	-0.11	0.39	0.40	0.08	1.75	1.79	187305
Rikubetsu	0.40	0.32	0.51	-0.14	1.87	1.78	14678
Xianghe	0.57	0.45	0.73	0.53	2.32	1.75	66766
Lamont	0.25	0.25	0.36	0.01	1.76	1.75	381097
Tsukuba	-0.23	0.18	0.29	0.02	1.69	1.81	96345
Edwards	-0.34	0.13	0.37	0.02	1.74	1.73	362397
Pasadena	-1.83	0.13	1.84	-0.08	1.99	1.76	230259
Saga	-0.27	0.08	0.28	0.31	1.76	1.80	178540
Hefei	1.01	0.22	1.03	-0.03	2.22	1.76	42340
Burgos	-0.20	0.31	0.37	-0.17	1.27	1.80	53607
Reunion Isl.	0.09	0.18	0.20	-0.30	1.34	1.81	124180
Lauder_lr	-0.02	0.15	0.15	-0.25	1.70	1.78	10766
Lauder	0.31	0.18	0.36	-0.04	1.59	1.75	13430
Summary	**0.03±0.55**	**0.23**	**0.59**	**-0.02±0.19**	**1.77**	**1.77**	**2329133**

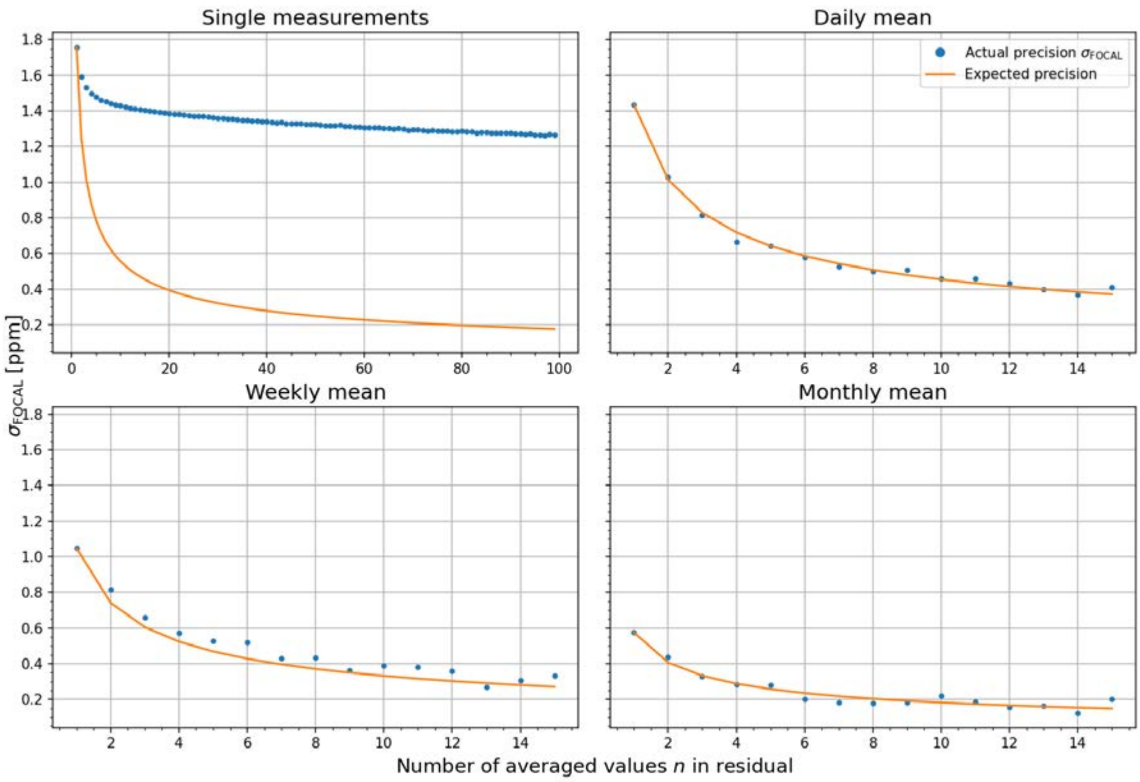

Figure 5.6: *Actual and expected retrieval precision of FOCAL computed from residuals with increasing bin size for the TCCON site Lamont for single measurements (top/left), daily (top/right), weekly (bottom/left), and monthly averages (bottom/right).*

The validation results for the individual soundings (Table 5.1) show that there is only a small overall average bias of 0.03ppm. Regional biases estimated from the site-to-site bias variability amount to 0.55ppm and are strongly influenced by the relatively large negative bias of -1.8ppm at the TCCON site Pasadena. The average seasonal and spatiotemporal bias amounts to 0.23ppm and 0.59ppm, respectively. The overall linear drift of -0.02ppm/a is much smaller than its site-to-site variability of 0.19ppm and, therefore, considered not significant.

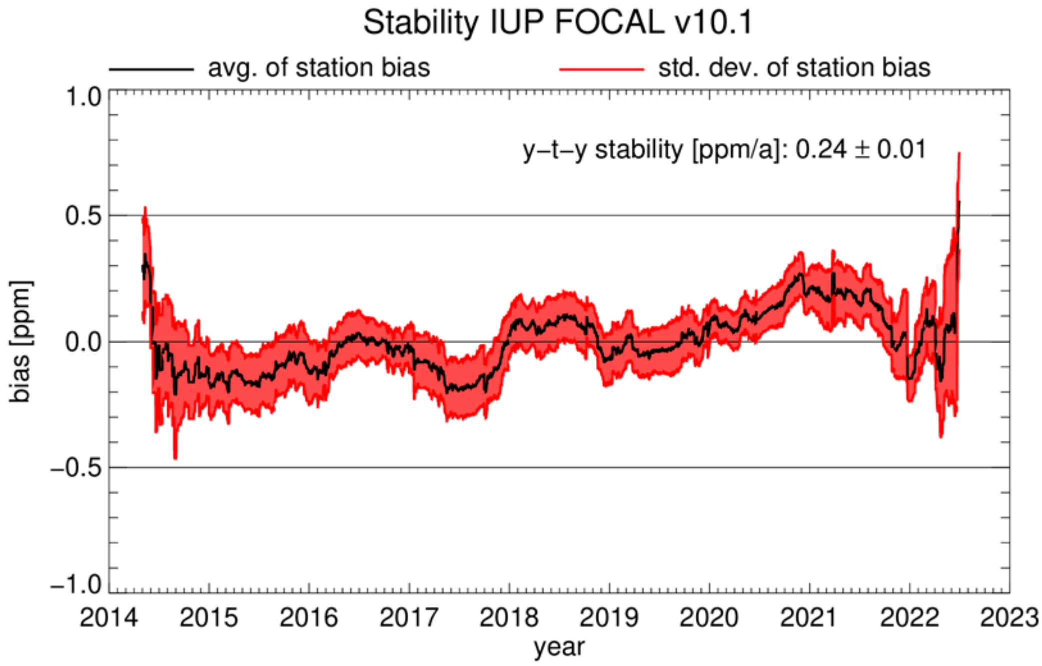

Figure 5.7: *Stability analyses for FOCAL. The black curve shows the average station bias and the red curves its uncertainty represented by the station-to-station standard deviation.*

Additionally, a measure for the year-to-year stability is computed as follows. For each TCCON site, the residual ε of the bias fit (Eq. 5-1) is smoothed by a running average of 365 days. Only days where more than 10 co-locations contribute to the running average of at least 5 TCCON sites are further considered. At these days, the station-to-station average is calculated (Figure 5.7, black line).

The corresponding expected uncertainty is computed from the standard error of the mean (derived from the station-to-station standard deviation and the number of stations) and by error propagation of the reported single sounding uncertainties (Figure 5.7, red line). For FOCAL, the average is always between about -0.2ppm and 0.5ppm with an uncertainty of typically about 0.15ppm. Most of the time, the average is not significantly different from zero, i.e., its two-sigma uncertainty is larger than its absolute value. Due to the relatively large uncertainty, we decided to compute not the maximum minus minimum as a measure for the year-to-year stability because this quantity can be expected to increase with length of the time series simply due to statistics. Therefore, we estimate the year-to-year stability by randomly selecting pairs of dates with a time difference of at least 365 days. For each selection we computed the difference modified by a random component corresponding to the estimated uncertainty. From 1000 of such pairs, we compute the standard deviation as estimate for the year-to-year stability. We repeat this experiment 1000 times and compute the average (0.24ppm) and standard deviation (0.01ppm). From this, we conclude that the year-to-year stability is 0.24ppm/a (Figure 5.7).

5.1.6 Summary

We validated the FOCAL v10.1 XCO_2 data product with TCCON GGG2020 data of the years 2014 – 2022. The validation has been performed for daily, weekly, and monthly averages as well as for single soundings. Analyzing the single soundings without temporal averaging, we find that the overall bias of the FOCAL data amounts to 0.03ppm. Regional biases vary from site to site by 0.55ppm. Seasonal and spatiotemporal biases amount on average to 0.23ppm and 0.59ppm, respectively. We found no significant linear drift (-0.02±0.19ppm). In the context of the systematic error characteristics, it shall be noted that **/Wunch et al., 2010, 2011/** specifies the accuracy (1σ) of TCCON to be about 0.4ppm. This means, e.g., that it cannot be expected to find regional biases considerably less than 0.4ppm using TCCON as reference. We find that the inferred systematic errors, i.e., regional, seasonal, and spatiotemporal biases as well as linear drift, do not critically depend on averaging. The year-to-year stability has been estimated to be 0.24ppm/a. The overall precision of the individual soundings is 1.77ppm which agrees well with the corresponding reported uncertainty of 1.77ppm. The overall precision improves for daily (1.45ppm), weekly (1.17ppm), and monthly (0.86ppm) averages. We find indications that the estimated precision of the individual soundings does actually comprise not only purely stochastic but also residual unknown systematic components. No such indications were found for the daily, weekly, and monthly averages. **Table 5.1-2** presents an overview of the estimated data quality as obtained from comparisons with TCCON ground-based reference observations.

Table 5.1-2: *Summary validation of product CO2_OC2_FOCA.*

Product Quality Summary Table for Product: CO2_OC2_FOCA Level: 2, Version: v10.1, Time period covered: 9.2014 – 02.2022 Assessment: Data Provider (DP)			
Parameter [unit]	**Achieved performance**	**Requirement**	**Comments**
Single measurement precision (1-sigma) in [ppm]	1.77	< 8 (T) < 3 (B) < 1 (G)	Computed as standard deviation of the difference to TCCON
Uncertainty ratio [-]: Ratio reported uncertainty to standard deviation of satellite-TCCON difference	1.00	-	No requirement but value close to unity expected for a high quality data product with reliable reported uncertainty.
Mean bias (global offset) [ppm]	0.03	-	No requirement but value close to zero expected for a high quality data product.
Accuracy: Relative systematic error [ppm]	Spatial: 0.55 Spatiotemporal: 0.61	< 0.5	Spatial: Computed as standard deviation of the biases at the various TCCON sites. Spatio-temporal: As "Spatial" but also considering seasonal biases.
Stability: Drift [ppm/year]	-0.02±0.19 (1-sigma)	< 0.5	Linear drift

5.2 Validation and intercomparison results for product CO2_TAN_OCFP

Development of this product ended at the end of Phase 1 with CRDP7. Please see the relevant CRDP7 CO2_TAN_OCFP documents available from https://climate.esa.int/en/projects/ghgs/key-documents/.

5.3 Validation and intercomparison results for product CO2_GO2_SRFP

The CO2_GO2_SRFP product is retrieved from GOSAT-2 TANSO-FTS SWIR spectra using the RemoTeC algorithm that has been jointly developed by SRON and KIT **/Butz et al., 2011; Schepers et al., 2012/**. The retrievals are performed globally for the time period between February 2019 and December 2021 and are evaluated against ground based TCCON observations.

5.3.1 Detailed results

To assess the quality of SRFP retrieval XCO_2 observations against TCCON values, SRFP soundings are matched to TCCON observations spatially and temporally. GOSAT-2 observations are co-located with TCCON sites based on a square latitude and longitude region around each TCCON site (in ±2.5º latitude/longitude box). For the temporal co-location we select only the TCCON measurements whose observation time falls within ±2 hour of each GOSAT-2 observation time. The TCCON observations that match these criteria are averaged for each individual GOSAT-2 observation.

We co-located GOSAT-2 and TCCON measurements with a maximum time difference of 2.5h, a maximum distance of 300 km in both longitudinal and latitudinal directions. In cases of multiple TCCON measurements of the same site collocating with a GOSAT-2 sounding, we averaged the TCCON measurements. In total we achieve 12,557 collocations for land soundings and 118 collocations over ocean.

The comparions for each TCCON site is shown in **Figure 5.3-1**. The statistics (mean bias, standard deviation) for each site are given in **Table 5.3-1**. The overall correlation between the GOSAT-2 and TCCON retrievals is given in **Figure 5.3-2**. The mean bias (global offset) amounts to -0.01 ppm. The standard deviation of the site biases (spatial accuracy or station-to-station variability) is 0.5 ppm. The single measurement precision of GOSAT-2 compared to TCCON amounts to 2.21 ppm.

Figure 5-3-1: Comparison of land single soundings of XCO_2 from the full physics retrieval (blue circles) with co-located TCCON (pink triangles) measurements at all TCCON sites for the period Feb 2019 to Dec 2021. Histograms are also given for each station indicating the number of GOSAT-2 retrievals present throughout the time series.

Figure 5-3-1cont.

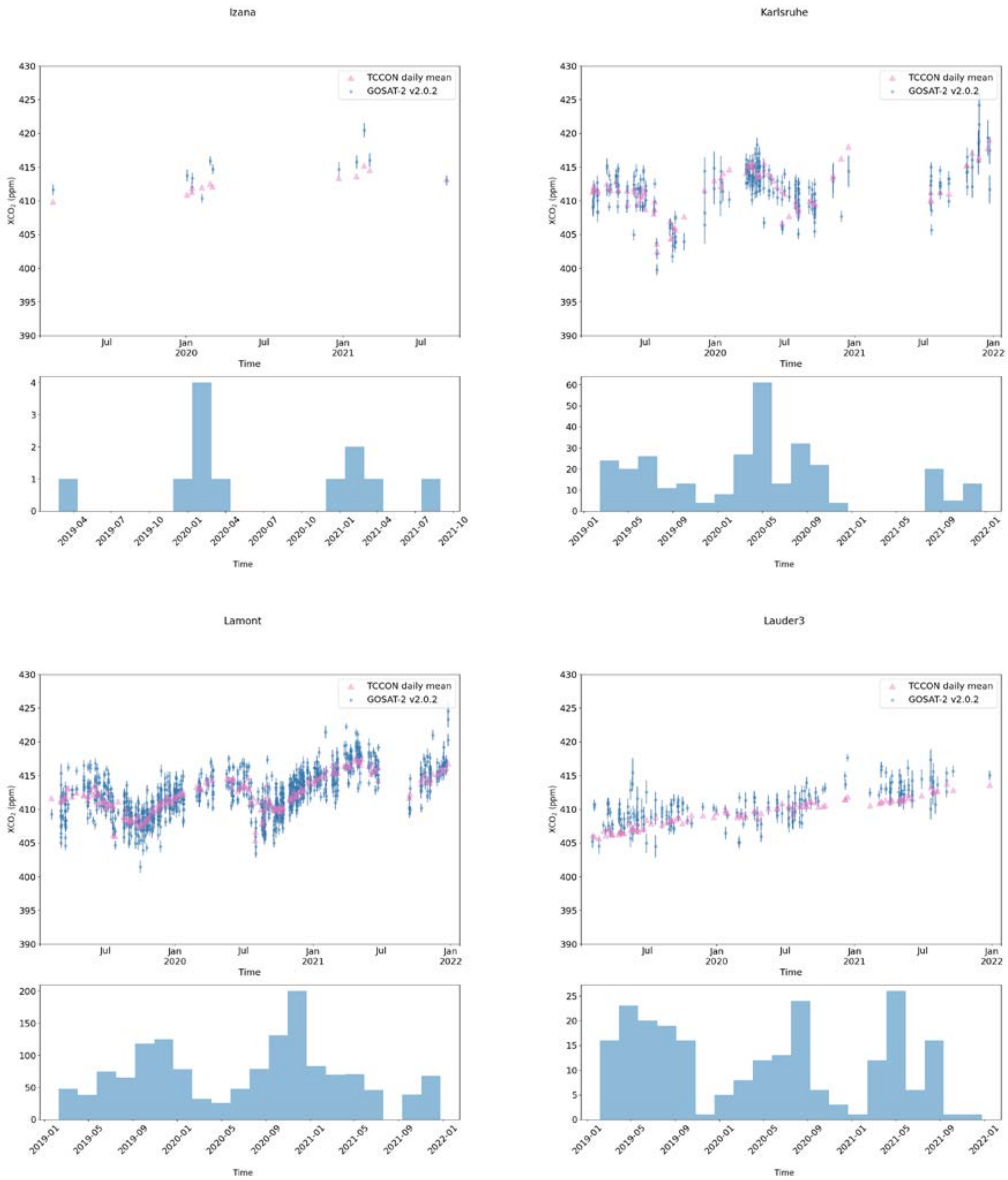

Figure 5-3-1 cont.

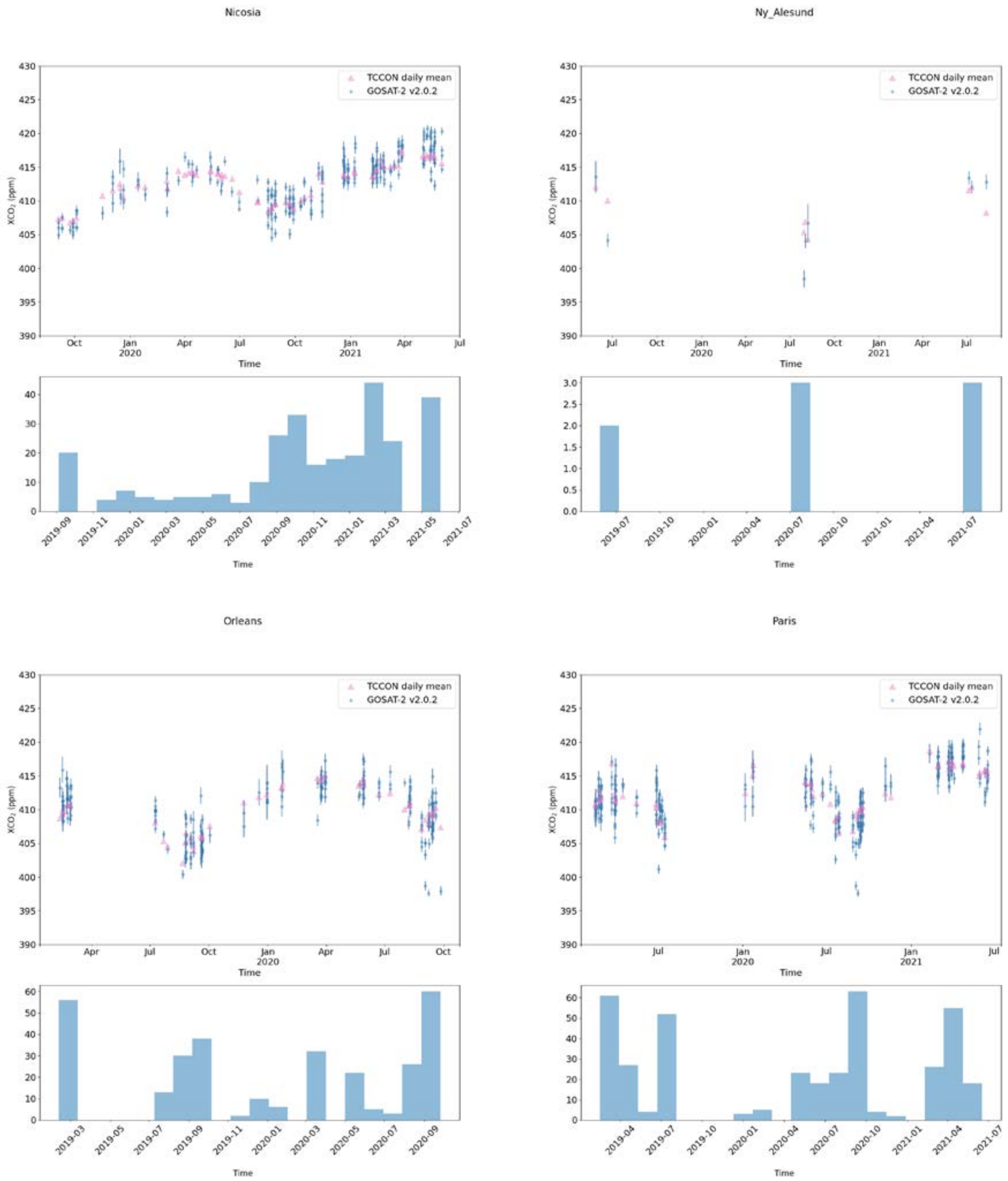

Figure 5-3-1 cont.

Figure 5-3-1 cont.

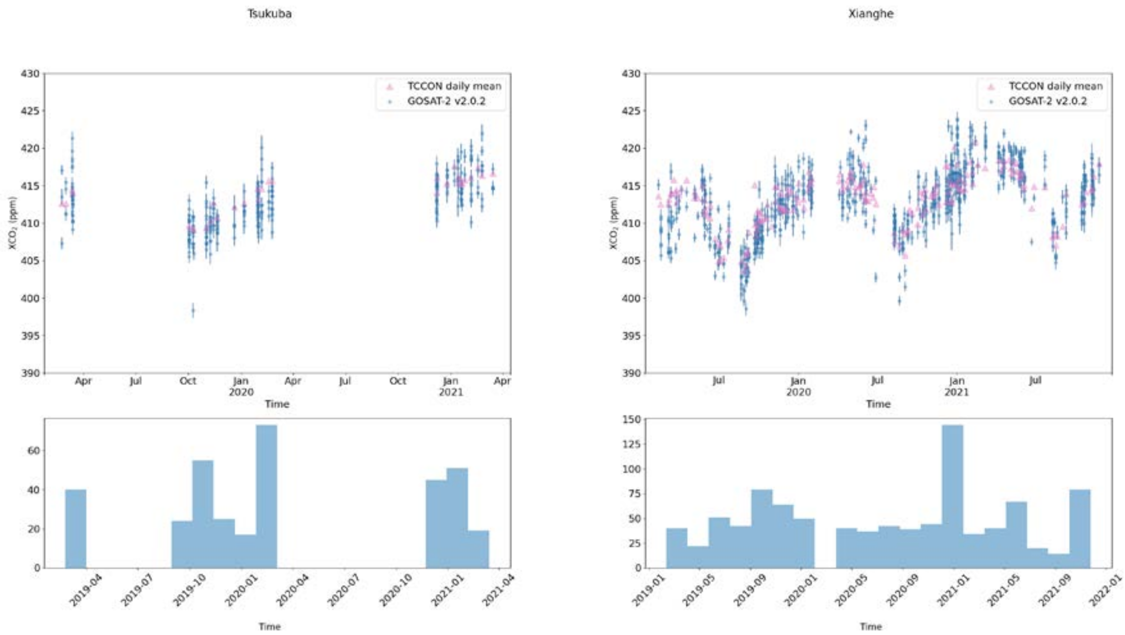

Figure 5-3-1 cont.

Table 5.3-1: Overview of the SRFP/RemoTeC XCO_2 validation with TCCON (after bias correction).

TCCON site [Land mode]	Number of co-locations [-]	Mean difference [ppm]	Standard deviation of difference [ppm]
Bremen	139	-0.18	1.91
Burgos	129	0.40	1.97
Caltech	2580	-1.02	2.09
East_Trout_Lake	353	0.48	2.48
Edwards	3158	0.64	2.02
Eureka	89	-0.26	3.90
Garmisch	324	0.09	2.33
Hefei	136	-0.49	2.62
Izana	12	1.73	1.67
Karlsruhe	303	-0.18	2.17
Lamont	1440	0.18	1.72
Lauder	229	1.08	1.85
Nicosia	288	0.31	1.77
Ny_Alesund	8	-0.69	3.87
Orleans	303	-0.19	2.16
Paris	384	-0.15	2.26
Park_Falls	420	0.26	2.11
Rikubetsu	170	0.53	2.07
Saga	627	0.33	2.09
Sodankyla	168	-0.49	2.33
Tsukuba	349	-0.83	2.26
Xianghe	948	-0.16	2.49
All observations	12557	-0.01	2.21

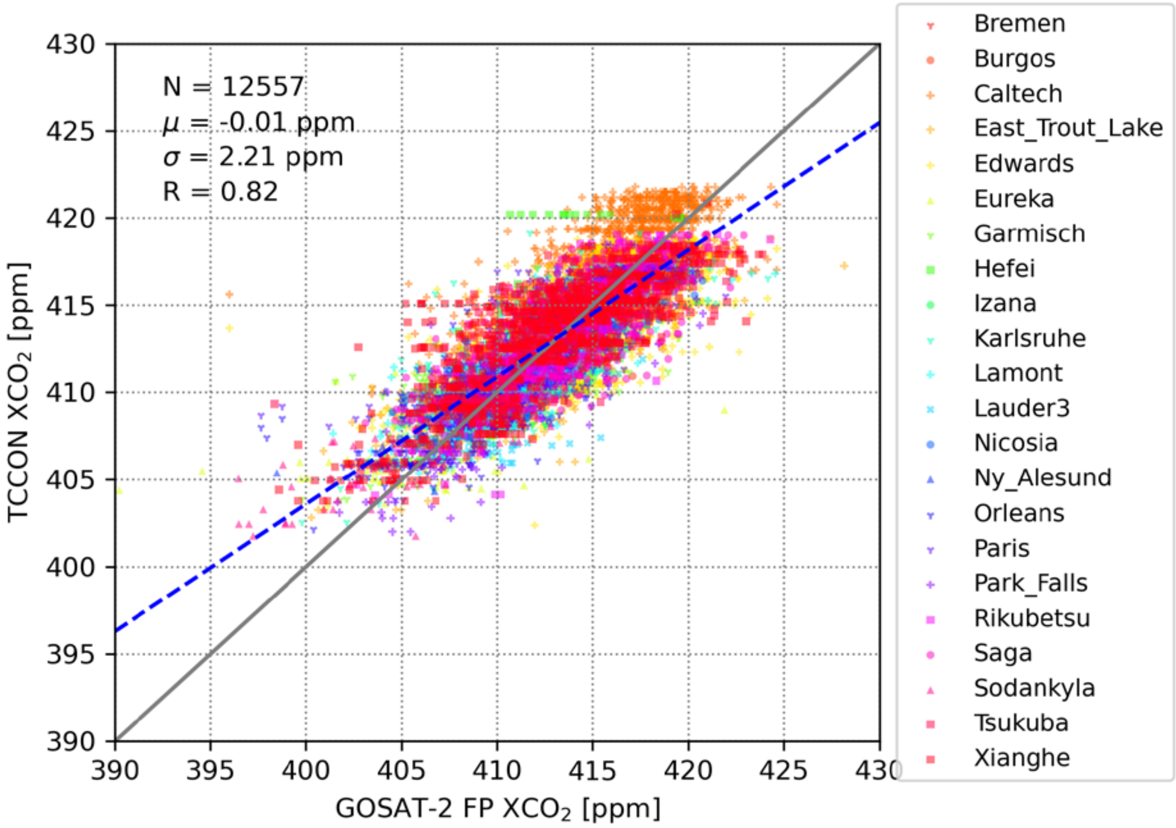

Figure 5-3-2: Validation of single soundings of FP XCO_2 with collocated TCCON measurements at all TCCON sites for the period Feb. 2019 - Dec 2021. Numbers in the figures: μ = bias, i.e., average of the difference; σ = single measurement precision, i.e., standard deviation of the difference; N = number of co-locations; R = Pearson correlation coefficient.

The error that comes out of the RemoTeC retrieval is just a purely statistical error on the radiance that has been propagated through the entire retrieval chain.

In order to more accurately estimate the actual random error on the GOSAT-2 sounding, we applied the following procedure to obtain a scaling factor with which to scale our statistical error. We take the absolute difference of every co-located sounding and divide it by the retrieved statistical error corresponding to that sounding. We then average these values to obtain the average scaling factor by which to scale the retrieved statistical error to obtain a more correct estimate of the random error.

Based on the analysis, we obtain the following scaling factors for the SRFP XCO_2 product, 2.36 for land retrievals and 3.24 for ocean retrievals and an uncertainty ratio of 0.83 and 0.82 for land and ocean, respectively.

5.3.2 Summary

The result of the validation of the CO2_GO2_SRFP dataset is given in **Table 5.3-2** and compared to the requirement. The mean estimate of the single-measurement precision is 2.21 ppm which exceeds the goal requirement but is within the breakthrough requirement of 3 ppm. The uncertainties provided by RemoTeC agree on average with the observed scatter of the data when compared to TCCON. The mean (global bias) of the GOSAT-2 XCO_2 retrieval is -0.01 ppm with a relative accuracy of 0.5 ppm which meets the requirement of 0.5 ppm.

Table 5.3-2: Summary validation of product CO2_GO2_SRFP by the data provider using TCCON ground-based reference data.

Product Quality Summary Table for Product: CO2_GO2_SRFP Level: 2, Version: v2.0.2, Time period covered: 2.2019 – 12.2021 Assessment: Data Provider (DP)			
Parameter [unit]	**Achieved performance**	**Requirement**	**Comments**
Single measurement precision (1-sigma) in [ppm]	2.21	< 8 (T) < 3 (B) < 1 (G)	Computed as standard deviation of the difference to TCCON
Uncertainty ratio [-]: Ratio reported uncertainty to standard deviation of satellite-TCCON difference	0.83 (0.82 sunglint)	-	No requirement but value close to unity expected for a high quality data product with reliable reported uncertainty.
Mean bias (global offset) [ppm]	-0.01	-	No requirement but value close to zero expected for a high quality data product.
Accuracy: Relative systematic error [ppm]	Spatial: 0.5 Spatio-temporal: 1.0	< 0.5	Spatial: Computed as standard deviation of the biases at the various TCCON sites. Spatio-temporal: As "Spatial" but also considering seasonal biases.
Stability: Drift [ppm/year]	0.46	< 0.5	Linear drift

5.4 Validation and intercomparison results for product CH4_S5P_WFMD

Validation results for XCH_4 retrieved from TROPOMI with the WFMDv1.8 algorithm **/Schneising et al., 2023/** are summarised in this section. The validation data set is the GGG2020 collection of the Total Carbon Column Observing Network (TCCON) (available from https://tccondata.org/). To ensure comparability, all TCCON sites use similar instrumentation (Bruker IFS 125HR) and a common retrieval algorithm. The TCCON data are tied to the WMO trace gas scale using airborne in situ measurements applying individual scaling factors for each species. The estimated TCCON accuracy (1σ) is about 3.5 ppb for XCH_4. From the validation with TCCON data at 26 TCCON sites, realistic error estimates of the satellite data are provided.

To compare the satellite data with TCCON quantitatively, it has to be taken into account that the sensitivities of the instruments differ from each other and that individual apriori profiles are used to determine the best estimate of the true atmospheric state, respectively. The first step is to correct for the apriori contribution to the smoothing equation by adjusting the measurements for a common apriori. Here we use the TCCON prior as the common apriori profile for all measurements:

$$\hat{c}_{adj} = \hat{c} + \frac{1}{m_0} \sum_l m_l \, (1 - A_l)(x_{a,T}^l - x_a^l)$$

In this equation, $\hat{c}$ represents the originally retrieved TROPOMI column-averaged dry air mole fraction, l is the index of the vertical layer, A_l the corresponding column averaging kernel of the TROPOMI algorithm, $\boldsymbol{x}_a$ and $\boldsymbol{x}_{a,T}$ the TROPOMI and TCCON apriori dry air mole fraction profiles. m_l is the mass of dry air determined from the dry air pressure difference between the upper and lower boundary of layer l and $m_0 = \sum_l m_l$ is the total mass of dry air. To minimise the smoothing error introduced by the averaging kernels we do not compare $\hat{c}_{adj}$ directly with the retrieved TCCON mole fractions $\hat{c}_T$ but rather with the adjusted expression

$$\hat{c}_{T,adj} = c_{a,T} + \left(\frac{\hat{c}_T}{c_{a,T}} - 1\right) \frac{1}{m_0} \sum_l m_l A_l x_{a,T}^l$$

Thereby, $c_{a,T}$ represents the TCCON apriori column-averaged dry air mole fraction associated with the apriori profile $\boldsymbol{x}_{a,T}$.

5.4.1 Detailed results

For the comparison a set of collocation criteria has been specified. The representativity is maximised by as strict as possible criteria while concurrently ensuring sufficient data for a sound and stable comparison. This trade-off is resolved by the following selection. The spatial collocation criterion requires the satellite measurements to lie within a radius of 100 km around the TCCON site and that the altitude difference is smaller than 250 m. The temporal collocation criterion is set to ±2 hours. For each satellite measurement within the collocation radius, all TCCON data meeting the temporal collocation criterion are averaged to obtain a unique satellite-TCCON data pair. This approach is consistent with the well-established methods used in previous GHG-CCI PVIRs.

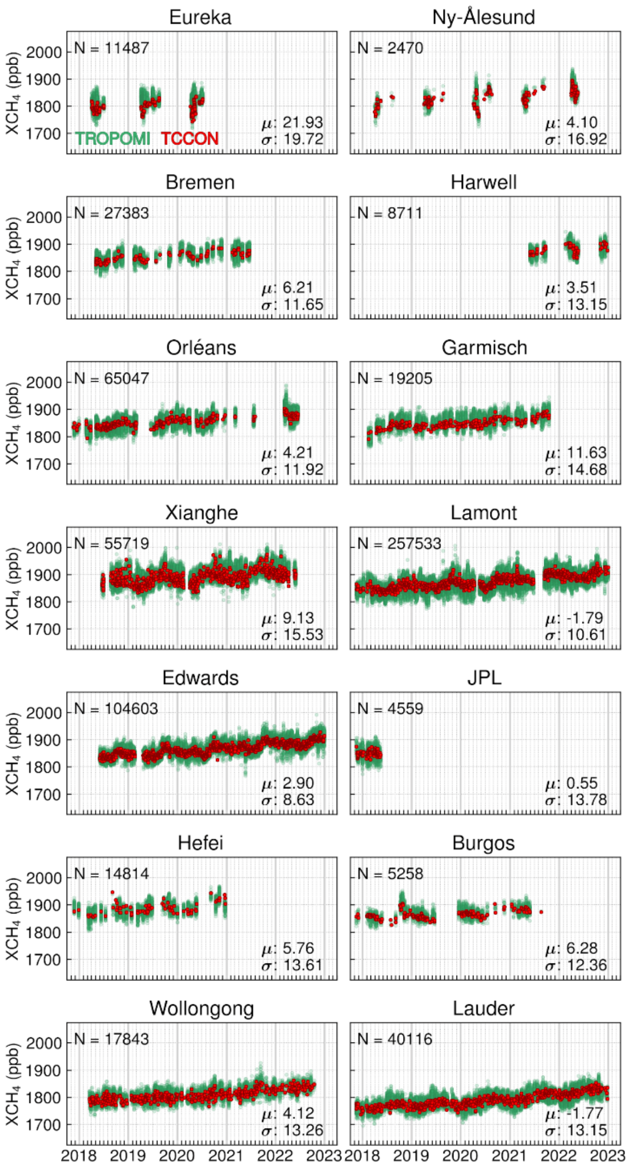

Figure 5.4-1: Comparison of the TROPOMI/WFMD v1.8 XCH_4 time series (green) with ground-based measurements from the TCCON (red). For each site, $\boldsymbol{N}$ is the number of collocations, $\boldsymbol{\mu}$ corresponds to the mean bias and $\boldsymbol{\sigma}$ to the scatter of the satellite data relative to TCCON in ppb.

The validation results are summarised in **Figure 5.4-1** including the mean bias μ and the scatter σ relative to TCCON for each site. As a consequence of the altitude representativity criterion, there are not enough collocations for a robust comparison at the mountain site Izaña. The parameter σ is estimated from Huber's Proposal-2 M-estimator, which is a well-established estimator of location and scale being robust against outliers of a normal distribution. This is an appropriate choice and preferred over the standard deviation, because one is interested in the actual single measurement precision without distortion of the results by a few outliers, which are rather attributed to systematic errors, e.g. due to residual clouds. As a consequence, outliers are fully included in the computation of the systematic error but get lower weight in the robust determination of the random error, which is interpreted as a measure of the repeatability of measurements.

It is also checked whether the respective site biases are sensitive to the selection of the spatial collocation radius, which is an indication of sources within the satellite collocation area with only marginal influence on the TCCON measurements itself. A considerable sensitivity was found for XCH_4 at Edwards. The collocation region intersects oil production areas in California's Central Valley (in contrast to Caltech and JPL, see **/Schneising et al., 2019/**) as well as the South Coast Air Basin (SoCAB), which has a well-known methane enhancement. As such nearby sources limit the representativity of affected satellite measurements, the collocation radius is reduced to 50 km for Edwards. A corresponding reduction of the collocation radius was also applied for the Chinese TCCON site Xianghe.

The results for the individual sites are condensed to the following parameters for the overall quality assessment of the satellite data: the global offset is defined as the mean of the local biases at the individual sites, the random error is the global scatter of the differences to TCCON after subtraction of the respective regional biases, and the spatial systematic error is the standard deviation of the local offsets relative to TCCON at the individual sites as a measure of the station-to-station biases. For XCH_4 the global offset amounts to 4.38 ppb, the random error is 12.37 ppb (13.72 ppb when using the standard deviation instead of Huber's Proposal-2 M-estimator), and the spatial systematic error is given by 5.24 ppb. The seasonal systematic error is defined as the standard deviation of the four overall seasonal offsets (using all sites combined after subtraction of the respective local offsets) relative to TCCON and amounts to 1.13 ppb. The spatio-temporal systematic error (defined as the the root-sum-square of the spatial and seasonal systematic errors) amounts to 5.36 ppb, which is on the order of the estimated (station-to-station) accuracy of the TCCON of about 3.5 ppb.

When using the previous GGG2014 collection of the TCCON, all derived figures of merit are largely consistent with the GGG2020 estimates, except that the global offset is only 0.8 ppb then.

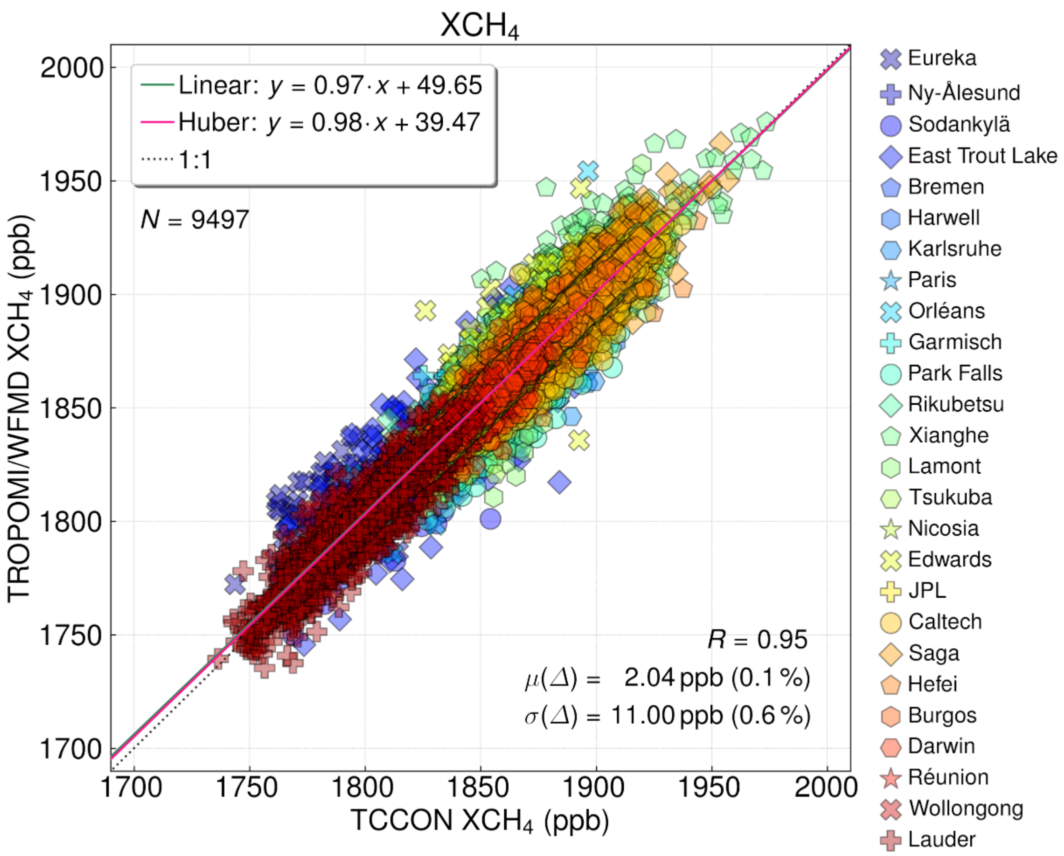

Figure 5.4-2: Comparison of the TROPOMI/WFMD data to the TCCON based on daily means. Specified are the linear regression results and the correlation of the data sets, as well as the mean and standard deviation of the difference. To analyse the impact of outliers, the regression is also performed for the Huber linear regression model, which is robust to outliers.

To further analyse how well the real temporal and spatial variations are captured by the TROPOMI data, **Figure 5.4-2** shows a comparison to TCCON based on daily means for days with more than three collocations. The obvious linear relationship with a high correlation of $R = 0.95$ underlines the typical good agreement of the satellite and validation data.

There are a few outliers where the satellite values are considerably lower than the TCCON values. These occasional instances are not site specific and can probably be ascribed to days with residual or partial cloud cover interfering with the satellite retrievals. Outliers at high latitude sites may be attributable to Arctic polar vortex air potentially causing the following related issues: associated fronts of different air masses may complicate the identification of collocations near the vortex edge and/or the stratospheric part of the methane profiles may be largely affected by the polar vortex leading to a considerable deviation from the assumed apriori profile shapes. It is verified that the impact of outliers on the regression is marginal by repeating the fit with the Huber linear regression model, which is robust to outliers and provides similar results to the standard linear regression here.

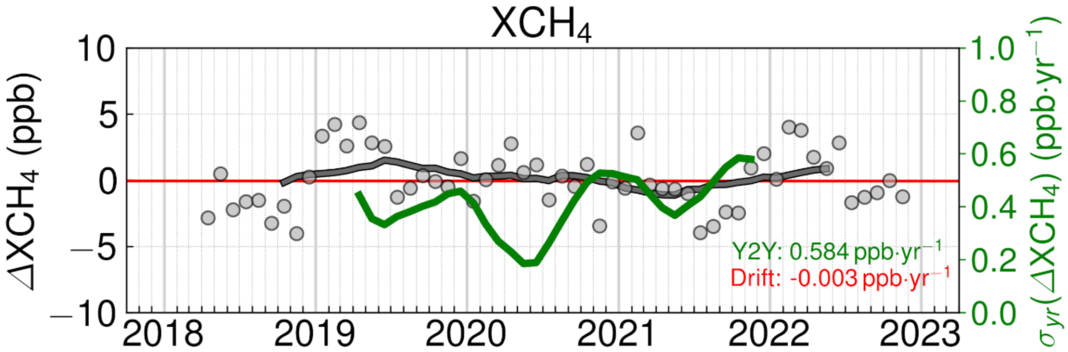

Figure 5.4-3: Long-term drift and year-to-year stability of TROPOMI/WFMD at TCCON sites.

To analyse the stability, we use comparisons with the TCCON since the start of the routine operations phase of Sentinel-5P to have sufficient data coverage. To assess the long-term drift stability, a robust Huber regression of the monthly mean differences relative to the reference (using all data combined after subtraction of the respective regional offsets) with time is used. The resulting stability estimate is -0.003 ppb/year (see red straight line in **Figure 5.4-3**).

The year-to-year stability allowing to detect potential jumps in the time series is defined in the following way: The one-year moving average of the differences relative to the reference (grey curve in **Figure 5.4-3**) is generated. For a given point in time t, let $\sigma_{yr}(t)$ be defined as the standard deviation of this deseasonalised difference within a one-year window around t (green curve in **Figure 5.4-3**). The year-to-year stability is then defined as the maximum of $\sigma_{yr}(t)$ over time, which amounts to 0.58 ppb/year here. Due to the moving average and the one-year moving standard deviation procedure, the green curve loses one year of data at the beginning and end of the time series. A longer time series of satellite data will allow a more sound and stable estimation of the year-to-year stability in the future.

The reported uncertainty of TROPOMI/WFMD v1.8 XCH_4 is validated based on a comparison to the measured scatter relative to the TCCON. After dividing up the reported uncertainties in equal sized bins of about 30000 measurements each, a robust regression provides the results shown in **Figure 5.4-4** (neglecting the random and systematic errors of the TCCON measurements) confirming that the reported estimates are realistic: The uncertainty ratio (reported uncertainty to measured scatter) is about 1.05, indicating a reliable estimation of the measurement uncertainties with a slight overestimation of the reported values.

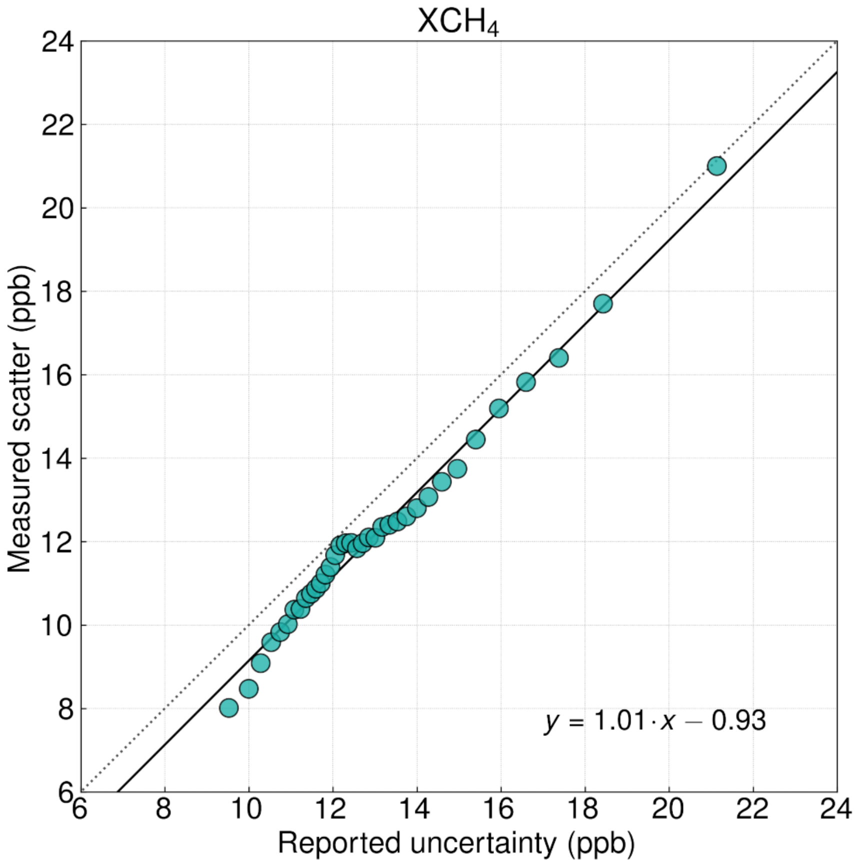

Figure 5.4-4: Comparison of the reported uncertainty of TROPOMI/WFMD v1.8 XCH_4 with the measured scatter relative to the TCCON after dividing up the reported uncertainties in equal sized bins.

5.4.2 Summary

In summary, the natural XCH_4 variations are well captured by the satellite data. We find a single measurement precision of the TROPOMI data of about 0.7%, while the station-to-station accuracy of the satellite data (0.3%) is comparable to the TCCON.

The single measurement precision is below the breakthrough requirement and the uncertainty ratio is close to 1. The accuracy also complies with the requirements and the mean bias is close to zero. The stability is well below the required value. **Table 5.4-1** presents an overview of the estimated data quality as obtained from comparisons with TCCON ground-based reference observations.

Table 5.4-1: Summary validation of product CH4_S5P_WFMD by the data provider using TCCON GGG2020 ground-based reference data.

Product Quality Summary Table for Product: CH4_S5P_WFMD Level: 2, Version: v1.8, Time period covered: 11.2017 – 12.2022 Assessment: Data Provider (DP)			
Parameter [unit]	**Achieved performance**	**Requirement**	**Comments**
Single measurement precision (1-sigma) in [ppb]	12.37	< 34 (T) < 17 (B) < 9 (G)	Computed as standard deviation of the difference to TCCON
Uncertainty ratio [-]: Ratio reported uncertainty to standard deviation of satellite-TCCON difference	1.05	-	No requirement but value close to unity expected for a high quality data product with reliable reported uncertainty.
Mean bias (global offset) [ppb]	4.38 (0.80 for GGG2014)	-	No requirement but value close to zero expected for a high quality data product.
Accuracy: Relative systematic error [ppb]	Spatial: 5.24 Spatio-temporal: 5.36	< 10	Spatial: Computed as standard deviation of the biases at the various TCCON sites. Spatio-temporal: As "Spatial" but also considering seasonal biases.
Stability: Drift [ppb/year]	-0.003	< 3	Linear drift

5.5 Validation and intercomparison results for product CH4_GO2_SRFP

The CH4_GO2_SRFP product is retrieved from GOSAT-2 TANSO-FTS SWIR spectra using the RemoTeC algorithm that has been jointly developed by SRON and KIT **/Butz et al., 2011; Schepers et al., 2012/**. The retrievals are performed globally for the time period between February 2019 and December 2021 and are evaluated against ground based TCCON observations.

5.5.1 Detailed results

To assess the quality of SRFP retrieval XCH_4 observations against ground based TCCON values, SRFP soundings are matched to TCCON observations spatially and temporally. GOSAT-2 observations are co-located with TCCON sites based on a square latitude and longitude region around each TCCON site (in ±2.5º latitude/longitude box). For the temporal co-location we select only the TCCON measurements whose observation time falls within ±2 hour of each GOSAT-2 observation time. The TCCON observations that match these criteria are averaged for each individual GOSAT-2 observation.

We co-located GOSAT-2 and TCCON measurements with a maximum time difference of 2.5h, a maximum distance of 300 km in both longitudinal and latitudinal directions. In cases of multiple TCCON measurements of the same site collocating with a GOSAT-2 sounding, we averaged the TCCON measurements. In total we achieve 8399 collocations for land soundings and 109 collocations over ocean.

The comparions for each TCCON site is shown in **Figure 5.5-1**. The statistics (mean bias, standard deviation) for each site are given in **Table 5.5-1**. The overall correlation between the GOSAT-2 and TCCON retrievals is given in **Figure 5.5-2**. The mean bias (global offset) amounts to -0.14 ppb. The standard deviation of the site biases (spatial accuracy or station-to-station variability) is 4.3 ppb. The single measurement precision of GOSAT-2 compared to TCCON amounts to 15.2 ppb.

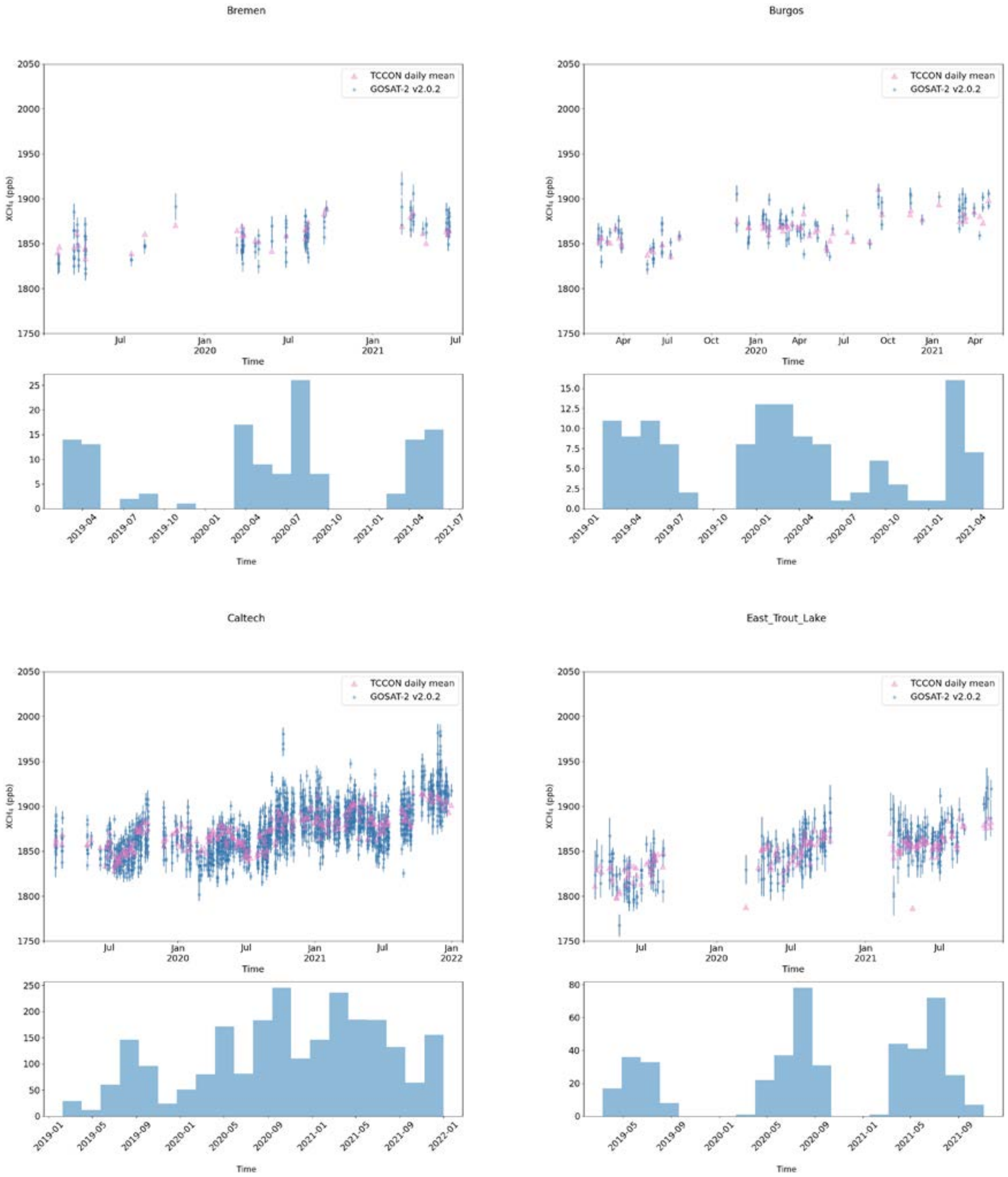

Figure 5.5-1: Comparison of land single soundings of XCH_4 from the full physics retrieval (blue circles) with co-located TCCON (pink triangles) measurements at all TCCON sites for the period Feb 2019 to Dec 2021. Histograms are also given for each station indicating the number of GOSAT-2 retrievals present throughout the time series.

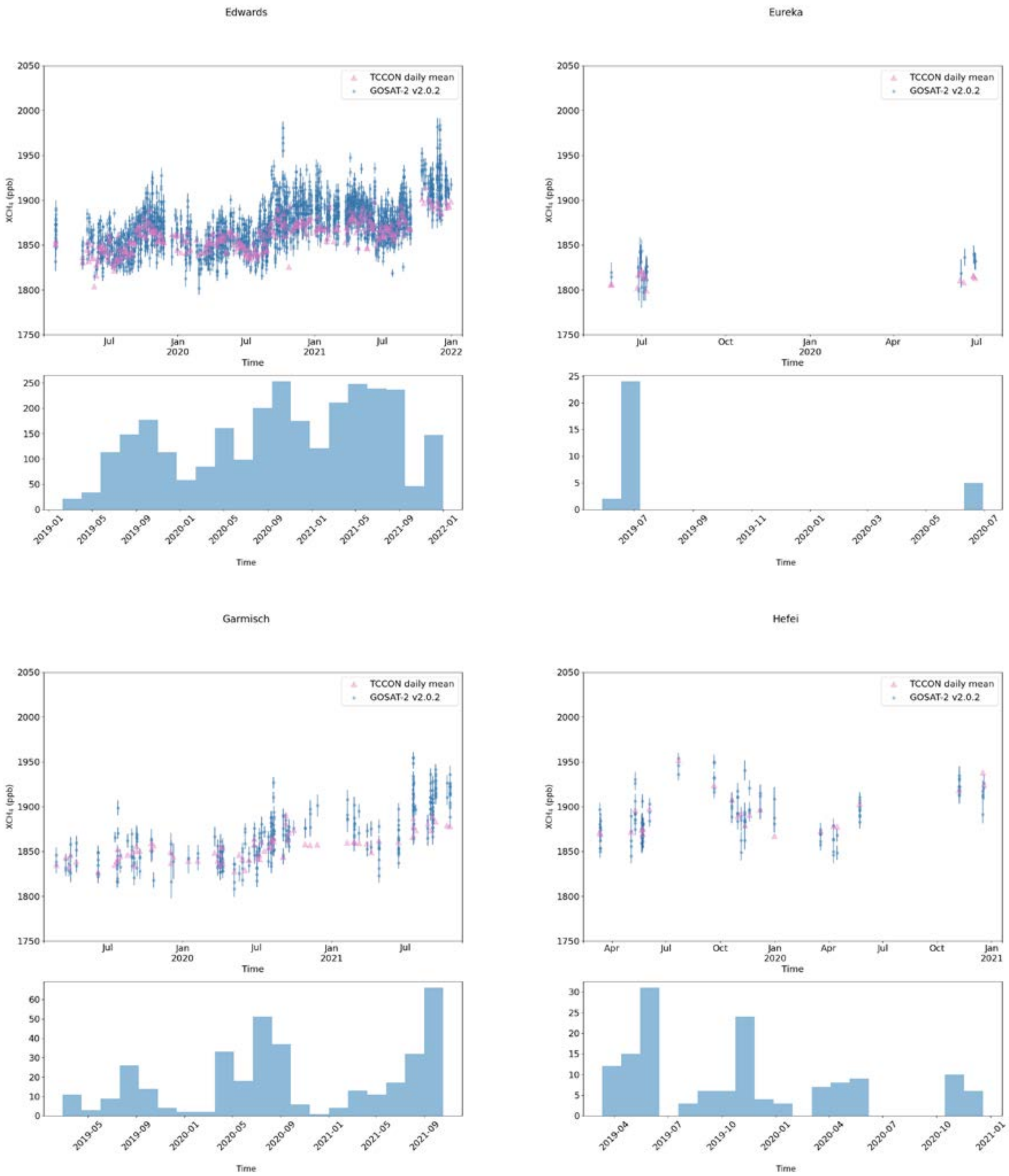

Figure 5.5-1cont.

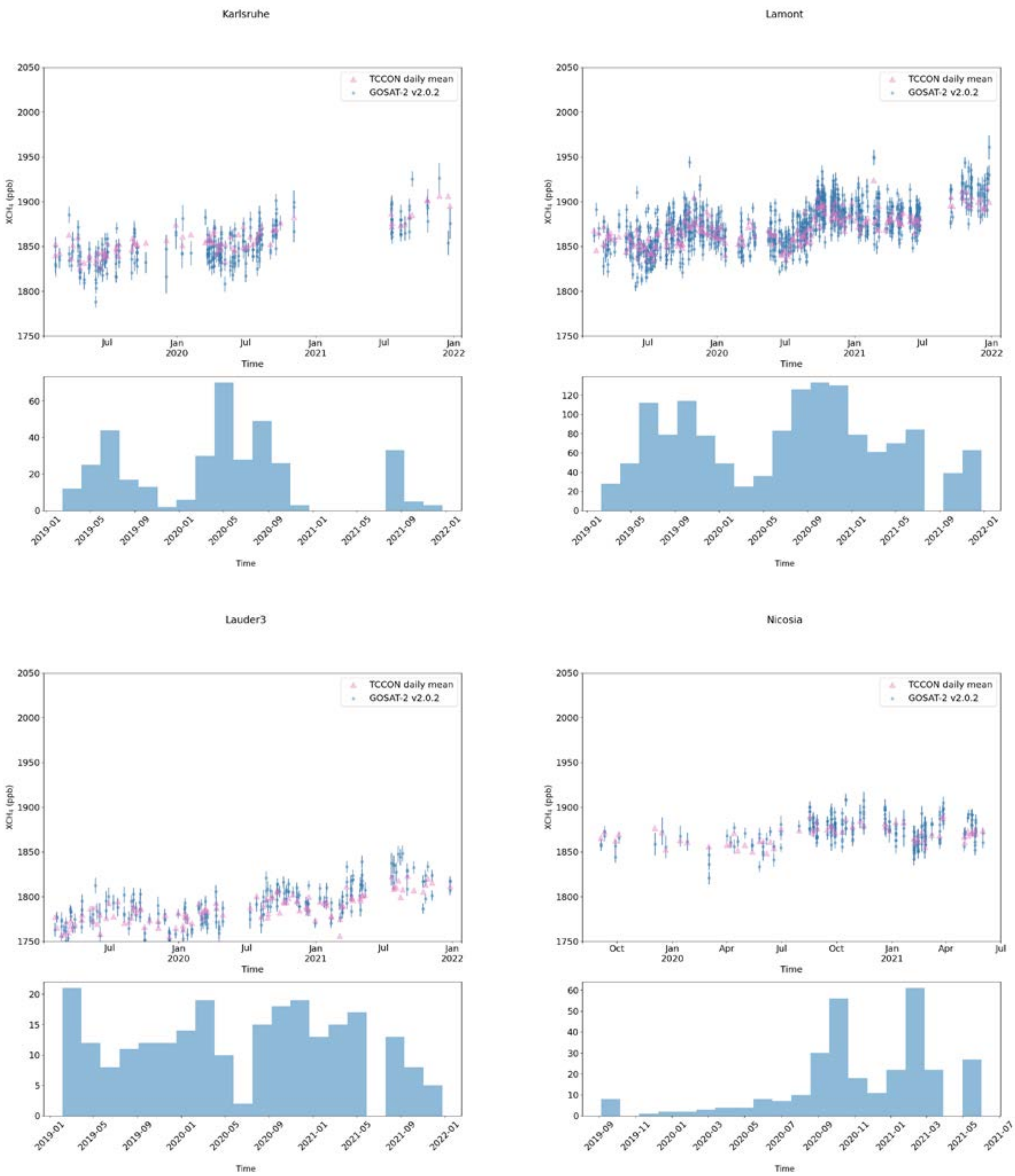

Figure 5.5-1 cont.

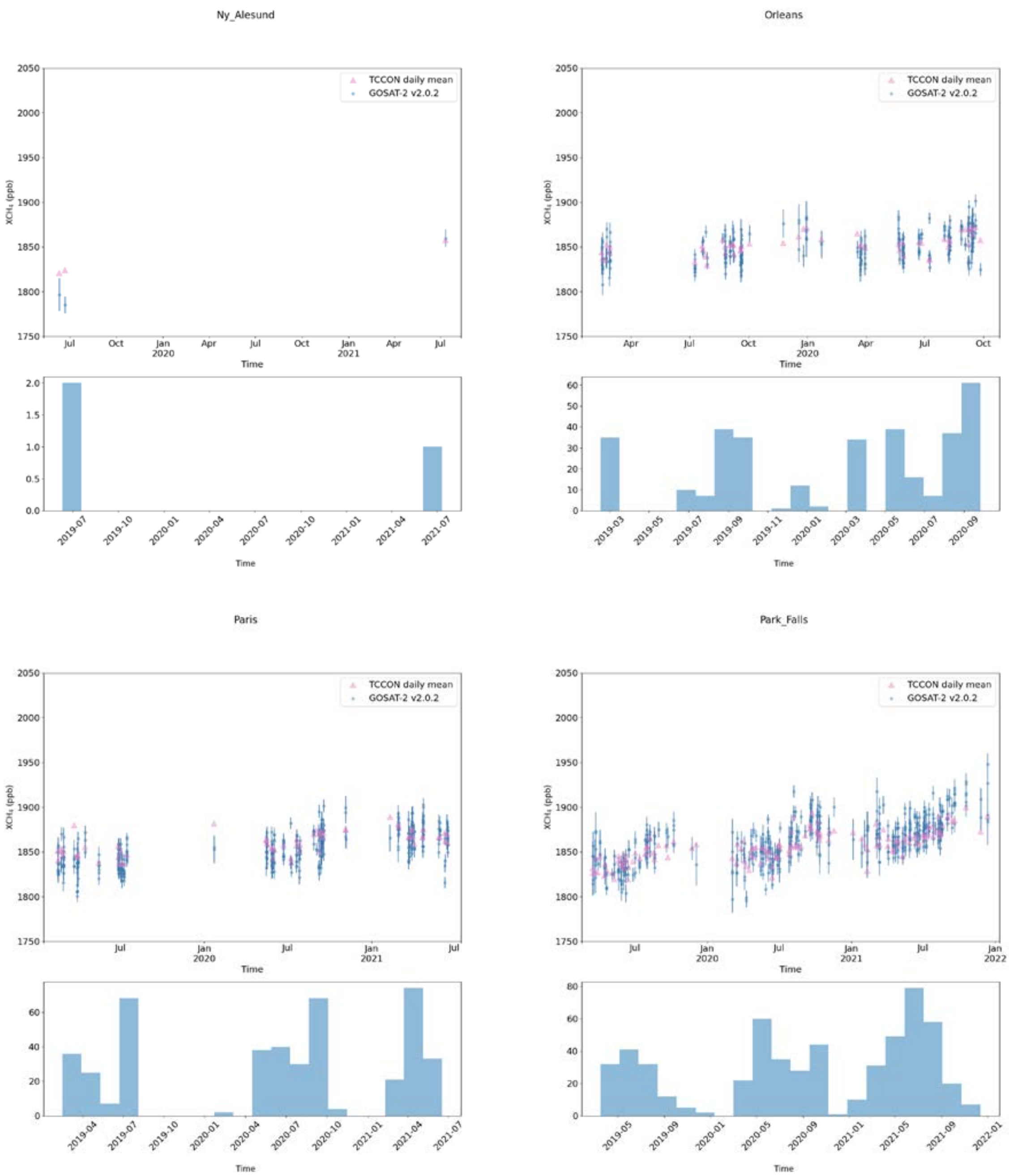

Figure 5.5-1cont.

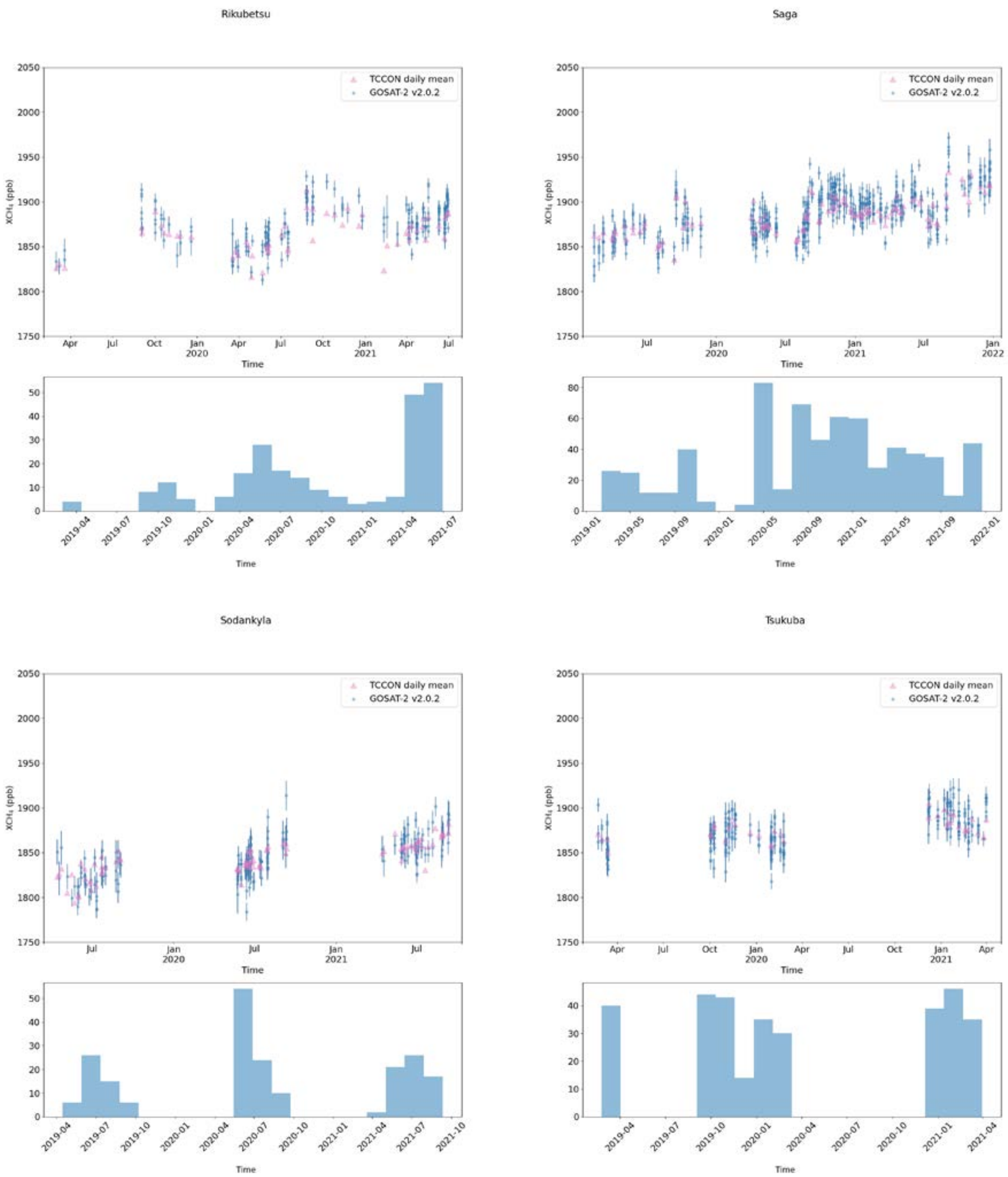

Figure 5.5-1cont.

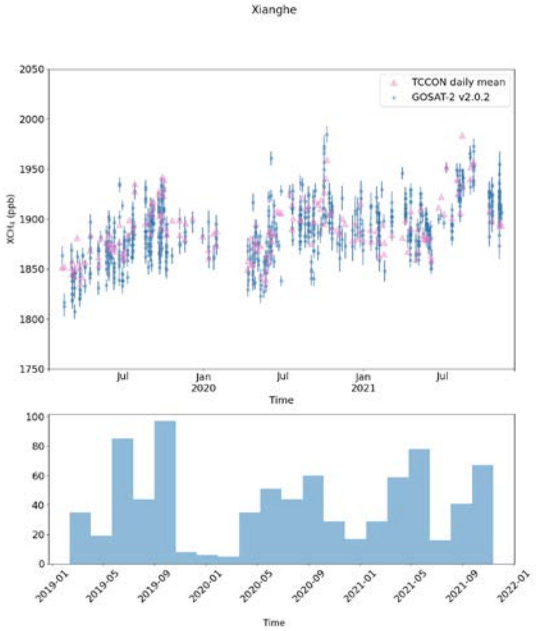

Figure 5.5-1 cont.

Table 5.5-1: Overview of the SRFP/RemoTeC XCH_4 validation with TCCON (after bias correction) for land retrievals.

TCCON site [Land mode]	Number of co-locations [-]	Mean difference [ppb]	Standard deviation of difference [ppb]
Bremen	132	-3.84	15.62
Burgos	129	0.54	12.07
Caltech	2390	-6.20	16.64
East_Trout_Lake	453	0.94	15.72
Edwards	2887	6.29	17.23
Eureka	31	4.83	14.14
Garmisch	360	7.80	20.28
Hefei	144	-2.11	15.56
Karlsruhe	366	-7.16	12.93
Lamont	1438	-0.39	14.52
Lauder	244	1.67	11.55
Nicosia	296	-1.28	11.24
Ny_Alesund	3	-20.55	16.89
Orleans	335	-5.10	13.06
Paris	446	-6.69	13.71
Park_Falls	568	3.09	14.85
Rikubetsu	241	6.09	13.80
Saga	653	0.45	13.31
Sodankyla	207	-2.53	14.69
Tsukuba	326	-1.42	13.41
Xianghe	825	-2.98	19.23
All observations	12471	-0.14	16.62

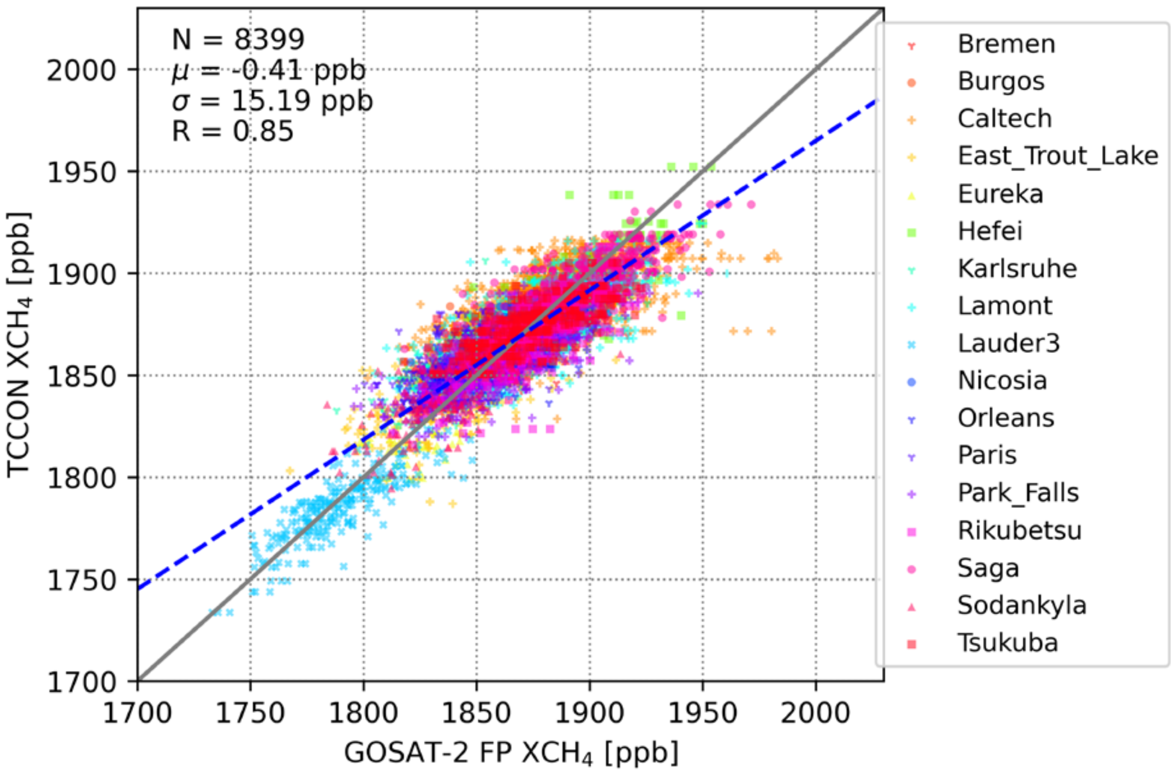

Figure 5.5-2: Validation of land single soundings of XCH_4 with co-located TCCON measurements at all TCCON sites for the period Feb 2019 to end Dec 2021. Numbers in the figures: μ = bias, i.e., average of the difference; σ = single measurement precision, i.e., standard deviation of the difference; N = number of co-locations; R the correlation coefficient. Stations that are along the coast and also sensitive to glint mode (ocean) measurements are indicated as circles. Those that have high latitudes in the northern and southern hemispheres are upward triangles and crosses, respectively. Stations in Asia, North America and Europe are indicated by squares, pluses and downward triangles respectively.

The error that comes out of the RemoTeC retrieval is just a purely statistical error on the radiance that has been propagated through the entire retrieval chain. In order to more accurately estimate the actual random error on the GOSAT-2 sounding, we applied the following procedure to obtain a scaling factor with which to scale our statistical error. We take the absolute difference of every co-located sounding and divide it by the retrieved statistical error corresponding to that sounding. We then average these values to obtain the average scaling factor by which to scale the retrieved statistical error to obtain a more correct estimate of the random error.

Based on the analysis, we obtain the following scaling factors for the SRFP XCH_4 product, 1.8 for the normal mode and 1.55 for the sunglint mode. Subsequently, we calculate the uncertainty ratio which is defined as the ratio of the mean value of the reported uncertainty and the standard deviation of the difference to TCCON. We obtain uncertainty ratios of 0.8 for the normal mode and 0.78 for the sunglint mode.

5.5.2 Summary

The result of the validation of the CH4_GO2_SRFP dataset is given in **Table 5.5-2** and compared to the requirement. The mean estimate of the single-measurement precision is 15.2 ppb which exceeds the goal requirement but is within the breakthrough requirement of 17 ppb. The uncertainties provided by RemoTeC agree on average with the observed scatter of the data when compared to TCCON. The mean, global bias of the GOSAT-2 XCH_4 retrieval is -0.41 ppb with a relative accuracy of 4.3 ppb which is smaller than the requirement of 10 ppb.

Table 5.5-2: Summary validation of product CH4_GO2_SRFP by the data provider using TCCON ground-based reference data.

Product Quality Summary Table for Product: CH4_GO2_SRFP Level: 2, Version: v2.0.2, Time period covered: 2.2019 – 12.2021 Assessment: Data Provider (DP)			
Parameter [unit]	**Achieved performance**	**Requirement**	**Comments**
Single measurement precision (1-sigma) in [ppb]	15.2	< 34 (T) < 17 (B) < 9 (G)	Computed as standard deviation of the difference to TCCON
Uncertainty ratio [-]: Ratio reported uncertainty to standard deviation of satellite-TCCON difference	0.80 (0.78 glint)	-	No requirement but value close to unity expected for a high quality data product with reliable reported uncertainty.
Mean bias (global offset) [ppb]	-0.41	-	No requirement but value close to zero expected for a high quality data product.
Accuracy: Relative systematic error [ppb]	Spatial: 4.3 Spatio-temporal: 3.8	< 10	Spatial: Computed as standard deviation of the biases at the various TCCON sites. Spatio-temporal: As "Spatial" but also considering seasonal biases.
Stability: Drift [ppb/year]	2.5 (1-sigma)	< 3	Linear drift

5.6 Validation and intercomparison results for product CH4_GO2_SRPR

The CH4_GO2_SRPR product is retrieved from GOSAT-2 TANSO-FTS SWIR spectra using the RemoTeC algorithm that has been jointly developed by SRON and KIT **/Butz et al., 2011; Schepers et al., 2012/**. The retrievals are performed globally for the time period between February 2019 and December 2021 and are evaluated against ground based TCCON observations.

5.6.1 Detailed results

To assess the quality of SRPR retrieval XCH_4 observations against ground based TCCON values, SRPR soundings are matched to TCCON observations spatially and temporally. GOSAT-2 observations are co-located with TCCON sites based on a square latitude and longitude region around each TCCON site (in ±2.5º latitude/longitude box). For the temporal co-location we select only the TCCON measurements whose observation time falls within ±2 hour of each GOSAT-2 observation time. The TCCON observations that match these criteria are averaged for each individual GOSAT-2 observation.

We co-located GOSAT-2 and TCCON measurements with a maximum time difference of 2.5h, a maximum distance of 300 km in both longitudinal and latitudinal directions. In cases of multiple TCCON measurements of the same site collocating with a GOSAT-2 sounding, we averaged the TCCON measurements. In total we achieve 27,263 collocations for land soundings and 329 collocations over ocean.

The comparions for each TCCON site is shown in **Figure 5.6-1**. The statistics (mean bias, standard deviation) for each site are given in **Table 5.6-1**. The overall correlation between the GOSAT-2 and TCCON retrievals is given in **Figure 5.6-2**. The mean bias (global offset) amounts to -0.12 ppb. The standard deviation of the site biases (spatial accuracy or station-to-station variability) is 5.9 ppb. The single measurement precision of GOSAT-2 compared to TCCON amounts to 16.56 ppb.

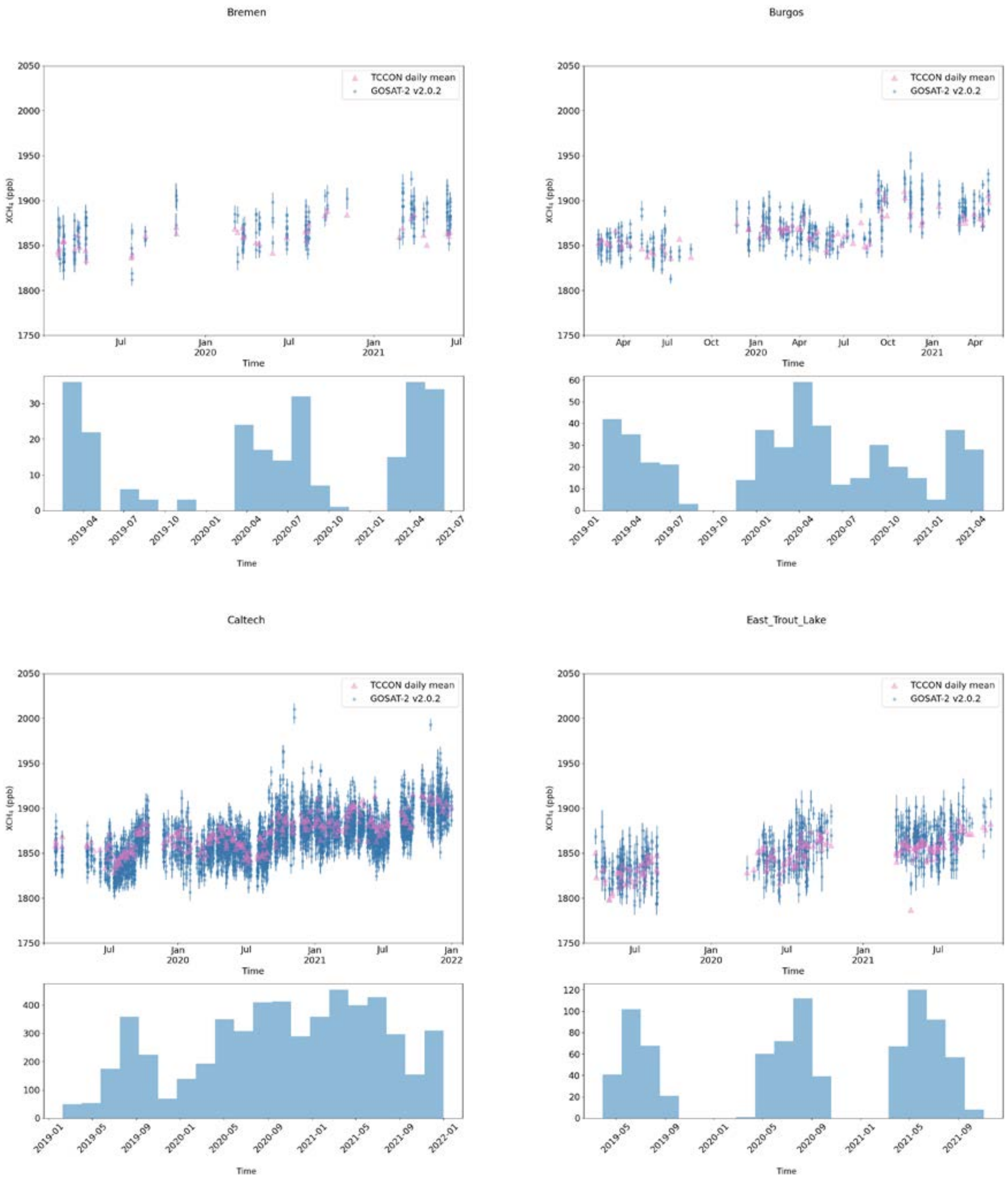

Figure 5.6-1: Comparison of land single soundings of XCH_4 from the proxy retrieval (blue circles) with co-located TCCON (pink triangles) measurements at all TCCON sites for the period Feb 2019 to Dec 2021. Histograms are also given for each station indicating the number of GOSAT-2 retrievals present throughout the time series.

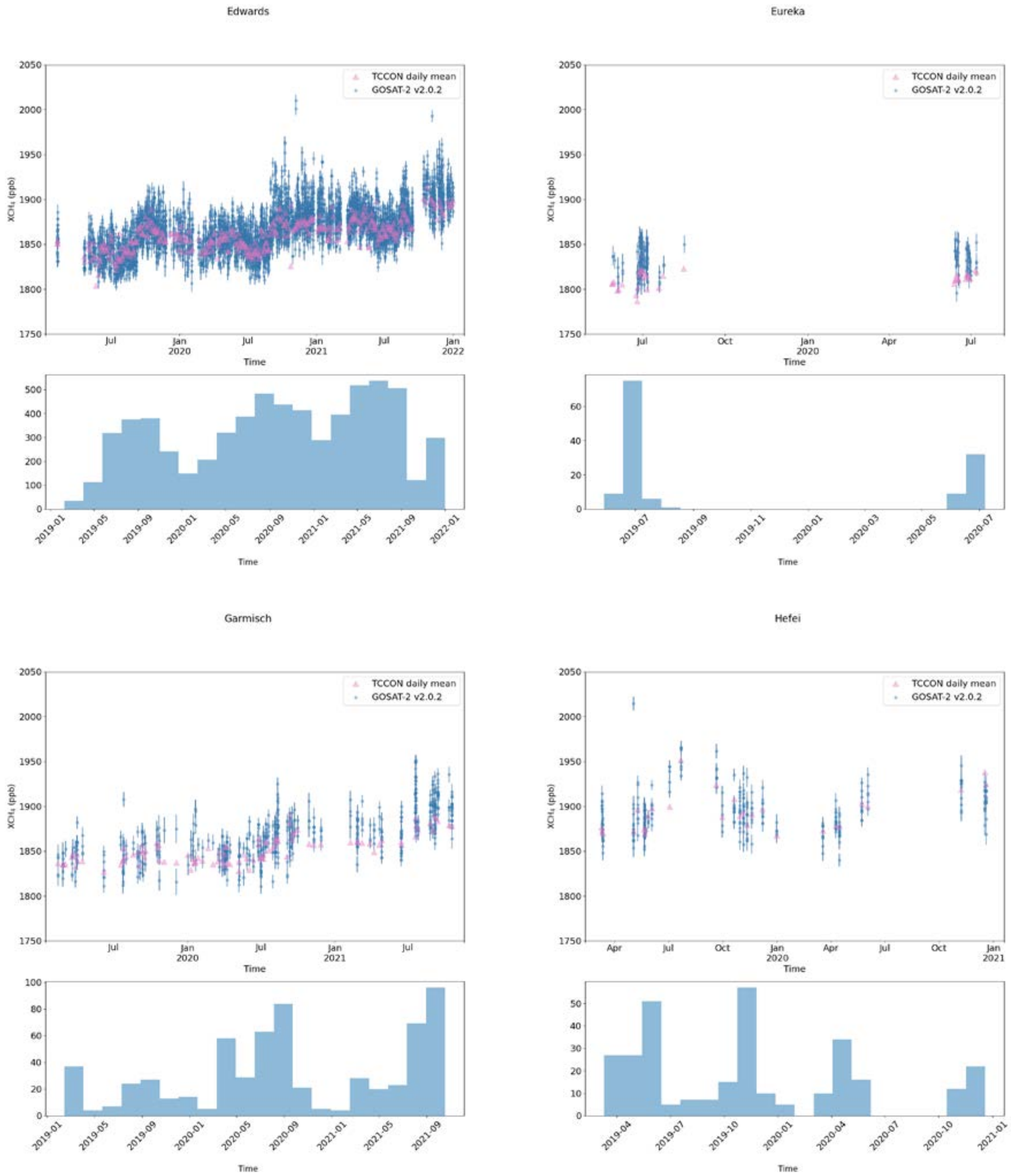

Figure 5.6-1Cont.

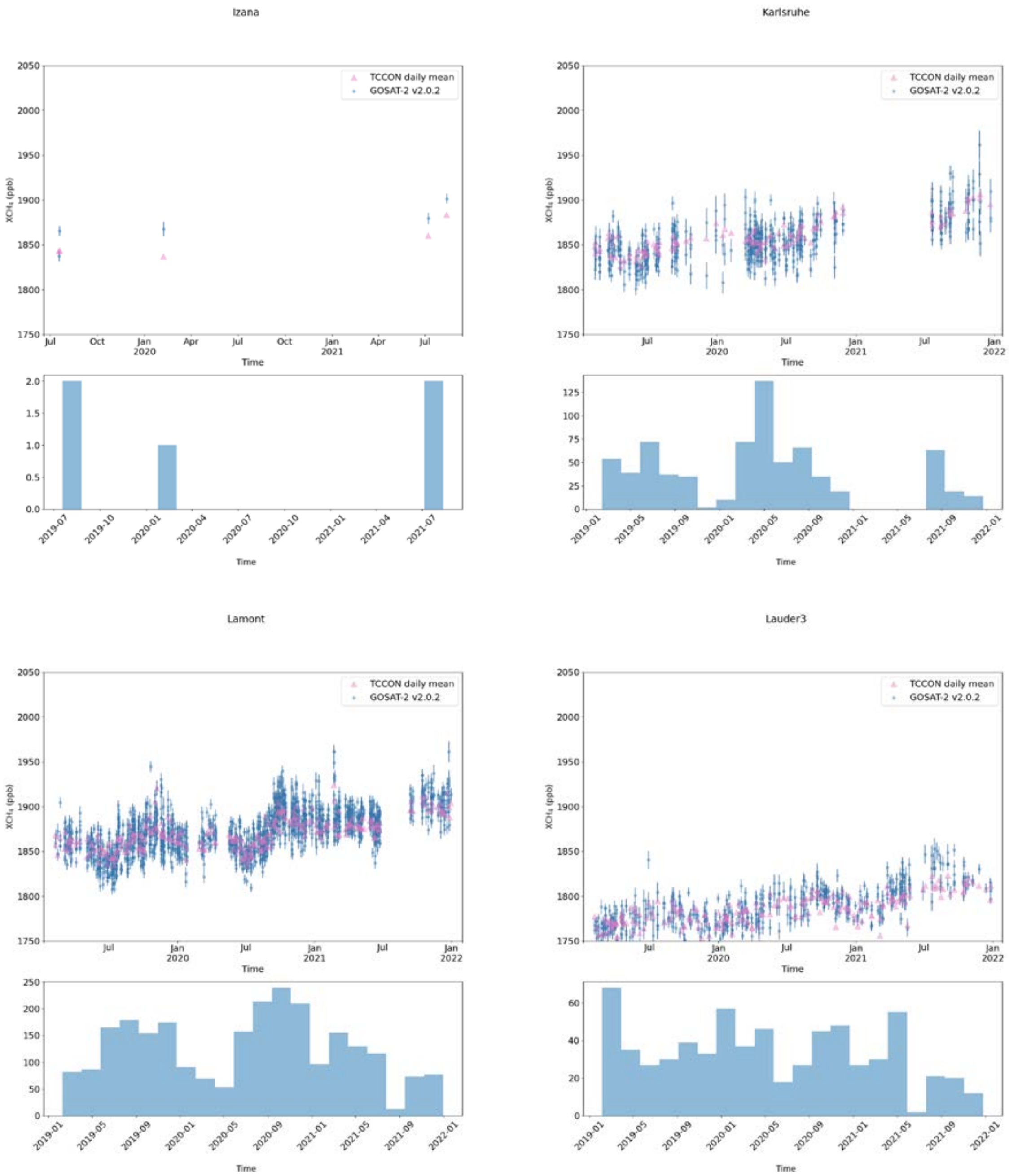

Figure 5.6-1 Cont.

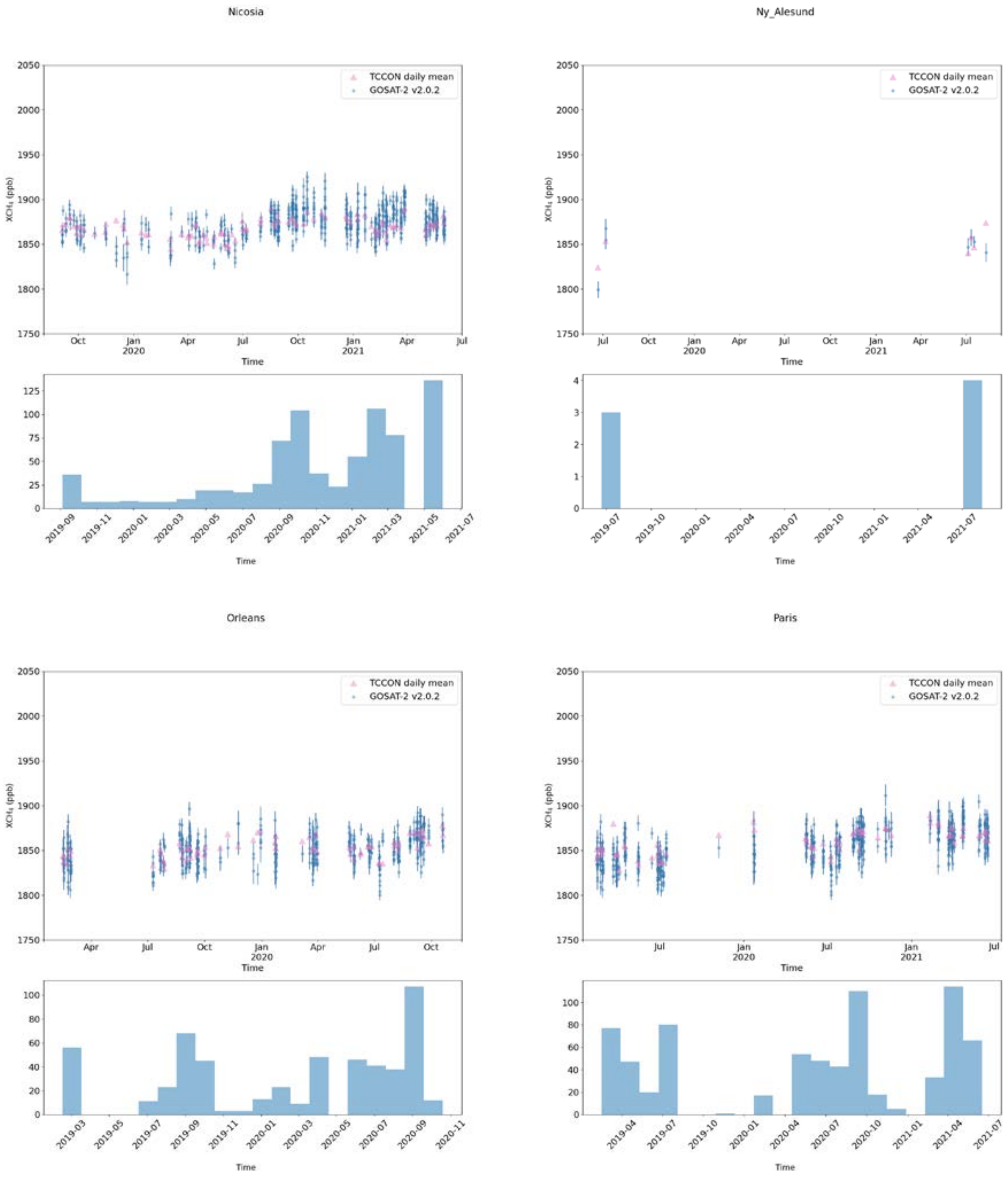

Figure 5.6-1 Cont.

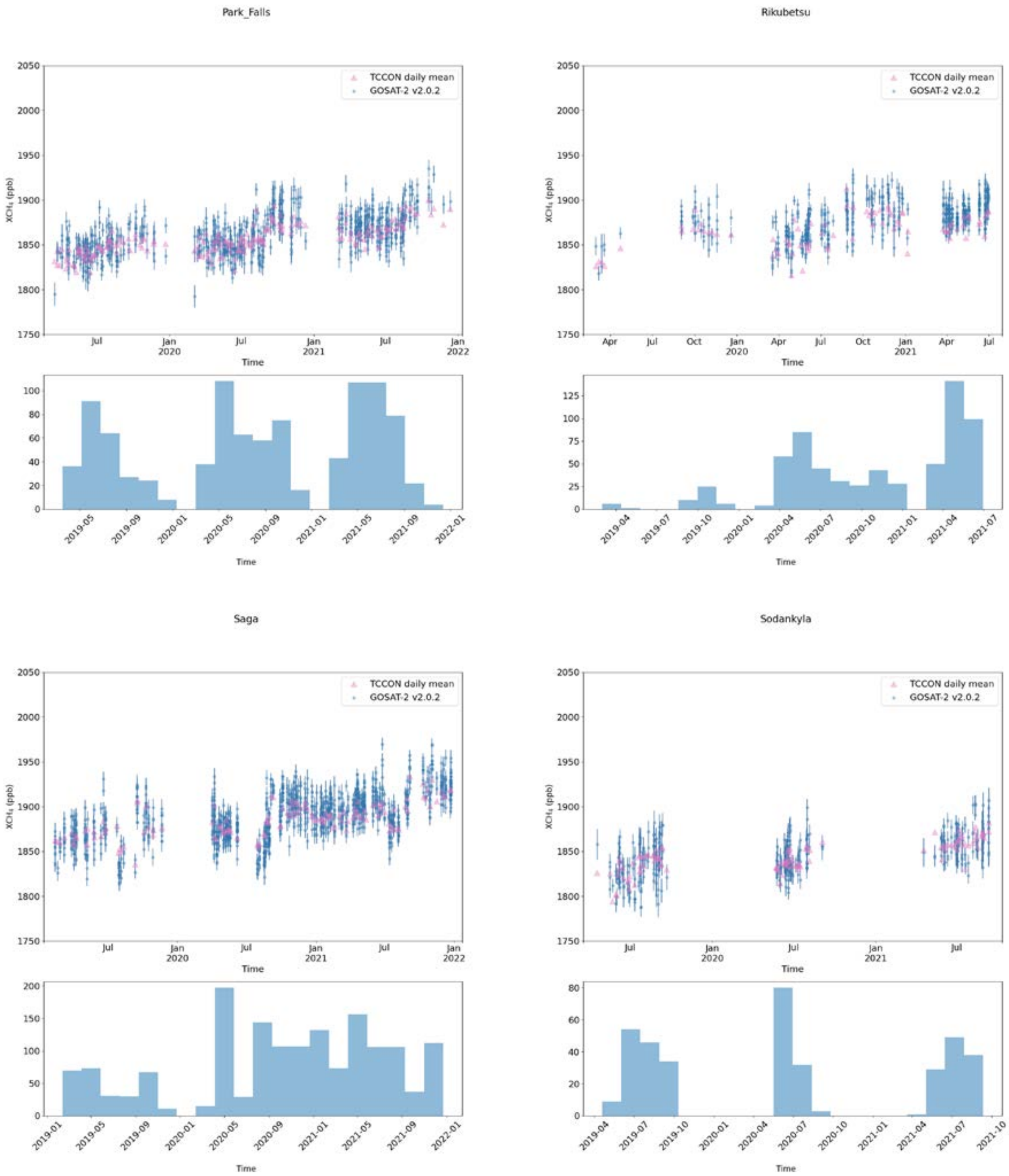

Figure 5.6-1 Cont.

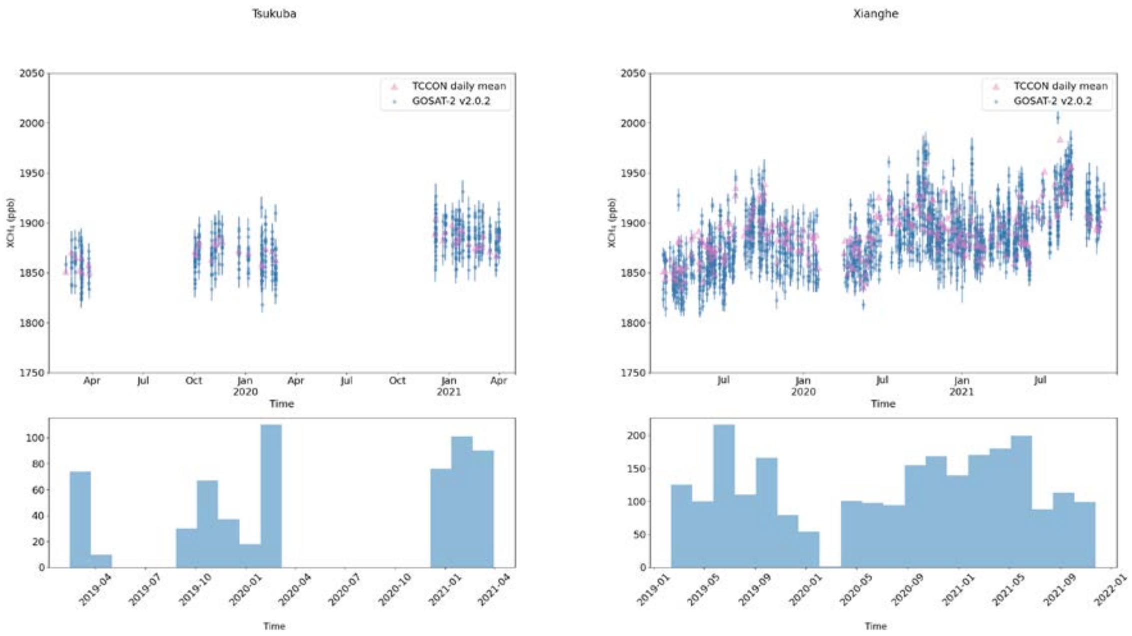

Figure 5.6-1 Cont.

Table 5.6-1: Overview of the SRPR/RemoTeC XCH_4 validation with TCCON (after bias correction) for land retrievals.

TCCON site [Land mode]	Number of co-locations [-]	Mean difference [ppb]	Standard deviation of difference [ppb]
Bremen	250	-2.47	18.27
Burgos	463	3.29	13.37
Caltech	5423	-8.00	15.27
East_Trout_Lake	860	4.74	16.83
Edwards	6524	4.21	15.85
Eureka	132	8.44	13.32
Garmisch	631	8.96	18.86
Hefei	305	1.87	19.01
Izana	5	16.64	12.01
Karlsruhe	724	-4.75	15.44
Lamont	2535	1.27	14.17
Lauder	677	3.07	11.90
Nicosia	774	2.94	13.32
Ny_Alesund	7	-4.49	16.30
Orleans	546	-3.68	14.02
Paris	733	-5.65	14.81
Park_Falls	970	3.86	15.47
Rikubetsu	658	11.04	14.61
Saga	1603	2.38	14.79
Sodankyla	375	0.10	17.10
Tsukuba	613	-0.87	14.79
Xianghe	2455	-4.93	18.94
All observations	27263	-0.12	16.56

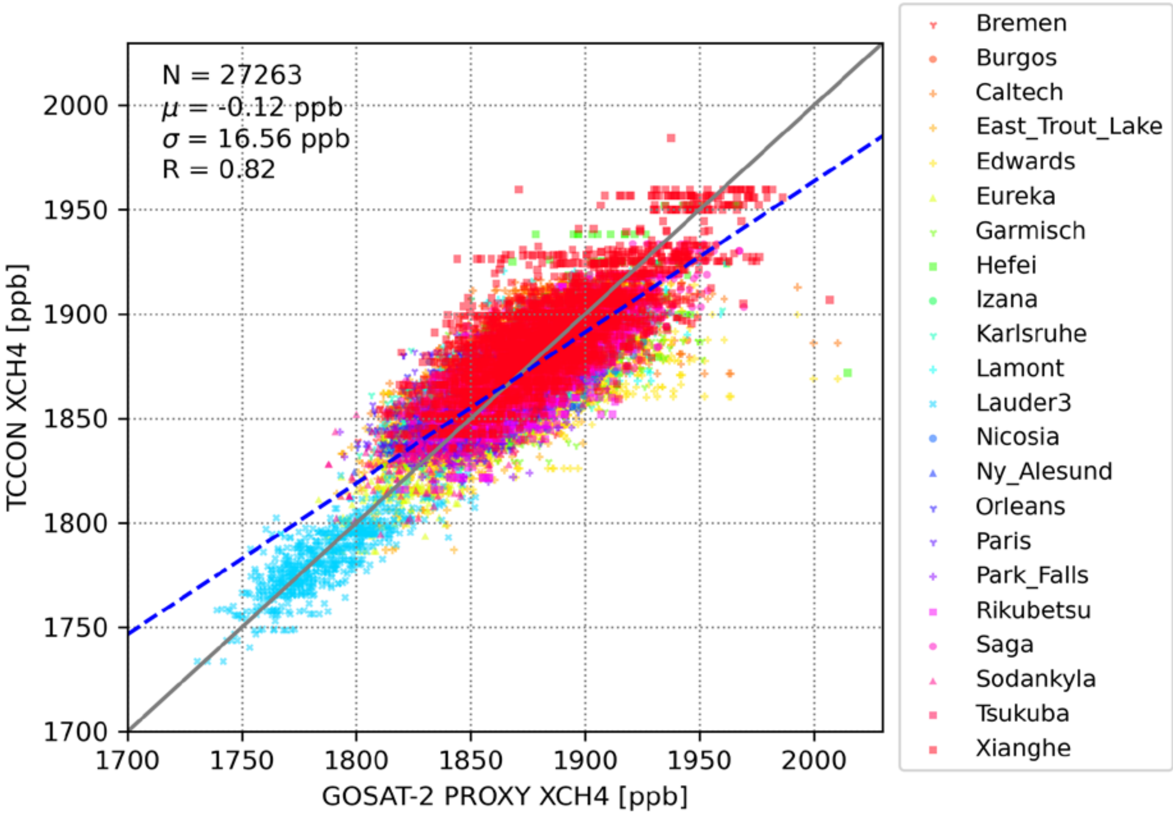

Figure 5.6-2: Validation of land single soundings of XCH_4 with co-located TCCON measurements at all TCCON sites for the period Feb 2019 to end Dec 2021. Numbers in the figures: μ = bias, i.e., average of the difference; σ = single measurement precision, i.e., standard deviation of the difference; N = number of co-locations; R the correlation coefficient. Stations that are along the coast and also sensitive to glint mode (ocean) measurements are indicated as circles. Those that have high latitudes in the northern and southern hemispheres are upward triangles and crosses, respectively. Stations in Asia, North America and Europe are indicated by squares, pluses and downward triangles respectively.

The error that comes out of the RemoTeC retrieval is just a purely statistical error on the radiance that has been propagated through the entire retrieval chain. In order to more accurately estimate the actual random error on the GOSAT-2 sounding, we applied the following procedure to obtain a scaling factor with which to scale our statistical error. We take the absolute difference of every co-located sounding and divide it by the retrieved statistical error corresponding to that sounding. We then average these values to obtain the average scaling factor by which to scale the retrieved statistical error to obtain a more correct estimate of the random error.

Based on the analysis, we obtain the following scaling factors for the SRPR XCH_4 product, 1.93 for the normal mode and 1.66 for the sunglint mode. Subsequently, we calculate the uncertainty ratio which is defined as the ratio of the mean value of the reported uncertainty and the standard deviation of the difference to TCCON. We obtain uncertainty ratios of 0.81 for the normal mode and 0.81 for the sunglint mode.

5.6.2 Summary

The result of the validation of the CH4_GO2_SRPR dataset is given in **Table 5.6-2** and compared to the requirement. The mean estimate of the single-measurement precision is 16.56 ppb which exceeds the goal requirement but is within the breakthrough requirement of 17 ppb. The uncertainties provided by RemoTeC agree on average with the observed scatter of the data when compared to TCCON. The mean, global bias of the GOSAT-2 XCH_4 retrieval is -0.12 ppb with a relative accuracy of 5.9 ppb which is smaller than the requirement of 10 ppb.

Table 5.6-2: Summary validation of product CH4_GO2_SRPR by the data provider using TCCON ground-based reference data.

Product Quality Summary Table for Product: CH4_GO2_SRPR Level: 2, Version: v2.0.2, Time period covered: 2.2019 – 12.2021 Assessment: Data Provider (DP)			
Parameter [unit]	**Achieved performance**	**Requirement**	**Comments**
Single measurement precision (1-sigma) in [ppb]	16.56	< 34 (T) < 17 (B) < 9 (G)	Computed as standard deviation of the difference to TCCON
Uncertainty ratio [-]: Ratio reported uncertainty to standard deviation of satellite-TCCON difference	0.81	-	No requirement but value close to unity expected for a high quality data product with reliable reported uncertainty.
Mean bias (global offset) [ppb]	-0.12	-	No requirement but value close to zero expected for a high quality data product.
Accuracy: Relative systematic error [ppb]	Spatial: 5.9 Spatio-temporal: Not evaluated	< 10	Spatial: Computed as standard deviation of the biases at the various TCCON sites. Spatio-temporal: As "Spatial" but also considering seasonal biases.
Stability: Drift [ppb/year]	Not evaluated (1-sigma)	< 3	Linear drift

6 References

/Aben et al., 2019/ Aben, I., L. Wu, O. Hasekamp, M. Buchwitz, M. Reuter, O. Schneising, H. Boesch, D. Yang, ESA Climate Change Initiative "Plus" (CCI+) System Specification Document (SSD) for the Essential Climate Variable (ECV) Greenhouse Gases (GHG): XCO_2 and/or XCH_4 from OCO-2, TanSat, Sentinel-5-Precursor and GOSAT-2, Version 1.0, 26-August-2019, pp. 33, 2019.

/Ackermann et al., 2010/ Ackerman, S.; Frey, R.; Strabala, K.; Liu, Y.; Gumley, L.; Baum, B.; Menzel, P. Discriminating Clear-Sky from Cloud with MODIS—Algorithm Theoretical Basis Document (MOD35); Version 6.1; Cooperative Institute for Meteorological Satellite Studies, University ofWisconsin—Madison: Madison, WI, USA, 2010.

/ATBDv1 FOCAL, 2019/ Reuter et al.: Algorithm Theoretical Basis Document Version 1 (ATBDv1) - Retrieval of XCO_2 from the OCO-2 satellite using the Fast Atmospheric Trace Gas Retrieval (FOCAL), ESA GHG-CCI project, 2019.

/ATBDv3, 2021/ M. Reuter, M. Hilker, S. Noël, M. Buchwitz, O. Schneising, H. Bovensmann, and J. P. Burrows: Algorithm Theoretical Basis Document Version 3 (ATBDv3) - Retrieval of XCO2 from the OCO-2 satellite using the Fast Atmospheric Trace Gas Retrieval (FOCAL), ESA Climate Change Initiative "Plus" (CCI+) for the Essential Climate Variable (ECV) Greenhouse Gases (GHG), ESA GHG CCI+, 2021.

/Batchelor at al., 2009/ Batchelor, R. L., Strong, K., Lindenmaier, R., Mittermeier, R. L.,Fast, H., Drummond, J. R., and Fogal, P. F.: A New Bruker IFS 125HR FTIR Spectrometer for the Polar Environment Atmospheric Research Laboratory at Eureka, Nunavut, Canada: Measurements and Comparison with the Existing Bomem DA8 Spectrometer, J. Atmos. Ocean. Tech., 26, 1328–1340,https://doi.org/10.1175/2009JTECHA1215.1, 2009.

/Blumenstock et al., 2020/ Blumenstock T., Raffalski U., and Matsumi Y., NDACC Metadata File for Eureka FTIR and references cited therein, https://www-air.larc.nasa.gov/pub/NDACC/PUBLIC/meta/ftir/Kiruna_ftir_tb_2020.pdf

/Boesch et al., 2011/ Boesch, H., Baker, D., Connor, B., Crisp, D., and Miller, C.: Global characterization of CO_2 column retrievals from shortwave-infrared satellite observations of the Orbiting Carbon Observatory-2 mission, Remote Sens., 3, 270–304, doi:10.3390/rs3020270, 2011.

/Bovensmann et al., 2010/ Bovensmann, H., Buchwitz, M., Burrows, J. P., Reuter, M., Krings, T., Gerilowski, K., Schneising, O., Heymann, J., Tretner, A., and Erzinger, J.: A remote sensing technique for global monitoring of power plant CO2 emissions from space and related applications, Atmospheric Measurement Techniques, 3, 781–811, doi:10.5194/amt-3-781-2010, URL http: //www.atmos-meas-tech.net/3/781/2010/, 2010.

/Buschmann et al. 2022/ Buschmann, M., Petri, C., Palm, M., Warneke, T., & Notholt, J. (2022). TCCON data from Ny-Ålesund, Svalbard (NO), Release GGG2020.R0 (Version R0) [Data set]. CaltechDATA. https://doi.org/10.14291/tccon.ggg2020.nyalesund01.R0.

/Butz et al., 2009/ Butz, André, Otto P. Hasekamp, Christian Frankenberg, and Ilse Aben, "Retrievals of atmospheric CO_2 from simulated space-borne measurements of backscattered near-infrared sunlight: accounting for aerosol effects," Appl. Opt. 48, 3322-3336 (2009)

/Butz et al., 2010/ Butz, André, Otto P. Hasekamp, Christian Frankenberg, Jerome Vidot, and Ilse Aben, ",CH4 retrievals from space-based solar backscatter measurements: Performance evaluation against simulated aerosol and cirrus loaded scenes" , J. Geophys. Res., 115, 24,302, doi:10.1029/2010JD014514, 2010.

/Butz et al., 2011/ Butz, A., S. Guerlet, O. Hasekamp, et al., Toward accurate CO_2 and CH_4 observations from GOSAT, Geophys. Res. Lett., Geophys. Res. Lett., doi:10.1029/2011GL047888, 2011.

/CECRv3 BESD, 2017/ M. Reuter, O. Schneising, M. Buchwitz, J. Heymann: Comprehensive Error Characterisation Report: BESD full-physics retrieval algorithm for XCO_2 for the Essential Climate Variable (ECV) Greenhouse Gases (GHG), ESA GHG-CCI project, 2017.

/CECRv3, 2017/ M. Reuter, O. Schneising, M. Buchwitz, J. Heymann: Comprehensive Error Characterisation Report: BESD full-physics retrieval algorithm for XCO2 for the Essential Climate Variable (ECV) Greenhouse Gases (GHG), ESA GHG-CCI project, 2017.

/De Mazière et al., 2017/ De Mazière, M., Sha, M. K., Desmet, F., Hermans, C., Scolas, F., Kumps, N., Metzger, J.-M., Duflot, V., and Cammas, J.-P.: TCCON data from Réunion Island (RE), Release GGG2014.R1, https://doi.org/10.14291/TCCON.GGG2014.REUNION01.R1, https://data.caltech.edu/records/322, 2017.

/De Mazière et al., 2018/ De Mazière, M., Thompson, A. M., Kurylo, M. J., Wild, J. D., Bernhard, G., Blumenstock, T., Braathen, G. O., Hannigan, J. W., Lambert, J.-C., Leblanc, T., McGee, T. J., Nedoluha, G., Petropavlovskikh, I., Seckmeyer, G., Simon, P. C., Steinbrecht, W., and Strahan, S. E.: The Network for the Detection of Atmospheric Composition Change (NDACC): history, status and perspectives, Atmos. Chem. Phys., 18, 4935–4964, https://doi.org/10.5194/acp-18-4935-2018, 2018.

/De Mazière et al., 2022/ De Mazière, M., Sha, M. K., Desmet, F., Hermans, C., Scolas, F., Kumps, N., Zhou, M., Metzger, J.-M., Duflot, V., & Cammas, J.-P. : TCCON data from Réunion Island (RE), Release GGG2020.R0 (Version R0) [Data set]. CaltechDATA. https://doi.org/10.14291/tccon.ggg2020.reunion01.R0, 2022.

/Deutcher et al, 2010/ Deutscher, N. M., Griffith, D. W. T., Bryant, G. W., Wennberg, P.O., Toon, G. C., Washenfelder, R. A., Keppel-Aleks, G., Wunch,D., Yavin, Y., Allen, N. T., Blavier, J.-F., Jiménez, R., Daube,B. C., Bright, A. V., Matross, D. M., Wofsy, S. C., and Park,S.: Total column CO2 measurements at Darwin, Australia – site description and calibration against in situ aircraft profiles, Atmos. Meas. Tech., 3, 947–958, https://doi.org/10.5194/amt-3-947-2010, 2010

/Deutscher et al., 2019/ Deutscher, N. M., Notholt, J., Messerschmidt, J., Weinzierl, C., Warneke, T., Petri, C., and Grupe, P.: TCCON data from Bialystok (PL), Release GGG2014.R2, https://doi.org/10.14291/TCCON.GGG2014.BIALYSTOK01.R2, https://data.caltech.edu/records/1300, 2019.

/E3UBv3, 2022/ M.Reuter, M.Hilker, M. Ingendahl, and M.Buchwitz: End-to-End ECV Uncertainty Budget Version 3 (E3UBv3) for the FOCAL XCO_2 OCO-2 Data Product CO2_OC2_FOCA (v10) for the Essential Climate Variable (ECV) Greenhouse Gases (GHG) ESA Climate Change Initiative "Plus" (CCI+), 2022

/Eldering et al., 2015/ Eldering, A.; Pollock, R.; Lee, R.; Rosenberg, R.; Oyafuso, F.; Crisp, D.; Chapsky, L.; Granat, R. Orbiting Carbon Observatory-2 (OCO-2) - LEVEL 1B - Algorithm Theoretical Basis; Version 1.2 Rev 1; National Aeronautics and Space Administration, Jet Propulsion Laboratory, California Institute of Technology: Pasadena, CA, USA, 2015.

/Feist et al.,2014/ Feist, D. G., Arnold, S. G., John, N., and Geibel, M. C.: TCCON data from Ascension Island (SH), Release GGG2014.R0, https://doi.org/10.14291/TCCON.GGG2014.ASCENSION01.R0/1149285, https://data.caltech.edu/records/210, 2014.

/Frankenberg et al., 2005/ Frankenberg, C., Meirink, J.F., van Weele, M., Platt, U., Wagner, T. (2005), Assessing methane emissions from global space-borne obseravtions, Science, ., doi:10.1126/science.1106644

/Frankenberg et al., 2011/ Frankenberg, C., Aben, I., Bergamaschi, P., et al. (2011), Global column-averaged methane mixing ratios from 2003 to 2009 as derived from SCIAMACHY: Trends and variability, J. Geophys. Res., doi:10.1029/2010JD014849.

/Garcia et al., 2022/ García, O. E., Schneider, M., Herkommer, B., Gross, J., Hase, F., Blumenstock, T., & Sepúlveda, E. (2022). TCCON data from Izana (ES), Release GGG2020.R1 (Version R1) [Data set]. CaltechDATA. https://doi.org/10.14291/tccon.ggg2020.izana01.R1.

/GCOS-154/ Global Climate Observing System (GCOS), SYSTEMATIC OBSERVATION REQUIREMENTS FOR SATELLITE-BASED PRODUCTS FOR CLIMATE, Supplemental details to the satellite-based component of the "Implementation Plan for the Global Observing System for Climate in Support of the UNFCCC (2010 update)", Prepared by World Meteorological Organization (WMO), Intergovernmental Oceanographic Commission, United Nations Environment Programme (UNEP), International Council for Science, Doc.: GCOS 154, link: http://cci.esa.int/sites/default/files/gcos-154.pdf, 2011.

/GCOS-195/ Status of the Global Observing System for Climate. GCOS-195. Link: https://library.wmo.int/pmb_ged/gcos_195_en.pdf, 2015.

/GCOS-200/ The Global Observing System for Climate: Implementation Needs, GCOS 2016 Implementation Plan, World Meteorological Organization (WMO), GCOS-200 (GOOS-214), pp. 325, link: https://library.wmo.int/opac/doc_num.php?explnum_id=3417, 2016.

/GCOS-245/ The 2022 GCOS ECVs Requirements, https://library.wmo.int/doc_num.php?explnum_id=11318, pp. 244, 2022.

/Goo et al., 2014/ Goo, T.-Y., Oh, Y.-S., & Velazco, V. A. (2014). *TCCON data from Anmeyondo (KR), Release GGG2014.R0* (Version GGG2014.R0) [Data set]. CaltechDATA. https://doi.org/10.14291/TCCON.GGG2014.ANMEYONDO01.R0/1149284, https://data.caltech.edu/records/266

/Griffith et al. 2014a/ Griffith, D. W., Deutscher, N. M., Velazco, V. A., Wennberg, P. O., Yavin, Y., Keppel-Aleks, G., Washenfelder, R. A., Toon, G. C., Blavier, J.-F., Paton-Walsh, C., Jones, N. B., Kettlewell, G. C., Connor, B. J., Macatangay, R. C., Roehl, C., Ryczek, M., Glowacki, J., Culgan, T., and Bryant, G. W.: TCCON data from Darwin (AU), Release GGG2014.R0, https://doi.org/10.14291/TCCON.GGG2014.DARWIN01.R0/1149290, https://data.caltech.edu/records/269, 2014a.

/Griffith et al. 2014b/ Griffith, D. W., Velazco, V. A., Deutscher, N. M., Paton-Walsh, C., Jones, N. B., Wilson, S. R., Macatangay, R. C., Kettlewell, G. C., Buchholz, R. R., and Riggenbach, M. O.: TCCON data from Wollongong (AU), Release GGG2014.R0, https://doi.org/10.14291/TCCON.GGG2014.WOLLONGONG01.R0/1149291, https://data.caltech.edu/records/291, 2014b.

/Hannigan et al., 2021/ Hannigan J. W., Ortega I. and Coffey M.: NDACC Metadata File for Thule FTIR and references cited therein, https://www-air.larc.nasa.gov/pub/NDACC/PUBLIC/meta/ftir/Thule_ftir_jh_2021.pdf

/Hase et al., 2015/ Hase, F., Blumenstock, T., Dohe, S., Groß, J., and Kiel, M.: TCCON data from Karlsruhe (DE), Release GGG2014.R1, https://doi.org/10.14291/TCCON.GGG2014.KARLSRUHE01.R1/1182416, https://data.caltech.edu/records/278, 2015.

/Hase et al., 2023/ Hase, F., Herkommer, B., Groß, J., Blumenstock, T., Kiel, M. ä ., & Dohe, S. (2023). TCCON data from Karlsruhe (DE), Release GGG2020.R1 (Version R1) [Data set]. CaltechDATA. https://doi.org/10.14291/tccon.ggg2020.karlsruhe01.R1

/HITRAN2016/ Gordon et al., The HITRAN2016 molecular spectroscopic database, J. Quant. Spectrosc. Radiat. Transfer, 203, 3-69, 2017.

/Iraci et al. 2016/ Iraci, L. T., Podolske, J. R., Hillyard, P. W., Roehl, C., Wennberg, P. O., Blavier, J.-F., Landeros, J., Allen, N., Wunch, D., Zavaleta, J., Quigley, E., Osterman, G. B., Albertson, R., Dunwoody, K., and Boyden, H.: TCCON data from Edwards (US), Release GGG2014.R1, https://doi.org/10.14291/TCCON.GGG2014.EDWARDS01.R1/1255068, https://data.caltech.edu/records/270, 2016.

/Iraci et al. 2022/ Iraci, L. T., Podolske, J. R., Roehl, C., Wennberg, P. O., Blavier, J.-F., Allen, N., Wunch, D., & Osterman, G. B. (2022). TCCON data from Edwards (US), Release GGG2020.R0 (Version R0) [Data set]. CaltechDATA. https://doi.org/10.14291/tccon.ggg2020.edwards01.R0.

/Kawakami et al. 2014/ Kawakami, S., Ohyama, H., Arai, K., Okumura, H., Taura, C., Fukamachi, T., and Sakashita, M.: TCCON data from Saga (JP), Release GGG2014.R0, https://doi.org/10.14291/TCCON.GGG2014.SAGA01.R0/1149283, https://data.caltech.edu/records/288, 2014.

/Kiel et al., 2019/ Kiel, M., O'Dell, C. W., Fisher, B., Eldering, A., Nassar, R., MacDonald, C. G., and Wennberg, P. O.: How bias correction goes wrong: measurement of XCO2 affected by erroneous surface pressure estimates, Atmos. Meas. Tech., 12, 2241–2259, https://doi.org/10.5194/amt-12-2241-2019, 2019.

/Kivi et al., 2014/ Kivi, R., Heikkinen, P., and Kyrö, E.: TCCON data from Sodankylä (FI), Release GGG2014.R0, https://doi.org/10.14291/TCCON.GGG2014.SODANKYLA01.R0/1149280, https://data.caltech.edu/records/289, 2014.

/Kivi et al., 2022/ Kivi, R., Heikkinen, P., & Kyrö, E. (2022). TCCON data from Sodankylä (FI), Release GGG2020.R0 (Version R0) [Data set]. CaltechDATA. https://doi.org/10.14291/tccon.ggg2020.sodankyla01.R0.

/Kuruz, 1994/ Kurucz, H.L. The Solar Spectrum: Atlases and Line Identifications, Workshop on Laboratory and Astronomical High Resolution Spectra. Astronomical Society of the Pacific Conference Series. In Proceedings of the ASP Conference, Brussels, Belgium, 29 August–2 September 1994; pp. 17–31.

/Langerock et al., 2015/ Langerock, B., De Mazière, M., Hendrick, F., Vigouroux, C., Desmet, F., Dils, B., and Niemeijer, S.: Description of algorithms for co-locating and comparing gridded model data with remote-sensing observations, Geosci. Model Dev., 8, 911–921, https://doi.org/10.5194/gmd-8-911-2015, 2015.

/Laughner et al., 2023/ Laughner, J. L., Roche, S., Kiel, M., Toon, G. C., Wunch, D., Baier, B. C., Biraud, S., Chen, H., Kivi, R., Laemmel, T., McKain, K., Quéhé, P.-Y., Rousogenous, C., Stephens, B. B., Walker, K., and Wennberg, P. O.: A new algorithm to generate a priori trace gas profiles for the GGG2020 retrieval algorithm, Atmos. Meas. Tech., 16, 1121–1146, https://doi.org/10.5194/amt-16-1121-2023, 2023.

/Liu et al. 2018/ Liu, C, Wang, W., Sun, Y., TCCON data from Hefei(PRC), Release GGG2014.R0, (Version GGG2014.R0) [Data set]. CaltechDATA. https://doi.org/10.14291/TCCON.GGG2014.HEFEI01.R0, https://data.caltech.edu/records/1092.

/Liu et al. 2022/Liu, C., Wang, W., Sun, Y., & Shan, C. (2022). TCCON data from Hefei (PRC), Release GGG2020.R0 (Version R0) [Data set]. CaltechDATA. https://doi.org/10.14291/tccon.ggg2020.hefei01.R0.

/Lunneborg, 2020/ Lunneborg, C. E. Data analysis by resampling: Concepts and applications. PacificGrove, CA: Duxbury, 2000.

/Mahieu 2017/ Mahieu, M. NDACC Metadata File for Jungraujoch FTIR and references cited therein https://www-air.larc.nasa.gov/pub/NDACC/PUBLIC/meta/ftir/Jungfraujoch_ftir_em_2017.pdf

/Makarova et al. 2017/, Marakova M.V., Virolainen Y., Polyakov A.: NDACC Metadata File for St. Petersburg FTIR and references cited therein https://www-air.larc.nasa.gov/pub/NDACC/PUBLIC/meta/ftir/StPetersburg_ftir_mm_2017.pdf

/Mellqvist et al., 2021/ Mellqvist J., Persson G., NDACC Metadata File for Harestua FTIR and references cited therein, https://www-air.larc.nasa.gov/pub/NDACC/PUBLIC/meta/ftir/Harestua_ftir_hrt_jm_2021.pdf

/Morino et al. 2018a/ Morino, I., Matsuzaki, T., and Horikawa, M.: TCCON data from Tsukuba (JP), 125HR, Release GGG2014.R2, https://doi.org/10.14291/TCCON.GGG2014.TSUKUBA02.R2, https://data.caltech.edu/records/958, 2018a.

/Morino et al. 2018b/ Morino, I., Yokozeki, N., Matsuzaki, T., and Horikawa, M.: TCCON data from Rikubetsu (JP), Release GGG2014.R2, https://doi.org/10.14291/TCCON.GGG2014.RIKUBETSU01.R2, https://data.caltech.edu/records/957, 2018b.

/Morino et al., 2018c/ Morino, I., Velazco, V. A., Hori, A., Uchino, O., & Griffith, D. W. T. (2018). *TCCON data from Burgos, Ilocos Norte (PH), Release GGG2014.R0* (Version GGG2014.R0) [Data set]. CaltechDATA. https://doi.org/10.14291/TCCON.GGG2014.BURGOS01.R0, https://data.caltech.edu/records/1090.

/Morino et al., 2022c/ Morino, I., Velazco, V. A., Hori, A., Uchino, O., & Griffith, D. W. T. (2022). TCCON data from Burgos, Ilocos Norte (PH), Release GGG2020.R0 (Version R0) [Data set]. CaltechDATA. https://doi.org/10.14291/tccon.ggg2020.burgos01.R0.

/Notholt et al., 2019/ Notholt, J., Petri, C., Warneke, T., Deutscher, N. M., Palm, M., Buschmann, M., Weinzierl, C., Macatangay, R. C., and Grupe, P.: TCCON data from Bremen (DE), Release GGG2014.R1, https://doi.org/10.14291/TCCON.GGG2014.BREMEN01.R1, https://data.caltech.edu/records/1290, 2019.

/Notholt et al., 2021a/ Notholt, J., Palm, M., NDACC Metadata File for Ny Alesund FTIR and references cited therein https://www-air.larc.nasa.gov/pub/NDACC/PUBLIC/meta/ftir/NyAlesund_ftir_jn_2021.pdf

/Notholt et al., 2021b/ Notholt, J., Palm, M., NDACC Metadata File for Bremen FTIR and references cited therein https://www-air.larc.nasa.gov/pub/NDACC/PUBLIC/meta/ftir/Bremen_ftir_jn_2021.pdf.

/Notholt et al., 2022/ Notholt, J., Petri, C., Warneke, T., & Buschmann, M. (2022). TCCON data from Bremen (DE), Release GGG2020.R0 (Version R0) [Data set]. CaltechDATA. https://doi.org/10.14291/tccon.ggg2020.bremen01.R0.

/O'Dell et al., 2012/ O'Dell, C.W.; Connor, B.; Bösch, H.; O'Brien, D.; Frankenberg, C.; Castano, R.; Christi, M.; Eldering, D.; Fisher, B.; Gunson, M.; et al. The ACOS CO_2 retrieval algorithm - Part 1: Description and validation against synthetic observations. Atmos. Meas. Tech. 2012, 5, 99–121.

/O'Dell et al., 2018/ O'Dell, C. W., Eldering, A., Wennberg, P. O., Crisp, D., Gunson, M. R., Fisher, B., Frankenberg, C., Kiel, M., Lindqvist, H., Mandrake, L., Merrelli, A., Natraj, V., Nelson, R. R., Osterman, G. B., Payne, V. H., Taylor, T. E., Wunch, D., Drouin, B. J., Oyafuso, F., Chang, A., McDuffie, J., Smyth, M., Baker, D. F., Basu, S., Chevallier, F., Crowell, S. M. R., Feng, L., Palmer, P. I., Dubey, M., García, O. E., Griffith, D. W. T., Hase, F., Iraci, L. T., Kivi, R., Morino, I., Notholt, J., Ohyama, H., Petri, C., Roehl, C. M., Sha, M. K., Strong, K., Sussmann, R., Te, Y., Uchino, O., and Velazco, V. A.: Improved retrievals of carbon dioxide from Orbiting Carbon Observatory-2 with the version 8 ACOS algorithm, Atmos. Meas. Tech., 11, 6539–6576, https://doi.org/10.5194/amt-11-6539-2018, 2018.

/Ortega et al., 2019/ Ortega, I., Buchholz, R. R., Hall, E. G., Hurst, D. F., Jordan, A. F.,and Hannigan, J. W.: Tropospheric water vapor profiles obtained with FTIR: comparison with balloon-borne frost point hygrometers and influence on trace gas retrievals, Atmos. Meas. Tech.,12, 873–890, https://doi.org/10.5194/amt-12-873-2019, 2019.

/Ostler et al., 2014/ Ostler, A., Sussmann, R., Rettinger, M., Deutscher, N. M., Dohe, S., Hase, F., Jones, N., and Palm, M.: Multistation intercomparison of column-averaged methane from NDACC and TCCON: Impact of dynamical variability, Atmos. Meas. Tech., 7, 4081–4101, https://doi.org/10.5194/amt-7-4081-2014, 2014.

/Parker et al., 2011/ Parker, R., Boesch, H, Cogan, A., et al. (2011), Methane Observations from the Greenhouse gases Observing SATellite: Comparison to ground-based TCCON data and Model Calculations, Geophys. Res. Lett., doi:10.1029/2011GL047871.

/Petri et al., 2020/ Petri, C., Vrekoussis M., Rousogenous, C., Warneke, T., Sciare, J., Notholt, J., TCCON data from Nicosia, Cyprus (CY), Release GGG2014.R0, https://doi.org/10.14291/TCCON.GGG2014.NICOSIA01.R0/, https://data.caltech.edu/records/1690.

/Petri et al., 2022/ Petri, C., Vrekoussis, M., Rousogenous, C., Warneke, T., Sciare, J., & Notholt, J. (2022). TCCON data from Nicosia (CY), Release GGG2020.R0 (Version R0) [Data set]. CaltechDATA. https://doi.org/10.14291/tccon.ggg2020.nicosia01.R0.

/PUGS, 2019/ Buchwitz, M., Aben, I., J., Armante, R., Boesch, H., Crevoisier, C., Di Noia, A., Hasekamp, O. P., Reuter, M., Schneising-Weigel, O., Wu, L.., Product User Guide and Specification (PUGS) – Main document for Greenhouse Gas (GHG: CO_2 & CH_4) data set CDR 3 (2003-2018), C3S project C3S_312b_Lot2_DLR, v3.1, 97 pages, https://www.iup.uni-bremen.de/carbon_ghg/docs/C3S/CDR3_2003-2018/PUGS/C3S_D312b_Lot2.3.2.3-v1.0_PUGS-GHG_MAIN_v3.1.pdf, 2019.

/PUGv4.1, 2023/ Reuter. M., M.Hilker, and M.Buchwitz: Product User Guide Version 4 (PUGv4.1) for the FOCAL XCO2 OCO-2 Data Product CO2_OC2_FOCA (v10.1) for the Essential Climate Variable (ECV) Greenhouse Gases (GHG) ESA Climate Change Initiative "Plus" (CCI+), 2023.

/PVIRv5, 2017/ Buchwitz et al., Product Validation and Intercomparison Report (PVIR), version 5, ESA GHG-CCI project, 2017

/PVIR v5, 2017/ Product Validation and Intercomparison Report" (PVIR), ESA Climate Change Initiative (CCI) GHG-CCI project, Version 5, 9 Feb 2017, 2017.

/PVIR GHG-CCI+ v1.1, 2020/ ESA Climate Change Initiative "Plus" (CCI+) Product Validation and Intercomparison Report (PVIR) for the Essential Climate Variable (ECV) Greenhouse Gases (GHG): XCO2 and/or XCH4 from OCO-2, TanSat, Sentinel-5-Precursor and GOSAT-2,13 Mar 2020, version 1.1, pp. 74, 2020.

/PVIR GHG-CCI+ v2.1, 2021/ ESA Climate Change Initiative "Plus" (CCI+) Product Validation and Intercomparison Report (PVIR) for the Essential Climate Variable (ECV) Greenhouse Gases (GHG): XCO2 and/or XCH4 from OCO-2, TanSat, Sentinel-5-Precursor and GOSAT-2,19 Mar 2021, version 2.1, pp. 118, 2021.

/PVIR GHG-CCI+ v3.0, 2022/ ESA Climate Change Initiative "Plus" (CCI+) Product Validation and Intercomparison Report (PVIR) for the Essential Climate Variable (ECV)

Greenhouse Gases (GHG): XCO2 and/or XCH4 from OCO-2, TanSat, Sentinel-5-Precursor and GOSAT-2,16 Feb 2022, version 3.0, pp. 148, 2022.

/Reuter et al., 2011/ Reuter, M., Bovensmann, H., Buchwitz, M., Burrows, J. P., Connor, B. J., Deutscher, N. M., Griffith, D.W. T., Heymann, J., Keppel-Aleks, G., Messerschmidt, J., and et al.: Retrieval of atmospheric CO_2 with enhanced accuracy and precision from SCIAMACHY: Validation with FTS measurements and comparison with model results., Journal of Geophysical Research, 116, doi:10.1029/2010JD015047, URL http://dx.doi.org/10.1029/2010JD015047, 2011.

/Reuter et al., 2012/ M. Reuter, M. Buchwitz, O. Schneising, F. Hase, J. Heymann, S. Guerlet, A.J. Cogan, H. Bovensmann, J.P. Burrows: A simple empirical model estimating atmospheric CO_2 background concentrations, Atmospheric Measurement Techniques, 5, 1349-1357, 2012.

/Reuter et al., 2013/ Reuter, M., H. Boesch, H. Bovensmann, A. Bril, M. Buchwitz, A. Butz, J. P. Burrows, C. W. O'Dell, S. Guerlet, O. Hasekamp, J. Heymann, N. Kikuchi, S. Oshchepkov, R. Parker, S. Pfeifer, O. Schneising, T. Yokota, and Y. Yoshida, A joint effort to deliver satellite retrieved atmospheric CO_2 concentrations for surface flux inversions: the ensemble median algorithm EMMA, Atmos. Chem. Phys., 13, 1771-1780, 2013.

/Reuter et al., 2017a/ M.Reuter, M.Buchwitz, O.Schneising, S.Noël, V.Rozanov, H.Bovensmann and J.P.Burrows: A Fast Atmospheric Trace Gas Retrieval for Hyperspectral Instruments Approximating Multiple Scattering - Part 1: Radiative Transfer and a Potential OCO-2 XCO_2 Retrieval Setup, Remote Sensing, 9(11), 1159; doi:10.3390/rs9111159, 2017.

/Reuter et al., 2017b/ M.Reuter, M.Buchwitz, O.Schneising, S.Noël, H.Bovensmann and J.P.Burrows: A Fast Atmospheric Trace Gas Retrieval for Hyperspectral Instruments Approximating Multiple Scattering - Part 2: Application to XCO_2 Retrievals from OCO-2, Remote Sensing, 9(11), 1102; doi:10.3390/rs9111102, 2017.

/Reuter et al., 2020/ M. Reuter, M. Buchwitz, O. Schneising, S. Noël, H. Bovensmann, J.P. Burrows, H. Boesch, A. Di Noia, J. Anand, R.J. Parker, P. Somkuti, L. Wu, O.P. Hasekamp, I. Aben, A. Kuze, H. Suto, K. Shiomi, Y. Yoshida, I. Morino, D. Crisp, C.W. O'Dell, J. Notholt, C. Petri, T. Warneke, V.A. Velazco, N.M. Deutscher, D.W.T. Griffith, R. Kivi, D.F. Pollard, F. Hase, R. Sussmann, Y.V. Té, K. Strong, S. Roche, M.K. Sha, M. De Mazière, D.G. Feist, L.T. Iraci, C.M. Roehl, C. Retscher, and D. Schepers: Ensemble-based satellite-derived carbon dioxide and methane column-averaged dry-air mole fraction data sets (2003-2018) for carbon and climate applications, Atmos. Meas. Tech., https://www.atmos-meas-tech.net/13/789/2020, 2020

/Rodgers, 2000/ Rodgers, C. D.: Inverse Methods for Atmospheric Sounding: Theory and Practice, World Scientific Publishing, 2000.

/Rozanov et al., 2014/ Rozanov, V., Rozanov, A., Kokhanovsky, A., and Burrows, J.: Radiative transfer through terrestrial atmosphere and ocean: Software package SCIATRAN, Journal of Quantitative Spectroscopy and Radiative Transfer, 133, 13 – 71, doi:https://doi.org/10.1016/j.jqsrt.2013.07.004,
URL http://www. sciencedirect.com/science/article/pii/S0022407313002872, 2014

/**Schepers et al., 2012/** Schepers, D., Guerlet, S., Butz, A., et al. (2012), Methane retrievals from Greenhouse Gases Observing Satellite (GOSAT) shortwave infrared measurements: Performance comparison of proxy and physics retrieval algorithms, *J. Geophys. Res*., 117, D10307, doi:10.1029/2012JD017549.

/Schneising et al., 2011/ Schneising, O., Buchwitz, M., Reuter, M., et al., Long-term analysis of carbon dioxide and methane column-averaged mole fractions retrieved from SCIAMACHY, Atmos. Chem. Phys., 11, 2881-2892, 2011.

/Schneising et al., 2012/ Schneising, O., Bergamaschi, P., Bovensmann, H., et al, Atmospheric greenhouse gases retrieved from SCIAMACHY: comparison to ground-based FTS measurements and model results, Atmos. Chem. Phys., 12, 1527-1540, 2012.

/Schneising et al., 2019/ Schneising, O., Buchwitz, M., Reuter, M., Bovensmann, H., Burrows, J. P., Borsdorff, T., Deutscher, N. M., Feist, D. G., Griffith, D. W. T., Hase, F., Hermans, C., Iraci, L. T., Kivi, R., Landgraf, J., Morino, I., Notholt, J., Petri, C., Pollard, D. F., Roche, S., Shiomi, K., Strong, K., Sussmann, R., Velazco, V. A., Warneke, T., and Wunch, D.: A scientific algorithm to simultaneously retrieve carbon monoxide and methane from TROPOMI onboard Sentinel-5 Precursor, Atmos. Meas. Tech., 12, 6771-6802, https://doi.org/10.5194/amt-12-6771-2019, 2019.

/Schneising et al., 2023/ Schneising, O., Buchwitz, M., Hachmeister, J., Vanselow, S., Reuter, M., Buschmann, M., Bovensmann, H., and Burrows, J. P.: Advances in retrieving XCH4 and XCO from Sentinel-5 Precursor: improvements in the scientific TROPOMI/WFMD algorithm, Atmos. Meas. Tech., 16, 669–694, https://doi.org/10.5194/amt-16-669-2023, 2023.

/Sherlock et al., 2014/ Sherlock, V., Connor, B., Robinson, J., Shiona, H., Smale, D., and Pollard, D. F.: TCCON data from Lauder (NZ), 125HR, Release GGG2014.R0, https://doi.org/10.14291/TCCON.GGG2014.LAUDER02.R0/1149298, https://data.caltech.edu/records/281, 2014.

/Sherlock et al., 2022/ Sherlock, V., Connor, B., Robinson, J., Shiona, H., Smale, D., & Pollard, D. F. (2022). TCCON data from Lauder (NZ), 120HR, Release GGG2020.R0 (Version R0) [Data set]. CaltechDATA. https://doi.org/10.14291/tccon.ggg2020.lauder01.R0.

/Shiomi et al., 2022/ Shiomi, K., Kawakami, S., Ohyama, H., Arai, K., Okumura, H., Ikegami, H., & Usami, M. (2022). TCCON data from Saga (JP), Release GGG2020.R0 (Version R0) [Data set]. CaltechDATA. https://doi.org/10.14291/tccon.ggg2020.saga01.R0.

/Stammes, 2002/ Stammes, P. OMI Algorithm Theoretical Basis Document, Volume III, Clouds, Aerosols, and Surface UV Irradiance (ATBD-OMI-03); Royal Netherlands Meteorological Institute (KNMI): De Bilt, The Netherlands, 2002.

/Strong et al., 2019/ Strong, K., Roche, S., Franklin, J. E., Mendonca, J., Lutsch, E., Weaver, D., Fogal, P. F., Drummond, J. R., Batchelor, R., and Lindenmaier, R.: TCCON data from Eureka (CA), Release GGG2014.R3, https://doi.org/10.14291/TCCON.GGG2014.EUREKA01.R3, https://data. caltech.edu/records/1171, 2019.

/Strong, 2021/ Strong K., NDACC Metadata File for Eureka FTIR and references cited therein, https://www-air.larc.nasa.gov/pub/NDACC/PUBLIC/meta/ftir/Eureka_ftir_ks_2021.pdf.

/Strong et al., 2022/ Strong, K., Roche, S., Franklin, J. E., Mendonca, J., Lutsch, E., Weaver, D., Fogal, P. F., Drummond, J. R., Batchelor, R., Lindenmaier, R., & McGee, E. (2022). TCCON data from Eureka (CA), Release GGG2020.R0 (Version R0) [Data set]. CaltechDATA. https://doi.org/10.14291/tccon.ggg2020.eureka01.R0.

/Sussmann et al., 2018a/ Sussmann, R. and Rettinger, M.: TCCON data from Garmisch (DE), Release GGG2014.R2, https://doi.org/10.14291/TCCON.GGG2014.GARMISCH01.R2, https://data.caltech.edu/records/956, 2018.

/Sussmann et al., 2018b/ Sussmann, R. and Rettinger, M.: NDACC Metadata File for Zugspitze FTIR and references cited therein M.: https://www-air.larc.nasa.gov/pub/NDACC/PUBLIC/meta/ftir/Zugspitze_ftir_rs_2018.pdf.

/Sussmann et al., 2023/ Sussmann, R., & Rettinger, M. (2023). TCCON data from Garmisch (DE), Release GGG2020.R0 (Version R0) [Data set]. CaltechDATA. https://doi.org/10.14291/tccon.ggg2020.garmisch01.R0

/Té et al., 2014/ Té, Y., Jeseck, P., & Janssen, C. (2014). *TCCON data from Paris (FR), Release GGG2014.R0* (Version GGG2014.R0) [Data set]. CaltechDATA. https://doi.org/10.14291/TCCON.GGG2014.PARIS01.R0/1149279, https://data.caltech.edu/records/284.

/Té et al., 2022/ Té, Y., Jeseck, P., & Janssen, C. (2022). TCCON data from Paris (FR), Release GGG2020.R0 (Version R0) [Data set]. CaltechDATA. https://doi.org/10.14291/tccon.ggg2020.paris01.R0.

/Thompson et al., 2012/ Thompson, D.R.; Chris Benner, D.; Brown, L.R.; Crisp, D.; Malathy Devi, V.; Jiang, Y.; Natraj, V.; Oyafuso, F.; Sung, K.; Wunch, D.; et al. Atmospheric validation of high accuracy CO_2 absorption coefficients for the OCO-2 mission. J. Quant. Spectrosc. Radiat. Transf. 2012, 113, 2265–2276.

/URDv2.1/ User Requirements Document (URD), ESA Climate Change Initiative (CCI) GHG-CCI project, Version 2.1, 38 pages, 19-Oct-2016, http://cci.esa.int/sites/default/files/URDv2.1_GHG-CCI_Final.pdf, 2016.

/URDv3.0/ Chevallier et al., GHG-CCI: User Requirements Document for the GHG-CCI+ project of ESA's Climate Change Initiative, pp. 42, version 3.0, 17-February-2020, https://www.iup.uni-bremen.de/carbon_ghg/docs/GHG-CCIplus/URD/URDv3.0_GHG-CCIp_Final.pdf, 2020.

/Warneke et al., 2019/ Warneke, T., Messerschmidt, J., Notholt, J., Weinzierl, C., Deutscher, N. M., Petri, C., and Grupe, P.: TCCON data from Orléans (FR), Release GGG2014.R1, https://doi.org/10.14291/TCCON.GGG2014.ORLEANS01.R1, https://data.caltech.edu/records/1301, 2019.

/Warneke et al., 2022/ Warneke, T., Petri, C., Notholt, J., & Buschmann, M. (2022). TCCON data from Orléans (FR), Release GGG2020.R0 (Version R0) [Data set]. CaltechDATA. https://doi.org/10.14291/tccon.ggg2020.orleans01.R0.

/Wennberg et al., 2015/ Wennberg, P. O., Wunch, D., Roehl, C. M., Blavier, J.-F., Toon, G. C., and Allen, N. T.: TCCON data from Caltech (US), Release GGG2014.R1, https://doi.org/10.14291/TCCON.GGG2014.PASADENA01.R1/1182415, https://data.caltech.edu/records/285, 2015.

/Wennberg et al., 2016a/ Wennberg, P. O., Roehl, C. M., Blavier, J.-F.,Wunch, D., and Allen, N. T.: TCCON data from Jet Propulsion Laboratory (US), 2011, Release GGG2014.R1, https://doi.org/10.14291/TCCON.GGG2014.JPL02.R1/1330096, https://data.caltech.edu/records/277, 2016a.

/Wennberg et al., 2016b/ Wennberg, P. O., Wunch, D., Roehl, C. M., Blavier, J.-F., Toon, G. C., and Allen, N. T.: TCCON data from Lamont (US), Release GGG2014.R1, https://doi.org/10.14291/TCCON.GGG2014.LAMONT01.R1/1255070, https://data.caltech.edu/records/279, 2016b.

/Wennberg et al., 2017/ Wennberg, P. O., Roehl, C. M., Wunch, D., Toon, G. C., Blavier, J.-F., Washenfelder, R., Keppel-Aleks, G., Allen, N. T., and Ayers, J.: TCCON data from Park Falls (US), Release GGG2014.R1, https://doi.org/10.14291/TCCON.GGG2014.PARKFALLS01.R1, https://data.caltech.edu/records/295, 2017.

/Wennberg et al., 2022/ Wennberg, P. O., Roehl, C. M., Wunch, D., Toon, G. C., Blavier, J.-F., Washenfelder, R., Keppel-Aleks, G., & Allen, N. T. (2022). TCCON data from Park Falls (US), Release GGG2020.R1 (Version R1) [Data set]. CaltechDATA. https://doi.org/10.14291/tccon.ggg2020.parkfalls01.R1.

/Wennberg et al., 2022b/Wennberg, P. O., Wunch, D., Yavin, Y., Toon, G. C., Blavier, J.-F., Allen, N. T., Keppel-Aleks, G., & Roehl, C. M. (2022). TCCON data from Jet Propulsion Laboratory (US), 2007, Release GGG2020.R0 (Version R0) [Data set]. CaltechDATA. https://doi.org/10.14291/tccon.ggg2020.jpl01.R0

/Wennberg et al., 2022c/ Wennberg, P. O., Roehl, C. M., Wunch, D., Blavier, J.-F., Toon, G. C., Allen, N. T., Treffers, R., & Laughner, J. (2022). TCCON data from Caltech (US), Release GGG2020.R0 (Version R0) [Data set]. CaltechDATA. https://doi.org/10.14291/tccon.ggg2020.pasadena01.R0.

/Wiacek et al., 2007/ Wiacek, A., Taylor, J. R., Strong, K., Saari, R., Kerzenmacher, T. E., Jones, N. B., and Griffith, D. W. T.: Ground-Based Solar Absorption FTIR Spectroscopy: Characterization of Retrievals and First Results from a Novel Optical Design Instrument at a New NDACC Complementary Station, J. Atmos. Ocean. Tech., 24,432–448, https://doi.org/10.1175/JTECH1962.1, 2007.

/Wiedmann et al. 2023/ Weidmann, D., Brownsword, R., & Doniki, S. (2023). TCCON data from Harwell, Oxfordshire (UK), Release GGG2020.R0 (Version R0) [Data set]. CaltechDATA. https://doi.org/10.14291/tccon.ggg2020.harwell01.R0.

/Wunch et al., 2010/ Wunch, D., Toon, G. C., Wennberg, P. O., Wofsy, S. C., Stephens, B. B., Fischer, M. L., Uchino, O., Abshire, J. B., Bernath, P., Biraud, S. C., Blavier, J.-F. L., Boone, C., Bowman, K. P., Browell, E. V., Campos, T., Connor, B. J., Daube, B. C., Deutscher, N. M., Diao, M., Elkins, J. W., Gerbig, C., Gottlieb, E., Griffith, D. W. T., Hurst, D. F., Jiménez, R., Keppel-Aleks, G., Kort, E. A., Macatangay, R., Machida, T., Matsueda, H., Moore, F., Morino, I., Park, S., Robinson, J., Roehl, C. M., Sawa, Y., Sherlock, V., Sweeney, C., Tanaka, T., and Zondlo, M. A.: Calibration of the Total Carbon Column Observing

Network using aircraft profile data, Atmospheric Measurement Techniques, 3, 1351–1362, doi:10.5194/amt-3-1351-2010, URL http://www.atmos-meas-tech.net/3/1351/2010/, 2010.

/Wunch et al., 2011/ Wunch, D., Toon, G. C., Blavier, J.-F. L., Washenfelder, R. A., Notholt, J., Connor, B. J., Griffith, D. W. T., Sherlock, V., and Wennberg, P. O.: The Total Carbon Column Observing Network (TCCON), Philosophical Transactions of the Royal Society of London, Series A: Mathematical, Physical and Engineering Sciences, 369, 2087–2112, doi:10.1098/rsta.2010.0240, 2011.

/Wunch et al., 2015/ Wunch, D., Toon, G. C., Sherlock, V., Deutscher, N. M., Liu, C., Feist, D. G., & Wennberg, P. O. (2015). Documentation for the 2014 TCCON Data Release. CaltechDATA. https://doi.org/10.14291/TCCON.GGG2014.DOCUMENTATION.R0/1221662, https://data.caltech.edu/records/249.

/Wunch et al., 2017/ Wunch, D., Mendonca, J., Colebatch, O., Allen, N. T., Blavier, J.-F., Springett, S., Neufeld, G., Strong, K., Kessler, R., & Worthy, D. (2017). *TCCON data from East Trout Lake, SK (CA), Release GGG2014.R0* (Version GGG2014.R0) [Data set]. CaltechDATA. https://doi.org/10.14291/TCCON.GGG2014.EASTTROUTLAKE01.R0/1348207, https://data.caltech.edu/records/296.

/Wunch et al., 2022/ Wunch, D., Mendonca, J., Colebatch, O., Allen, N. T., Blavier, J.-F., Kunz, K., Roche, S., Hedelius, J., Neufeld, G., Springett, S., Worthy, D., Kessler, R., & Strong, K. (2022). TCCON data from East Trout Lake, SK (CA), Release GGG2020.R0 (Version R0) [Data set]. CaltechDATA. https://doi.org/10.14291/tccon.ggg2020.easttroutlake01.R0.

/Yang et al., 2020/ Yang, D., H. Boesch, Y. Liu, P. Somkuti, Z. Cai, X. Chen, A. Di Noia, C. Lin, N. Lu, D. Lyu, R. J. Parker, L. Tian, M. Wang, A. Webb, L. Yao, Z. Yin, Y. Zheng, N. M. Deutscher, D. W. T. Griffith, F. Hase, R. Kivi, I. Morino, J. Notholt, H. Ohyama, D. F. Pollard, K. Shiomi, R. Sussmann, Y. Te, V. A. Velazco, T. Warneke, D. Wunch: Toward high precision XCO_2 retrievals from TanSat observations: Retrieval improvement and validation against TCCON measurements, Journal of Geophysical Research: Atmospheres, 125, e2020JD032794, https://doi.org/10.1029/2020JD032794, 2020.

/Zhou et al., 2022/ Zhou, M., Wang, P., Kumps, N., Hermans, C., & Nan, W. (2022). TCCON data from Xianghe, China, Release GGG2020.R0 (Version R0) [Data set]. CaltechDATA. https://doi.org/10.14291/tccon.ggg2020.xianghe01.R0.

7 List of Acronyms and Abbreviations

Abbreviation	Meaning
AAI	Absorbing Aerosol Index
ACA	Additional Constraints Algorithm
AOD	Aerosol Optical Depth
AOT	Aerosol Optical Thickness
ATBD	Algorithm Theoretical Basis Document
BIRA-IASB	Royal Belgian Institute for Space Aeronomy
CCI	Climate Change Initiative
CDR	Climate Data Record
CMUG	Climate Modelling User Group (of ESA's CCI)
COD	Cloud Optical Depth
CRG	Climate Research Group
D/B	Data base
DOAS	Differential Optical Absorption Spectroscopy
DPM	Detailed Processing Model
EC	European Commission
ECA	ECV Core Algorithm
ECMWF	European Centre for Medium Range Weather Forecasting
ECV	Essential Climate Variable
EO	Earth Observation
ESA	European Space Agency
ESM	Earth System Model
FCDR	Fundamental Climate Data Record
FOCAL	Fast atmOspheric traCe gAs retrievaL
FoM	Figure of Merit
FP	Full Physics
FTIR	Fourier Transform InfraRed

FTS	Fourier Transform Spectrometer
GCOS	Global Climate Observing System
GEO	Group on Earth Observation
GEOSS	Global Earth Observation System of Systems
GHG	GreenHouse Gas
GMES	Global Monitoring for Environment and Security
GOSAT	Greenhouse Gas Observing Satellite
IDL	Interactive Data Language
ITT	Invitation To Tender
IODD	Input Output Data Definition
IPCC	International Panel in Climate Change
IPR	Intellectual Property Right
IUP	Institute of Environmental Physics (IUP) of the University of Bremen, Germany
JCGM	Joint Committee for Guides in Metrology
LMD	Laboratoire de Météorologie Dynamique
LUT	Look-up table
MACC	Monitoring Atmospheric Composition and Climate, EU GMES project
MERIS	Medium Resolution Imaging Spectrometer
MIPAS	Michelson Interferometer for Passive Atmospheric Sounding
MODIS	Moderate Resolution Imaging Spectrometer
N/A	Not applicable
NDACC	Network for the Detection of Atmospheric Composition Change
NASA	National Aeronautics and Space Administration
NIES	National Institute for Environmental Studies
NIWA	National Institute Of Water & Atmospheric Research
NOAA	National Oceanic and Atmospheric Administration
OCO	Orbiting Carbon Observatory
OD	Optical Depth

OE	Optimal Estimation
PBL	Planetary Boundary Layer
PMD	Polarization Measurement Device
PR	Proxy (retrieval method)
PVP	Product Validation Plan
PVR	Product Validation Report
RA	Relative Accuracy
RD	Reference Document
RMS	Root-Mean-Square
RTM	Radiative transfer model
S5P	Sentinel-5 Precursor
SoW	Statement of work
SQWG	SCIAMACHY Quality Working Group
SRA	Seasonal Relative Accuracy
SRD	Software Requirements Document
SRON	Netherlands Institute for Space Research
SUM	Software User Manual
SVR	Software Verification Report
TANSAT	CarbonSat
TANSO	Thermal And Near infrared Sensor for carbon Observation
TBC	To be confirmed
TCCON	Total Carbon Column Observing Network
TBD	To be defined / to be determined
TROPOMI	TROPOspheric Monitoring instrument
UNAM	Universidad Nacional Autónoma de México
WFM-DOAS (or WFMD)	Weighting Function Modified DOAS
WG	Working Group

***** End of Document *****